Title
Dissecting the Roles of mTOR Complexes in the Neurologic Manifestations of Tuberous Sclerosis Complex

Author
Karalis, Vasiliki

Publication Date
2021

Peer reviewed|Thesis/dissertation

Dissecting the Roles of mTOR Complexes in the Neurologic Manifestations of Tuberous Sclerosis Complex

By

Vasiliki P. Karalis

A dissertation submitted in partial satisfaction of the

requirements for the degree of

Doctor of Philosophy

in

Molecular and Cell Biology

in the

Graduate Division

of the

University of California, Berkeley

Committee in Charge:

Professor Helen Bateup, Chair
Professor Dan Feldman
Professor Linda Wilbrecht
Professor Roberto Zonku

Fall 2021

Abstract

Dissecting the Roles of mTOR Complexes in the Neurologic Manifestations of Tuberous Sclerosis Complex

by

Vasiliki Karalis

Doctor of Philosophy in Molecular and Cell Biology

University of California, Berkeley

Professor Helen Bateup, Chair

The mechanistic target of rapamycin (mTOR) is a kinase found in two multi-protein complexes, mTOR complex 1 (mTORC1) and 2 (mTORC2). These complexes are integral parts of an evolutionarily conserved signaling pathway known as the mTOR pathway. mTORC1 and mTORC2 are controlled by an array of intra and extracellular stimuli via different upstream regulators. The two complexes are known to exert distinct functions by phosphorylating downstream targets and ultimately orchestrate cell growth and metabolism. Aberrant mTOR activity is associated with numerous diseases, with particularly profound impact on the nervous system. Specifically, mutations in genes encoding for mTOR regulators result in a collection of neurodevelopmental disorders known as mTORopathies.

Tuberous Sclerosis Complex (TSC) is one of the most well characterized mTORopathies. TSC is caused by mutations in the *TSC1* or *TSC2* genes, which encode proteins that negatively regulate mTORC1 signaling. Current therapeutic strategies focus on rapamycin and its analogs that are inhibitors of mTORC1. However, several studies have shown that chronic rapamycin inhibits both mTORC1 and mTORC2 in a cell-type specific manner, raising the possibility that mTORC2 suppression might also exert therapeutic benefits in TSC. This idea has been corroborated by some studies showing that mTORC2 is involved in cellular processes that are altered in TSC, such as myelination and mGluR-dependent synaptic long-term depression. Most recently a study showed that mTORC2 suppression can provide therapeutic benefits in other mTORopathies.

It is currently unknown which mTOR complex is most relevant for TSC-related brain phenotypes. To model TSC we used *in vitro* systems of primary hippocampal cultures where we examined postnatal loss of *Tsc1* and we also used the Emx1-Cre mouse line to conditionally delete *Tsc1* embryonically from forebrain excitatory neurons.

To investigate which mTOR complex is responsible for TSC neurologic manifestations we used genetic strategies to target Raptor and Rictor and selectively reduce mTORC1 or mTORC2 activity respectively. Interestingly, our study revealed that the two complexes regulate each other's activity and loss of either Raptor or Rictor affects the activity of both complexes.

As it has been previously shown loss of *Tsc1* results in increased mTORC1 activity and decreased mTORC2. We found that reduction of Raptor, but not Rictor, rebalances both mTORC1 and mTORC2 signaling and improves the morphology of *Tsc1* knock-out neurons *in vitro*. We also observed that Raptor reduction *in vivo,* was sufficient to prevent several neurologic phenotypes in a mouse model of TSC, including mTORC1 hyperactivity, neuronal hypertrophy, demyelination, network hyperactivity and premature mortality.

Finally, we examined Raptor manipulation as a therapeutic strategy by postnatally injecting shRNA in mice with embryonic loss of *Tsc1*. We found that postnatal Raptor downregulation can rescue both cell and non-cell autonomous mechanisms including mTORC1 hyperactivity, neuronal hypertrophy, and myelination. We also found that shRptor can significantly extend survival and improve the overall development of Tsc1-KO mice. Notably, when we examined the effects of Raptor manipulation as therapeutic strategy for TSC-related seizure activity we found that downregulation of Raptor did not improve the phenotype. Interestingly, neither rapamycin treatment was able to rescue this phenotype suggesting that this seizure like activity in our *in vitro* model, cannot be rescued via mTORC1 suppression after it has been established.

Overall, this thesis provides novel insights in the regulation and function of the mTOR pathway in neurons. We identify mTORC1 as the complex that drives neurologic manifestations in mouse models of TSC and propose that Raptor manipulation could be a promising therapeutic strategy for TSC and potentially other mTORopathies. We have also established an *in vitro* model where we can study TSC related seizure-like activity. This model reveals that cell-autonomous changes that drive neuronal hyperactivity due to *Tsc1* loss can become mTORC1 independent over time. Together this data generates new insights that will aid in understanding more in depth the molecular mechanisms that drive TSC neurologic manifestations and provide important information for the development of novel preventative and therapeutic strategies.

Acknowledgements

I would like to acknowledge and thank all the people who have supported me, influenced me, and guided me throughout my time at UC Berkeley.

I must start by thanking the people who helped me and guided me during the very first steps of this exciting journey. George Gaitanaris, thank you for trusting me, guiding me and for always being there to give me your advice. Io Dolka, thank you for your unconditional support since the very first day I moved to the US!

I would also like to extend my gratitude to all the people who inspired me and helped me achieve my goal to pursue my PhD at Berkeley. Rene Onrust, working with you was an amazing experience! Thank you for your continuous support! Alex Rohde, thank you for teaching me a lot of the things I know today! Anna Sadusky, I cannot count how many times I came to you to ask for your help and advice and I cannot remember a single time you did not kindly offer both! Linda Buck, thank you for giving me the opportunity to be part of your team. It was an honor to work with you and learn from you. Pia Hoellerbauer, thank you for being a great friend when I needed one the most! Mike Luoma, I am grateful for your unconditional support. I am not sure I would have done it without you!

Joining UC Berkeley as a graduate student has been an amazing experience, and I want to thank all the people who contributed to this. I must start by thanking Helen Bateup, a truly inspiring scientist whom I was fortunate to have as my research mentor. Helen, thank you for trusting me and giving me the time and space to grow as a scientist while simultaneously gently guiding me towards the right direction. It has been an honor to work with you! I also must thank my thesis committee: Dan Feldman, Linda Wilbrecht and Robert Zoncu for their guidance and support throughout graduate school. Finally, a sincere thanks to Ehud Isacoff who has been supporting me and advising me since I rotated in his lab during my first year.

I also would like to say thank you to all the members of the Bateup lab current and past! John Blair, Dan Kramer, Katie Benthall, Polina Kosillo, Jilian Iafrati, Bipan Deb, Katie Cording, Erin Aisenberg, Jesse Dunnack, Laura Haetzel, Victoria Du, Mahmoud Farhan, Kamran Ahmed and Alex Agopyan-Miu. It has been an honor to be part of such an inspiring group of scientists, exchange ideas and learn from you. Katie B. and Polina thank you for besides being incredible scientists and colleagues you have also been amazing friends! Katie B. thank you for forcing me outside lab every now and then and for all the fun adventures we shared! Polina, being able to confide in you has helped more than I can describe. You have inspired me and helped me in so many ways! I cannot imagine going through these last years of graduate school without you there!

I am grateful to consider myself part of the MCB and Neuro community at UC Berkeley. It has been a privilege to meet, collaborate and make friends with such diverse and amazing people. A huge thanks to Carlos Pantoja, Liliya Khasin, Kurtresha Worden, Laura Craciun, Malak El-Quessny, Adam Hoagland, Franklin Caval-Holme, Mathew Summers, Chris Habrian and Victoria Chu. Mathew, I always knew we'd turn out to be best buddies! I will miss our crepes and movie nights and I hope we will have more in the future. Chris, thank you for being a great friend, supporting me and keeping me sane

during some rather rough times. Victoria, thank you for always having time to chat and advise me for both scientific and non-scientific matters!

A heartfelt thank you to my incredible roommates Laura Craciun and Prince Craciun. You both have made my life so much more fun and exciting! Having you around helped way more than you can think! Also, a huge thanks to both of you for supporting (Laura) and putting up (Prince) with one of the most impulsive decisions I've ever made which was to adopt Mera.

To my support network: Mera, while you are probably not aware of this (or maybe you are at this point) you are one of the main reasons I have managed to make it this far. Sebastian Palluk, I am also not sure you are aware of this, but I truly thank you for putting up with the worst and the best of me with the same patience and compassion. I am truly grateful for having you in my life especially during the difficult times of the pandemic.

To my close friends from back home who have always been there for me and inspired me in their own unique ways: Eleni Malaktari, Katerina Adam, Lina Giotopoulou, Evi Iliopoulou and Velissarios Pliatsikas, thank you! Evi and Velissarie, 15 years and counting full of amazing memories. Even though we've been so far you are always a phone call away. I am grateful to have you both in my life!

Finally, I must extend the most whole-hearted thanks to my family. To my parents Rita and Petros, and my brother Yiannis. I am grateful for the way you raised me to be, for your unwavering support, and for your unconditional love. I would not have made it this far if it weren't for you. Ευχαριστώ!

Table of Contents

Chapter 1: Introduction
Current approaches and future directions for the treatment of mTORopathies

This chapter is modified from the review article published as “Current approaches and future directions for the treatment of mTORopathies” in Developmental Neuroscience, 2021; 1-16. doi:10.1159/000515672 by Vasiliki Karalis and Helen S. Bateup. It has been modified and reproduced here with full permission of the authors

Vasiliki Karalis

Department of Molecular and Cell Biology
University of California, Berkeley

The history of rapamycin

In 1964 a scientific expedition in Easter Island led to the discovery of one of the most widely studied compounds today. Microbiologist Georges Nógrády was intrigued by the fact that while the presence of horses was associated with a bacterial infection called tetanus, in Easter Island, where horse population was larger than the human population, the prevalence of tetanus was very low. To understand this paradox Nógrády collected soil samples from the island[1].

These samples were later given to a scientific team in Ayerst Pharmaceuticals that was interested in naturally occurring medicinal compounds. The team there identified a novel antifungal compound produced by the Streptomyces hygroscopicus bacteria and named it rapamycin after Rapa Nui, the Polynesian name for Easter Island. Dr. Suren N. Sehgal who was part of that team went on to demonstrate that in addition to acting as an antifungal, rapamycin showed strong immunosuppressant and anti-tumor properties [1]. In 1991 Michael N Hall and George P. Livi working independently identified the molecular target of rapamycin (TOR) in budding yeast [2, 3] and a few years later followed the discovery of the mammalian TOR homologue that was later named mechanistic target of rapamycin or mTOR [4, 5].

The mechanistic target of rapamycin

The serine/threonine-protein kinase mTOR (mechanistic target of rapamycin) was discovered just over 25 years ago [4, 5]. Initial studies on mTOR focused on its role in cancer, as it is a key regulator of cell growth and proliferation [6]. However, subsequent studies revealed broader roles for mTOR as a signaling hub, coordinating information between the intra and extracellular environment. mTOR was found to respond to various stimuli including amino acids, trophic factors and energy status and in turn regulate the balance between anabolic (i.e. protein synthesis) and catabolic (i.e. autophagy) processes [7].

mTOR's role in protein synthesis made this pathway a point of interest for neuroscientists in the early 2000s. *De novo* protein synthesis had been identified as a requirement for long-term synaptic plasticity in neurons [8, 9] and mTOR was known to control the translational regulators ribosomal protein S6 kinase beta-1 (S6K1 or p70S6K1) and 4E binding proteins (4E-BPs) [10]. Indeed, in 2002, mTOR was shown to be required for the late phase of hippocampal long-term potentiation (LTP), as LTP was inhibited by rapamycin in brain slices [11]. From then on, the list of mTOR's functions in neurons has steadily expanded. Today, mTOR signaling has been linked to fundamental neural processes such as progenitor proliferation, neuronal migration, cell survival, axon and dendrite development, membrane excitability and synaptic properties [12, 13]. Consistent with its multifaceted roles in the nervous system, deregulation of mTOR signaling is associated with numerous neurological and psychiatric disorders [14-16].

In this chapter I will discuss: 1) how mutations in genes that encode mTOR regulators lead to disorders with shared neurological manifestations ("mTORopathies"), 2) the current status of therapeutic interventions for mTORopathies in patients and animal models, and 3) potential considerations for developing improved treatment strategies for mTOR-related disorders.

The architecture and function of the mTOR complexes

The regulatory-associated protein of mTOR (RAPTOR) was the first mTOR binding partner to be discovered and was identified as an obligatory component of mTOR complex 1 (mTORC1) [17, 18]. A few years later, a second mTOR complex was found (mTOR complex 2, mTORC2), after the discovery of a protein that bound to mTOR independently of RAPTOR, the rapamycin-insensitive companion of mTOR (RICTOR) [19]. mTORC1 and mTORC2 share some of the same protein components, while others are unique to each complex (shown in Fig. 1A). Shared proteins include the mTOR kinase itself, mTOR-associated protein, LST8 homolog (mLST8 also known as GβL), DEP domain-containing mTOR interacting protein (DEPTOR), TELO 2 interacting protein 1 (TTI1) and telomere maintenance 2 (TELO2) [20-22]. Specific to mTORC1 are RAPTOR and proline-rich AKT1 substrate 1 (AKT1S1 or PRAS40) [23]. Besides RICTOR, mTORC2 also contains proline-rich protein 5 or 5-like (PRR5/5L or PROTOR1/2) and target of rapamycin complex 2 subunit MAPKAP1 (MAPKAP1 or mSIN1) [24, 25] (shown in Fig. 1A).

Both complexes work as integrators of extra and intracellular signals to orchestrate cellular responses [12, 26] (shown in Fig. 1A). mTORC1 is regulated by various inputs including nutrients, growth factors, neuropeptides, and neurotransmitters [12]. In response to these stimuli, mTORC1 controls fundamental cellular processes such as protein synthesis, metabolism and autophagy. In neurons, mTORC1 controls differentiation, migration, cell morphology, intrinsic excitability and synaptic properties [12, 13]. Our knowledge of the functions of mTORC2 in the central nervous system is still limited. Several studies, however, have shown that mTORC2 responds to growth factors, hormones and neurotransmitters to regulate cytoskeletal organization and thus can impact neuronal morphology and synaptic physiology [12, 27, 28].

mTORopathies

The critical importance of balanced mTOR signaling is underscored by the fact that mutations in genes encoding mTOR regulators cause neurodevelopmental disorders collectively termed mTORopathies (Table 1) [29, 30]. Some of the most well characterized genes associated with mTORopathies are *TSC1*, *TSC2*, *PTEN*, *AKT*, *STRADA*, and *DEPDC5* [31]. While mutations in these genes can affect multiple organ systems, I will focus on their shared neurologic and psychiatric manifestations, which can include cortical malformations, intellectual disability, epilepsy, and autism spectrum disorder (ASD).

Phosphatase and tensin homolog (PTEN) hamartoma tumor syndrome (PHTS)

PHTS is a spectrum of multi-system disorders caused by LoF germline mutations in *PTEN* [32]. PTEN is a phosphatase that negatively regulates the PI3K/AKT/mTOR pathway by dephosphorylating phosphatidylinositol (3,4,5)-trisphosphate (PIP3) at the cell membrane. LoF mutations in *PTEN* cause elevated PIP3 that recruits several proteins including 3-phosphoinositide-dependent protein kinase-1 (PDK1) and AKT family members. PDK1 and subsequently mTORC2 phosphorylate and fully activate AKT, which

in turn phosphorylates and inhibits TSC2 leading to increased mTORC1 activity (shown in Fig. 1C) [33].

PHTS disorders include Cowden syndrome (CS), Bannayan–Riley–Ruvalcaba syndrome and adult Lhermitte–Duclos disease [32]. These disorders are associated with increased cancer and tumor risk [32]. Neuropsychiatric manifestations associated with LoF mutations in *PTEN* include macrocephaly, developmental delay, ASD, and intellectual disability [32]. Some studies have also identified patients carrying *PTEN* mutations who present with cortical malformations and seizures [34-36]. In addition, *PTEN* mutations have been linked to ASD and *PTEN* is one of the most prominent risk genes in idiopathic ASD [37, 38].

Malformations of cortical development (MCD)

MCD is a group of disorders characterized by abnormal development of the cerebral cortex, such as focal cortical dysplasia (FCD), megalencephaly (ME), and hemimegalencephaly (HME) [39]. FCD is defined by focal regions of the cortex that contain enlarged, dysplastic, and mislaminated neurons and glia, which can be observable by MRI and vary in size and location [40]. ME is defined by increased head circumference two standard deviations above the age-related mean, which is caused by increased growth of brain structures. HME is the enlargement of an individual hemisphere of the cerebral cortex [41, 42]. MCDs are common causes of pediatric epilepsy, ID and neurological deficits [43]. Epilepsy in MCD patients is often intractable, occasionally life-threatening, and can require surgical resection [44, 45]. Studies of resected tissue from FCD and HME patients have shown increased phosphorylation of the mTORC1 downstream target, ribosomal protein S6 [46-49]. More recent sequencing studies revealed that somatic brain mutations in mTOR regulators including *mTOR* itself, *PIK3CA*, *RHEB*, *AKT3*, *TSC1* and *TSC2* [50-53] can result in focal cortical dysplasia (Table 1), which share several features with syndromic disorders including cortical malformations and epilepsy [52, 54]. In addition, mutations in *DEPDC5*, *NPRL2* and *NPRL3*, which are components of the mTORC1 inhibitor GATOR complex 1 [55], have been linked to FCD, infantile spasms, focal epilepsy and sudden unexpected death in epilepsy (SUDEP) [56-58].

Mutations in *STRADA* and *NF1*, which encode negative regulators of mTORC1 [59, 60] have been identified in syndromes that present with MCD, epilepsy and cognitive deficits. Specifically, LoF mutations in *STRADA* cause polyhydramnios, megalencephaly, and symptomatic epilepsy syndrome (PMSE) [61] and LoF mutations in *NF1* cause neurofibromatosis type 1 (NF1) syndrome [62]. Polyhydramnios refers to excess amniotic fluid during pregnancy, which is a hallmark of PMSE. Aside from mTORopathies, aberrant mTOR signaling has been detected in several neurodevelopmental disorders such as Fragile X syndrome, Down syndrome and idiopathic ASD [63-65]. In addition, mTOR dysregulation has been observed in several psychiatric disorders and neurodegenerative diseases [12, 14, 15, 66]. However, a direct causal link between mTOR and these disorders has yet to be defined. In particular, given that mTOR signaling is highly responsive to neuronal activity [67], it is possible that altered mTOR signaling may occur as a secondary phenotype to changes in network activity in many of these diseases.

Tuberous Sclerosis Complex (TSC)

TSC is a multisystem developmental disorder with varying symptom severity caused by mutations in either the *TSC1* or *TSC2* genes that encode for the proteins tuberin and hamartin, respectively [68, 69]. TSC1, TSC2 and TBC1 domain family member 7 (TBC1D7) form a protein complex that acts as an essential negative regulator of mTORC1 [70-72] (shown in Fig. 1B). Loss of either TSC1 or TSC2 results in destabilization of the complex, leading to loss of its GTPase activating protein (GAP) activity towards the GTP-binding protein Rheb (RHEB), a direct activator of mTORC1 [73]. Loss-of-function (LoF) mutations in *TSC1* or *TSC2* therefore lead to constitutive mTORC1 activity.

TSC neuropathology includes focal malformations called tubers that contain enlarged and dysplastic neurons, astrocytes, and so called “giant” or “balloon” cells [74]. Tubers form during embryonic development and are primarily found in the cortex and occasionally in other regions such as the cerebellum [75, 76]. Tubers, or the peri-tuberal cortex can become seizure foci [77, 78] and may be surgically resected as a treatment for intractable epilepsy in TSC [79]. Approximately 80% of individuals with TSC develop benign growths emanating from the ventricular walls called subependymal nodules (SENs) [80]. In 5-15% of TSC patients, SENs can progress to benign glioneuronal tumors called subependymal giant cell astrocytomas (SEGAs) [80]. A prevailing model is that TSC-associated brain lesions including SEGAs and tubers are caused by somatic second-hit mutations [31, 81]. According to this model, individuals with TSC have a germline heterozygous LoF mutation in *TSC1* or *TSC2* and during brain development a small number of neural progenitor cells acquire a somatic mutation that disrupts the expression of the functional allele, causing bi-allelic inactivation. In this scenario, progenitor cells with a second-hit mutation give rise to abnormal, dysplastic tuber cells that are surrounded by cells with normal-appearing morphology, which are derived from heterozygous progenitors. This model, in which the secondary mutation occurs stochastically, is consistent with the variable number, size and location of cortical tubers observed in individuals with TSC. Second-hit mutations have been consistently observed in resected SEGAs and TSC-associated tumors (called hamartomas) in peripheral organs [82-84]. However, they have only been identified in a subset of cortical tubers, resulting in some debate over the origins of cortical tuber cells [85-88].

TSC is also associated with several neuropsychiatric conditions, collectively termed “TAND” (TSC-Associated Neuropsychiatric Disorders) [89]. Approximately 80-90% of TSC patients develop seizures that can begin in infancy (infantile spasms) [90]. Earlier onset and increased severity of TSC-related seizures is correlated with greater risk of intellectual disability (ID), ASD, and attention deficit hyperactivity disorder (ADHD) [90-94]. Impaired and disordered myelination has also been observed in individuals with TSC using brain imaging techniques [95, 96]. Interestingly, while mutations in *TBC1D7* have not been reported in TSC patients, they have been identified in individuals with macrocephaly/megalencephaly and ID [97, 98], presentations that are shared among several mTORopathies.

Current treatment strategies for TSC and other mTORopathies

Several clinical studies have demonstrated the utility of rapamycin and its analogues (rapalogs), such as sirolimus and everolimus, as treatments for TSC and other mTORopathies including PHTS, NF1 and PMSE [99-101]. Rapamycin is an allosteric mTOR inhibitor that binds to FK506-binding protein 12 (FKBP12). The rapamycin-FKBP12 complex then binds to the FKBP-rapamycin binding domain on mTOR and blocks its catalytic domain [4, 102]. The first clinical evidence of rapalog efficacy for neurological manifestations came from Franz et al. in 2006 who showed SEGA regression in five TSC patients following rapamycin treatment [103]. Several larger follow-up studies corroborated the effectiveness of everolimus treatment in TSC patients with SEGAs [104-106]. Clinical studies have also shown that rapalogs can be useful treatments for other TSC-related phenotypes including seizures [106-108], with one study demonstrating 40% reduction of seizure severity in 40% of patients in a trial of over 300 patients spanning a broad age range [107]. However, not all studies have reported successful outcomes with rapalogs in individuals with TSC-related seizures [109]. Recent clinical studies such as "Stopping TSC Onset and Progression 2: Epilepsy Prevention in TSC Infants (STOP2) (https://clinicaltrials.gov/ct2/show/NCT04595513)" have focused on early treatment or prevention of seizures in infants and children with TSC, as it may be difficult to control seizures with rapalogs or other drugs after prolonged occurrence [110, 111]. Notably, other antiseizure medications, including vigabatrin for infantile spasms, have been successfully used in TSC patients [112].

A limited number of studies have explored the effect of rapalogs on the cognitive and psychiatric conditions associated with TSC. In 2017, Krueger et al. found that a 6-month long everolimus treatment did not significantly improve neurocognitive function or behavioral abnormalities in children with TSC [113]. Similarly, in 2019, Overwater et al, showed that 12-month everolimus treatment in children with TSC did not improve intelligence quotient (IQ) or ASD symptoms [114]. However, a study involving 35 Japanese patients showed promising results of everolimus treatment on both TSC-related ASD behavioral symptoms and seizures [115]. The mixed results of these studies suggest that while rapalogs can be effective at treating neuropsychiatric aspects of TSC in some individuals, further research and development of therapeutic approaches is warranted.

While rapalogs are extensively used in clinical trials as therapeutic interventions for mTORopathies, there are limitations to their usage. For instance, rapamycin does not equally block the phosphorylation of all mTORC1 substrates [116]. Specifically, while rapamycin abolishes phosphorylation of ribosomal protein S6, inhibition of 4E-BP1 phosphorylation is incomplete [117], suggesting that phenotypes arising due to 4E-BP1 deregulation may be largely rapalog-resistant. In addition, while the phenotypes of mTORopathies are generally thought to be due to mTORC1 hyperactivity (although see further discussion below), it is known that chronic rapamycin treatment inhibits both mTORC1 and mTORC2, likely via sequestering mTOR kinase and prohibiting mTORC2 formation [118]. This non-selective inhibition, in addition to on-target off-tissue effects, has been shown to contribute to the adverse effects associated with rapalog treatment such as glucose intolerance, insulin resistance and new-onset diabetes [119-121]. These side-effects are an important consideration given that long-term treatment with rapalogs may be required as the beneficial results can be reversible. For example, upon cessation

of rapalog treatment, seizures can resume and SEGAs can regrow [103]. However, studies in mice have shown that intermittent, low-level dosing of rapamycin can maintain the mTOR inhibiting effects while minimizing unwanted systemic side effects [122]. Consistent with this, it was shown that the antiepileptic properties of rapamycin in a mouse model of TSC could be maintained with as long as 24 day inter-treatment intervals [123].

Development of novel drug-based therapeutics

Currently, much research is geared towards the development of new drugs, including novel rapalogs, with more favorable pharmacokinetic characteristics, greater selectivity towards mTORC1, and fewer or less severe side effects. A recently developed rapalog, DL001, showed higher selectivity for mTORC1 when compared to rapamycin and had substantially fewer side effects when tested in mice [124]. In addition to rapalogs, a second generation of ATP-competitive mTOR kinase inhibitors have been under development [125]. These inhibitors target the catalytic site of mTOR and while all downstream mTORC1 targets are equally affected, these inhibitors exhibit no selectivity between the two mTOR complexes, similar to extended rapamycin treatment. Recent studies have attempted to improve selectivity by targeting mTOR regulators. For example, the small molecule NR1 potently binds to Rheb and selectively inhibits mTORC1 activity in mice [126]. More recently, another small molecule, EN6, inhibits mTORC1 by binding to an ATP-proton pump that normally aids mTORC1 recruitment onto the lysosome, which is necessary for its activation [127]. *In vitro*, EN6 was shown to suppress phosphorylation of both S6 and 4E-BP1, increase autophagy, and did not affect the mTORC2 target AKT [127].

The off-tissue effects of systemically administered small molecules are often a challenge in drug development. The ability to selectively target aberrant mTOR signaling in the brain would be transformative to long-term management of patient care. One recently developed strategy is a dual-molecule approach aiming to restrict mTOR inhibition to the brain. Specifically, Shokat et al. used RapaLink-1, a brain permeable mTOR inhibitor, along with RapaBlock, a brain impermeable FKB12 ligand. RapaBlock inhibits RapaLink-1 function outside the brain and thus prevents mTOR inhibition in peripheral tissues [128]. This approach has the potential to overcome the problem of systemic side effects.

While small molecule mTOR inhibitors are an active area of research, the question of whether we fully understand the functions of the mTOR complexes and the consequences of manipulating these functions remain. The variability of the clinical data underscores the importance of further exploring the mechanisms underlying neuropsychiatric presentations in mTORopathies. In addition, treatment strategies may need to be optimized and tailored toward specific phenotypes. For example, when targeting cells in tumors, complete suppression of mTORC1 activity may be beneficial to inhibit cell growth and eventually induce cell death. However, balancing mTOR activity rather than completely inhibiting it, may be a more desirable outcome for treating neuropsychiatric conditions. Thus, it will be important to examine alternative treatment strategies and utilize robust models to study these disorders.

Animal models of mTORopathies

Various animal models have been generated to enable investigations into the underlying mechanisms of mTORopathies. In early studies, drosophila and rat models of TSC were used to uncover the roles of *Tsc1* and *Tsc2* in the cell cycle, proliferation and cancer [129-133]. Subsequently, numerous genetic mouse models have been developed harboring mutations in genes that encode for mTOR regulators including *Strada* [134, 135], *Nf1* [136] and *Depc5* [137] (Table 2). Here, we will focus on several of the most well-studied mouse models with mutations in the *Tsc1*, *Tsc2* or *Pten* genes (Table 2). Germline homozygous loss of these genes is embryonically lethal [138-141]. While mice with heterozygous LoF mutations in *Tsc1*, *Tsc2* or *Pten* can exhibit some synaptic, cellular and behavioral phenotypes [140, 142-149], they often do not fully recapitulate the spectrum and severity of human disease phenotypes. In particular, mice with heterozygous *Tsc1* or *Tsc2* mutations do not exhibit robust mTORC1 hyperactivity, cortical malformations, or significant spontaneous seizures.

The use of Cre-dependent conditional knock-out mice avoids the confound of embryonic lethality and enables the generation of models with cell type- and developmental stage-specific mutations. Several mouse models with deletion of either *Tsc1, Tsc2* or *Pten* in specific cell types have been generated, which recapitulate various disease phenotypes including dysmorphic neurons, astrogliosis, hypomyelination, mislamination, seizures and behavioral alterations (as reviewed previously [12, 150]). In these models, the onset and severity of phenotypes depend on the developmental stage of the genetic perturbation. For example, studies of Tsc1 conditional knock-out mice (Tsc1-cKO) have shown that Cre expression driven by the Emx1 or Syn1 promoters, which lead to loss of Tsc1 from neurons during mid-embryogenesis, causes spontaneous seizures first observable at two weeks of age with premature mortality and a median survival of ~18-35 days *[151, 152]*. Loss of Tsc1 or Pten from postmitotic neurons between 2-4 weeks of age using *Camk2a*-Cre mice results in seizures that begin later, between 5-10 weeks of age**,** with a median survival of approximately 50 days *[153-155]*. This demonstrates that seizures can occur independent of early developmental alterations. A study by Zou et al. using a tamoxifen-inducible system showed that GFAP-Cre-driven Tsc1 loss primarily from astrocytes at 2 weeks of age, but not at 6 weeks, was sufficient to cause seizures, signifying that the timing of the perturbation affects the phenotypic severity *[156]*. These findings are important to consider when interpreting the results of therapeutic interventions in these models. For example, later-onset seizures may arise from distinct cellular or circuit mechanisms and may therefore respond differently to treatment compared to early developmental seizures. In addition, studies that provide treatment prior to or at the onset of seizures (i.e. prevention) may have a better outcome than those in which treatment occurs after seizures have already begun.

Cell type-specific disruption of mTOR regulators has revealed brain regions and cell types that may be key drivers of cognitive and behavioral deficits in TSC and PHTS. For instance, LoF mutations in *Tsc1*, *Tsc2* or *Pten* in Purkinje cells (PC) of the cerebellum induce ASD-like phenotypes including altered sociability and cognitive inflexibility [157-159]. Selective loss of *Tsc1* from dopaminergic (DA) neurons using *Slc6a3*(DAT)-Cre mice leads to cognitive inflexibility in a reversal learning task [160], while DA-neuron specific loss of *Pten* impairs social preference and novelty [145]. Selective loss of *Tsc1*

from serotonergic neurons using *Slc6a4*(SERT)-Cre mice was also sufficient to cause autism-like behaviors including social behavior deficits and increased repetitive behaviors [161]. Deletion of *Tsc1* from one of the primary targets of dopamine neurons, striatal projection neurons (SPNs), results in enhanced motor routine learning, which only occurs when Tsc1 is lost from direct pathway, but not indirect pathway, SPNs [162]. In addition, deletion of *Tsc1* from thalamic neurons during mid-embryonic development leads to repetitive grooming [163]. Notably, loss of Tsc1 from cerebellar, dopaminergic, serotonergic or striatal neurons can induce behavioral alternations in the absence of seizures. Therefore, different cell types and circuits may be responsible for the distinct neuropsychiatric manifestations of TSC and related disorders.

Novel approaches have emerged to capture the focal nature of mTOR-driven cortical malformations using *in utero* electroporation in mice to induce mutations in a small population of cortical cells. In one study, Cre was electroporated at ~E15 into the cortex of *Tsc1*$^{flox/-}$ mouse embryos to induce a second-hit mutation. This led to the formation of cortical heterotopic nodules with neuronal hypertrophy and abnormal migration together with decreased seizure threshold [164]. Similarly, Lim et al. used *in utero* electroporation to induce CRISPR/Cas9-based gene disruption of *Tsc1* or *Tsc2*. These mice exhibited spontaneous seizures, neuronal hypertrophy and cortical mislamination [53]. Focal, constitutive activation of Rheb in the developing mouse cortex, which results in robust mTORC1 hyperactivity, has also been shown to result in neuronal hypertrophy, misplacement and spontaneous seizures [165].

As a complement to these animal models, human stem cell-based models of TSC and other mTORopathies have emerged over recent years due to advances in human stem cell and genome engineering [166-170]. These systems can capture human or patient-specific aspects of cell biology, genetics and brain development and thus provide an important complement to mouse models. Together, animal and human cellular models of mTORopathies provide a platform from which investigate key outstanding questions, in particular: 1) what is the neurodevelopmental impact of mutations in mTOR regulators? 2) what are the molecular, cellular and circuit mechanisms that drive pathophysiology? 3) which brain regions and cell types are responsible for different disease manifestations? and 4) what is the best therapeutic approach to maximize improvement and minimize side effects?

Drug-based therapies in animal models

There is a large literature examining the effects of rapalogs in animal models of mTOR-related disorders. These studies have revealed a range of possible outcomes including full reversal of neuropsychiatric phenotypes even after they have been established, prevention of phenotypes by pre-symptomatic mTOR inhibition, rescue within certain critical treatment windows, or a lack of response to rapalog treatment. One of the first studies to show efficacy of rapalogs in treating brain phenotypes was in a conditional mouse model of TSC. Meikle et al. showed that by administering rapamycin every other day starting at P7-P9 in *Syn1*-Cre*;Tsc1*-cKO mice they could shift median survival from 33 to over 100 days and reverse neuronal hypertrophy and demyelination phenotypes [171]. In subsequent work, Carson et al began rapamycin treatment at P13 in *Emx1*-Cre*;Tsc1*-cKO mice and were able to prevent premature mortality and largely

reverse glial pathology. However, abnormal neuronal lamination was rapamycin-resistant [152]. Lin et al. showed that mislamination in a mouse model of hyperactive mTORC1 could, in fact, be prevented through administration of a constitutively active mutant 4E-BP1 if this occurred at the same time as the manipulation that caused mTORC1 hyperactivity [172]. Similarly, a study examining *Pten* loss from dentate gyrus neurons showed that rapamycin could prevent but not reverse abnormal migration [173]. Together, these studies show that while seizures may be partly treatable with postnatal rapamycin, abnormal lamination and neuronal migration are early developmental phenotypes that may be preventable by mTORC1 suppression but cannot be reversed at later stages of development. For phenotypes such as these it will be key to determine how much they contribute to disease manifestations and whether functional improvement can be achieved in the absence of complete rescue of these abnormalities.

The idea of critical periods for treatment has gained attention in recent studies. Two studies led by Tsai et al. showed that mice which lack *Tsc1* from cerebellar Purkinje cell's exhibit social deficits and repetitive behaviors [157, 174]. The authors demonstrated that treatment starting within the first week of life could rescue both phenotypes [157]. However, treatment starting at 6 weeks of age, after the phenotypes were already established, could only reverse social behavior aberrations, but not behavioral inflexibility or repetitive behaviors [174]. Cox et al. characterized the effects of rapamycin on dendritic arborization and spine deficits caused by embryonic Tsc1 deletion from cortical neurons at two different time points. In the early treatment group (P1-P7) they could rescue abnormal arborization and with later treatment (P15-P27) they could reverse abnormal spine maturation *[175]*. Critical periods might also exist for treatment of seizures in mTORopathies. Studies reporting the most success have either treated animals prior to symptom onset or have shown rescue in models in which the mutation occurs later in life *[150]*. It is possible that early on, potentially during epileptogenesis, seizures are sensitive to rapamycin *[176]* but once epilepsy is established, seizures are less responsive to mTOR inhibition. Together, these data suggest that it is important to identify critical periods for disease phenotypes in order to determine the optimal timing of treatment. Treatment given past the critical window may be responsible for some of the differential drug effectiveness observed in clinical studies.

Rapalogs have been the main pharmacological approach used in animal and cell models to inhibit mTORC1 in the context of genetic mTORopathies. However, as discussed above, chronic rapamycin inhibits both mTOR complexes and may not be effective at targeting all cell types in the brain, for example dopamine neurons [160]. In addition, a study assessing the effect of prenatal rapamycin treatment in wild-type animals showed that a single dose at embryonic day 16 resulted in adverse effects including motor abnormalities and increased anxiety that persisted in adulthood [177]. Thus, strong and non-specific suppression of mTOR activity, particularly in the developing brain, may not be an optimal therapeutic approach. Further work is needed to understand the basic biology of the two mTOR complexes, especially in neurons, the contribution of each complex to specific disease endophenotypes, and whether selective targeting of one complex will yield improved treatment with fewer side effects.

Genetic approaches to manipulating mTORC1 and mTORC2 in disease models

Several studies have attempted to selectively manipulate mTORC1 or mTORC2 in the mouse brain by disrupting their specific components, Raptor or Rictor, respectively. Such studies have revealed that while the two complexes share some common functions such as regulation of somatodendritic morphology [178], they also have distinct functions and differentially impact a range of processes from development to synaptic transmission to behavior [27, 28, 179]. The distinct contributions of the two mTOR complexes to neural development and function suggest that therapeutic approaches for modifying disease phenotypes may benefit from an ability to control each complex independently and in a temporally precise manner.

Recent studies have begun disentangling the contribution of mTORC1 and mTORC2 to disease phenotypes in genetic mouse models of mTORopathies. Huang et al. crossed germline *Pten*$^{+/-}$ mice with mice that had heterozygous loss of *Rptor* from forebrain neurons (*Emx1*-Cre*;Rptor*$^{fl/+}$) [180]. *Pten*$^{+/-}$ mice exhibited neuronal hypertrophy in cortical layer V and a deficit in social approach behavior. Partial downregulation of mTORC1 in *Pten*$^{+/-}$ mice was sufficient to correct both neuronal hypertrophy and social deficits [180]. Chen et al. used *CamK2a*-Cre mice to induce loss of *Pten* in postmitotic forebrain neurons [155]. *Pten*-cKO animals exhibited hyperactivity of both mTORC1 and mTORC2 signaling, macrocephaly, seizures, premature mortality, and behavioral abnormalities. Concomitant deletion of *Rictor* in *Pten*-cKO mice prolonged their lifespan by approximately two-fold (i.e. median survival shifted from ~50 to ~110 days postnatal) but did not completely prevent premature mortality as all mice died between ~P90-P130. In this study, mTORC2 downregulation also prevented seizures and corrected behavioral abnormalities. Postnatal intracerebroventricular injection with an antisense oligonucleotide (ASO) targeting *Rictor* at four weeks of age was sufficient to improve seizures and behavioral deficits in *Pten*-cKO mice. *Rptor* deletion in *Pten*-cKO mice normalized brain size; however, surprisingly, neither seizures nor behavioral impairments were improved, and the median survival was only modestly increased by a few days [155]. These studies show that both mTORC1 and mTORC2 complexes contribute to *Pten*-related pathology in mice. One discrepancy between the ability to prevent behavioral phenotypes with Raptor (Huang et al.) or Rictor (Chen et al.) manipulation might be because Huang et al. used constitutive *Pten*$^{+/-}$ animals while Chen et al. studied homozygous loss of *Pten* from postnatal forebrain neurons. It would be interesting to investigate whether embryonic *Pten* haploinsufficiency can also be rescued via manipulation of mTORC2.

While TSC phenotypes tend to be ascribed to mTORC1 hyperactivity, the studies described above in *Pten* mouse models suggest that there could be a potential contribution of mTORC2. It should be noted, however, that while Akt signaling is elevated in response to *Pten* loss, phosphorylation of Akt at the mTORC2 site (Ser473) is consistently reduced in the context of *Tsc1* or *Tsc2* mutations [166, 181]. Prior to study described in chapter 2, the contribution of mTORC1 and mTORC2 signaling to the neuropsychiatric presentations of TSC had not been comprehensively investigated. However, a recent study demonstrated that heterozygous loss of *Rptor* restored several TSC-related phenotypes in mice with loss of *Tsc1* from dopamine neurons (*Slc6a3*-Cre*;Tsc1*-cKO) [160]. These mice exhibited dopamine neuron hypertrophy and impaired

striatal dopamine release that led to deficits in cognitive flexibility. Concomitant heterozygous loss of *Rptor*, while not sufficient to prevent somatic hypertrophy, significantly improved striatal dopamine release and prevented cognitive inflexibility. Notably, the authors showed that homozygous deletion of *Rptor* in *Tsc1*-cKO dopamine neurons caused neuronal hypotrophy and was not able to improve dopamine release deficits [160]. This demonstrates that complete suppression of mTORC1 can be just as detrimental to neuronal function as mTORC1 hyperactivation. These findings underscore the idea that rebalancing rather than completely suppressing mTORC1 signaling may be a preferable therapeutic approach for mTOR-related brain disorders.

The importance of considering tissue- and mTOR complex-selectivity of therapeutic approaches was signified by two studies conducted in a mouse model of fragile X syndrome (*Fmr1*-KO), which exhibits mTORC1 hyperactivity [182]. Yan et al. selectively downregulated mTORC1 by injecting shRNA targeting *Rptor* directly into the hippocampal CA1 region of *Fmr1*-KO mice; rescuing, in part, aberrant spine morphology, synaptic function and memory deficits [183]. In contrast, a different study showed that orally administered rapamycin in *Fmr1*-KO mice did not reverse behavioral deficits and had adverse effects on social behavior and sleep in both control and *Fmr1*-KO mice [184]. These studies suggest that selective manipulation of a specific mTOR complex within a targeted brain region, as opposed to systemic non-specific inhibition, might be a more beneficial strategy for the treatment of disorders with altered mTOR signaling.

Conclusions

While the mTOR pathway has been extensively studied in many systems, it remains enigmatic due to its significant complexity and breadth of actions. Research using *in vitro* and *in vivo* models has revealed a multitude of upstream regulators and downstream targets can vary significantly based on cell type and developmental stage. Given this complexity, it is not surprising that results from treatment with rapamycin and its analogues have had mixed success. In both people and in animal models, rapalogs exhibit variability in their efficacy and side effects. While it will be interesting to see how recently developed dual-drug strategies that enable brain-specific targeting of rapalogs affect neuropathophysiology, the development of alternative therapeutic strategies is warranted. One exciting approach currently under development is gene therapy [185]. While this has traditionally meant the delivery of a gene that is lacking via a virus-based carrier, it has expanded to include approaches such as ASOs and CRISPR/Cas9-based systems, including those that modify gene expression without altering the genome sequence [186, 187]. Although there are still several limitations and barriers to the wide-spread implementation of these technologies, gene-based therapies offer potential advantages of selective brain region- and cell type-targeting [188, 189].

In summary, building off the initial success of rapalogs as therapeutic treatments for mTORopathies, new insights into the basic biology of the mTOR complexes and their functions in different neural cell types will facilitate the generation of improved treatments for mTOR-related disorders. Based on our current information, therapeutic strategies that 1) target the most relevant mTOR complex for disease phenotypes, 2) are given at the optimal age and stage of disease progression, 3) act on disease-relevant cellular targets

with minimal off-tissue activity, and 4) rebalance signaling to physiologic levels, are likely to be most successful.

Dissertation research goals

Several recent studies have challenged the mTORC1-centric view in the field of mTORopathies and drawn attention to the possibility that mTORC2 is involved in pathophysiology. These studies suggest that while mTORopathies share neurologic phenotypic manifestations, the underlying mechanisms might differ. Such findings highlight the need to 1) study each mTORopathy as a unique disorder, 2) dissect the molecular mechanisms that underlie each phenotypic manifestation within each disorder independently, and finally 3) further our understanding of the mTOR signaling cascade in the nervous system both in physiological and disease-like states.

The overall goal of my dissertation project was to elucidate which mTOR complex underlies the neurologic manifestations in Tuberous Sclerosis Complex and determine whether selective manipulation of this complex can provide a promising therapeutic strategy. Further, I explored therapeutic interventions for seizure-like activity in an *in vitro* model of TSC, and finally I performed experiments to dissect the signaling crosstalk between the mTOR complexes in neurons.

Figures and Tables

Figure 1

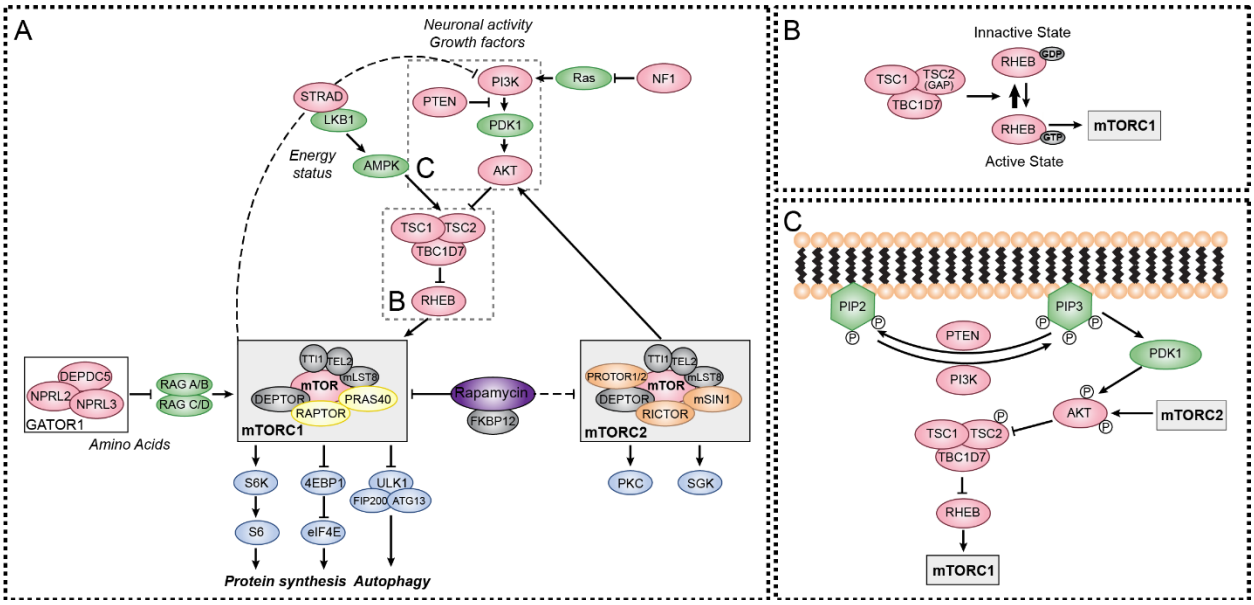

Figure 1. Mutations in regulators of mTOR signaling cause mTORopathies.
(A) mTOR is a protein kinase found in two distinct multiprotein complexes, mTORC1 and mTORC2, which are composed of shared and unique protein components. Several upstream regulators collectively work to control the activity of the two complexes in response to various stimuli including growth factors and nutrients. Mutations in genes that encode for mTOR regulators (denoted in pink) result in neurodevelopmental disorders, collectively termed mTORopathies (see Table 1). Current treatments for mTORopathies include rapalogs, which are derivatives of rapamycin that suppress mTORC1 activity and indirectly inhibit mTORC2 signaling when administered chronically.
(B) The TSC complex functions as a GTPase activating protein (GAP) for the small GTPase Rheb, which is a direct activator of mTORC1.
(C) PI3K converts PIP2 into PIP3 via phosphorylation at the cell membrane. PIP3 recruits the kinase PDK1 that, along with mTORC2, phosphorylates and activates AKT. In turn, AKT phosphorylates TSC2, inhibiting the TSC1/TSC2/TBC1D7 complex, and promoting mTORC1 activity. PTEN is a phosphatase that negatively regulates mTOR signaling by dephosphorylating and converting PIP3 to PIP2.

Table 1. mTORopathy genes, disorders and clinical manifestations

Gene mutations	Associated Diseases and Syndromes		Clinical Manifestations*		Refs
		Abbreviation	Neurological	Psychiatric	
TSC1 *TSC2*	Tuberous Sclerosis Complex	TSC	Tubers, SENs, SEGAs, Epilepsy, Infantile spasms, Altered white matter	ID, ASD, ADHD, other behavioral conditions	[36, 38, 42, 51-58]
PTEN	PTEN hamartoma tumor syndrome (incl. Cowden syndrome, Bannayan-Riley-Ruvalcaba syndrome and Lhermitte-Duclos disease)	PHTS	Macrocephaly	ID, ASD	[61, 63-67]
MTOR *PIK3CA* *RHEB* *AKT3* *TSC1* *TSC2* *DEPDC5* *NPRL2* *NPRL3*	Malformations of cortical development	MCD	FCD, HME, ME, Epilepsy, Infantile spasms	ID	[68-74, 85-87]
NF1	Neurofibromatosis type 1	NF1	Macrocephaly,	ID, ASD, ADHD,	[91]

			Epilepsy, Ataxia, Altered white matter	Learning disabilities	
STRADA	Polyhydramnios, megalencephaly, and symptomatic epilepsy syndrome	PMSE	ME, Epilepsy	ID, Psychomotor retardation	[90]
TBC1D7	-		Macrocephaly/ ME	ID	[59-60]

(ADHD) Attention deficit hyperactivity disorder, (ASD) Autism spectrum disorder, (FCD) Focal cortical dysplasia, (HME) Hemimegalencephaly, (ID) Intellectual disability, (ME) megalencephaly, (SENs) subependymal nodules, (SEGAs) subependymal giant cell astrocytomas
*Listed are the primary neuropsychiatric presentations of these diseases as listed in the references noted, the NIH Genetic and Rare Diseases Information Center, and OMIM database. Other manifestations may be present in these disorders and not all patients may present with all manifestations listed here.

Table 2 Summary of mouse models discussed in this chapter

Disorder	**Animal model**	**Refs**
	Tsc1$^{-/-}$ (germline KO)	[136]
	Tsc2$^{-/-}$ (germline KO)	[137,138]
	Tsc1$^{+/-}$ (germline Het)	[136,140-141],
	Tsc2$^{+/-}$ (germline Het)	[137-138, 140,145,147]
	Tsc1$^{fl/fl}$*;Emx1*^{Cre}	[150]
	Tsc1$^{fl/fl}$*;Syn1*^{Cre}	[149]
	Tsc1$^{fl/fl}$*;Camk2a*^{Cre}	[151-152]
	Tsc1$^{fl/fl}$*;GFAP*^{CreER}	[154]

TSC	*Tsc1*$^{fl/fl}$;*L7*^{Cre}	[155, 172]
	Tsc2$^{-/fl}$;*L7*^{Cre}	[156]
	Tsc1$^{fl/fl}$;*Slc6a3*^{Cre}	[158]
	Tsc1$^{fl/fl}$;*Slc6a4*^{Cre}	[159]
	Tsc1$^{fl/fl}$;*Drd1a-Cre*	[160[
	Tsc1$^{fl/fl}$;*Adora2a-Cre*	[160]
	Tsc1$^{fl/fl}$;*Gbx2*^{CreER}	[161]
	Tsc1$^{fl/fl}$ + Cre *in utero* electroporation	[173]
	Tsc1$^{flox/-}$ + Cre *in utero* electroporation	[162]
PHTS	*PTEN*$^{-/-}$ (germline KO)	[139]
	PTEN$^{+/-}$ (germline Het)	[139,143-144, 180]
	PTEN $^{fl/fl}$;*CamK2a*^{Cre}	[152-153]
	PTEN $^{fl/fl}$;*L7*^{Cre}	[157]
	PTEN$^{fl/fl}$;*Slc6a3*^{Cre}	[143]
	PTEN $^{fl/fl}$ + AAV-Cre	[171]
PMSE	*Strada*$^{-/-}$ (germline KO)	[133]
	Strada shRNA *in utero* electroporation	[132]
	Depdc5 $^{fl/fl}$;*Syn1*^{Cre}	[135]
	Rheb^{CA} *in utero* electroporation	[163, 170]

MCD	*Tsc1* CRISPR/Cas9 editing *in utero* electroporation	[82]
	Tsc2 CRISPR/Cas9 editing *in utero* electroporation	[82]

Listed are the primary mouse models discussed in this chapter. Comprehensive reviews of animal models of mTORopathies can be found in references [12, 134, 142, 148]

Chapter 2
Raptor downregulation rescues neuronal phenotypes in mouse models of Tuberous Sclerosis Complex

This chapter was previously published in its entirety as " Raptor downregulation rescues neuronal phenotypes in mouse models of Tuberous Sclerosis Complex" in bioRxiv, 2021 July (DOI: 10.1101/2021.07.21.453275) by Vasiliki Karalis, Franklin Caval-Holme and Helen S. Bateup. It has been reproduced in here with full permission of the authors.

Vasiliki Karalis

Department of Molecular and Cell Biology
University of California, Berkeley

Introduction

Tuberous Sclerosis Complex (TSC) is a neurodevelopmental disorder resulting in benign tumors in multiple organs and focal cortical malformations called tubers[74]. Some of the most significant problems associated with TSC are the neurological and psychiatric aspects[76]. Approximately 85% of TSC patients develop epilepsy, which often begins in infancy and becomes intractable in two-thirds of cases[90, 94]. TSC is also associated with varying degrees of intellectual disability, cognitive impairments, and behavioral conditions including autism spectrum disorder and attention deficit hyperactivity disorder[89].

Current treatment strategies for TSC include inhibitors of mTOR signaling called rapalogs, which are analogs of the naturally occurring macrolide rapamycin[4, 102]. Rapamycin has been successful in treating neuropsychiatric phenotypes in rodent models of TSC, especially when treatment is started early in development[171, 190]. In the clinic, rapalogs are moderately effective at treating seizures and subependymal giant cell astrocytomas (SEGAs), which are benign brain tumors that affect about 5-15% of TSC patients[103-107]. However, symptoms can return after treatment cessation[103] and chronic rapalog use is associated with significant side-effects including immunosuppression and systemic metabolic changes such as insulin resistance[119]. In addition, several recent clinical trials have reported that rapalogs did not significantly improve the cognitive and psychiatric aspects of TSC[113, 114]. As a result, additional therapeutic interventions are needed.

TSC is caused by loss-of-function mutations in either the *TSC1* or *TSC2* genes[68, 69]. At the biochemical level, the protein products of *TSC1* and *TSC2* form a complex that inhibits Rheb, a small GTPase that activates mTOR complex 1 (mTORC1)[73]. The Tsc2 protein harbors the GTPase activating protein (GAP) domain, while Tsc1 is required for complex stability[191]. mTORC1 is composed of several proteins including mTOR and the obligatory component Regulatory-associated protein of mTOR (Raptor)[17, 18, 192]. mTORC1 is a kinase that phosphorylates several targets including p70S6K and the 4E binding proteins (4E-BPs), which are involved in translational control[10, 193, 194]. P70S6K in turn phosphorylates ribosomal protein S6, a canonical read-out of mTORC1 activity[195]. The activity of mTORC1 is regulated by various intra- and extracellular signals including growth factors, insulin, nutrients, and neural activity[12, 67]. When active, mTORC1 promotes anabolic cellular processes such as protein, lipid and nucleotide synthesis and suppresses catabolic processes, including autophagy[12, 26]. In the absence of regulation by the TSC1/2 complex, mTORC1 is constitutively active[73].

Rapamycin is thought to suppress mTORC1 signaling by inducing a trimeric complex between itself, mTOR and FK506-binding protein 12 (FKBP12)[192]. Binding of rapamycin-FKBP12 on mTORC1 occludes access of some substrates to the catalytic site of the mTOR kinase[192]. While acute administration of rapamycin selectively reduces mTORC1 signaling, chronic treatment also suppresses the activity of a second mTOR complex, mTORC2, potentially by preventing *de novo* mTORC2 assembly[118]. mTORC2 shares several protein components with mTORC1 but instead of Raptor, mTORC2 contains Rapamycin-insensitive companion of mTOR (Rictor) as an essential component[19, 26, 196]. mTORC2 has been reported to control aspects of cytoskeletal organization, cell survival and metabolism[12], although its functions in neurons are not

well understood. The most well characterized phosphorylation target of mTORC2 is Ser473 of Akt[197]. While mTORC1 and mTORC2 have conventionally been thought to have distinct upstream regulators and targets, studies in various systems have revealed potential points of crosstalk between the two complexes[198, 199].

TSC-related phenotypes are canonically thought to be due to mTORC1 hyperactivity; however, recent studies have raised the possibility that mTORC2 may also be involved. In particular, a study in mice with forebrain-specific disruption of Pten, a negative regulator of mTORC1 that is upstream of Tsc1/2, showed that downregulation of mTORC2, but not mTORC1, could prevent behavioral abnormalities, seizures, and premature mortality[155]. Moreover, it was shown that mTORC2, but not mTORC1, is required for hippocampal mGluR-dependent long-term depression (LTD)[27], a form of synaptic plasticity that is altered in mouse models of TSC[149, 200-202]. Therefore, a careful investigation of the relationships between Tsc1/2, mTORC1, and mTORC2 in the context of brain development and function is needed to design the most effective therapeutic strategy for TSC.

Here we used *in vitro* and *in vivo* mouse models of TSC to investigate whether manipulation of mTORC1 or mTORC2 signaling via genetic reduction of Raptor or Rictor, respectively, could prevent TSC-related brain phenotypes. We find that reduction, but not complete elimination, of Raptor rebalances both mTORC1 and mTORC2 signaling in the context of Tsc1 loss. We show that heterozygous deletion of *Rptor* in conditional *Tsc1* knock-out mice (Tsc1-cKO) improves several phenotypes including neuronal hypertrophy, neural network hyperactivity, impaired myelination, altered cortical and hippocampal architecture, and premature mortality. By contrast, heterozygous or homozygous loss of *Rictor* does not ameliorate TSC-related neural phenotypes. Finally, we demonstrate that postnatal Raptor downregulation rescues neuronal hypertrophy, myelination deficits, improves overall development and extends survival of Tsc1-cKO mice. Our results highlight the central role of mTORC1 in driving TSC-related brain phenotypes in mouse models and establish Raptor as a potential target for treating the neurological presentations of TSC.

Results

Chronic rapamycin treatment suppresses mTORC1 and mTORC2 signaling in Tsc1-cKO hippocampal cultures

To investigate how loss of Tsc1 affects mTORC1 and mTORC2 signaling, we generated primary hippocampal cultures from *Tsc1*$^{fl/fl}$ mice[203] and treated them with adeno-associated virus (AAV) expressing GFP (control) or Cre (Tsc1-cKO) at two days *in vitro* (DIV 2) (Fig. 1a and Supplementary Fig. 1a,b). To assess mTORC1 signaling status we quantified Raptor protein levels and two canonical downstream phosphorylation targets, ribosomal protein S6 (p-S6 Ser240/244) and 4E-BP1 (p-4E-BP1 Thr37). To measure mTORC2 signaling we quantified Rictor protein levels and Akt phosphorylation at Ser 473 (p-Akt Ser473). We found that on DIV 14, Tsc1-cKO cultures had complete loss of Tsc1 and a small increase in Raptor protein suggesting potentially enhanced mTORC1 assembly (Fig. 1b-d). No significant changes in Rictor protein were observed (Fig. 1e). Phosphorylation of S6 was increased in Tsc1-cKO cultures, as expected (Fig. 1f). However, we did not observe significant changes in p-4E-BP1 in this system (Fig. 1g), which may be due to the timing of Tsc1 loss, as discussed further below. In terms of mTORC2, we found that *Tsc1* deletion decreased Akt phosphorylation at Ser473 (Fig. 1h), indicating reduced mTORC2 activity. Together these data show that in hippocampal cultures, loss of *Tsc1* has opposing effects on the two mTOR complexes: it increases mTORC1 signaling, particularly the p70S6K/S6 branch, and decreases mTORC2 activity.

We next examined the effects of rapamycin on neuronal mTOR signaling to provide a benchmark for comparing the effects of genetic manipulation of the two mTOR complexes. Four-day treatment with 50 nM rapamycin had no effect on Tsc1 levels but reduced Raptor and modestly increased Rictor levels in Tsc1-cKO cultures (Fig. 1c-e). We observed the expected complete loss of p-S6 and partial reduction of p-4E-BP1 in both control and Tsc1-cKO cultures (Fig. 1f,g), indicative of suppressed mTORC1 signaling. Notably, we observed a strong reduction of p-Akt in both control and Tsc1-cKO neurons treated chronically with rapamycin that was greater than with Tsc1 loss alone (Fig. 1h). Together, these data demonstrate that rapamycin treatment does not restore balanced mTOR signaling in Tsc1-cKO hippocampal cultures but rather strongly suppresses the p70S6K branch of mTORC1, partially decreases p-4E-B1, and further reduces mTORC2-dependent Akt phosphorylation.

Downregulation of Raptor, but not Rictor, improves mTOR signaling abnormalities in Tsc1-cKO neurons

To investigate whether genetic disruption of mTORC1 or mTORC2 could improve signaling abnormalities in Tsc1-cKO neurons, we crossed *Tsc1*$^{fl/fl}$ mice to mice with either floxed *Rptor[204]* or *Rictor[205, 206]* alleles for simultaneous Cre-dependent deletion of *Tsc1* and *Rptor* or *Tsc1* and *Rictor*, respectively (Fig. 2a,b and Supplementary Fig. 1c,d). We found that mTORC1 hyperactivity persisted in Tsc1-cKO cultures with deletion of *Rictor*, evidenced by significantly increased levels of p-S6 in Tsc1-cKO;Rictor-cKO cultures compared to controls (Fig. 2c,d). p-Akt-473 was strongly reduced in Tsc1-cKO;Rictor-cKO neurons (Fig. 2c,d), similar to Tsc1-cKO cells. Thus, the mTOR signaling perturbations in Tsc1-cKO hippocampal cultures were not improved by genetic reduction of Rictor.

We next examined how reduction of Raptor affected mTOR signaling in Tsc1-cKO cultures. Homozygous deletion of *Rptor* effectively normalized p-S6 levels in Tsc1-cKO cultures harvested on DIV 14 (Fig. 2e,f). Deletion of *Rptor* also reversed the reduction of p-Akt caused by Tsc1 loss, suggesting a boosting of mTORC2 activity (Fig. 2e,f). The enhanced Akt phosphorylation resulting from Raptor loss may be due to relief of mTORC1-dependent negative feedback, either on mTORC2 itself or upstream regulators of both mTOR complexes[199]. These data indicate that Raptor downregulation could be an effective strategy for rebalancing mTOR signaling abnormalities due to loss of *Tsc1*.

During this experiment, we noted that low levels of Raptor protein remained in the cultures, which could have accounted for the incomplete suppression of mTORC1 signaling compared to rapamycin treatment (see Fig. 1 vs. Fig. 2e,f). To investigate this further, we added AAV-Cre to Tsc1-cKO;Rptor-cKO cultures on DIV 2 and harvested the cells at different time points. We found that while Tsc1 protein was virtually undetectable by DIV 14, residual Raptor protein remained. Raptor levels decreased over time such that by DIV 18 (16 days post-Cre) there was less than 1% of Raptor protein remaining (Supplementary Fig. 2a-g). This slow turn-over may reflect higher stability of Raptor protein bound within mTORC1. We therefore harvested Tsc1-cKO;Raptor-cKO cultures on day 18 to assess the consequences of more complete loss of Raptor on mTORC1 and mTORC2 signaling. At this time point, we found that concomitant deletion of *Tsc1* and *Rptor* strongly reduced p-S6 and increased p-Akt levels (Fig. 3a,b). Interestingly, we did not observe a consistent reduction in 4E-BP1 phosphorylation (Fig. 3b), suggesting that, as with rapamycin[117], mTORC1 targets are differentially susceptible to Raptor downregulation.

Our findings suggest that relatively low levels of Raptor protein may be sufficient to sustain mTORC1 signaling in the absence of negative regulation by the Tsc1/2 complex. To further evaluate the relationships between Raptor, mTORC1, and mTORC2, we analyzed results from cultures harvested at different time points, which had complete loss of Tsc1 protein and variable loss of Raptor protein (as in Supplementary Fig. 2b,c). We plotted the correlation of Raptor protein levels with p-S6 and p-Akt, expressed as a percentage of control cultures from the same genotype and time point. We observed a non-linear relationship whereby p-S6 remained elevated in Tsc1-cKO cultures even when Raptor protein levels were reduced by up to 80% (Fig. 3c). Only when Raptor levels dropped below 20% of control did we observe a reduction in p-S6 levels. The inverse relationship was observed for p-Akt, which was consistently reduced with Tsc1 loss and increased sharply as Raptor levels fell below 20% (Fig. 3d). Similar relationships were observed in hippocampal cultures with downregulation of Raptor alone, which were wild-type for *Tsc1* (Supplementary Fig. 2h-j). In this case, mild mTORC1 suppression was observed with 20-80% loss of Raptor protein; however, when Raptor levels were less than 15% of control, p-S6 was strongly suppressed and p-Akt was robustly increased. Together, these analyses reveal a non-linear relationship between Raptor and mTORC1 signaling such that relatively low Raptor protein levels appear to be sufficient to maintain mTORC1 activity in neuronal cultures.

These results suggest that partial reduction of Raptor protein may be an effective strategy to normalize both mTORC1 and mTORC2 signaling in Tsc1-cKO neurons. This would avoid the strong suppression of both complexes observed with rapamycin

treatment and the inhibition of mTORC1 and increase in mTORC2 activity observed with complete Raptor loss. To test this, we assessed mTOR signaling in cultures from *Tsc1*$^{fl/fl}$;*Rptor*$^{wt/fl}$ mice, which had partial loss of Raptor in the Tsc1-cKO background. We harvested Tsc1-cKO;Raptor-cHet cultures on DIV 18 and found that the elevation in p-S6 was reduced compared to *Tsc1* deletion alone (Fig. 3e,f) (Tsc1-cKO;Raptor-cHet 125.9% +/- 6.6 % of control vs. Tsc1-cKO 181.6% +/-15.5% of control). In addition, while p-Akt-473 was slightly reduced compared to control, the reduction was less than in Tsc1-cKO cultures (Fig. 3e,f) (Tsc1-cKO;Raptor-cHet 74.5% +/- 9.1% of control vs. Tsc1-cKO 58.2% +/- 4.0% of control). These data show that loss of one copy of *Rptor* can significantly ameliorate, although not completely prevent, the mTORC1 and mTORC2 signaling abnormalities associated with Tsc1 loss. Supplementary Figure 2k provides a summary of the effects of rapamycin, Rictor, and Raptor manipulations on p-S6 and p-Akt levels in Tsc1-cKO cultures.

Reduction of Raptor prevents hypertrophy of Tsc1-cKO neurons

Cellular hypertrophy is a well-established consequence of mTORC1 hyperactivity[26]. To test whether genetic reduction of Raptor could improve somatic hypertrophy, we sparsely labeled cultured neurons with florescent proteins and measured soma size. In this experiment, control cells expressed GFP and mutant cells within the same culture expressed nuclear Cre-mCherry and cytoplasmic tdTomato (Fig. 3g). We observed the expected increase in soma size of Tsc1-cKO neurons compared to controls, which was reversed by four-day treatment with rapamycin (Fig. 3h and Supplementary Fig. 3a-f). Homozygous deletion of *Rictor* did not prevent cellular hypertrophy as Tsc1-cKO;Rictor-cKO neurons exhibited significantly increased soma size compared to controls (Fig. 3h and Supplementary Fig. 3g-i). By contrast, both homozygous and heterozygous deletion of *Rptor* reduced the size of Tsc1-cKO neurons, effectively normalizing soma area to control levels (Fig. 3h and Supplementary Fig. 3j-o). Together, these results demonstrate that genetic reduction of Raptor, but not Rictor, is sufficient to prevent hypertrophy of Tsc1-cKO neurons *in vitro*.

Genetic reduction of Raptor, but not Rictor, extends the life span of Tsc1-cKO mice

To test whether Raptor reduction could improve TSC-related phenotypes *in vivo*, we used the *Emx1*^{IRESCre} (Emx1-Cre)[207] mouse line to induce *Tsc1* deletion around embryonic day 9.5 (E9.5), primarily in excitatory neurons of the cortex and hippocampus (Fig. 4a). Deletion of *Tsc1* in Emx1-expressing cells leads to a severe phenotype characterized by poor development, seizures, and premature mortality in the first few weeks of life[152, 208]. To test whether genetic reduction of mTORC1 or mTORC2 could prevent these phenotypes, we generated mice with heterozygous or homozygous deletion of *Rptor* or *Rictor* in the Tsc1-cKO;Emx1-Cre background (Fig. 4b). We monitored the survival and body weight of mice born from these crosses for the first 40 postnatal days. As expected, *Tsc1*$^{fl/fl}$;*Emx1-Cre*$^{+}$ (Tsc1-cKO) mice exhibited premature mortality with a median survival of 18.5 days (Fig. 4c,d and Supplementary Table 1). Tsc1-cKO mice of both sexes also had reduced body weight, although the timing of death was not correlated to weight (Fig. 4e-h, Supplementary Fig. 4a, and Supplementary Table 2).

Loss of Raptor extended the life span of Tsc1-cKO mice in a gene dose-dependent manner, with homozygous *Rptor* deletion resulting in near normal survival (16/17 *Tsc1*$^{fl/fl}$*;Rptor*$^{fl/fl}$*;Emx1-Cre*$^{+}$ animals survived until at least P40, Fig. 4c and Supplementary Table 1). Heterozygous deletion of *Rptor* led to a significant shift in the median survival of Tsc1-cKO mice from 18.5 to 24.5 postnatal days and 26% of the Tsc1-cKO;Raptor-cHet mice survived past P40 (Fig. 4c). While Tsc1-cKO;Raptor-cHet males and females had identical median survival, the length of life span extension was sex-dependent. After P26, the surviving female population stabilized with 40% of Tsc1-cKO;Raptor-cHet females surviving past P40 (Supplementary Fig. 4b and Supplementary Table 1). By contrast, the Tsc1-cKO;Raptor-cHet male population steadily declined and only 5% of mice survived past P40 (Supplementary Fig. 4b and Supplementary Table 1). Notably, while Tsc1-cKO;Raptor-cKO mice regularly survived past P40, they exhibited significantly decreased body weight (Fig. 4e,f and Supplementary Table 2). Similar body weight changes were observed with homozygous loss of *Rptor* in mice WT for *Tsc1* (Supplementary Table 2). Compared to WT mice, Tsc1-cKO;Raptor-cHet mice had reduced body weight but were significantly larger than Tsc1-cKO;Raptor-WT mice, suggesting improved physical development (Fig. 4e,f and Supplementary Table 2). The body weight differences between Tsc1;Raptor mice of different genotypes generally persisted among surviving mice at P150 (Supplementary Fig. 4c).

A recent report in *Pten*$^{fl/fl}$*;CamKII-Cre*$^{+}$ mice (Pten-cKO) showed that concurrent deletion of *Pten* and *Rictor* significantly shifted median survival from P~50 to ~110 days; however, no mice survived past P130. Surprisingly, homozygous *Rptor* deletion did not significantly affect the median survival age of Pten-cKO mice[155]. We generated *Tsc1;Rictor;Emx1-Cre* mice and found that heterozygous loss of *Rictor* did not affect the survival of Tsc1-cKO mice and homozygous loss of *Rictor* only slightly shifted the median survival from P18 to P20, with no Tsc1-cKO;Rictor-cKO animals surviving past P24 (Fig. 4d and Supplementary Table 1). It was previously shown that *Rictor*$^{fl/fl}$*;Emx1-Cre*$^{+}$ animals exhibited reduced body weight[209]. Consistent with this, we observed decreased body weight in mice with homozygous loss of *Rictor*, independent of *Tsc1* genotype (Fig. 4g,h and Supplementary Table 2). Together, these findings indicate that premature mortality due to loss of Tsc1 in forebrain excitatory neurons can be prevented by concomitant downregulation of mTORC1, but not mTORC2.

Genetic downregulation of Raptor improves multiple TSC-related brain phenotypes

Given that downregulation of Raptor extended the life span of Tsc1-cKO mice in a gene-dose dependent manner, we next examined whether TSC-related brain phenotypes could be improved. We explored a battery of common phenotypes in mouse models of TSC including macrocephaly, hypertrophic neurons, impaired myelination, and reactive astrogliosis[151, 152, 208]. We harvested brain tissue from P14-15 mice and found the expected cortical hypertrophy and elevated p-S6 phosphorylation in the forebrain of Tsc1-cKO mice (Fig. 4i,j and Supplementary Fig. 4g,h). Strikingly, when we examined the brains of Tsc1-cKO;Raptor-cKO mice, we found decreased overall brain size, severely reduced cortical thickness, and lack of a clear hippocampal structure (Fig. 4k and Supplementary Fig. 4d,e,i), despite near normal survival of these mice (see Fig. 4c). Underdeveloped cortical and hippocampal structures were also observed in Tsc1-WT;Raptor-cKO mice (Supplementary Fig. 4f), indicating that impaired forebrain

development was due to *Rptor* deletion alone, independent of *Tsc1* genotype. In contrast, heterozygous deletion of *Rptor* did not cause changes in overall brain architecture (Supplementary Fig. 4f). These results demonstrate that while loss of Tsc1 causes cortical hypertrophy, embryonic suppression of mTORC1 signaling leads to severely impaired cortical and hippocampal development.

Given the significant neurodevelopmental abnormalities associated with complete loss of Raptor, we tested whether partial Raptor reduction could improve developmental brain phenotypes in Tsc1-cKO mice. We found that loss of one copy of *Rptor* improved overall brain architecture, reduced cortical hypertrophy, ameliorated hippocampal CA1 and dentate gyrus (DG) lamination defects, and improved cortical myelination, resulting in an intermediate phenotype between WT and Tsc1-cKO mice (Fig. 4l-s and Supplementary Fig. 4j and Fig. 5a-c). At the cellular level, heterozygous loss of *Rptor* reduced mTORC1 signaling, as measured by p-S6 levels, and partially prevented neuronal hypertrophy in the cortex, CA1 and DG regions (Fig. 5a-n and Supplementary Fig. 5d-g).

Glial abnormalities have previously been observed in the *Tsc1$^{fl/fl}$;Emx1-Cre^{+}* mouse model[152, 208]. Astrocytes specifically appear dysmorphic, exhibiting hypertrophic processes and increased expression of glial fibrillary acidic protein (GFAP)[152, 208]. Consistent with these findings, we observed a significant increase in GFAP fluorescence intensity across all cortical layers of Tsc1-cKO mice, that was partially attenuated in Tsc1-cKO;Raptor-cHet mice (Fig. 5o-q). We also observed a significant increase in GFAP fluorescence intensity in the hippocampal CA1 region of Tsc1-cKO mice that was restored to near WT levels in Tsc1-cKO;Rptor-cHet mice (Fig. 5r-t). Similar to prior studies, the GFAP-positive cells within the hippocampus of Tsc1-cKO mice did not exhibit high p-S6 levels[152, 208] (Fig. 5u). The severity of phenotypes caused by Tsc1 loss and their ability to be prevented by Raptor reduction were both cell type- and sex-dependent (Supplementary Fig. 5h-k and Supplementary Table 3). Taken together, these results demonstrate that partial reduction of Raptor in the forebrain is sufficient to improve multiple developmental brain phenotypes resulting from loss of Tsc1.

Hyperexcitability of Tsc1-cKO neurons is reduced by Raptor downregulation

Tsc1$^{fl/fl}$;Emx1-Cre^{+} mice exhibited behavioral seizures that were observable after the first two weeks of life. Given the challenges of performing *in vivo* EEG analysis in very young animals, and reports that cultured neurons with TSC-associated mutations show network hyperactivity[153, 210, 211], we used calcium imaging of hippocampal cultures from *Tsc1$^{fl/fl}$;Rptor$^{wtl/fl}$;Emx1-Cre^{+}* mice to test whether Raptor reduction could prevent epileptiform activity. We delivered an AAV encoding the fluorescent calcium indicator jRGECO1a[212] on DIV 2 and imaged calcium dynamics on DIV 14 (Fig. 6a-j and Supplementary Fig. 6a,b). Analysis of individual Ca^{2+} transients (Supplementary Fig. 6c,d) showed that cultures from Tsc1-cKO mice exhibited more frequent events, which were, on average, larger in amplitude and longer in duration than in control neurons (Fig. 6k-n). We calculated the area under the curve (AUC) for each Ca^{2+} transient and found that the average AUC was significantly larger in Tsc1-cKO neurons (Fig. 6o). In cultures from Tsc1-cKO;Raptor-cHet mice, Raptor downregulation significantly reduced the average frequency, amplitude, and AUC but had no effect on the duration of Ca^{2+}

transients compared to Tsc1 loss alone (Fig. 6k-o). These results show that neuronal hyperactivity caused by Tsc1 loss can be ameliorated by Raptor reduction.

To investigate how loss of Tsc1 affects network activity patterns, we analyzed 'network events', which were defined by synchronous activity of more than 20% of neurons in the field of view (see Fig. 6h-j). We found that a significantly larger proportion of neurons participated in each network event in Tsc1-cKO cultures compared to controls and that these events occurred with greater frequency (Supplementary Fig. 6e,f). We measured the percentage of time each culture exhibited coordinated network activity during the recording period and found that this was significantly increased in Tsc1-cKO cultures compared to controls (Supplementary Fig. 6g). We analyzed the individual Ca^{2+} transients that occurred during network events and found that these were larger and lasted longer in Tsc1-cKO neurons compared to controls (Supplementary Fig. 6h-j). While partial Raptor downregulation did not significantly reduce the frequency or duration of network activity, it was sufficient to reduce the proportion of neurons participating in network events (Supplementary Fig. 6e-g). Heterozygous deletion of *Rptor* also reduced the amplitude and AUC, but not the duration, of individual Ca^{2+} transients occurring within network events (Supplementary Fig. 6h-j). Collectively, these data show that heterozygous loss of *Rptor* reduces but does not completely prevent network hyperactivity caused by loss of Tsc1.

Heterozygous loss of *Tsc1* does not induce network hyperexcitability

Whether partial loss of Tsc1/2 complex function is sufficient to drive neuronal hyperactivity remains inconclusive as reports using cultured human neurons derived from TSC patient cells, which are heterozygous for the *TSC1* or *TSC2* mutation, present conflicting findings[211, 213, 214]. To investigate this in our model, we generated *Tsc1*$^{wt/fl}$*;Emx1-Cre*$^{+}$ (Tsc1-cHet) mice and found that they had normal body weight and survival (Supplementary Fig. 7a-c), with no spontaneous seizures observed. We prepared hippocampal cultures from these mice and found that in contrast to homozygous *Tsc1* deletion, heterozygous loss of *Tsc1* did not induce somatic hypertrophy, increase p-S6, or reduce p-Akt levels (Supplementary Fig. 7d-j).

We transduced Tsc1-cHet cultures with AAV-jRGECO1a and examined whether loss of one copy of *Tsc1* altered Ca^{2+} activity dynamics (Supplementary Fig. 8a-f). Tsc1-cHet neurons showed no difference in the frequency of Ca^{2+} transients per culture and had a small decrease in the frequency of events per neuron (Supplementary Fig. 8g,h). While the average event duration and AUC per neuron were not different between Tsc1-cHet and control neurons, the average amplitude of these events was larger in Tsc1-cHet neurons. (Supplementary Fig. 8i-k). Analysis of network events showed that a smaller proportion of Tsc1-cHet neurons participated in these events compared to control (Supplementary Fig. 8l). The frequency and total duration of network events were similar between control and Tsc1-cHet cultures, as was the amplitude of individual transients (Supplementary Fig. 8m-o). The duration and AUC of Ca^{2+} transients occurring within network events were slightly decreased in Tsc1-cHet neurons (Supplementary Fig. 8p,q). Together these data indicate that while loss of one copy of *Tsc1* causes some alterations in Ca^{2+} dynamics in mouse hippocampal neurons, it is not sufficient to induce neuronal or network hyperactivity.

Postnatal Raptor reduction using AAV-shRptor

The results described above showed that ~50% reduction of Raptor protein concurrent with *Tsc1* deletion reduced mTORC1 hyperactivity and improved multiple developmental and functional phenotypes resulting from Tsc1 loss. To determine whether Raptor reduction could be used therapeutically, we used a viral approach to reduce Raptor expression postnatally in the forebrain of Tsc1-cKO mice. Our biochemical experiments indicated that ~80% loss of Raptor may be most effective at normalizing mTORC1 and mTORC2 signaling in neurons with *Tsc1* deletion (see Fig. 3). Therefore, we generated AAVs encoding an shRNA targeting Raptor (shRptor)[215] or a scrambled control (shControl) under a ubiquitously expressed promoter. We transduced hippocampal cultures from *Tsc1*$^{wt/wt\ or\ fl/fl}$*;Emx1-Cre*$^{+}$ mice with these viruses and found that shRptor reduced Raptor protein levels by ~90% in WT neurons and 65-70% in Tsc1-cKO neurons (Supplementary Fig. 9a-h). The lesser reduction of Raptor in Tsc1-cKO cultures compared to WT was likely due to upregulation of Raptor protein in these cells (Supplementary Fig. 9d). In Tsc1-cKO cultures, shRptor reduced p-S6 levels, relieved p-Akt suppression, and completely rescued neuronal hypertrophy (Supplementary Fig. 9f,h-j). In this experiment, in which *Tsc1* was deleted embryonically, we observed a significant increase in 4E-BP1 phosphorylation in Tsc1-cKO neurons treated with shControl (Supplementary Fig. 9g). However, similar to rapamycin treatment[215], 4E-BP1 phosphorylation was resistant to shRptor treatment (Supplementary Fig. 9g).

To examine the efficacy of postnatal Raptor downregulation as a therapeutic strategy, we injected AAV9-shRptor-EYFP or shControl into the cortex and hippocampus of P0 *Tsc1*$^{fl/fl}$*;Emx1-Cre*$^{+}$ (Tsc1-cKO) and *Tsc1*$^{wt/wt}$*;Emx1-Cre*$^{+}$ (WT) mice (Fig. 7a). We examined brain sections from P16 mice and found that shRptor consistently reduced the p-S6 levels and soma size of Tsc1-cKO neurons within the cortex and hippocampus (Fig. 7b-m and Supplementary Fig. 10). We noted that the degree of reduction compared to shControl-treated WT neurons varied by brain region, ranging from an intermediate phenotype in the DG, normalization to WT levels in CA1, and reduction below WT levels in the somatosensory cortex (Fig. 7b-m and Supplementary Fig. 10). In WT mice, shRptor strongly downregulated neuronal p-S6 levels in the cortex and CA1, but not in the DG, and modestly reduced soma size within all regions (Fig. 7b-m and Supplementary Fig. 10). Thus, postnatal downregulation of Raptor improved cellular phenotypes in mice with prenatal *Tsc1* deletion.

Decreased myelination in Tsc1-cKO mouse models can arise directly from changes in oligodendrocytes[216, 217] or can occur via a non-cell-autonomous mechanism due to altered neuronal signaling[151, 218]. In *Tsc1*$^{fl/fl}$*;Syn-Cre*$^{+}$ mice, there is impaired myelination due to increased secretion of connective tissue growth factor from Tsc1-cKO neurons, which negatively regulates oligodendrocyte development[218]. In Emx1-Cre mice, Cre is expressed primarily in neurons, although some glial cells can exhibit Cre expression[152, 207]. We tested whether shRptor injection into the forebrain of Tsc1-cKO mice could rescue decreased myelination. We found that shRptor boosted bulk cortical MBP fluorescence in Tsc1-cKO mice to WT levels (Fig. 7n-r). Since *Rptor* deletion from oligodendrocytes leads to reduced myelination[216, 219], the increased MBP expression observed here was likely a result of Raptor reduction in Tsc1-cKO neurons, which led to a non-cell-autonomous increase in cortical myelination. Finally,

while Tsc1-cKO mice injected with shRptor still exhibited some handling-induced seizures, their body weight and life span were significantly improved in comparison to Tsc1-cKO mice injected with control shRNA (Fig. 8a-c).

Discussion

The goal of this study was to test whether genetic downregulation of mTORC1 or mTORC2 activity could be used to improve brain phenotypes in mouse models of TSC. We found that mTORC1 suppression via Raptor reduction was able to rebalance the activity of both mTOR complexes in the context of Tsc1 loss. While complete embryonic Raptor loss caused severe defects in forebrain development, 50% reduction of Raptor was sufficient to ameliorate several TSC-related phenotypes including signaling abnormalities, cellular alterations, network hyperactivity, and changes in brain architecture. Notably, mTORC2 suppression via loss of Rictor did not confer significant benefit in TSC mouse models. To extend the potential therapeutic relevance of our findings, we showed that postnatal downregulation of Raptor rescued Tsc1-cKO cellular phenotypes to a significant extent. Together, these data suggest that mTORC1 hyperactivity is primarily responsible for TSC-related brain phenotypes and that Raptor downregulation could be a potential therapeutic approach for the neurological presentations of TSC.

The contribution of mTORC1 vs. mTORC2 to TSC-related brain phenotypes

The manifestations of TSC have traditionally been thought to arise from mTORC1 hyperactivity[31, 76]. However, there are several lines of evidence suggesting that mTORC2 may also be involved. First, rapamycin and its derivatives, which are used to treat TSC, not only strongly inhibit the p70S6K arm of mTORC1 signaling but also suppress mTORC2 activity in neurons[118] (see Fig. 1). Second, a recent study in mice lacking *Pten*, an upstream negative regulator of mTORC1, showed that disease-related phenotypes could be prevented by inhibition of mTORC2 but not mTORC1[155]. Third, several different mouse models of TSC exhibit a defect in mGluR-dependent LTD[149, 200-202]. It was recently shown that mTORC2 is the most relevant complex that regulates this form of hippocampal synaptic plasticity, which was not affected by deletion of *Rptor*[27]. Taken together, this leaves open the possibility that mTORC2 may be a relevant therapeutic target for TSC.

Here we deleted *Rptor* or *Rictor* in mouse models of TSC to determine whether suppression of mTORC1 or mTORC2 could improve disease-related phenotypes. We found that while reduction of Raptor levels ameliorated multiple TSC-related phenotypes, loss of Rictor did not significantly improve mTOR signaling abnormalities, neuronal hypertrophy, physical development, or premature mortality of Tsc1-cKO mice. This indicates that while reductions in Pten or the Tsc1/2 complex both increase mTORC1 signaling, the differences in how loss of these proteins affects other parts of the PI3K/Akt/mTOR signaling network need to be considered when designing a therapeutic strategy. In the case of *Pten* deletion, Akt, mTORC1 and mTORC2 signaling are all upregulated since Pten normally suppresses PI3K-dependent activation of Akt upstream of mTORC1 and mTORC2[155, 181, 220-222]. Disruption of the Tsc1/2 complex also leads to increased mTORC1 signaling, which is due to loss of its GAP activity towards Rheb, a direct activator of mTORC1[223]. However, in contrast to Pten, loss of Tsc1/2 leads to decreased mTORC2-dependent phosphorylation of Akt[208, 216, 224, 225].

Here we observed an interesting relationship between mTORC1 and mTORC2 signaling in neurons, indicating significant crosstalk between the two complexes. We

found that while chronic rapamycin treatment suppressed both mTORC1 and mTORC2 signaling, *Rptor* deletion led to increased Akt phosphorylation at the mTORC2 site, in both WT and Tsc1-cKO neurons, suggesting enhanced mTORC2 activity. A similar effect has been reported in oligodendrocytes with conditional deletion of *Rptor* and in cancer cell lines with Raptor siRNA[216, 226]. In addition, Chen et al. showed that concomitant deletion of *Rptor* and *Pten* from forebrain neurons led to a stronger upregulation of p-Akt than observed with loss of *Pten* alone[155]. This phenotype is opposite of what we observed with Tsc1 loss, where mTORC2 signaling was reduced. There are several possible mechanisms whereby this crosstalk between mTORC1 and mTORC2 may occur. First, in conditions of high mTORC1 signaling, there may be enhanced negative feedback to upstream regulators of Akt, which would lead to reduced Akt phosphorylation[199, 225, 227, 228]. Second, it has been shown in other systems that p70S6K1, a direct target of mTORC1, can phosphorylate two mTORC2 components, Rictor and mSin1, and inhibit mTORC2-dependent Akt phosphorylation[229-231]. In this case, Raptor reduction and reduced mTORC1 activity would lead to decreased Rictor phosphorylation, thereby boosting mTORC2-dependent phosphorylation of Akt. Third, in the case of Raptor reduction, it is possible that limited Raptor protein availability leads to decreased formation of mTORC1, which in turn may free up more mTOR protein to form mTORC2, leading to its enhanced activity. Further work is needed to clarify the mechanistic interactions between mTORC1 and mTORC2 signaling in neurons. Regardless of the mechanism, our data show that partial reduction of Raptor alone, in the absence of direct manipulations to mTORC2, can rebalance the signaling of both mTOR complexes in Tsc1 KO neurons by constraining mTORC1 signaling and releasing inhibition of mTORC2.

The consequences of heterozygous versus homozygous loss of *Tsc1*

The mouse model of TSC used here has embryonic deletion of *Tsc1* from most forebrain excitatory neurons. This model recapitulates several disease-relevant phenotypes including spontaneous seizures, abnormalities in brain anatomy, neuronal hypertrophy, hypomyelination and astrogliosis[152, 208]. However, the phenotypes are generally more severe than in individuals with TSC as $Tsc1^{fl/fl};Emx1\text{-}Cre^{+}$ mice also have reduced body weight, fail to thrive, and exhibit premature mortality in the first few weeks of life. It is important to note that individuals with TSC generally carry germline heterozygous mutations in either the *TSC1* or *TSC2* genes, although somatic mosaicism can also occur[232-234]. The prevailing model is that during embryonic brain development, somatic second-hit mutations cause loss of heterozygosity and mTORC1 hyperactivity, leading to the formation of cortical malformations, which can become seizure foci[31, 166]. In support of this model, we found that loss of one copy of *Tsc1* from excitatory forebrain neurons was not sufficient to induce seizures, consistent with previous reports[142, 143]. To further investigate this, we generated primary hippocampal cultures from Tsc1-cHet mice and found that they did not exhibit spontaneous hyperactivity or mTORC1 activation. Previous reports have demonstrated that heterozygous loss of *Tsc1* or *Tsc2* from other neuronal types can induce synaptic and behavioral changes[142, 143, 147, 149, 235]. Therefore, further work is needed to clarify

which TSC-related phenotypes may be driven by haploinsufficiency and which require complete disruption of TSC1/2 complex activity.

Importance of the developmental timing of mTOR perturbations

Balanced mTOR signaling is crucial for proper embryonic brain development[208, 209, 236-238]. In line with this, we found that embryonic mTORC1 suppression via homozygous deletion of *Rptor* from forebrain excitatory neurons led to stunted body and brain development. In particular, Raptor-cKO mice had a severely underdeveloped cortex and failed to form a discernable hippocampal structure, which occurred independent of *Tsc1* genotype. These results are consistent with a prior study that disrupted Raptor expression broadly in neuronal progenitors (using *Rptor*$^{fl/fl}$*;Nestin-Cre*$^{+}$ mice), which led to microcephaly and perinatal mortality of Raptor-cKO mice[237]. Despite significant deficits in forebrain development, here we found that *Rptor*$^{fl/fl}$*;Emx1-Cre*$^{+}$ mice had remarkably normal survival, with the majority of Raptor-cKO mice surviving into adulthood (> P150). Postnatal disruption of Raptor has also been investigated using *Rptor*$^{fl/fl}$*;CamkIIa-Cre*$^{+}$ mice. In this model, Raptor-cKO mice had fully developed hippocampal and cortical structures, however, these brain regions were smaller compared to WT littermates[239]. Together these studies show that the developmental timing and number or type of cells impacted by mTORC1 alterations defines the severity of the phenotypes.

Therapeutic considerations

One of the goals of this study was to test whether genetic suppression of mTORC1 could have beneficial outcomes in mouse models of TSC and avoid side-effects associated with rapalog treatment, which strongly inhibits both mTORC1 and mTORC2 signaling. While mTORC2/Akt suppression might be beneficial for anti-tumor drugs, suppression of Akt in the brain is associated with neuronal cell death[240] and has been implicated in synaptic alterations underlying bipolar disorder[241, 242]. Here we found that it was possible to titrate Raptor protein levels to achieve near complete normalization of mTOR signaling in Tsc1-cKO neurons, as measured by p-S6 and p-Akt. Importantly, reduction of Raptor did not strongly suppress mTORC2, as chronic rapamycin does, and in fact boosted mTORC2-dependent phosphorylation of Akt and normalized it in the context of Tsc1 loss. However, disruption of Raptor showed a similar substrate bias as rapamycin, in which the p70S6K branch of mTORC1 signaling was preferentially suppressed with less impact on 4E-BP1 phosphorylation. Despite this, reduction of Raptor was sufficient to improve neuronal hypertrophy, network excitability, brain architecture, myelination, and survival in Tsc1-cKO mice. Therefore, genetic Raptor reduction is a promising therapeutic approach. Compared to systemic administration of small molecule drugs, a gene-based therapy has the advantage of potentially being targetable to specific tissues or cell types, which would avoid on-target, off-tissue side-effects that are a limitation to the chronic use of rapalogs[119].

The Raptor manipulations tested here were consistently effective across multiple functional and anatomical read-outs both *in vitro* and *in vivo*. However, they did not provide complete prevention or rescue of all TSC-related phenotypes. In the genetic prevention experiments, this is likely because we could maximally achieve 50% loss of Raptor with heterozygous deletion, whereas our biochemical data suggest that ~80% loss

would be most beneficial. With Raptor shRNA, we were able to achieve 60-70% Raptor downregulation in Tsc1-cKO neurons, which was sufficient to improve cellular phenotypes, body weight, and survival; however stronger suppression may show even more benefit. That said, even a partial rescue can have overall beneficial outcomes, as was recently shown in Tsc1-cKO dopamine neurons. In *Tsc1$^{fl/fl}$;Slc6a3-Cre^{+}* mice, heterozygous, but not homozygous, deletion of *Rptor* prevented functional deficits in dopamine release and cognitive flexibility, despite not rescuing somatic hypertrophy[160].

Importantly, postnatal reduction of Raptor should avoid the severe developmental impairments caused by embryonic mTORC1 suppression. Given our findings of a non-linear relationship between Raptor protein levels and mTORC1 signaling, it would be interesting to test other strategies for fine-tuning Raptor levels, for example using antisense oligonucleotides or CRISPR/Cas-based approaches, to achieve the optimal level and developmental timing of Raptor reduction. In addition, it would be worthwhile testing Raptor reduction in a mouse model with milder or later onset phenotypes to allow more time for therapeutic intervention.

In summary, our study confirms the importance of mTORC1 hyperactivity as a key driver of TSC-related brain phenotypes in mouse models and highlights Raptor as a relevant therapeutic target that has potential advantages over current pharmacologic approaches.

Materials and Methods

Mice

All animal procedures were carried out in accordance with protocols approved by the University of California, Berkeley Institutional Animal Care and Use Committee (IACUC) AUP-2016-04-8684. Mice of both sexes were used, and the ages are indicated in the methods for each experiment. Mice were on a mixed genetic background. Mice were housed with same-sex littermates in groups of 5–6 animals per cage and kept on a regular 12 h light/dark with ad libitum access to standard chow and water. Mice used for shRNA experiments were housed on an inverse 12 h light/dark cycle. Mouse genotypes were confirmed by PCR using genomic DNA obtained from tail samples. See Supplementary Table 4 for a list of the transgenic mouse lines used and genotyping primers.

Primary hippocampal cultures

Dissociated hippocampal cultures were prepared from postnatal day 0-1 (P0-1) mice using standard protocols. Briefly, hippocampi from 2-3 pups (floxed mouse lines, Figs. 1-3 and Supplementary Figs. 1-3) or from single pups (Emx1-Cre mouse lines, Fig. 7 and Supplementary Figs. 6-9) were dissected on ice. The tissue was dissociated using 34.4 μg/ml papain in dissociation media (HBSS Ca^{2+}, Mg^{2+} free, 1 mM sodium pyruvate, 0.1% D-glucose, 10 mM HEPES buffer) and incubated for 3 min at 37°C. Tissue digestion was stopped by incubation in trypsin inhibitor (1 mg/ml) in dissociation media at 37°C for 4 min. After trypsin inhibition, dissociation media was carefully removed and the tissue was gently manually triturated in 5 ml plating media (MEM, 10% FBS, 0.45% D-Glucose, 1 mM sodium pyruvate, 1 mM L-glutamine). Cell density was counted using a TC10 Automated cell counter (Bio-Rad) and ~2-2.25 × 10^5 neurons were plated for each experiment. For western blotting and Ca^{2+} imaging experiments, neurons were plated onto 24-well plates pre-coated with Poly-D-Lysine (PDL) (Corning, Cat # 08774271). For immunocytochemistry, neurons were plated onto 12 mm glass coverslips precoated overnight at room temperature (RT) with 0.5 mg/ml PDL in 0.1 M borate buffer (pH 8.5). On the plating day, the coverslips were rinsed 4 times with sterile water and then coated with 20 μg/ml laminin (GIBCO, 23017015) in 1x PBS for ~1.5h at 37°C. Subsequently, coverslips were rinsed 3 times with sterile water, and 400 μl of plating media were added prior to adding the dissociated neurons. For all cultures, plating media was removed after 3 h and 900 μl maintenance media (Neurobasal media (Fisher Scientific # 21103-049) with 2 mM glutamine, pen/strep, and B-27 supplement (Invitrogen # 17504-044)) were added per well. After 4 days *in vitro* (DIV 4), 1 μM Cytosine β-D-arabinofuranoside (Sigma-Aldrich # C6645) was added to prevent glial proliferation. Cultures were maintained in maintenance media for 14 - 18 days with partial media changes every 4 days.

Adeno-associated virus (AAV) transduction of primary cultures

For hippocampal culture experiments, AAVs were added on DIV 2, except for the shRNA experiments in which AAVs were added on DIV 1. Amounts of AAVs were chosen after titration experiments for each virus to accomplish either maximum or sparse

transduction efficiency while maintaining low toxicity levels. In primary cultures from *Tsc1*$^{fl/fl}$, *Tsc1*$^{fl/fl}$*;Rptor*$^{fl/fl}$, *Tsc1*$^{fl/fl}$*;Rptor*$^{wt/fl}$ and *Tsc1*$^{fl/fl}$*;Rictor*$^{fl/fl}$ mice that were used for western blotting experiments, we aimed for >95% transduction efficiency using AAV1 human Synapsin 1 (*SYN1,* "hSyn") promoter-driven Cre-GFP or GFP to generate mutant and control cultures, respectively. For immunocytochemistry experiments, we aimed for sparse transduction to resolve individual neurons using AAV1-CBA-mCherry-Cre (nuclear localized), AAV9-CAG-FLEX-tdTomato, and AAV5-hSyn-GFP. To determine the percentage of Cre-expressing neurons in primary hippocampal cultures from Emx1-Cre-positive pups we used AAV1-CAG-FLEX-GFP at a high titer (see Supplementary Fig 6a). For calcium imaging experiments, we transduced neurons with AAV1-hSyn-jRGECO1a aiming for >95% transduction efficiency. For shRNA experiments, we transduced neurons with AAV9-hU6-shRNA-EYFP on DIV 1 and achieved 85-90% transduction. See Supplementary Table 5 for the list of viruses, source, titer and number of viral genomes (vg) used.

Protein extraction and western blot analysis

Hippocampal cultures were harvested on DIV 14 -18. Neurobasal media was aspirated from one well at a time, wells were quickly rinsed with ice cold 1x PBS with Ca^{2+}/Mg^{2+} and then 75 μl of lysis buffer were added (lysis buffer: 2 mM EDTA (Sigma: E5134), 2 mM EGTA (Sigma: E3889), 1% Triton-X (Sigma: T8787), and 0.5% SDS (Sigma: 71736) in 1× PBS with Halt phosphatase inhibitor cocktail (ThermoFisher: PI78420) and Complete mini EDTA-free protease inhibitor cocktail (Roche: 4693159001)). Wells were thoroughly scraped, and lysates were collected and sonicated for 5 sec. Total protein was determined by BCA assay (ThermoFisher: PI23227) and 10 µg of protein in 1X Laemmli sample buffer (Bio-Rad:161-0747) were loaded onto 4-15% Criterion TGX gels (Bio-Rad: 5671084). Proteins were transferred overnight at low voltage to PVDF membranes (Bio-Rad: 1620177), blocked in 5% milk in 1x TBS-Tween for one hour at RT, and incubated with primary antibodies diluted in 5% milk in 1x TBS-Tween overnight at 4°C. The following day, membranes were washed 3 x 10 min in 1x TBS-Tween and incubated with HRP-conjugated secondary antibodies (1:5000) for one hour at RT, washed 6 x 10 min in 1x TBS-Tween, incubated with chemiluminescence substrate (Perkin-Elmer: NEL105001EA) and developed on GE Amersham Hyperfilm ECL (VWR: 95017-661). Membranes were stripped by two 7 min incubations in stripping buffer (6 M guanidine hydrochloride (Sigma: G3272) with 1:150 β-mercaptoethanol) with shaking followed by four 2 min washes in 1x TBS with 0.05% NP-40 to re-blot on subsequent days. Bands were quantified by densitometry using ImageJ software (NIH). Phospho-proteins were normalized to their respective total proteins. Histone-3 was used as a loading control for every experiment. Antibody vendors, catalog numbers, and dilutions are listed in Supplementary Table 6.

Immunocytochemistry

On DIV 14, Neurobasal media was carefully aspirated from all wells and coverslips were briefly rinsed with ice cold 1× PBS with Ca^{2+}/Mg^{2+} followed by fixation in freshly made 4% PFA (Electron Microscopy Sciences: 15713) in 1x PBS for 10 min. PFA was then removed and the coverslips were washed for 5 min with 1x PBS three times. Coverslips were blocked for one hour at RT in buffer containing 5% normal goat serum

(NGS) (ThermoFisher: PCN5000) and 0.3% Triton-X in 1x PBS and incubated in primary antibodies in antibody dilution buffer (1% BSA and 0.3% Triton-X in 1x PBS) overnight at 4°C. The following day, coverslips were washed three times for 5 min in 1x PBS, incubated with secondary antibodies in antibody dilution buffer (1:500) for one hour at RT and washed three times for 5 min in 1x PBS. Coverslips were mounted onto slides with ProLong Gold Antifade mountant with or without DAPI (ThermoFisher: P36934 or P36935) and allowed to set for one day before imaging. For soma size quantification, neuronal cultures from the floxed mouse lines were imaged on an FV1000 Olympus FluoView confocal microscope with a 20x objective. Neuronal cultures from the Emx1-Cre lines were imaged with a Hamamatsu Orca-er digital camera with a 10× objective and Micro-Manager 1.4 software. Soma area was quantified by manually tracing neuronal cell bodies using ImageJ software. Antibody vendors, catalog numbers, and dilutions are listed in Supplementary Table 6.

Rapamycin treatment *in vitro*

Primary hippocampal cultures were treated chronically for 4 days with rapamycin from DIV 10-14. A stock solution of 0.5 mM rapamycin (LC Laboratories: R-5000) was prepared in ethanol and stored at −20°C. Rapamycin stock was diluted in Neurobasal media 1:100 prior to use and then added to a final concentration of 50 nM. Rapamycin was first added on DIV 10 and in the final media change on DIV 12.

Survival and body weight monitoring

Breeder cages from the *Tsc1;Rptor;Emx1-Cre* and *Tsc1;Rictor;Emx1-Cre* lines were monitored daily with minimal disturbance. The birth date of each litter was noted, and the number of pups was recorded. At P11, pups were genotyped, and their body weight was measured. Weight was measured every two days from P11-P21 and every 5 days from P21-P40. Each pup that was found dead in the cage was immediately removed and re-genotyped for confirmation. Mice were handled minimally and with care to reduce stressors that could promote seizures.

For AAV-shRaptor *in vivo* experiments, breeder cages from the *Tsc1;Emx1-Cre* lines were monitored daily with minimal disturbance. On the birth date each litter received intracranial injections (see methods below) and the number of pups was recorded. Pups found dead before P4 were excluded from the study. At P10 pups were genotyped and their body weight was measured. Weight was measured every 2 days from P10-P22, every 3 days from P22-31 and then on P35 and P40. Each pup that was found dead in the cage was immediately removed and re-genotyped for confirmation. Mice were handled minimally and with care to reduce stressors that could promote seizures.

Perfusion and immunohistochemistry

P14-P15 mice were deeply anesthetized by isoflurane and transcardially perfused with ice-cold 1x PBS, followed by 4% PFA solution (Electron Microscopy Sciences: 15713) in 1x PBS using a peristaltic pump (Instech). The brains were removed and post-fixed by immersion in 4% PFA in 1x PBS overnight at 4 °C. Brains were then suspended in 30% sucrose in 0.1 M PB solution at 4°C until processed. Brains were sectioned coronally at 30 µm on a freezing microtome (American Optical AO 860).

Free-floating brain sections were batch processed to include matched control and experimental samples. With gentle shaking, sections were washed 3x 15 min in 1x PBS, followed by 1 h incubation at RT with BlockAid blocking solution (Life Tech: B10710). Primary antibodies were diluted in 1x PBS-T (PBS + 0.25% Triton-X-100) and applied for 48 h at 4 °C. Sections were washed with cold 1x PBS 3 x 15 min and incubated for 1h at RT with secondary antibodies diluted 1:500 in 1x PBS-T. Sections were then washed in cold 1x PBS 5 x 15 min, mounted on SuperFrost slides (VWR: 48311-703), and coverslipped with Vectashield hard-set mounting media with DAPI (Vector Labs: H-1500). See Supplementary Table 6 for a list of antibodies and dilutions used for immunohistochemistry.

Confocal microscopy and image analysis

Images of brain sections were taken on either a Zeiss LSM 710 AxioObserver with 10x or 20x objectives, or an FV3000 Olympus FluoView confocal microscope with 4x or 20x objectives. For all quantitative comparison experiments, the same microscope and acquisition settings were used for each image and samples were processed in batches to include matched control and experimental samples. All images were processed using ImageJ software.

To quantify p-S6 levels and soma area, regions of interest (ROIs) were manually drawn around neuronal bodies on max-projected Z-stack images. The location and the size of the brain region selected for analysis was consistent across genotypes for each experiment. For the cortex, a region within the somatosensory area spanning all layers was selected and ~200 neurons per section were traced. For the CA1, ~70 neurons per section were traced and analyzed. For the dentate gyrus, ~50 neurons per section from a sub-region of the suprapyramidal blade were analyzed per animal. To quantify ectopic cells above CA1, the number of cells with a strong p-S6 signal within a 249 x 83 µm ROI between the CA1 pyramidal layer and white matter were counted.

For myelin basic protein (MBP) analysis, the average bulk fluorescence intensity was calculated from a ~468 x 468 µm sized ROI from a region spanning the retrosplenial area and secondary motor area drawn on max-projected Z-stack images. To examine GFAP expression in the cortex, a line was drawn across the cortical plate spanning from layer I to the border with the white matter. Mean GFAP fluorescence along the line was plotted using plot profile function in ImageJ. To examine GFAP expression in CA1, bulk average fluorescence intensity was calculated from a sub-region of CA1 approximately 232 x 81 µm.

For animals that received intracranial injections of AAV9-shRNA-EYFP bilaterally, neurons from both hemispheres were analyzed and pooled to account for potential differences in the injection efficiency. To quantify p-S6 levels, ~ 185 EYFP+ neurons were manually outlined within the primary somatosensory area including all cortical layers. For the hippocampus, ~85 neurons in CA1 and ~65 neurons in DG from a middle region (along the anterior/posterior axis) of the hippocampus were analyzed per animal. To quantify MBP, two ~621.5 x 621.5 µm ROIs (one per hemisphere) in the primary somatosensory cortex were drawn and bulk MBP fluorescence intensity was quantified and averaged per mouse. All ROIs were drawn on max-projected Z-stack images using ImageJ.

Calcium Imaging

Primary hippocampal cultures from P0-1 *Tsc1;Rptor;Emx1-Cre* mice of different genotypes were plated onto 24 well plates pre-coated with PDL (Corning, Cat # 08774271). On DIV 2, cultures were transduced with AAV1-jRGECO1a (Supplementary Table 5) and maintained for 12 days in Neurobasal media. On DIV 14, neurons were imaged on an AxioObserver.A1 (Zeiss) inverted microscope using a 10x Zeiss A-Plan objective (Numerical Aperture: 0.25) with wide field fluorescence illumination (X-Cite series 120Q, Lumen Dynamics). Images were taken at 8.91 Hz with a Hamamatsu Orca-er digital camera and Micro-Manager 1.4 software. For all Ca^{2+} imaging experiments excitation light intensity, camera sensor gain, and exposure time used were identical. A single field of view (FOV) was imaged from at least 2-3 individual wells per culture (prepped from 1 pup) and approximately 40 neurons were randomly selected and analyzed. Before proceeding to the analysis, we verified that the neurons selected were active at least once during the recording period. At least 3 mice per genotype were examined from at least 3 different litters.

Calcium imaging analysis

Data analysis was performed using ImageJ 1.53c and custom programs written in Matlab 2020a.

Pre-processing

Circular ROIs corresponding to neuronal somata, were drawn manually in ImageJ on mean intensity projection images of the recorded FOV. Forty ROIs were drawn per FOV, beginning in the upper left quadrant of the image, and extending outward as necessary (to the right, bottom left, and bottom right quadrants, respectively), and were imported into Matlab for further analysis. Movies were motion corrected using the normcorre function[243], then normalized with respect to baseline, taken to be the minimum intensity projection of the FOV, to generate a ΔF/F movie. It was necessary to use the minimum projection as Tsc1-cKO neurons exhibited high Ca^{2+} activity and thus contained few baseline frames. Ca^{2+} traces were extracted as ΔF/F by computing the mean fluorescence within each ROI at each movie frame.

Single event analysis

Individual Ca^{2+} transients were detected by first filtering the ΔF/F traces with a four-frame moving mean, then using Matlab's findpeaks function to identify peaks in the ΔF/F trace. Event amplitude was defined as the difference between the event's peak ΔF/F and the minimum ΔF/F in the preceding inter-event-interval (see Supplementary Fig. 6c). Events with an amplitude < 0.5% were excluded from further analysis. Prior to measurement of event duration and area under the curve (AUC), Matlab's msbackadj function was used to shift the 1st percentile of the ΔF/F trace within 15 second time windows to zero. This reduced the reliance of event AUC on preceding bouts of Ca^{2+} activity, which would otherwise contribute significantly to AUC values in Tsc1-cKO neurons due to their high frequency activity. Event initiation and termination were identified by finding the 0.5% ΔF/F threshold (see Supplementary Fig. 6d) crossing

preceding and following the event peak. Event termination was alternatively identified when the Ca^{2+} decay following the event peak ΔF/F was interrupted by a ΔF/F increase >1%, indicating the initiation of another event. Events without a clear initiation or termination were excluded from further analysis. AUC was defined as the area under the ΔF/F trace during the event (see Supplementary Fig. 6d) and measured using trapezoidal numerical integration implemented by the trapz function in Matlab.

Network event analysis

Network Ca^{2+} events were defined as time intervals over which more than 20% of neuronal ROIs in the imaged area were simultaneously active (activity for a single neuron was defined as ΔF/F ≥ 0.5%) (See gray highlighted zones in Fig. 6e-g and Supplementary Fig. 8c,d). We did not use a standard deviation-based threshold, as it would have selectively reduced event detection in Tsc1-cKO cultures, due to their persistent Ca^{2+} activity. Events with a duration < 2.5 seconds were excluded from further analysis. Cell participation in events was defined as the percentage of neurons that were active at any time during the event. Response amplitude within a single neuron during a network event was defined as the difference between the maximum ΔF/F during the event and the minimum ΔF/F in the preceding inter-event-interval. Area under the curve (AUC) was defined as the area under the ΔF/F trace occurring during the event.

shRNA constructs

The AAV-Tet3-shRNA plasmid (Addgene plasmid # 85740) was used as a backbone to generate the AAV9-hU6-shRptor-EYFP construct. The restriction enzymes BamHI and XbaI were used to excise the Tet-3 shRNA sequence. The oligonucleotide sequence: 5'-GATCCGCCTCATCGTCAAGTCCTTCAAGAAGCTTGTTGAAGGACTTGACGATGAGG CTTTTTTT -3' that contains the *Rptor* shRNA sequence[215] flanked by restriction sites for BamHI and XbaI was subcloned into the plasmid backbone. AAV-hU6-shControl-EYFP (Addgene plasmid # 85741) that contains the 5'-GTTCAGATGTGCGGCGAGT-3' shRNA sequence was used as a control. For large-scale isolation and purification of the plasmids, DH5α NEB competent cells (New England Biolabs #C2987H) were transformed and Endofree Megaprep (Qiagen # 12381) was performed to generate plasmids for high titer viral packaging.

Intracranial neonatal mouse injections

Neonatal mice (P0) were cryo-anesthetized by placing on ice for ~2-3 min. When the animal was fully anesthetized, confirmed by lack of movement, it was placed in a head mold. Each pup received a total of 500 nl of 4x diluted AAV9 (AAV9-hU6-shRptor-EYFP or AAV9-hU6-shControl-EYFP, see Supplementary Table 5 for titer information) spread across 4 injections (2 per hemisphere): two 150 nl injections were made into the cortex and two 100 nl injections were made into the dorsal hippocampus. Cortical injections were made halfway between bregma and lambda approximately 0.6 mm from the sagittal suture and 0.5-0.6 mm ventral to the surface of the skull. Hippocampal injections were made approximately 0.5 mm anterior to lambda with the injection sites ~0.5 mm from the sagittal suture and 1 mm ventral to the surface of the skull.

Statistical Analysis

Statistical analyses and graphing were performed using GraphPad Prism software (versions 7-9). All datasets were first analyzed using the D'Agostino and Pearson normality test, and then parametric or non-parametric two-tailed statistical tests were employed accordingly to determine significance. Normally distributed datasets were analyzed using Welch's t-tests when comparing two groups or a one-way ANOVA with Holm-Sidak's multiple comparison tests when comparing three or more groups. Datasets that did not pass the normality test were analyzed using a Mann-Whitney test when comparing two groups or the Kruskal–Wallis test with Dunn's multiple comparisons tests when comparing three or more groups. Cumulative distributions were analyzed using Kolmogorov–Smirnov tests (when comparing two groups) or the Kruskal–Wallis test with Dunn's multiple comparisons tests (when comparing three or more groups). Survival curves were analyzed using the Log-rank (Mantel-Cox) test. Regression models were analyzed either with Pearson correlation (linear regression) or Spearman correlation (non-linear regression). Body weigh graphs were analyzed with Mixed-effects model (REML) statistics. Significance was set as $*p < 0.05$, $**p < 0.01$, $***p < 0.001$, and $****p < 0.0001$. P values were corrected for multiple comparisons.

Figures

Figure 1

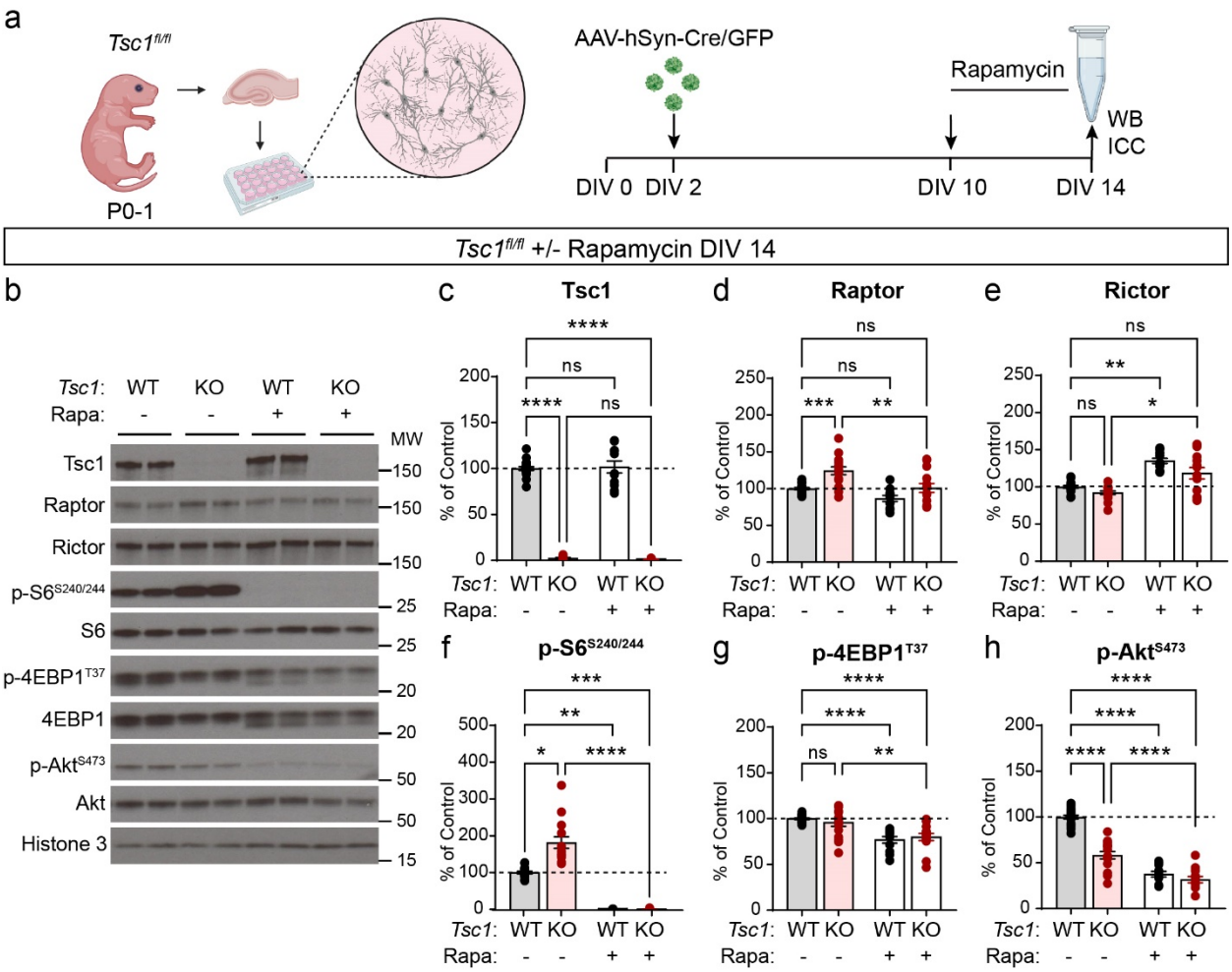

Figure 1. Chronic rapamycin suppresses mTORC1 and mTORC2 signaling in cultured Tsc1-cKO neurons.

a) Schematic of the experiment. Primary hippocampal cultures were prepared from *Tsc1*$^{fl/fl}$ mice on postnatal day (P) 0-1. AAV-GFP or AAV-Cre-GFP was added on DIV 2 and rapamycin or vehicle was added on DIV 10. Cells were collected for analysis by western blot (WB) or immunocytochemistry (ICC) on DIV 14. Created with BioRender.com

b) Representative western blots from *Tsc1*$^{fl/fl}$ cultures with (+) or without (-) four-day rapamycin (Rapa) treatment. MW indicates molecular weight. WT=*Tsc1*$^{fl/fl}$ + AAV-GFP; KO=*Tsc1*$^{fl/fl}$ + AAV-Cre-GFP. Two independent samples per genotype are shown; this experiment was replicated seven times.

c-h) Bar graphs display western blot quantification (mean +/- SEM) for the indicated proteins, expressed as a percentage of Control (WT) levels. Phospho-proteins were normalized to their respective total proteins. Dots represent data from individual culture wells. WT n=18, KO n=15, WT+Rapa n=11 and KO+Rapa n=14 culture wells from 7 independent cultures; 2 mice per culture. ns=non-significant. Dashed lines at 100% indicate Control levels.

c) Tsc1, Kruskal-Wallis, p<0.0001; WT vs KO, ****p<0.0001; WT vs WT+Rapa, p>0.9999; WT vs KO+Rapa, **** p<0.0001; KO vs KO+Rapa, p>0.9999; Dunn's multiple comparisons tests.

d) Raptor, One-way ANOVA, p<0.0001, F (3, 54) = 11.89; WT vs KO, ***p=0.0004; WT vs WT+Rapa, p=0.1541; WT vs KO+Rapa, p=0.9997; KO vs KO+Rapa, **p=0.0016; Sidak's multiple comparisons tests.
e) Rictor, Kruskal-Wallis, p<0.0001; WT vs KO p=0.3281; WT vs WT+Rapa, ** p=0.0023; WT vs KO+Rapa, p=0.7348; KO vs KO+Rapa, *p=0.0144, Dunn's multiple comparisons tests.
f) p-S6 Ser240/244, Kruskal-Wallis, p<0.0001; WT vs KO, *p=0.0310; WT vs WT+Rapa, ** p=0.0022; WT vs KO+Rapa, ***p=0.0008; KO vs KO+Rapa, ****p<0.0001; Dunn's multiple comparisons tests.
g) p-4E-BP1 T37, One-way ANOVA, p<0.0001, F (3, 54) = 12.40; WT vs KO, p=0.3293; WT vs WT+Rapa, ****p<0.0001; WT vs KO+Rapa, ****p<0.0001; KO vs KO+Rapa, **p=0.0021; Holm-Sidak's multiple comparisons tests.
h) p-Akt Ser473, One-way ANOVA, p<0.0001, F (3, 54) = 103.2; WT vs KO, ****p<0.0001; WT vs WT+Rapa, ****p<0.0001; WT vs KO+Rapa, ****p<0.0001; KO vs KO+Rapa, ****p<0.0001; Sidak's multiple comparisons tests.
See also Supplementary Figure 1.

Figure 2

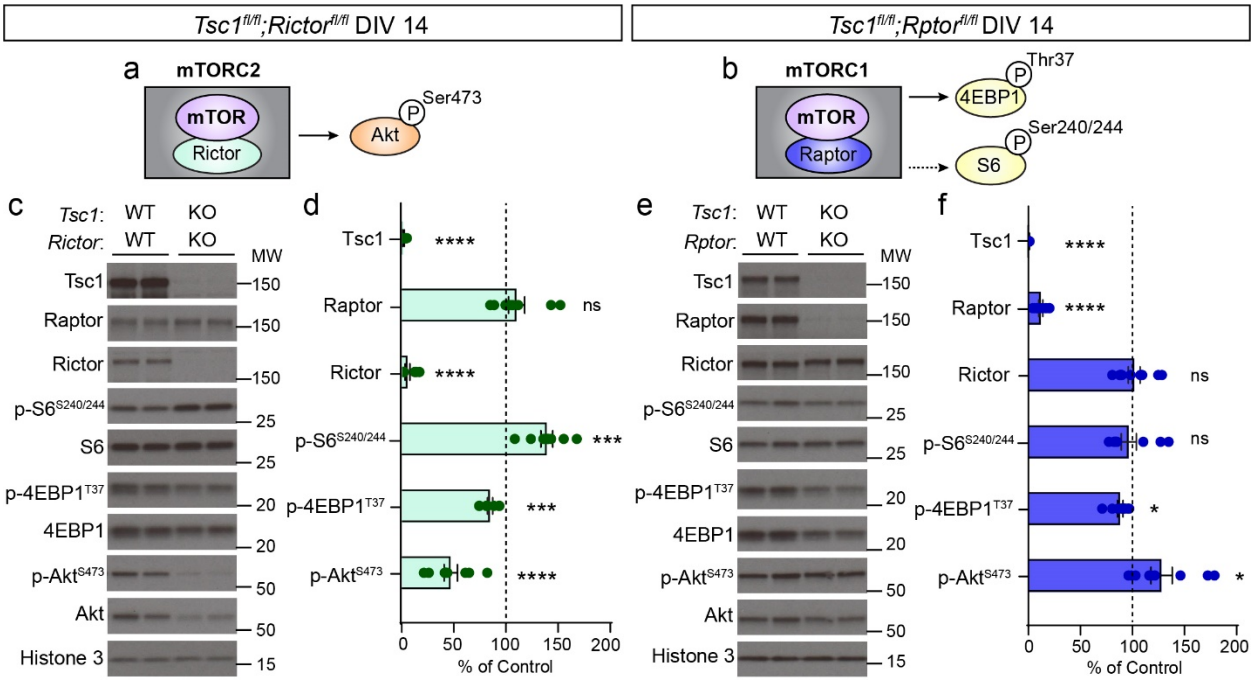

Figure 2. Genetic reduction of Raptor, but not Rictor, ameliorates mTOR signaling abnormalities in Tsc1-cKO neurons.

a) Simplified schematic of mTORC2 showing mTOR and its obligatory binding partner Rictor. mTORC2 phosphorylates Ser473 on Akt.

b) Simplified schematic of mTORC1 showing mTOR and its obligatory binding partner Raptor. mTORC1 phosphorylates 4E-BP1 (Thr37) and p70S6K, which in turn phosphorylates S6 at Ser240/244 (represented by the dashed line).

c) Representative western blots from *Tsc1$^{fl/fl}$;Rictor$^{fl/fl}$* hippocampal cultures treated with AAV-GFP (WT;WT) or AAV-Cre-GFP (KO;KO) and harvested on DIV 14. MW indicates molecular weight. Two independent samples per genotype are shown; this experiment was replicated three times.

d) Bar graphs display western blot quantification (mean +/- SEM) for the indicated proteins, expressed as a percentage of Control (WT) levels. n=9 culture wells from 3 independent cultures per genotype; 2 mice per culture. Tsc1 ****p<0.0001; Raptor p=0.2380; Rictor **** p<0.0001; p-S6 Ser240/244 *** p=0.0007; p-4EBP1 T37 *** p=0.0002; p-Akt Ser473 **** p<0.0001; Welch's t-tests.

e) Representative western blots of lysates collected from *Tsc1$^{fl/fl}$;Rptor$^{fl/fl}$* hippocampal cultures treated with AAV-GFP (WT;WT) or AAV-Cre-GFP (KO;KO) and harvested on DIV 14. Two independent samples per genotype are shown; this experiment was replicated three times.

f) Bar graphs display western blot quantification (mean +/- SEM) for the indicated proteins, expressed as a percentage of Control (WT) levels. n=9 culture wells from 3 independent cultures per genotype; 2 mice per culture. Tsc1 ****p<0.0001; Raptor ****p<0.0001; Rictor p=0.8199; p-S6 Ser240/244 p=0.6616; p-4EBP1 T37 *p=0.0146; p-Akt Ser473 *p=0.0283; Welch's t-tests.

For panels d and f, phospho-proteins were normalized to their respective total proteins. Dots represent data from individual culture wells. Dashed lines at 100% indicate Control levels. ns=non-significant.

See also Supplementary Figure. 1.

Figure 3

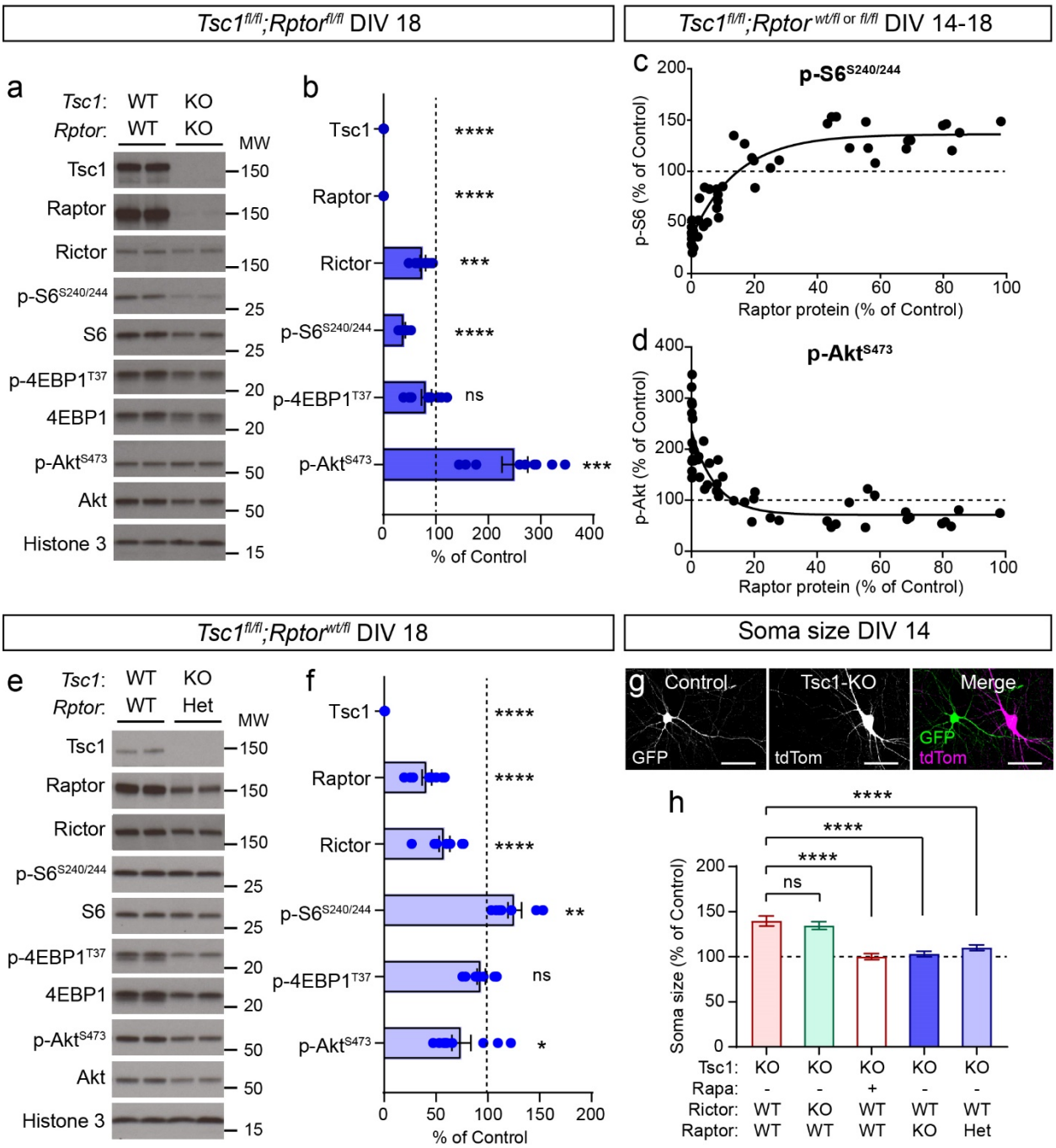

Figure 3. Partial reduction of Raptor normalizes mTOR signaling in Tsc1-cKO cultures.
a) Representative western blots from *Tsc1*$^{fl/fl}$*;Rptor*$^{fl/fl}$ hippocampal cultures treated with AAV-GFP (WT;WT) or AAV-Cre-GFP (KO;KO) and harvested on DIV 18. MW indicates molecular weight. Two independent samples per genotype are shown; this experiment was replicated three times.
b) Bar graphs display western blot quantification (mean +/- SEM) for the indicated proteins, expressed as a percentage of Control (WT) levels. n=9 culture wells from 3 independent cultures per genotype; 2 mice per culture. Tsc1 ****p<0.0001, Mann-Whitney test; Raptor ****p<0.0001, Mann-Whitney test; Rictor

***p=0.0005, Mann-Whitney test; p-S6 Ser240/244 ****p<0.0001, Welch's t-test; p-4EBP1 T37 p=0.1018, Welch's t-test; p-Akt Ser473 ***p=0.0003, Welch's t-test. ns=non-significant.
c,d) Correlation of Raptor protein levels to p-S6 Ser240/244 (c) or p-Akt Ser473 (d) levels within each culture, expressed as a percentage of Control. Samples were pooled across hippocampal cultures from *Tsc1*$^{fl/fl}$*;Rptor*$^{wt/fl\ or\ fl/fl}$ mice treated with AAV-GFP or AAV-Cre-GFP and harvested on different days (DIV 14-18) to generate a range of Raptor protein levels (includes data from Figs. 2e-f, 3a-b & e-f, and Fig. S2a-g). Solid line depicts non-linear regression. n=48 culture wells. For panel c, r= 0.8907, ****p<0.0001, Spearman correlation. For panel d, r= -0.8662, ****p<0.0001, Spearman correlation.
e) Representative western blots from *Tsc1*$^{fl/fl}$*;Rptor*$^{wt/fl}$ hippocampal cultures treated with AAV-GFP (WT;WT) or AAV-Cre-GFP (KO;KO) and harvested on DIV 18. Two independent samples per genotype are shown; this experiment was replicated three times.
f) Bar graphs display western blot quantification (mean +/- SEM) for the indicated proteins, expressed as a percentage of Control (WT) levels. n=9 culture wells from 3 independent cultures per genotype; 2 mice per culture. Tsc1 ****p<0.0001; Raptor ****p<0.0001; Rictor ****p<0.0001; p-S6 Ser240/244 **p=0.0052; p-4EBP1 T37 p=0.1621; p-Akt Ser473 *p=0.0235; Welch's t-tests.
For panels b,c,d and f, phospho-proteins were normalized to their respective total proteins. Dots represent data from individual culture wells. Dashed lines at 100% indicate control levels.
g) Representative images showing a GFP-expressing control neuron (left panel) and a neighboring AAV-Cre + AAV-Flex-tdTomato transduced Tsc1 KO neuron (middle panel) within the same hippocampal culture. Right panel shows the merged image is on the right. Scale bars=50 μm.
h) Quantification (mean +/- SEM) of the average soma area of cultured hippocampal neurons of the indicated genotypes, expressed as a percentage of Control (WT) neurons from the same culture. One-way ANOVA, p<0.0001, F (4, 705) = 19.33; Tsc1-KO vs Tsc1-KO;Rictor-KO, p=0.4030; Tsc1-KO vs Tsc1-KO+Rapa, ****p<0.0001; Tsc1-KO vs Tsc1-KO;Rptor-KO, ****p<0.0001; Tsc1-KO vs. Tsc1-KO;Rptor-Het, ****p<0.0001; Holm-Sidak's multiple comparisons tests.
See also Supplementary Figures 2 and 3.

Figure 4

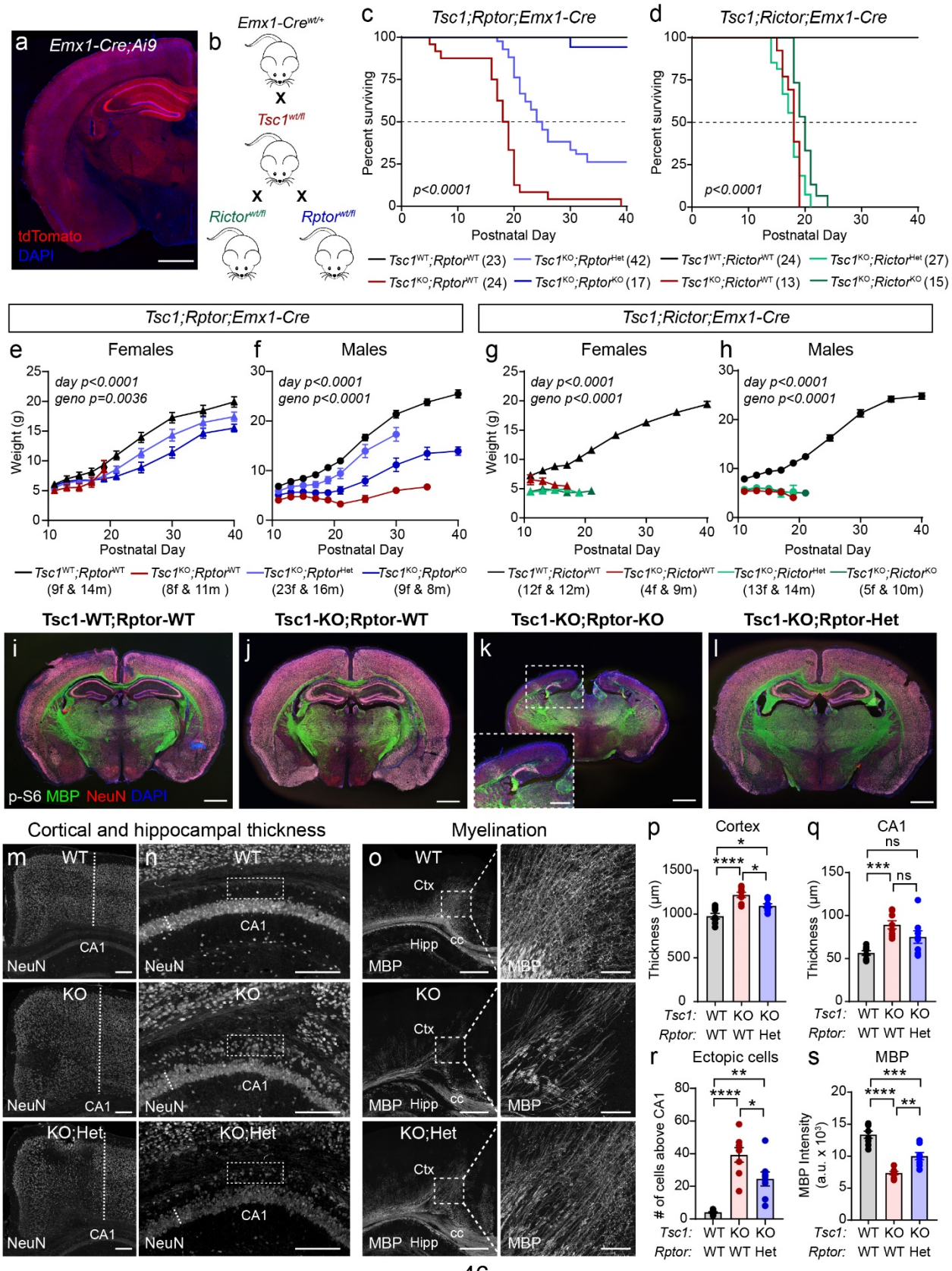
a Emx1-Cre;Ai9
tdTomato
DAPI
b
Emx1-Cre^wt/+
x
Tsc1^wt/fl
x x
Rictor^wt/fl
Rptor^wt/fl
c Tsc1;Rptor;Emx1-Cre
Percent surviving
p<0.0001
Postnatal Day
d Tsc1;Rictor;Emx1-Cre
Percent surviving
p<0.0001
Postnatal Day
Tsc1^WT;Rptor^WT (23)
Tsc1^KO;Rptor^Het (42)
Tsc1^WT;Rictor^WT (24)
Tsc1^KO;Rictor^Het (27)
Tsc1^KO;Rptor^WT (24)
Tsc1^KO;Rptor^KO (17)
Tsc1^KO;Rictor^WT (13)
Tsc1^KO;Rictor^KO (15)
Tsc1;Rptor;Emx1-Cre
Tsc1;Rictor;Emx1-Cre
e Females
f Males
g Females
h Males
Weight (g)
day p<0.0001
geno p=0.0036
day p<0.0001
geno p<0.0001
day p<0.0001
geno p<0.0001
day p<0.0001
geno p<0.0001
Postnatal Day
Tsc1^WT;Rptor^WT (9f & 14m)
Tsc1^KO;Rptor^WT (8f & 11m)
Tsc1^KO;Rptor^Het (23f & 16m)
Tsc1^KO;Rptor^KO (9f & 8m)
Tsc1^WT;Rictor^WT (12f & 12m)
Tsc1^KO;Rictor^WT (4f & 9m)
Tsc1^KO;Rictor^Het (13f & 14m)
Tsc1^KO;Rictor^KO (5f & 10m)
Tsc1-WT;Rptor-WT
Tsc1-KO;Rptor-WT
Tsc1-KO;Rptor-KO
Tsc1-KO;Rptor-Het
i
j
k
l
p-S6 MBP NeuN DAPI
Cortical and hippocampal thickness
Myelination
m WT
n WT
o WT
CA1
NeuN
Ctx
Hipp
cc
MBP
KO
KO;Het
p Cortex
q CA1
Thickness (µm)
ns
Tsc1: WT KO KO
Rptor: WT WT Het
r Ectopic cells
# of cells above CA1
s MBP
MBP Intensity (a.u. x 10³)

Figure 4. Reduction of *Rptor* prolongs the life span and improves forebrain development of Tsc1-cKO mice.

a) Representative image showing one hemisphere of a coronal section from an *Emx1-Cre*$^{+}$*;Ai9*$^{+}$ mouse. The Cre-dependent tdTomato reporter (red) is expressed broadly in the cortex and hippocampus. DAPI labels cell nuclei (blue). Scale bar=1 mm

b) Schematic of the crosses used to generate experimental mice. *Emx1-Cre*$^{+}$ mice were crossed with *Tsc1*$^{wt/fl}$ mice. This line was subsequently bred to either *Rictor*$^{wt/fl}$ or *Rptor*$^{wt/fl}$ mice.

c,d) Survival analysis of *Tsc1;Rptor;Emx1-Cre* (c) and *Tsc1;Rictor;Emx1-Cre* (d) mice of the indicated genotypes. The number of mice for each genotype is indicated in parentheses. Dashed lines indicate 50% of the population surviving. P values from Log-rank Mantel-Cox tests are shown on the graphs.

e-h) Mean +/- SEM body weight in grams measured from postnatal day 11 to 40 for mice of the indicated sex and genotype. The number of mice for each genotype and is indicated in parentheses. f=females, m=males. Mixed-effects model (REML) statistics: *Tsc1;Rptor;Emx1-Cre* females (e), day p<0.0001, F(1.447, 51.30) = 398.9; geno p=0.0036, F(3, 45) = 5.192. *Tsc1;Rptor;Emx1-Cre* males (f), day p<0.0001, F(2.287, 79.03) = 197.4; geno p<0.0001, F (3, 45) = 26.85. *Tsc1;Rictor;Emx1-Cre* females (g), day p<0.0001, F (4.257, 69.52) = 221.1; geno p<0.0001, F (3, 30) = 53.74. *Tsc1;Rictor;Emx1-Cre* males (h), day p<0.0001, F (2.389, 48.04) = 370.4; geno ****p<0.0001, F (3, 41) = 28.86.

i-l) Representative whole brain coronal sections from mice of the indicated genotypes. Immunostaining for p-S6 Ser240/244 is in grey, myelin basic protein (MBP) is in green, NeuN is in red and DAPI-labeled nuclei are in blue. In panel k, inset shows zoomed-in image of the cortex and hippocampal region. Scale bars=1 mm. Panel k inset, scale bar=500 µm (See also Suppl. Fig 4g-j)

m) Representative images of the cortex with NeuN immunostaining. Dashed lines denote the measurement of cortical thickness. WT=Tsc1-WT;Rptor-WT, KO=Tsc1-KO;Rptor-WT, KO;Het=Tsc1-KO;Rptor-Het. Scale bars=500 µm.

n) Representative images of the CA1 region of the hippocampus with NeuN immunostaining from mice of the indicated genotypes. Dashed lines denote the measurement of CA1 thickness. Boxed regions highlight the area above the CA1 that contains ectopic p-S6 expressing neurons in Tsc1-KO;Rptor-WT mice, which are reduced in Tsc1-KO;Rptor-Het mice (quantified in panel r). Scale bars=250 µm

o) Representative images of MBP immunostaining in the cortex (Ctx) & dorsal hippocampus (Hipp) from mice of the indicated genotypes. cc=corpus callosum. Scale bars=500 µm. Right panels show higher magnification of the boxed regions in the cortex. Scale bars=100 µm.

p) Mean +/- SEM cortical thickness for the indicated genotypes. For panels p-s, dots represent values from individual mice, n=8 mice per genotype. One-way ANOVA, p<0.0001, F (2, 21) = 18.40; WT vs KO, ****p<0.0001; WT vs KO;Het, *p=0.0226; KO vs KO;Het, *p=0.0157, Sidak's multiple comparisons tests.

q) Mean +/- SEM CA1 thickness for the indicated genotypes. One-way ANOVA, p=0.0010, F (2, 21) = 9.703; WT vs KO, ***p=0.0008; WT vs KO;Het, p=0.0628; KO vs KO;Het, p=0.1968 Sidak's multiple comparisons tests. ns=non-significant.

r) Mean +/- SEM number of p-S6 positive neurons above the CA1 (boxed regions in panel n) for the indicated genotypes. One-way ANOVA, p<0.0001, F (2, 21) = 24.77; WT vs KO, ****p<0.0001; WT vs KO;Het, **p=0.0016; KO vs KO;Het, *p=0.0237 Sidak's multiple comparisons tests.

s) Mean +/- SEM bulk MBP fluorescence intensity in the boxed cortical region shown in panel o for the indicated genotypes. One-way ANOVA, p<0.0001, F (2, 21) = 39.19; WT vs KO, ****p<0.0001; WT vs KO;Het, ***p=0.0002; KO vs KO;Het, **p=0.0025; Sidak's multiple comparisons tests.

See also Supplementary Figure 4 and Supplementary Tables 1 and 2.

Figure 5

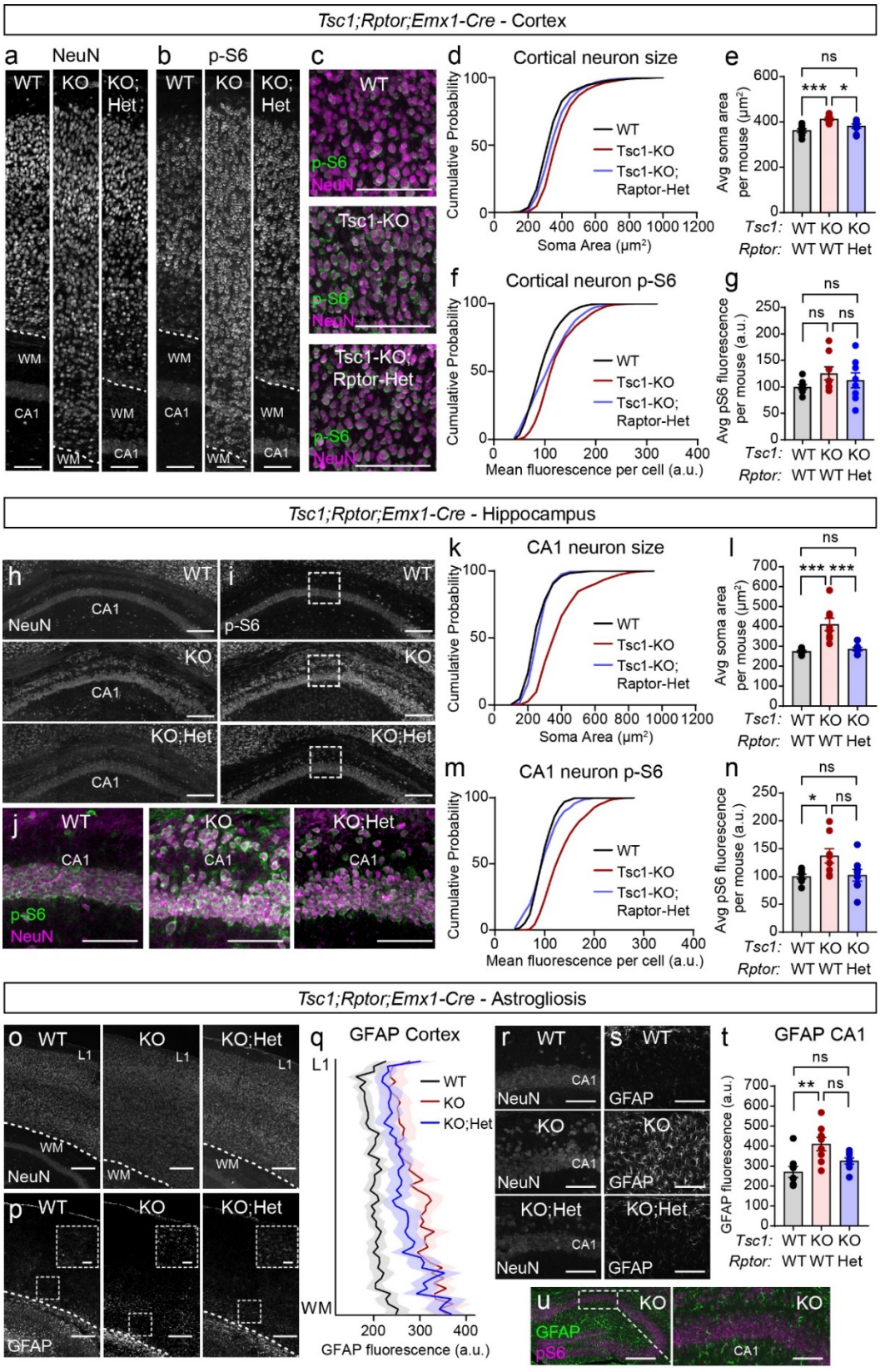
Tsc1;Rptor;Emx1-Cre - Cortex
a NeuN
b p-S6
c
WT
KO
KO; Het
WM
CA1
p-S6
NeuN
Tsc1-KO
Tsc1-KO; Rptor-Het
d Cortical neuron size
Cumulative Probability
Soma Area (μm²)
WT
Tsc1-KO
Tsc1-KO; Raptor-Het
e
Avg soma area per mouse (μm²)
ns
***
*
Tsc1: WT KO KO
Rptor: WT WT Het
f Cortical neuron p-S6
Mean fluorescence per cell (a.u.)
g
Avg pS6 fluorescence per mouse (a.u.)
Tsc1-KO; Rptor-Het
Tsc1;Rptor;Emx1-Cre - Hippocampus
h
i
j
KO;Het
k CA1 neuron size
l
m CA1 neuron p-S6
n
Tsc1;Rptor;Emx1-Cre - Astrogliosis
o
p
q GFAP Cortex
L1
GFAP fluorescence (a.u.)
r
s
t GFAP CA1
GFAP
u
pS6

Figure 5. Heterozygous deletion of *Rptor* improves cellular phenotypes in Tsc1-cKO mice.
a,b) Representative images of somatosensory cortex showing NeuN (left panels, a) and p-S6 Ser240/244 (right panels, b) immunostaining in Tsc1-WT;Rptor-WT (WT), Tsc1-KO;Rptor-WT (KO), and Tsc1-KO;Rptor-Het (KO;Het) mice. Dashed lines indicate the border of cortical layer 6 and the corpus callosum. Scale bars=100 μm. WM=white matter
c) Representative zoomed-in images of the cortex (midway between the cortical plate and white matter) showing p-S6 Ser240/244 (green) and NeuN (magenta) immunostaining for the indicated genotypes. Scale bars=100 μm.
d) Cumulative distributions of cortical neuron soma area for the indicated genotypes. n=1601 WT, 1605 Tsc1-KO, and 1602 Tsc1-KO;Rptor-Het neurons from 8 mice per genotype. Kruskal-Wallis test, p<0.0001; WT vs KO, p<0.0001; WT vs KO;Het, p<0.0001; KO vs KO;Het, p<0.0001; Dunn's multiple comparisons tests.
e) Mean +/- SEM cortical neuron soma area per mouse for the indicated genotypes. Dots represent values from individual mice. n=8 mice per genotype. One-way ANOVA, p=0.0011, F (2, 21) = 9.629; WT vs KO, ***p=0.0008, WT vs KO;Het, p=0.2760; KO vs KO;Het, *p=0.0447 Sidak's multiple comparisons tests. ns=non-significant.
f) Cumulative distributions of cortical p-S6 levels per neuron for the indicated genotypes. n is the same as for panel d. Kruskal-Wallis test, p<0.0001; WT vs KO, p<0.0001; WT vs KO;Het, p<0.0001; KO vs KO;Het, p<0.0001; Dunn's multiple comparisons tests.
g) Mean +/- SEM cortical neuron p-S6 levels per mouse for the indicated genotypes. Dots represent values from individual mice. n=8 mice per genotype. One-way ANOVA, p=0.2881, F (2, 21) = 1.321; WT vs KO, p=0.3162; WT vs KO;Het, p= 0.8216, KO vs KO;Het, p=0.7989; Sidak's multiple comparisons tests.
h,i) Representative images of hippocampal area CA1 from mice of the indicated genotypes. Left panels show NeuN (h) and right panels show p-S6 Ser240/244 (i) immunostaining. Scale bars=250 μm.
j) Representative zoomed-in images of the boxed region in panel i, showing p-S6 Ser240/244 (green) and NeuN (magenta) immunostaining for the indicated genotypes. Scale bars=100 μm.
k) Cumulative distributions of CA1 neuron soma area for the indicated genotypes. n=568 WT, 561 Tsc1-KO, and 561 Tsc1-KO;Rptor-Het neurons from 8 mice per genotype.
Kruskal-Wallis test, p<0.0001; WT vs KO, ****p<0.0001; WT vs KO;Het, *p=0.0133; KO vs KO;Het, ****p<0.0001; Dunn's multiple comparisons tests.
l) Mean +/- SEM CA1 neuron soma area per mouse for the indicated genotypes. Dots represent values from individual mice. n=8 mice per genotype. One-way ANOVA, p<0.0001, F(2, 21) = 15.89; WT vs KO, ***p=0.0001; WT vs KO;Het, p=0.9655; KO vs KO;Het, ***p=0.0004; Sidak's multiple comparisons tests.
m) Cumulative distributions of CA1 p-S6 levels per neuron for the indicated genotypes. n is the same as for panel k. Kruskal-Wallis test, p<0.0001; WT vs KO, p<0.0001; WT vs KO;Het, p=0.7622; KO vs KO;Het, p<0.0001; Dunn's multiple comparisons tests.
n) Mean +/- SEM CA1 neuron p-S6 levels per mouse for the indicated genotypes. Dots represent values from individual mice. n=8 mice per genotype. One-way ANOVA, p=0.0263, F (2, 21) = 4.346; WT vs KO, *p=0.0464; WT vs KO;Het, p=0.9981; KO vs KO;Het, p=0.0650; Sidak's multiple comparisons tests.
o,p) Representative images of the somatosensory cortex from mice of the indicated genotypes. Top panels show NeuN (o) and bottom panels show GFAP (p) immunostaining. Scale bars=250 μm. Dashed lines indicate the border of cortical layer 6 and the beginning of white matter of the corpus callosum. L1=cortical layer 1. Zoomed-in inset scale bars=100μm.
q) GFAP immunofluorescence across cortical layers for mice of the indicated genotypes. Lines represent the mean, shaded regions represent the SEM. n=8 mice per genotype.
r,s) Representative images of the hippocampal CA1 region from mice of the indicated genotypes. Left panels show NeuN (r) and right panels show GFAP (s) immunostaining. Scale bars=100 μm.
t) Mean +/- SEM bulk GFAP fluorescence in the CA1 region per mouse for the indicated genotypes. Dots represent values from individual mice. n=8 mice per genotype. Kruskal-Wallis test, p=0.0087; WT vs KO, **p=0.0063; WT vs KO;Het, p=0.2691; KO vs KO;Het, p=0.5038; Dunn's multiple comparisons tests.
u) Representative images showing GFAP (green) and p-S6 Ser240/244 (magenta) immunostaining in the hippocampus of a Tsc1-KO mouse Scale bar=500 μm. Right panel shows a zoomed-in image of the boxed region. Scale bar=100μm.
See also Supplementary Figure 5 and Supplementary Table 3.

Figure 6

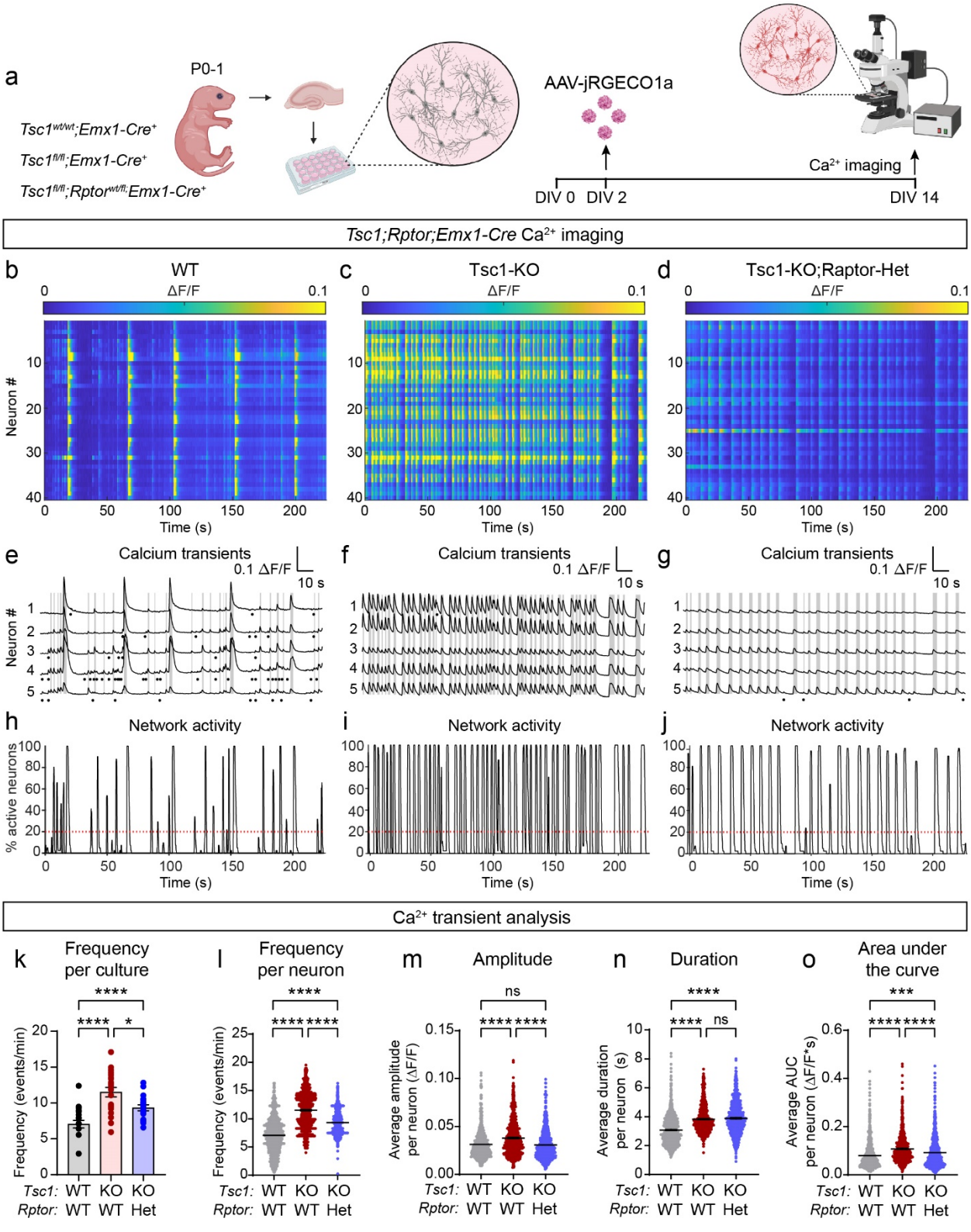
a
P0-1
Tsc1wt/wt;Emx1-Cre+
Tsc1fl/fl;Emx1-Cre+
Tsc1fl/fl;Rptorwt/fl;Emx1-Cre+
AAV-jRGECO1a
Ca2+ imaging
DIV 0
DIV 2
DIV 14
Tsc1;Rptor;Emx1-Cre Ca2+ imaging
b WT
c Tsc1-KO
d Tsc1-KO;Raptor-Het
ΔF/F
0
0.1
Neuron #
Time (s)
e Calcium transients
f Calcium transients
g Calcium transients
0.1 ΔF/F
10 s
h Network activity
i Network activity
j Network activity
% active neurons
Ca2+ transient analysis
k Frequency per culture
l Frequency per neuron
m Amplitude
n Duration
o Area under the curve
Frequency (events/min)
Average amplitude per neuron (ΔF/F)
Average duration per neuron (s)
Average AUC per neuron (ΔF/F*s)
ns
Tsc1: WT KO KO
Rptor: WT WT Het

Figure 6. Raptor downregulation reduces hyperactivity of Tsc1-cKO neurons.
a) Schematic of the experiment. Primary hippocampal cultures were prepared from P0-1 mice of different genotypes. An AAV expressing the calcium indicator jRGeco1a was added on DIV 2 and cells were imaged on DIV 14. Created with BioRender.com
b-d) Representative heatmaps of ΔF/F for 40 neurons imaged in a field of view from *Tsc1*$^{wt/wt}$*;Emx1-Cre*$^{+}$ (WT, b), *Tsc1*$^{fl/fl}$*;Emx1-Cre*$^{+}$ (Tsc1-KO, c), and *Tsc1*$^{fl/fl}$*;Rptor*$^{wt/fl}$*;Emx1-Cre*$^{+}$ (Tsc1-KO;Raptor-Het, d) cultures.
e-g) Ca^{2+} transients from 5 representative neurons imaged in a field of view in WT (e), Tsc1-KO (f) and Tsc1-KO;Raptor-Het (g) cultures. Grey lines indicate network events with more than 20% of neurons in the field of view active at the same time. Black dots represent spontaneous Ca^{2+} transients that were not part of network events.
h-j) Graphs display the percentage of neurons in the field of view that were active at a given time for a representative WT (h), Tsc1-KO (i) and Tsc1-KO;Raptor-Het (j) culture. Red dashed lines at 20% indicate the threshold for what was considered a network event.
k) Mean +/- SEM calcium transient frequency per culture. Dots represent values from individual cultures. n=20 culture wells from 6-7 independent culture preps per genotype, 1 pup per prep. One-way ANOVA, $p<0.0001$, $F(2, 57) = 16.88$; WT vs KO, ****$p<0.0001$; WT vs KO;Het, *$p=0.0130$; KO vs KO;Het, *$p=0.0187$; Sidak's multiple comparisons tests.
l) Scatter dot plot of the Ca^{2+} transient frequency per neuron for the indicated genotypes. Black lines indicate mean +/- SEM. n=800 neurons per genotype. Kruskal-Wallis test, $p<0.0001$; WT vs KO, $p<0.0001$; WT vs KO;Het, $p<0.0001$. KO vs. KO;Het, $p<0.0001$; Dunn's multiple comparisons tests.
m) Scatter dot plot of the average Ca^{2+} transient amplitude per neuron for the indicated genotypes. n is the same as for panel l. Kruskal-Wallis test, $p<0.0001$; WT vs KO, ****$p<0.0001$; WT vs KO;Het, $p=0.9211$; KO vs. KO;Het, ****$p<0.0001$; Dunn's multiple comparisons tests. ns=non-significant.
n) Scatter dot plot of the average Ca^{2+} transient duration per neuron for the indicated genotypes. n is the same as for panel l. Kruskal-Wallis test, $p<0.0001$; WT vs KO, ****$p<0.0001$; WT vs KO;Het, ****$p<0.0001$; KO vs. KO;Het, $p>0.9999$; Dunn's multiple comparisons tests.
o) Scatter dot plot of the average Ca^{2+} transient area under the curve (AUC) per neuron for the indicated genotypes. n is the same as for panel l. Kruskal-Wallis test, $p<0.0001$; WT vs KO, ****$p<0.0001$; WT vs KO;Het, ***$p=0.0001$; KO vs. KO;Het, ****$p<0.0001$; Dunn's multiple comparisons tests.
See also Supplementary Figures 6-8.

Figure 7

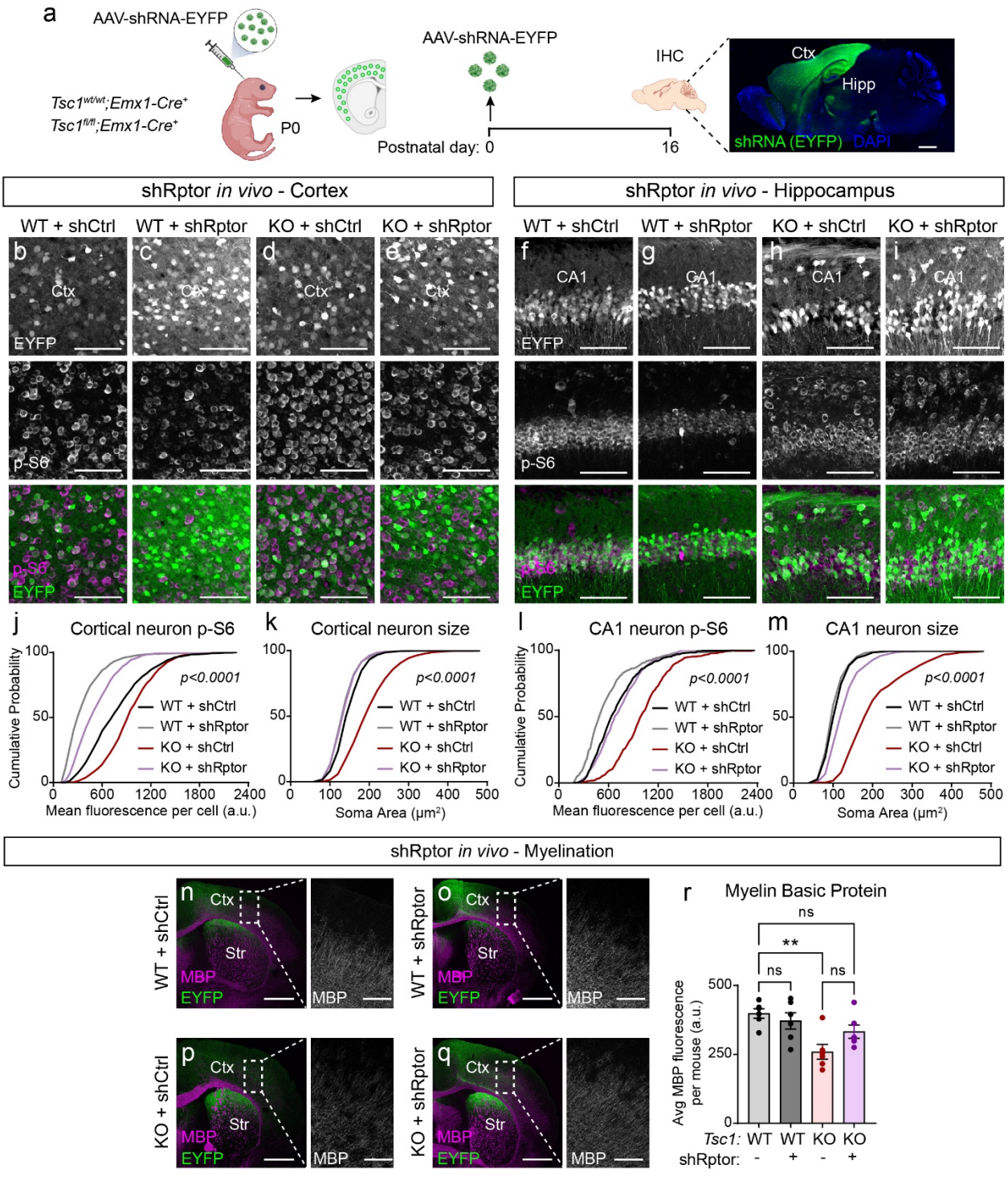
a
AAV-shRNA-EYFP
Tsc1wt/wt;Emx1-Cre+
Tsc1fl/fl;Emx1-Cre+
P0
AAV-shRNA-EYFP
Postnatal day: 0
16
IHC
Ctx
Hipp
shRNA (EYFP) DAPI
shRptor in vivo - Cortex
shRptor in vivo - Hippocampus
WT + shCtrl
WT + shRptor
KO + shCtrl
KO + shRptor
EYFP
p-S6
CA1
j Cortical neuron p-S6
k Cortical neuron size
l CA1 neuron p-S6
m CA1 neuron size
Cumulative Probability
p<0.0001
Mean fluorescence per cell (a.u.)
Soma Area (μm²)
shRptor in vivo - Myelination
MBP
Str
r Myelin Basic Protein
Avg MBP fluorescence per mouse (a.u.)
ns
**
Tsc1:
shRptor:

Figure 7. Postnatal Raptor reduction improves cellular phenotypes in Tsc1-cKO mice.
a) Schematic of the experiment. P0 pups received intracranial injections with AAV-shRptor-EYFP or AAV-shControl-EYFP (shCtrl). Brains were analyzed by immunohistochemistry at P16. Example sagittal brain image of an injected mouse at P16 showing EYFP expression in green and DAPI in blue. Ctx=cortex; Hipp=hippocampus. Scale bar=1 mm. Created with BioRender.com.
b-e) Representative images of the primary somatosensory cortex of *Tsc1*$^{wt/wt}$*;Emx1-Cre*$^{+}$ (WT, b-c) and *Tsc1*$^{fl/fl}$*;Emx1-Cre*$^{+}$ (KO, d-e) mice injected with shRptor-EYFP or shCtrl-EYFP virus showing EYFP (top panels) and p-S6 240/244 immunostaining (middle panels). Bottom panels show merged images. Scale bars=100 µm.
f-i) Representative images of the CA1 region of WT (f-g) and KO (h-i) mice injected with shRptor-EYFP or shCtrl-EYFP virus showing EYFP (top panels) and p-S6 240/244 immunostaining (middle panels). Bottom panels show merged images. Scale bars=100 µm.
j) Cumulative distributions of p-S6 levels in cortical EYFP+ neurons for the indicated genotypes. n=1086 WT+shCtrl, 1095 WT+shRptor, 1095 Tsc1-KO+shCtrl, and 1087 Tsc1-KO+shRptor neurons from 6 mice per group. Kruskal-Wallis test, p<0.0001; WT+shCtrl vs WT+shRptor, p<0.0001; WT+shCtrl vs Tsc1-KO+shCtrl, p<0.0001; WT+shCtrl vs Tsc1-KO+shRptor, p<0.0001; Tsc1-KO+shCtrl vs Tsc1-KO+shRptor, p<0.0001; Dunn's multiple comparison tests.
k) Cumulative distributions of EYFP+ cortical neuron soma area for the indicated genotypes. n is the same as in panel j. Kruskal-Wallis test, p<0.0001; WT+shCtrl vs WT+shRptor, p<0.0001; WT+shCtrl vs Tsc1-KO+shCtrl, p<0.0001; WT+shCtrl vs Tsc1-KO+shRptor, p<0.0001; Tsc1-KO+shCtrl vs Tsc1-KO+shRptor, p<0.0001; Dunn's multiple comparison tests.
l) Cumulative distributions of p-S6 levels in CA1 EYFP+ neurons for the indicated genotypes. n=514 WT+shCtrl, 507 WT+shRptor, 512 Tsc1-KO+shCtrl, and 497 Tsc1-KO +shRptor neurons from 6 mice per group. Kruskal-Wallis test, p<0.0001; WT+shCtrl vs WT+shRptor, p<0.0001; WT+shCtrl vs Tsc1-KO+shCtrl, p<0.0001; WT+shCtrl vs Tsc1-KO+shRptor, p=0.4315; Tsc1-KO+shCtrl vs Tsc1-KO+shRptor, p<0.0001; Dunn's multiple comparison tests.
m) Cumulative distributions of EYFP+ CA1 neuron soma area for the indicated genotypes. n is the same as for panel l. Kruskal-Wallis test, p<0.0001; WT+shCtrl vs WT+shRptor, p=0.2318; WT+shCtrl vs Tsc1-KO+shCtrl, p<0.0001; WT+shCtrl vs Tsc1-KO+shRptor, p<0.0001; Tsc1-KO+shCtrl vs Tsc1-KO+shRptor, p<0.0001; Dunn's multiple comparison tests.
n-q) Representative images of primary somatosensory cortex from mice of the indicated genotypes and treatments showing EYFP (green) and myelin basic protein (MBP, magenta) immunostaining. Scale bars=1 mm. Str=striatum. Right panels show zoomed-in images of MBP immunostaining within the boxed cortical regions; scale bars=250 µm
r) Mean +/- SEM bulk MBP fluorescence intensity in the boxed cortical regions shown in panels n-q for the indicated genotypes. n=6 animals per condition. Kruskal-Wallis, p=0.0114; WT+shCtrl vs WT+shRptor, p>0.9999; WT+shCtrl vs Tsc1-KO+shCtrl, **p=0.0077; WT+shCtrl vs Tsc1-KO+shRptor, p=0.4833; Tsc1-KO+shCtrl vs Tsc1-KO+shRptor, p=0.4833; Dunn's multiple comparison tests. ns=non-significant.
See also Supplementary Figures 9 and 10.

Figure 8

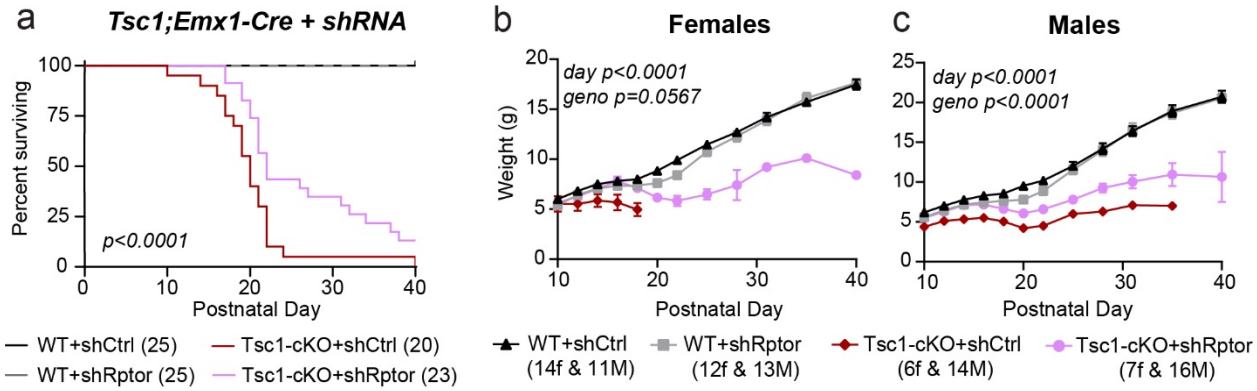

Figure 8. Postnatal Raptor reduction extends survival and improves development of Tsc1-cKO mice.
a) Survival analysis of *Tsc1$^{wt/wt}$;Emx1-Cre^{+}* (WT) and *Tsc1$^{fl/fl}$;Emx1-Cre^{+}* (KO) injected with AAV-shRptor or AAV-shControl. The number of mice for each genotype is indicated in parentheses. P values from Log-rank Mantel-Cox tests are shown on the graphs.
b-c) Mean +/- SEM body weight in grams measured from postnatal day 10 to 40 for mice of the indicated sex and genotype. The number of mice for each genotype and is indicated in parentheses. f=females, m=males. Mixed-effects model (REML) statistics: *Tsc1;Emx1-Cre* females (b), day p<0.0001, F(2.310, 70.56) = 380.3; geno p=0.0567, F(3, 35) = 2.759. *Tsc1;Emx1-Cre* males (c), day p<0.0001, F(1.638, 62.53) = 299.7; geno p<0.0001, F(3, 50) = 13.58
.

Supplementary Figures and Tables

Supplementary Figure 1

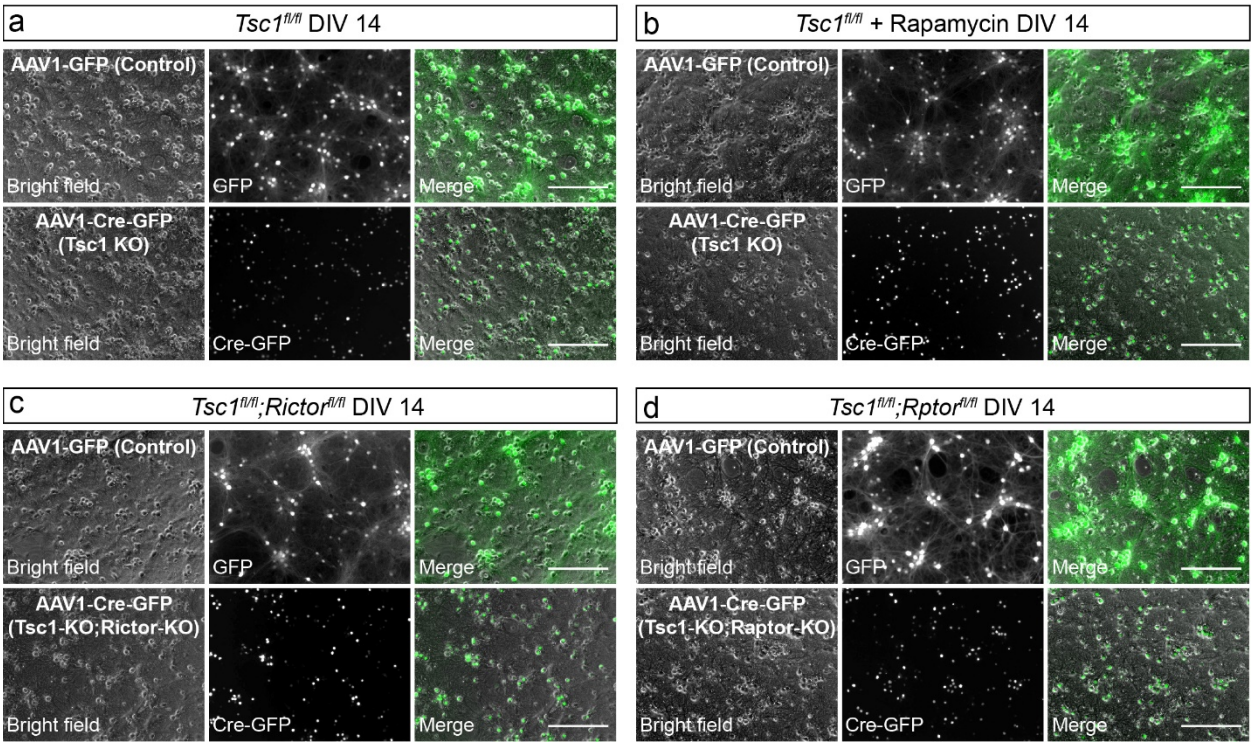

Supplementary Figure 1. Example images of primary hippocampal cultures.
Related to Figures 1-3.
Representative bright-field and fluorescence images of primary hippocampal cultures from P0-P1 pups imaged on DIV 14. The cultures were transduced on DIV 2 with AAV-GFP (cytosolic expression) or AAV-Cre-GFP (nuclear localized).
a) *Tsc1*$^{fl/fl}$ cultures + GFP (Control, top panels) or Cre-GFP (Tsc1 KO, bottom panels)
b) *Tsc1*$^{fl/fl}$ cultures + GFP (Control, top panels) or Cre-GFP (Tsc1 KO, bottom panels) treated with rapamycin (50 nM) from DIV 10-14.
c) *Tsc1*$^{fl/fl}$*;Rictor*$^{fl/fl}$ cultures + GFP (Control, top panels) or Cre-GFP (Tsc1-KO;Rictor-KO, bottom panels).
d) *Tsc1*$^{fl/fl}$*;Rptor*$^{fl/fl}$ cultures + GFP (Control, top panels) or Cre-GFP (Tsc1-KO;Raptor-KO, bottom panels)
All scale bars=250 µm

Supplementary Figure 2

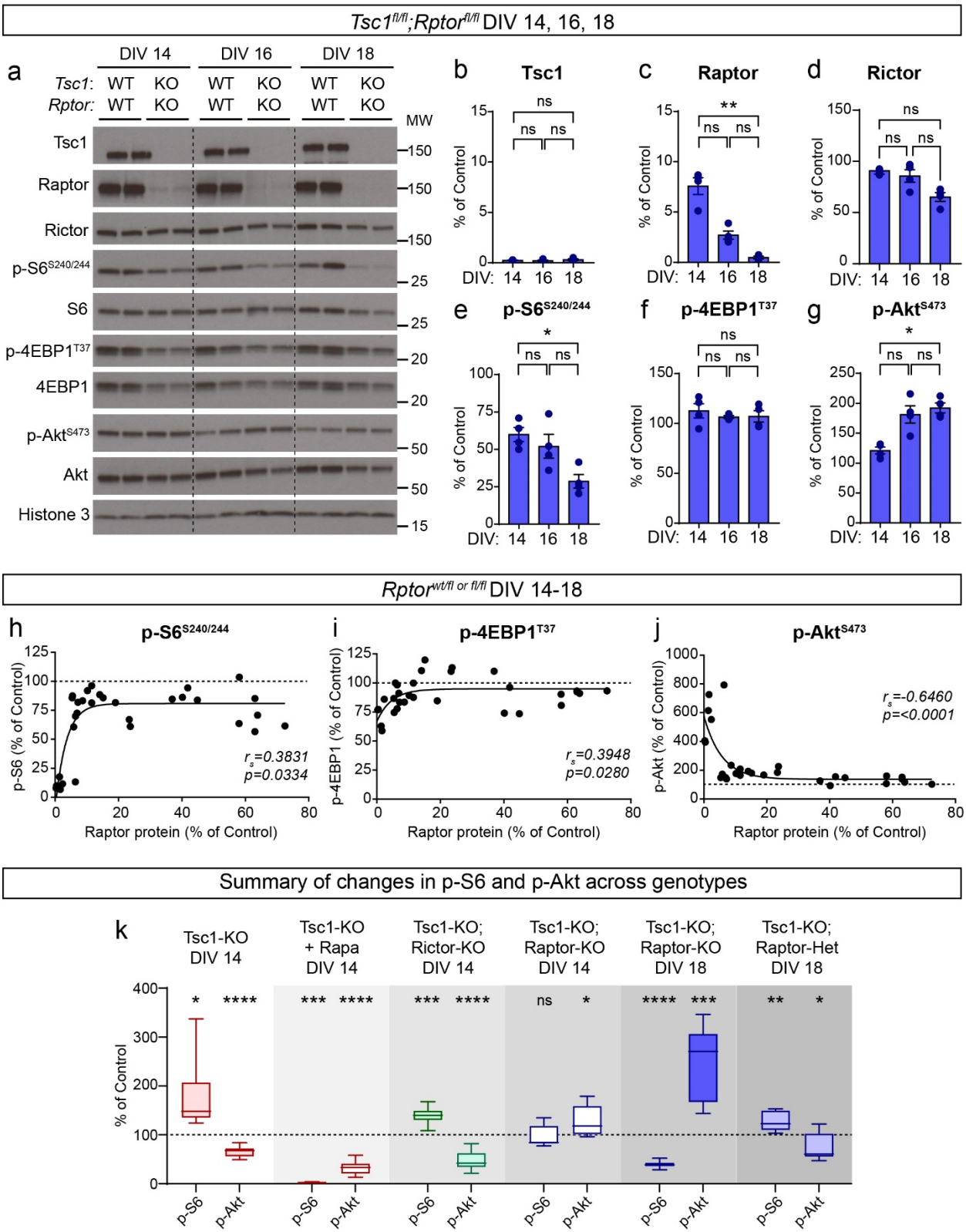

Supplementary Figure 2. Raptor reduction affects both mTORC1 and mTORC2 signaling. Related to Figures 1-3.

a) Representative western blots of lysates from *Tsc1$^{fl/fl}$;Rptor $^{fl/fl}$* hippocampal cultures treated with GFP (WT;WT) or Cre-GFP (KO;KO) on DIV 2 and collected at different time points (DIV 14, 16, and 18). MW indicates molecular weight. Two samples per genotype are shown; this experiment was replicated two times.

b-g) Bar graphs display western blot quantification (mean +/- SEM) for the indicated proteins. The data have been normalized to control values (WT;WT samples) for each DIV. Phospho-proteins were normalized to their respective total proteins. Dots represent data from individual culture wells. For all genotypes n=2 culture wells from 2 independent cultures; 2 mice per culture.

b) Tsc1, Kruskal-Wallis, p=0.5101; D14 vs D16, p>0.9999; D16 vs D18, p=0.7179; D14 vs D18, p>0.9999; Dunn's multiple comparisons tests. ns=non-significant.

c) Raptor, Kruskal-Wallis, p=0.0002; D14 vs D16, p=0.3500; D16 vs D18, p=0.3500; D14 vs D18, **p=0.0051; Dunn's multiple comparisons tests.

d) Rictor, Kruskal-Wallis, p=0.0263; D14 vs D16, p>0.9999; D16 vs D18, p=0.1184; D14 vs D18, p=0.0558 Dunn's multiple comparisons tests.

e) p-S6 240/244, Kruskal-Wallis, p=0.0194; D14 vs D16, p>0.9999; D16 vs D18, p=0.1873; D14 vs D18, *p=0.0324; Dunn's multiple comparisons tests.

f) p-4EBP1 T37, Kruskal-Wallis, p=0.7463; D14 vs D16, p>0.9999; D16 vs D18, p>0.9999; D14 vs D18, p>0.9999; Dunn's multiple comparisons tests.

g) p-Akt Ser473, Kruskal-Wallis, p=0.0132; D14 vs D16, p=0.0723; D16 vs D18, p>0.9999; D14 vs D18, *p=0.0427; Dunn's multiple comparisons tests.

h-j) Correlation of Raptor protein levels to p-S6 Ser240/244 (h), p-4EBP1 T37 (i), or p-Akt Ser473 (j) levels within each culture, expressed as a percentage of Control. Samples were pooled across hippocampal cultures from *Rptor$^{wt/fl\ or\ fl/fl}$* mice treated with AAV-GFP or AAV-Cre-GFP and harvested on different days (DIV 14-18) to generate a range of Raptor protein levels. Solid lines depict non-linear regression. Dashed lines represent control levels. Dots represent individual culture wells, n=31 culture wells. For panel h, r= 0.3831, p=0.0334, Spearman correlation. For panel i, r=0.3948, p =0.0280, Spearman correlation. For panel j, r= -0.6460, ****p<0.0001, Spearman correlation.

k) Box-and-whisker plots (min to max) displaying the p-S6 Ser240/244 and p-Akt Ser473 western blot results for the indicated conditions, expressed as a percentage of their respective controls. Data are replotted from Figs. 1-3. Dashed line indicates control levels.

Supplementary Figure 3

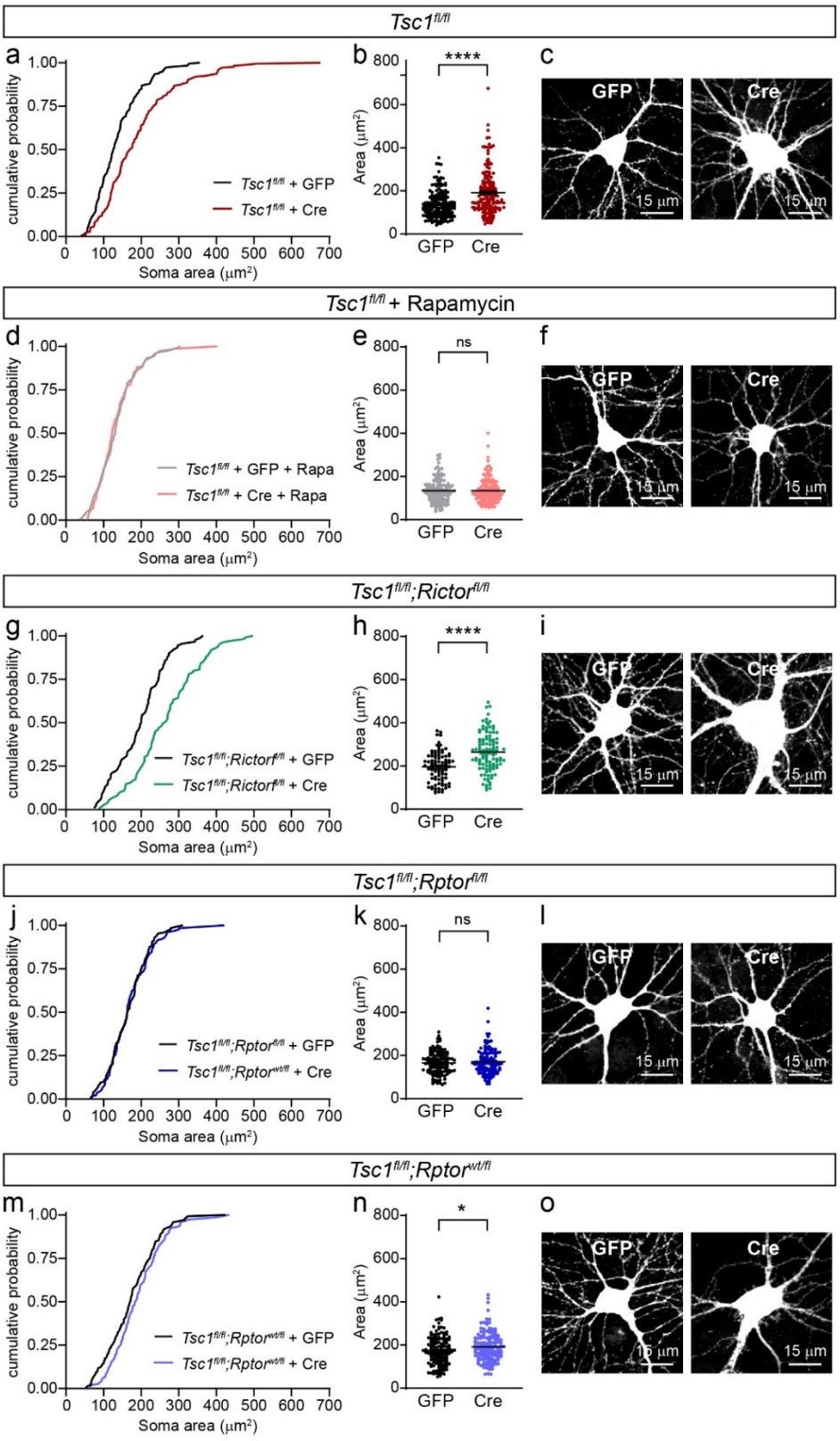

Supplementary Figure 3. Hypertrophy of Tsc1-cKO neurons is prevented by genetic reduction of Raptor but not Rictor.
Related to Figure 3.
a) Cumulative distributions of soma area for cultured *Tsc1$^{fl/fl}$* neurons treated with AAV-GFP (control) or AAV-Cre-mCherry and AAV-FLEx-tdTomato (Tsc1-KO). n=182 GFP+ and 175 Cre+ neurons.
b) Scatter dot plot of the data in panel a. Black lines indicated mean +/- SEM. Mann-Whitney, ****p<0.0001.
c) Example fluorescence images of *Tsc1$^{fl/fl}$* neurons expressing GFP (control) or mCherry and Cre-dependent tdTomato (Tsc1-KO).
d) Cumulative distributions of soma area for cultured *Tsc1$^{fl/fl}$* neurons treated with AAV-GFP (control) or AAV-Cre-mCherry and AAV-FLEx-tdTomato (Tsc1-KO). Cultures were treated with 50 nM rapamycin from DIV 10-14. n=147 GFP+ and 150 Cre+ neurons.
e) Scatter dot plot of the data in panel d. Black lines indicated mean +/- SEM. Mann-Whitney, p=0.7508.
f) Example fluorescence images of *Tsc1$^{fl/fl}$* neurons treated with rapamycin expressing GFP (control) or mCherry and Cre-dependent tdTomato (Tsc1-KO).
g) Cumulative distributions of soma area for cultured *Tsc1$^{fl/fl}$;Rictor$^{fl/fl}$* neurons treated with AAV-GFP (control) or AAV-Cre-mCherry and AAV-FLEx-tdTomato (Tsc1-KO;Rictor-KO). n=90 GFP+ and 109 Cre+ neurons.
h) Scatter dot plot of the data in panel g. Black lines indicated mean +/- SEM. Welch's t-test, ****p<0.0001.
i) Example fluorescence images of *Tsc1$^{fl/fl}$;Rictor$^{fl/fl}$* neurons expressing GFP (control) or mCherry and Cre-dependent tdTomato (Tsc1-KO;Rictor-KO).
j) Cumulative distributions of soma area for cultured *Tsc1$^{fl/fl}$;Rptor$^{fl/fl}$* neurons treated with AAV-GFP (control) or AAV-Cre-mCherry and AAV-FLEx-tdTomato (Tsc1-KO;Raptor-KO). n=128 GFP+ and 130 Cre+ neurons.
k) Scatter dot plot of the data in panel j. Black lines indicated mean +/- SEM. Mann-Whitney, p=0.8062.
l) Example fluorescence images of *Tsc1$^{fl/fl}$;Rptor$^{fl/fl}$* neurons expressing GFP (control) or mCherry and Cre-dependent tdTomato (Tsc1-KO;Raptor-KO).
m) Cumulative distributions of soma area for cultured *Tsc1$^{fl/fl}$;Rptor$^{wt/fl}$* neurons treated with AAV-GFP (control) or AAV-Cre-mCherry and AAV-FLEx-tdTomato (Tsc1-KO;Raptor-Het). n=144 GFP+ and 146 Cre+ neurons.
n) Scatter dot plot of the data in panel n. Black lines indicated mean +/- SEM. Mann-Whitney, *p=0.0452.
o) Example fluorescence images of *Tsc1$^{fl/fl}$;Rptor$^{wt/fl}$* neurons expressing GFP (control) or mCherry and Cre-dependent tdTomato (Tsc1-KO;Raptor-Het).
For all panels, cultures were harvested on DIV 14. Neurons were imaged from 4-5 culture wells from 3 independent culture preps, 2 pups per prep. ns=non-significant. Scale bars=15 μm.

Supplementary Figure 4

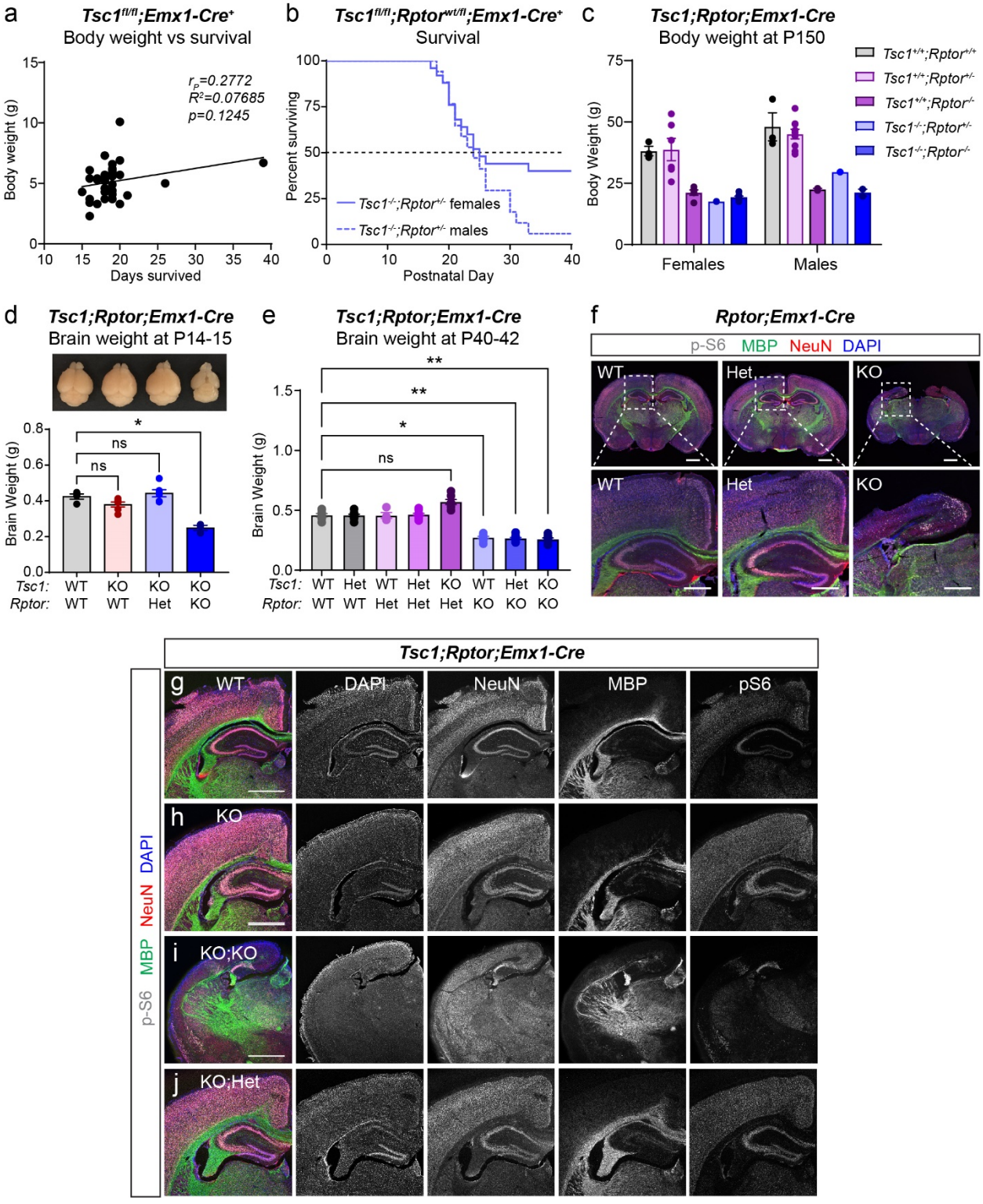

Supplementary Figure 4. Raptor reduction impacts brain and body weight, survival, and forebrain development
Related to Figure 4.

a) Scatterplot displaying the number of days *Tsc1$^{fl/fl}$;Emx1-Cre^{+}* (Tsc1-KO) mice survived versus their final recorded body weight. Dots represent individual mice, n=32. Tsc1-KO mice were pooled from the *Tsc1;Rptor;Emx1-Cre* and *Tsc1;Rictor;Emx1-Cre* lines. r= 0.2772, p=0.1245, Pearson correlation.

b) Survival analysis of *Tsc1$^{fl/fl}$;Rptor$^{wt/fl}$;Emx1-Cre^{+}* mice by sex. n=17 male and 25 female mice. Log-rank (Mantel-Cox) test, p=0.1024. Dashed black line indicates 50% of the population surviving.

c) Mean +/- SEM body weight of *Tsc1;Rptor;Emx1-Cre* mice of the indicated sex and genotype on postnatal day 150. Dots represent individual mice. n=3 male and 3 female Tsc1-WT;Raptor-WT mice; 9 male and 6 female Tsc1-WT;Raptor-Het mice; 2 male and 5 female Tsc1-WT;Raptor-KO mice; 1 male and 1 female Tsc1-KO;Raptor-Het mouse; and 2 male and 7 female Tsc1-KO;Raptor-KO mice.

d) Top, representative whole brain images from mice of the genotypes indicated under the respective bar graph. Bottom, mean +/- SEM brain weight from P14-15 mice of the indicated genotypes. Dots represent individual mice. n=4 Tsc1-WT;Raptor-WT mice, 6 Tsc1-KO;Raptor-WT mice, 6 Tsc1-KO;Raptor-Het mice, and 3 Tsc1-KO;Raptor-KO mice. Kruskal-Wallis, p=0.0027; WT;WT vs KO;WT, p=0.5730; WT;WT vs KO;Het, p>0.9999; WT;WT vs KO;KO, *p=0.0371; Dunn's multiple comparison tests. ns=non-significant.

e) Mean +/- SEM brain weight of P40-42 *Tsc1;Rptor;Emx1-Cre* mice of the indicated genotypes. Dots represent individual mice. n=8 Tsc1-WT;Raptor-WT, 10 Tsc1-Het;Rptor-WT, 4 Tsc1-WT;Rptor-Het, 10 Tsc1-Het;Rptor-Het, 7 Tsc1-KO;Rptor-Het, 8 Tsc1-WT;Rptor-KO, 11 Tsc1-Het;Rptor-KO, and 8 Tsc1-KO;Rptor-KO mice. Kruskal-Wallis, p<0.0001. Dunn's multiple comparisons tests to WT;WT: Het;WT, p>0.9999; WT;Het, p>0.9999; Het;Het, p>0.9999; KO;Het, p=0.4700; WT;KO, *p=0.0258; Het;KO, **p=0.0057; KO;KO, **p=0.0067.

f) Representative images of coronal brain sections showing p-S6 Ser240/244 (gray), myelin basic protein (MBP, green), and NeuN (red) immunostaining in P14 *Rptor$^{wt/wt}$;Emx1-Cre^{+}* (WT), *Rptor$^{wt/fl}$;Emx1-Cre^{+}* (Het) and *Rptor$^{fl/fl}$;Emx1-Cre^{+}* mice (all *Tsc1$^{wt/wt}$*). DAPI staining is in blue. Scale bars=1 mm. Bottom panels show zoomed-in images of the hippocampal regions indicated by the dashed boxes. Scale bars=500 μm.

g-j) Zoomed in regions from panels in Fig. 4i-l. Immunostaining of WT, Tsc1-KO (KO), Tsc1-KO;Raptr-Het (KO-Het) and Tsc1-KO;Raptor-KO (KO-KO) for p-S6 Ser240/244 is in grey, myelin basic protein (MBP) is in green, NeuN is in red and DAPI-labeled nuclei are in blue. Scale bars=1 mm

Supplementary Figure 5

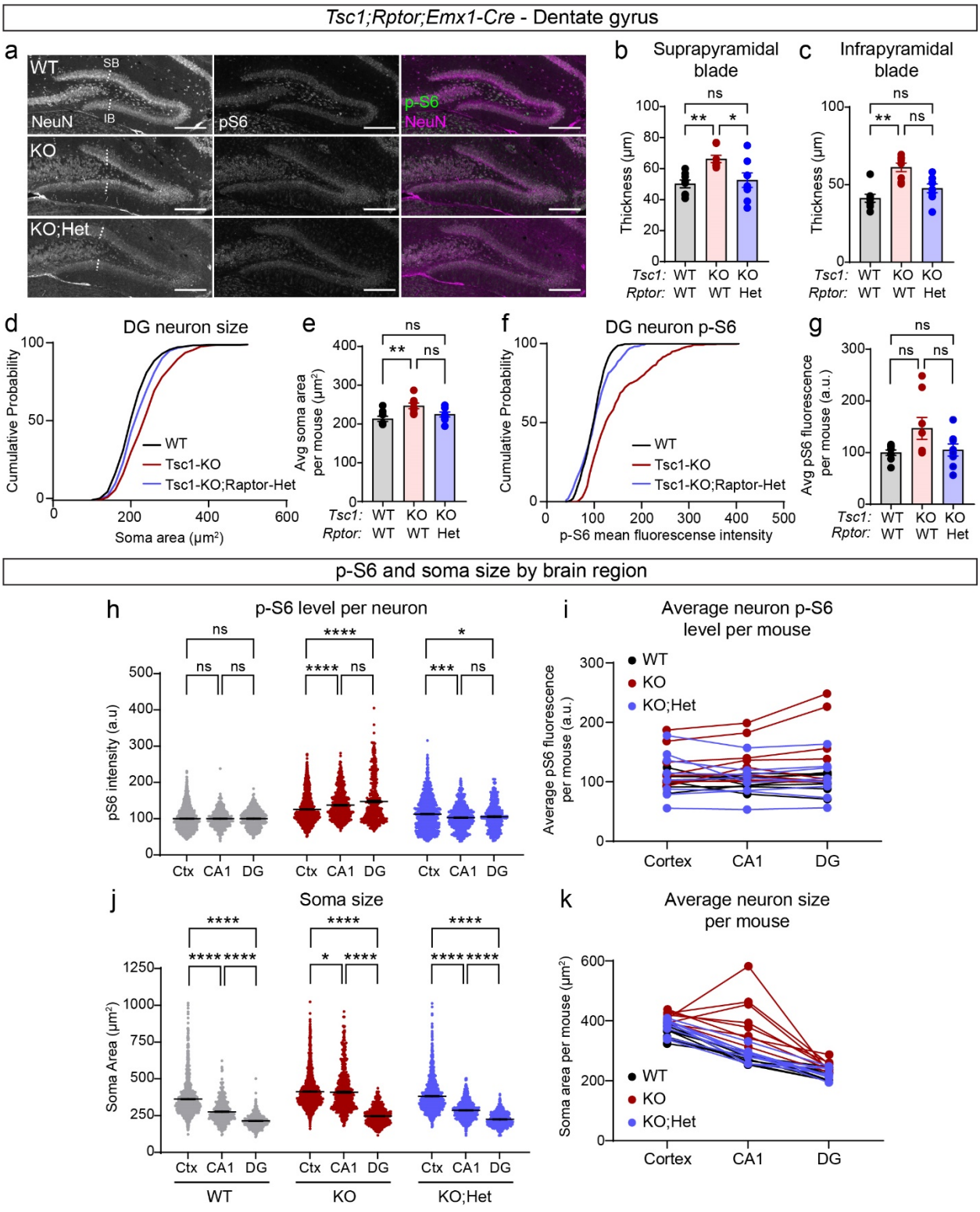

Supplementary Figure 5. p-S6 and soma size exhibit brain region-specific differences. Related to Figure 5.

a) Representative images from the dentate gyrus (DG) showing NeuN (left panels) and p-S6 Ser240/244 (middle panels) immunostaining in *Tsc1*$^{wt/wt}$*;Rptor*$^{wt/wt}$*;Emx1-Cre*$^{+}$ (WT), *Tsc1*$^{fl/fl}$*;Rptor*$^{wt/wt}$*;Emx1-Cre*$^{+}$ (KO), and *Tsc1*$^{fl/fl}$*;Rptor*$^{wt/fl}$*;Emx1-Cre*$^{+}$ (KO;Het) mice. Merged images on the right show NeuN in magenta and p-S6 in green. SB = Suprapyramidal blade, IB = Infrapyramidal blade. Lines denote the measurement of IB and SB thickness. Scale bars=250 µm

b) Mean +/- SEM thickness of the suprapyramidal blade for the indicated genotypes. Dots represent values from individual mice, n=8 mice per genotype. One-way ANOVA, p=0.0055, F(2, 21) = 6.745; WT vs KO, **p=0.0081; WT vs KO;Het, p=0.9473; KO vs KO;Het, *p=0.0253; Sidak's multiple comparisons tests. ns=non-significant.

c) Mean +/- SEM thickness of the infrapyramidal blade for the indicated genotypes. Dots represent values from individual mice, n=8 mice per genotype. Kruskal-Wallis, p=0.0019; WT vs KO, **p=0.0014; WT vs KO;Het, p=0.6093; KO vs KO;Het, p=0.0778; Sidak's multiple comparisons tests.

d) Cumulative distributions of dentate gyrus (DG) neuron soma area for the indicated genotypes. n=403 WT, 401 Tsc1-KO, and 400 Tsc1-KO;Rptor-Het neurons from 8 mice per genotype. Kruskal-Wallis, p<0.0001; WT vs KO, p<0.0001; WT vs KO;Het, p=0.0022; KO vs KO;Het, p<0.0001; Dunn's multiple comparisons tests.

e) Mean +/- DG neuron soma area per mouse for the indicated genotypes. Dots represent values from individual mice, n=8 mice per genotype. One-way ANOVA, p=0.0074, F(2, 21) = 6.257; WT vs KO, **p=0.0067; WT vs KO;Het, p=0.5700; KO vs KO;Het, p=0.0951; Sidak's multiple comparisons tests.

f) Cumulative distributions of DG p-S6 levels per neuron for the indicated genotypes. n is the same as for panel d. Kruskal-Wallis, p<0.0001; WT vs KO, p<0.0001; WT vs KO;Het, p=0.4109; KO vs KO;Het, p<0.0001; Dunn's multiple comparisons tests.

g) Mean +/- SEM DG neuron p-S6 levels per mouse for the indicated genotypes. Dots represent values from individual mice, n=8 mice per genotype. One-way ANOVA, p=0.0591, F (2, 21) = 3.246; WT vs KO, p=0.0883; WT vs KO;Het, p=0.9923; KO vs KO;Het, p=0.1456; Sidak's multiple comparisons tests.

h) Scatter dot plots of p-S6 levels per neuron for the cortex (Ctx), CA1 and DG regions for WT (grey dots), KO (red dots) and KO;Het (blue dots) mice. Black lines indicate mean +/- SEM. n=1601 WT Ctx neurons, 1605 KO Ctx neurons, 1602 KO;Het Ctx neurons, 561 WT CA1 neurons, 561 KO CA1 neurons, 561 KO;Het CA1 neurons, 403 WT DG neurons, 401 KO DG neurons, and 400 KO;Het DG neurons from 8 mice per genotype. WT p-S6 levels: Kruskal-Wallis test, p=0.0669; Ctx vs CA1, p=0.1806; Ctx vs DG, p=0.2338; CA1 vs DG, p>0.9999; Dunn's multiple comparison tests. KO p-S6 levels: Kruskal-Wallis test, p<0.0001; Ctx vs CA1, ****p<0.0001; Ctx vs DG, ****p<0.0001; CA1 vs DG, p>0.9999; Dunn's multiple comparison tests. KO;Het p-S6 levels: Kruskal-Wallis test, p=0.0001; Ctx vs CA1, ***p=0.0002, Ctx vs DG, *p=0.0485, CA1 vs DG, p>0.9999, Dunn's multiple comparison tests.

i) Average p-S6 levels per mouse for neurons in the cortex, CA1 and DG regions for WT (black dots), KO (red dots) and KO;Het (blue dots) mice. Lines connect data points from the same mouse. n=8 mice per genotype.

j) Scatter dot plots of soma area for neurons in the Ctx, CA1 and DG regions for WT (grey dots), KO (red dots) and KO;Het (blue dots) mice. n is the same as in panel h. WT soma area: Kruskal-Wallis test, p<0.0001; Ctx vs CA1, ****p<0.0001; Ctx vs DG, ****p<0.0001, CA1 vs DG, ****p<0.0001; Dunn's multiple comparison tests. KO soma area: Kruskal-Wallis test, p<0.0001; Ctx vs CA1, *p=0.0299, Ctx vs DG, ****p<0.0001; CA1 vs DG, ****p<0.0001, Dunn's multiple comparison tests. KO;Het soma area: Kruskal-Wallis test, p<0.0001; Ctx vs CA1, p<0.0001; Ctx vs CA1, ****p<0.0001; Ctx vs DG, ****p<0.0001, CA1 vs DG, ****p<0.0001, Dunn's multiple comparison tests.

k) Average soma size per mouse for neurons in the cortex, CA1 and DG regions for WT (black dots), KO (red dots) and KO;Het (blue dots) mice. Lines connect data points from the same mouse. n=8 mice per genotype.

Supplementary Figure 6

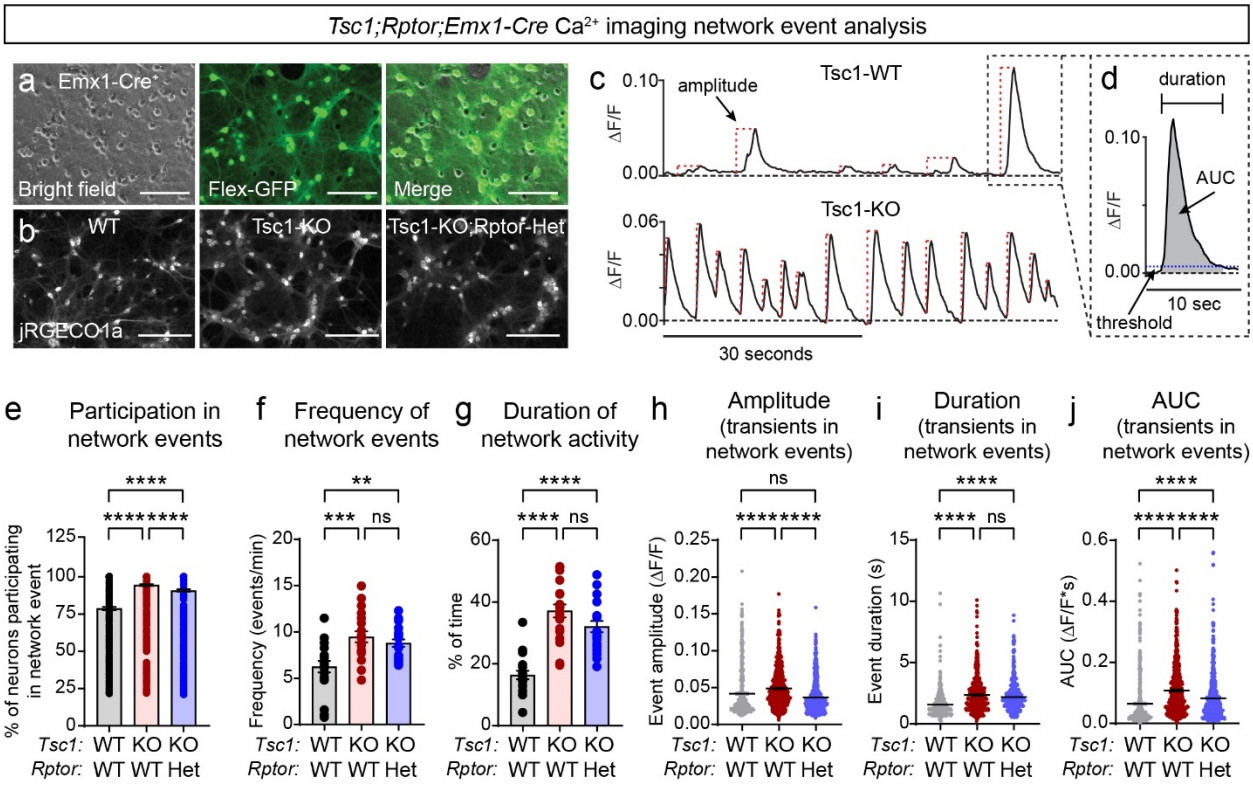

Supplementary Figure 6. Heterozygous deletion of *Rptor* partially improves network hyperactivity of Tsc1-cKO hippocampal cultures.
Related to Figure 6.

a) Representative images of a primary hippocampal culture from a *Tsc1$^{wt/wt}$;Emx1-Cre^{+}* mouse transduced with a Cre-dependent GFP expressing virus (AAV-Flex-GFP). Bright field (left panel), GFP fluorescence (middle panel) and merged (right panel) images are shown. Scale bars=150 µm

b) Representative images of cultures from *Tsc1$^{wt/wt}$;Rptor$^{wt/wt}$;Emx1-Cre^{+}* (WT), *Tsc1$^{fl/fl}$;Rptor$^{wt/wt}$;Emx1-Cre^{+}* (KO), and *Tsc1$^{fl/fl}$;Rptor$^{wt/fl}$;Emx1-Cre^{+}* (KO;Het) mice expressing jRGeco1a. Scale bars=250 µm.

c) Example of Ca^{2+} imaging analysis showing individual Ca^{2+} transients from a Tsc1-WT (top) and Tsc1-KO (bottom) neuron. Vertical red dashed lines indicate amplitude measurements. See Methods for additional details.

d) Example analysis of a single Ca^{2+} transient showing the duration, area under the curve (AUC, grey shaded region) and threshold (crossings of the threshold define event initiation and termination) measurements.

e) Mean +/- SEM percentage of neurons in a field of view that participated in a network event for the indicated genotypes. Each dot represents a network event. n=467 WT, 708 KO, and 657 KO;Het network events from 20 individual culture wells per genotype. Culture wells were from 6-7 independent culture preps, 1 pup per prep. Kruskal-Wallis, p<0.0001; WT vs KO, ****p<0.0001; WT vs KO;Het, ****p<0.0001; KO vs KO;Het, ****p<0.0001; Dunn's multiple comparisons tests.

f) Mean +/- SEM frequency of network events per culture for the indicated genotypes. Each dot represents a single culture well. n=20 individual culture wells per genotype, from 6-7 independent culture preps, 1 pup per prep. One-way ANOVA, p=0.0002, F (2, 57) = 9.773; WT vs KO, ***p=0.0003; WT vs KO;Het, **p=0.0049; KO vs KO;Het, p=0.7599; Sidak's multiple comparisons tests. ns=non-significant.

g) Mean +/- SEM duration of network activity, expressed as the percent of the recording time during which network events occurred for the indicated genotypes. Each dot represents a single culture well. n=20 individual culture wells per genotype, from 6-7 independent culture preps, 1 pup per prep. Kruskal-Wallis,

p<0.0001; WT vs KO, ****p<0.0001; WT vs KO;Het, ****p<0.0001; KO vs KO;Het, p=0.5496; Dunn's multiple comparisons tests.
h) Scatter dot plot of the average Ca^{2+} transient amplitude per network event for the indicated genotypes. Black lines indicate the mean +/- SEM. n is the same as for panel e. Kruskal-Wallis, p<0.0001; WT vs KO, ****p<0.0001; WT vs KO;Het, p>0.9999; KO vs KO;Het, ****p<0.0001; Dunn's multiple comparison tests.
i) Scatter dot plot of the average Ca^{2+} transient duration per network event for the indicated genotypes. Black lines indicate the mean +/- SEM. n is the same as for panel e. Kruskal-Wallis, p<0.0001; WT vs KO, ****p<0.0001; WT vs KO;Het, ****p<0.0001; KO vs KO;Het, p>0.9999; Dunn's multiple comparison tests.
j) Scatter dot plot the average Ca^{2+} transient AUC per network event for the indicated genotypes. Black lines indicate the mean +/- SEM. n is the same as for panel e. Kruskal-Wallis, p<0.0001; WT vs KO, ****p<0.0001; WT vs KO;Het, ****p<0.0001; KO vs KO;Het, ****p<0.0001; Dunn's multiple comparison tests.

Supplementary Figure 7

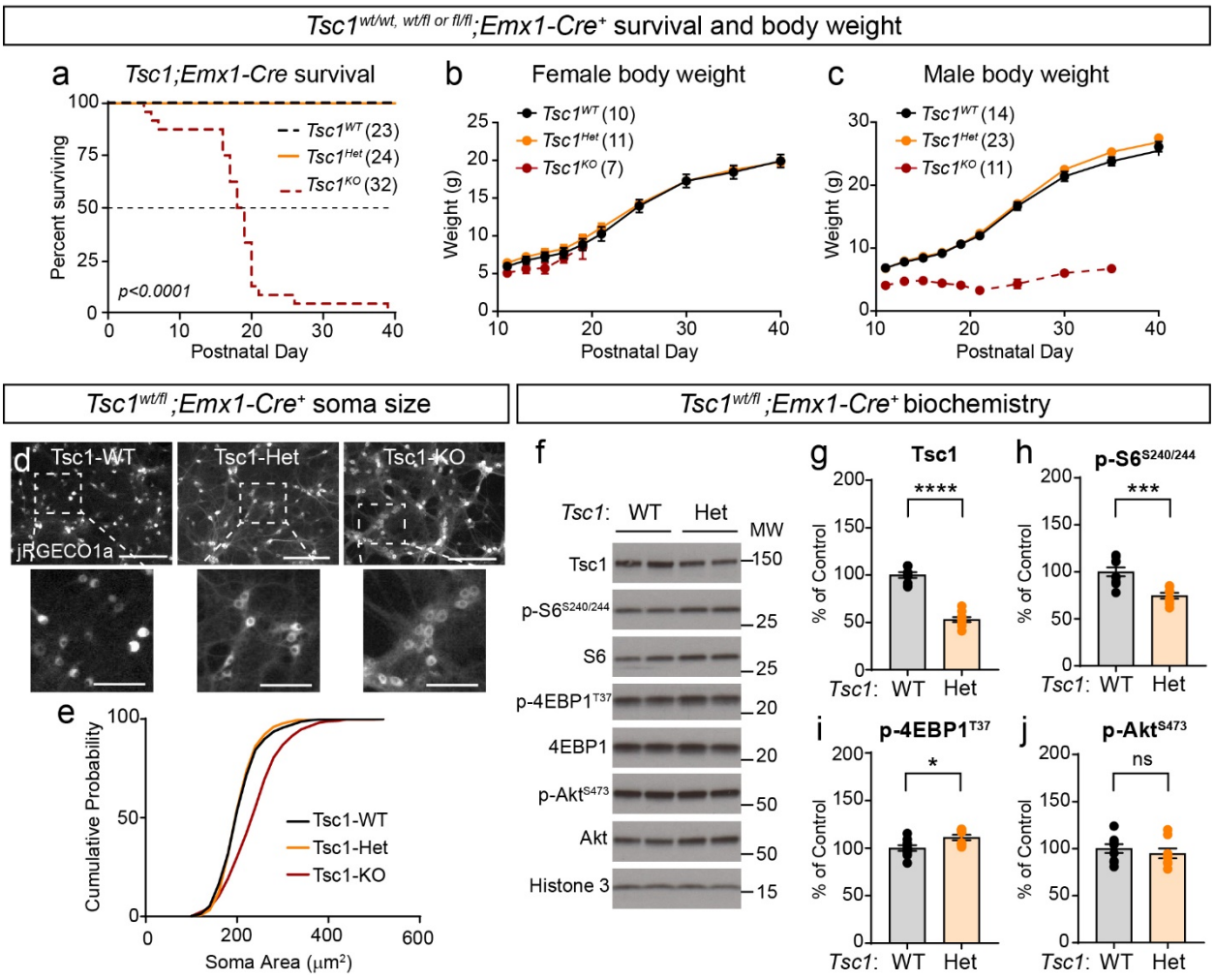

Supplementary Figure 7. Heterozygous deletion of *Tsc1* does not affect survival, body weight, or soma size.

Related to Figures 1, 4 and 6.

a) Survival analysis of *Tsc1*$^{wt/wt}$;*Rptor*$^{wt/wt}$;*Emx1*-Cre^{+} (*Tsc1*^{WT}), *Tsc1*$^{wt/fl}$;*Rptor*$^{wt/wt}$;*Emx1*-Cre^{+} (*Tsc1*^{Het}), and *Tsc1*$^{fl/fl}$;*Rptor*$^{wt/wt}$;*Emx1*-Cre^{+} (*Tsc1*^{KO}) mice. Data for *Tsc1*^{WT} and *Tsc1*^{KO} mice are re-plotted from Fig. 4c for reference. The number of mice for each genotype is indicated in parentheses. Dashed line indicates 50% of the population surviving. P value from Log-rank Mantel-Cox tests is shown.

b,c) Mean +/- SEM body weight in grams measured from postnatal day 11 to 40 for female (b) and male (c) mice of the indicated genotypes. Data for *Tsc1*^{WT} and *Tsc1*^{KO} mice are re-plotted from Fig. 4e,f for reference. The number of mice for each genotype is indicated in parentheses. Mixed-effects model (REML) statistics: Females (b), day p<0.0001, F (1.199, 25.84) = 1056; geno p=0.0569, F (2, 25) = 3.221. Males (c), day p<0.0001, F (1.792, 71.09) = 1113; geno p<0.0001, F (2, 44) = 29.07.

d) Representative images of *Tsc1*$^{wt/wt}$;*Emx1*-Cre^{+} (WT), *Tsc1*$^{wt/fl}$;*Emx1*-Cre^{+} (Tsc1-Het) and *Tsc1*$^{fl/fl}$;*Emx1*-Cre^{+} (Tsc1-KO) primary hippocampal cultures expressing jRGeco1a on DIV 14. Scale bars for top panels=250 μm. Scale bars for in zoomed-in images (bottom panels)=100 μm.

e) Cumulative distributions of soma area for WT, Tsc1-Het and Tsc1-KO cultured hippocampal neurons. n=454 WT, 451 Tsc1-Het and 453 Tsc1-KO neurons from 5 independent culture preps, 1 pup per prep. Kruskal-Wallis test, p<0.0001; WT vs Het, p>0.9999; WT vs KO, ****p<0.0001; Het vs KO, ****p<0.0001; Dunn's multiple comparison tests.

f) Representative western blots of lysates collected from Tsc1-WT and Tsc1-Het primary hippocampal cultures. MW indicates molecular weight. Two independent samples per genotype are shown; this experiment was replicated three times.
g-j) Bar graphs display western blot quantification (mean +/- SEM) for Tsc1 (g) Welch's test, ****p<0.0001; p-S6 Ser240/244 (h) Welch's test, ***p= 0.0005; p-4EBP1 T37 (i) Mann-Whitney test, *p= 0.0152; and p-Akt Ser473 (j) Welch's test, p= 0.4734. Phospho-proteins were normalized to their respective total proteins. Dots represent data from individual culture wells. n=9 WT and 8 Tsc1-Het culture wells from 3 independent culture preps, 1 pup per prep.

Supplementary Figure 8

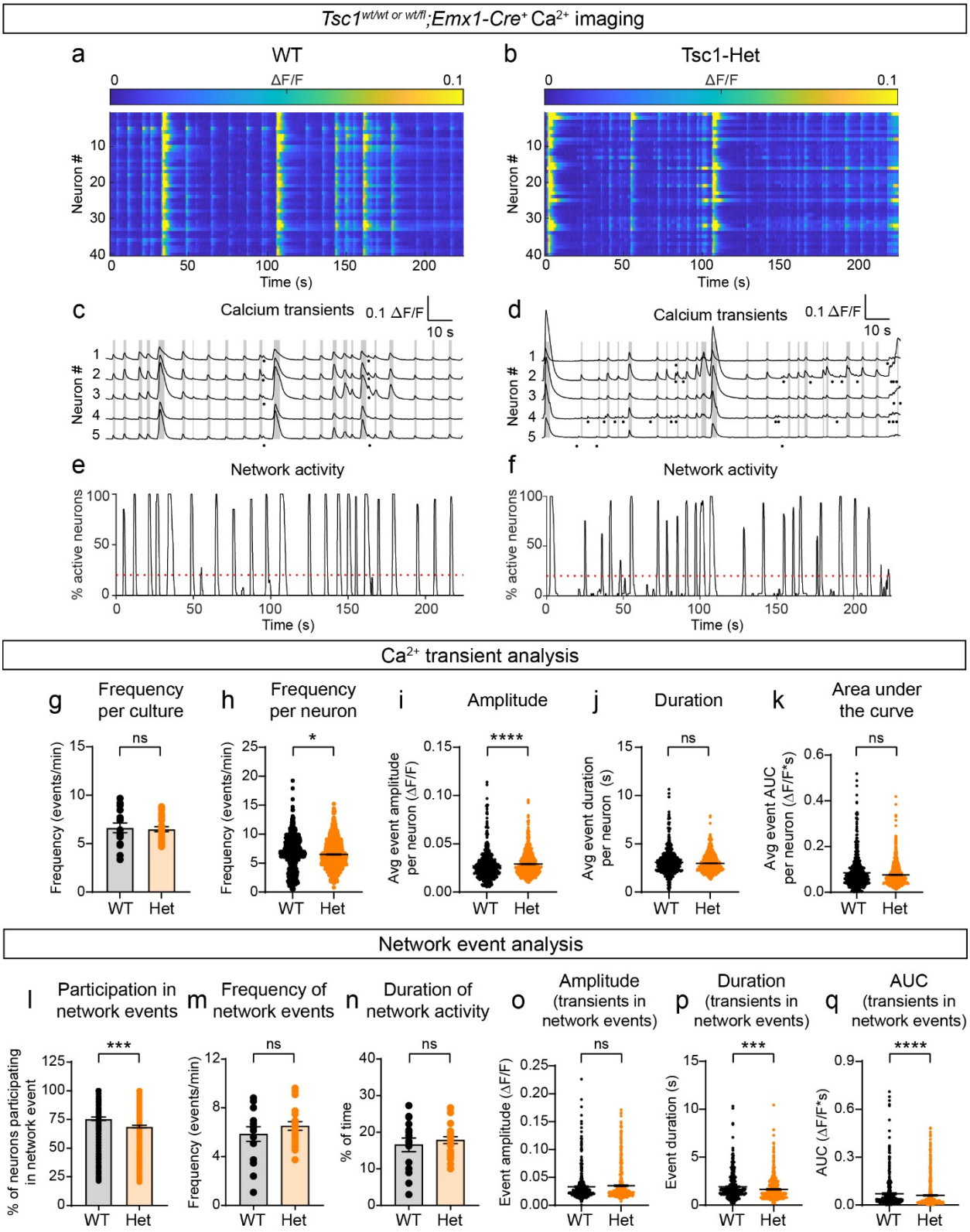

Supplementary Figure 8. Loss of one copy of *Tsc1* does not induce neuronal or network hyperexcitability.
Related to Figure 6.

a,b) Representative heatmaps of ΔF/F for 40 neurons imaged in a field of view from *Tsc1*$^{wt/wt}$;*Emx1*-Cre^{+} (WT) and *Tsc1*$^{wt/fl}$;*Emx1*-Cre^{+} (Tsc1-Het) cultures.

c,d) Ca^{2+} transients from 5 representative neurons imaged in a field of view from WT (c) and Tsc1-Het (d) cultures. Grey lines indicate network events with more than 20% of neurons in the field of view active at the same time. Black dots represent spontaneous Ca^{2+} transients that were not part of network events.

e,f) Graphs show the percentage of neurons in the field of view that were active at a given time for WT (d) and Tsc1-Het (e) cultures. One representative culture is shown per genotype. Red dashed lines at 20% indicate the threshold for a network event.

g) Mean +/- SEM Ca^{2+} transient frequency per culture. Dots represent values from individual cultures. For WT: n=15 individual culture wells from 5 independent culture preps, 1 pup per prep for WT. For Tsc1-Het: n=24 individual culture wells from 9 independent culture preps, 1 pup per prep. Welch's test, p=0.8128; ns=non-significant.

h) Scatter dot plot of the Ca^{2+} transient frequency per neuron for the indicated genotypes. Black lines indicate mean +/- SEM. For WT: n=600 neurons from 15 individual culture wells from 5 independent culture preps, 1 pup per prep. For Tsc1-Het: n=960 neurons from 24 individual culture wells from 9 independent culture preps, 1 pup per prep. Mann-Whitney test, *p = 0.0402.

i) Scatter dot plot of the average Ca^{2+} transient amplitude per neuron for the indicated genotypes. n is the same as for panel h. Mann-Whitney test, ****p<0.0001.

j) Scatter dot plot of the average Ca^{2+} transient duration per neuron for the indicated genotypes. n is the same as for panel h. Mann-Whitney test, p=0.0932.

k) Scatter dot plot of the average Ca^{2+} transient area under the curve (AUC) per neuron for the indicated genotypes. n is the same as for panel h. Mann-Whitney test, p=0.4472.

l) Mean +/- SEM percentage of neurons in a field of view that participated in a network event for the indicated genotypes. Each dot represents a network event. For WT: n=362 network events from 15 individual culture wells from 5 independent culture preps, 1 pup per prep. For Tsc1-Het: n=585 network events from 24 individual culture wells from 9 independent culture preps, 1 pup per prep. Mann-Whitney test, ***p=0.0005.

m) Mean +/- SEM frequency of network events per culture for the indicated genotypes. Each dot represents a single culture well. For WT: n=15 individual culture wells from 5 independent culture preps, 1 pup per prep. For Tsc1-Het: n=24 individual culture wells from 9 independent culture preps, 1 pup per prep. Welch's test, p=0.3462.

n) Mean +/- SEM duration of network activity, expressed as the percent of the recording time during which network events occurred for the indicated genotypes. Each dot represents a single culture well. n is the same as for panel m. Welch's test, p=0.5464

o) Scatter dot plot of the average Ca^{2+} transient amplitude per network event for the indicated genotypes. Black lines indicate the mean +/- SEM. n is the same as for panel l. Mann-Whitney, p=0.8654.

p) Scatter dot plot of the average Ca^{2+} transient duration per network event for the indicated genotypes. Black lines indicate the mean +/- SEM. n is the same as for panel l. Mann-Whitney, ***p=0.0003.

q) Scatter dot plot of the average Ca^{2+} transient AUC per network event for the indicated genotypes. Black lines indicate the mean +/- SEM. n is the same as for panel l.
Mann-Whitney, ****p<0.0001.

Supplementary Figure 9

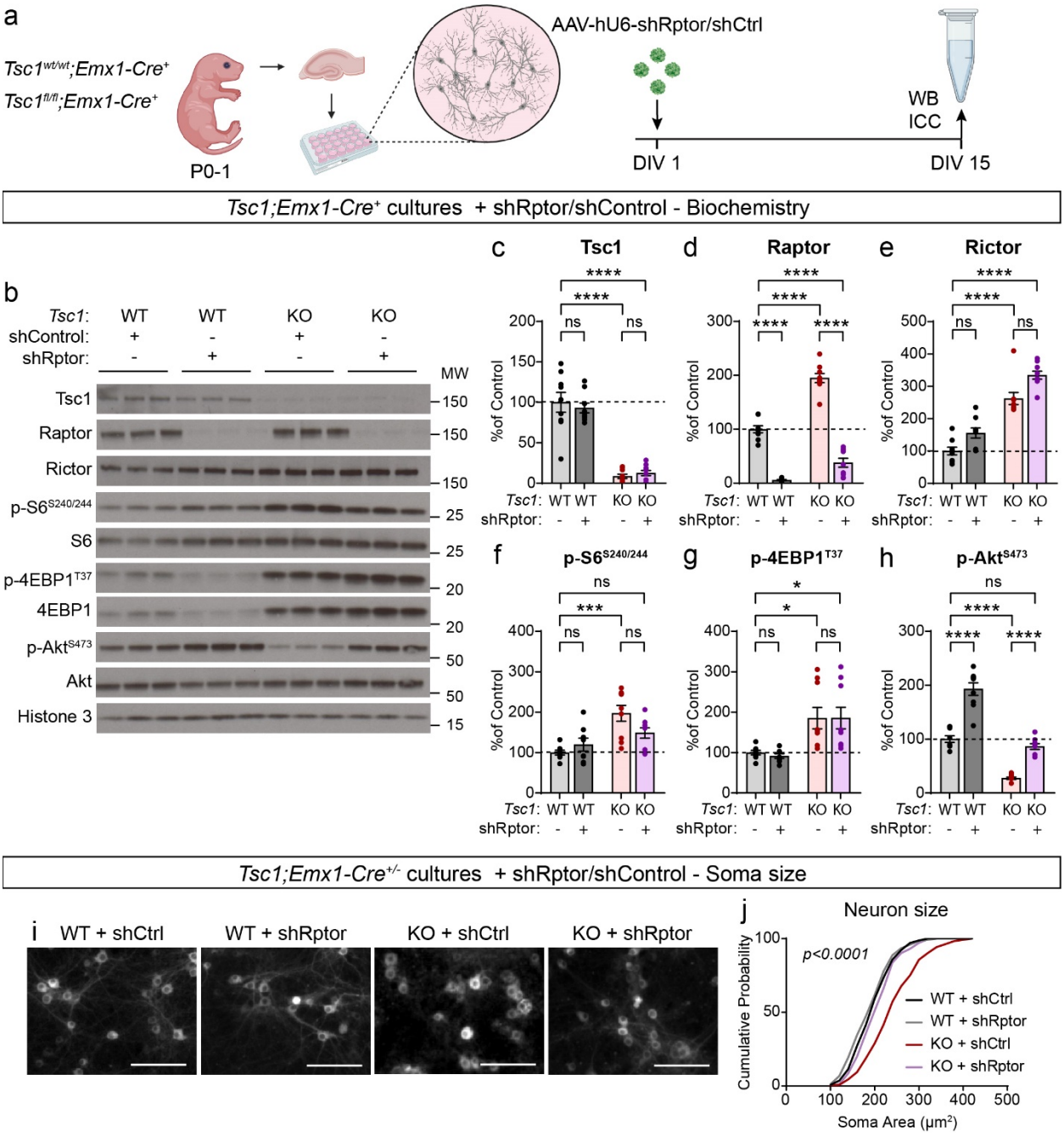

Supplementary Figure 9. shRptor rebalances mTOR signaling and rescues neuronal hypertrophy in cultured Tsc1-KO neurons.
Related to Figure 7.
a) Schematic of the experiment. Primary hippocampal cultures were prepared from P0-1 *Tsc1$^{wt/wt}$;Emx1-Cre^{+}* (WT) and *Tsc1$^{fl/fl}$;Emx1-Cre^{+}* (Tsc1-KO) mice and transduced with AAV-shControl-EYFP (shControl) or AAV-shRptor-EYFP (shRptor) on DIV 1. Cell were collected for analysis by western blot (WB) or immunocytochemistry (ICC) on DIV 15. Created with BioRender.com

b) Representative western blots of lysates collected from WT and Tsc1-KO primary hippocampal cultures treated with shControl or shRptor. MW indicates molecular weight. Three samples per genotype and treatment are shown; this experiment was replicated three times.
c-h) Bar graphs display western blot quantification (mean +/- SEM) for the indicated proteins, expressed as a percentage of control (WT + shControl) levels. Phospho-proteins were normalized to their respective total proteins. Dots represent data from individual culture wells. n=8-9 culture wells per condition from 3 independent culture preps, 1 pup per prep.
c) Tsc1, One-way ANOVA, $p<0.0001$, $F(3, 32) = 48.58$; WT+shControl vs WT+shRptor, $p= 0.9360$; WT+shControl vs KO+shControl, ****$p<0.0001$; WT+shControl vs KO+shRptor, ****$p<0.0001$; KO+shControl vs KO+shRptor, $p=0.9918$; Sidak's multiple comparison tests. ns=non-significant.
d) Raptor, One-way ANOVA, $p<0.0001$, $F(3, 32) = 153.6$; WT+shControl vs WT+shRptor, ****$p<0.0001$; WT+shControl vs KO+shControl, ****$p<0.0001$; WT+shControl vs KO+shRptor, ****$p<0.0001$; KO+shControl vs KO+shRptor, ****$p<0.0001$; Sidak's multiple comparison tests.
e) Rictor, Kruskal-Wallis, $p<0.0001$; WT+shControl vs WT+shRptor, $p=0.8411$; WT+shControl vs KO+shControl, **$p=0.0023$; WT+shControl vs KO+shRptor, ****$p<0.0001$; KO+shControl vs KO+shRptor, $p=0.5592$; Dunn's multiple comparison tests.
f) p-S6 Ser240/244, One-way ANOVA, $p=0.0004$, $F(3, 30) = 8.234$; WT+shControl vs WT+shRptor, $p=0.8388$; WT+shControl vs KO+shControl, ***$p=0.0003$; WT+shControl vs KO+shRptor, $p=0.1045$; KO+shControl vs KO+shRptor, $p=0.0894$; Sidak's multiple comparison tests.
g) p-4EBP1 T37, One-way ANOVA, $p=0.0015$, $F(3, 30) = 6.582$; WT+shControl vs WT+shRptor, $p=0.9973$; WT+shControl vs KO+shControl, *$p=0.0224$; WT+shControl vs KO+shRptor,* $p=0.0220$; KO+shControl vs KO+shRptor, $p>0.9999$; Sidak's multiple comparison tests.
h) p-Akt Ser473, One-way ANOVA, $p<0.0001$, $F(3, 32) = 92.30$; WT+shControl vs WT+shRptor, ****$p<0.0001$; WT+shControl vs KO+shControl, ****$p<0.0001$; WT+shControl vs KO+shRptor, $p=0.5561$; KO+shControl vs KO+shRptor, ****$p<0.0001$; Sidak's multiple comparison tests.
i) Representative images of DIV 15 WT and Tsc1-KO primary hippocampal cultures transduced with shControl or shRptor expressing jRGeco1a. Scale bars=100 µm.
j) Cumulative distributions of soma area for WT and Tsc1-KO cultured hippocampal neurons treated with shControl or shRptor. n=246 WT+shControl, 249 WT+shRptor, 245 Tsc1-KO+shControl and 246 Tsc1-KO+shRptor neurons from 8 culture wells from 4 independent culture preps, 1 pup per prep. Kruskal-Wallis, $p<0.0001$; WT+shControl vs WT+shRptor, $p= 0.4789$; WT+shControl vs KO+shControl, $p<0.0001$; WT+shControl vs KO+shRptor, $p=0.2352$; KO+shControl vs KO+shRptor, $p<0.0001$; Dunn's multiple comparison tests.

Supplementary Figure 10

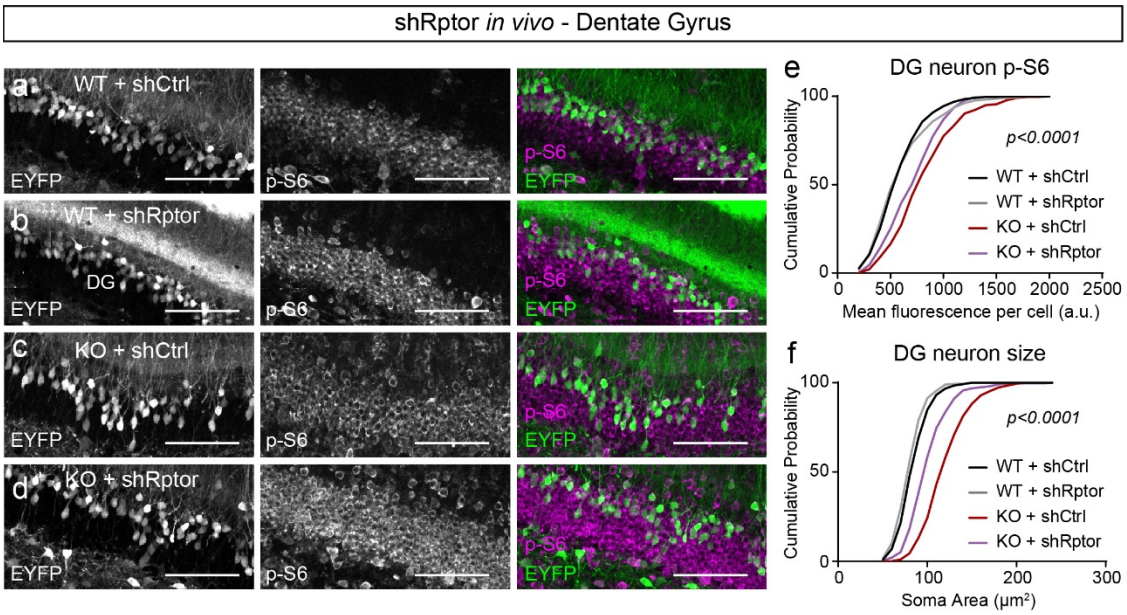

Supplementary Figure 10. shRptor improves cellular phenotypes in the dentate gyrus of Tsc1-cKO mice.

Related to Figure 7.

a-d) Representative images of the dentate gyrus (DG) of *Tsc1*$^{wt/wt}$*;Emx1-Cre*$^{+}$ (WT, a-b) and *Tsc1*$^{fl/fl}$*;Emx1-Cre*$^{+}$ (KO, c-d) mice injected with AAV-shRptor-EYFP or AAV-shCtrl-EYFP virus showing EYFP fluorescence (left panels) and p-S6 240/244 immunostaining (middle panels). Right panels show merged images. Scale bars=100 μm.

e) Cumulative distributions of p-S6 levels in DG EYFP+ neurons for the indicated genotypes. n=396 WT+shCtrl, 396 WT+shRptor, 382 Tsc1-KO+shCtrl and 350 Tsc1-KO+shRptor neurons from 6 mice per group. Kruskal-Wallis, p<0.0001; WT+shCtrl vs WT+shRptor, p>0.9999; WT+shCtrl vs Tsc1-KO+shCtrl, p<0.0001; WT+shCtrl vs Tsc1-KO+shRptor, p<0.0001; Tsc1-KO+shCtrl vs Tsc1-KO+shRptor, p=0.0026; Dunn's multiple comparison tests.

f) Cumulative distributions of EYFP+ DG neuron soma area for the indicated genotypes. n is the same as in panel e. Kruskal-Wallis, p<0.0001; WT+shCtrl vs WT+shRptor, p=0.0241; WT+shCtrl vs Tsc1-KO+shCtrl, p<0.0001; WT+shCtrl vs Tsc1-KO+shRptor, p<0.0001; Tsc1-KO+shCtrl vs Tsc1-KO+shRptor, p<0.0001; Dunn's multiple comparison tests.

Supplementary Table 1. Survival analysis of *Tsc1;Rptor;Emx1-Cre* and *Tsc1;Rictor;Emx1-Cre* mice. Related to Figure 4.

Mouse line	Genotype	Sex	Day of first mortality (P0-P40)[1]	Median survival in days (P0-P40)[1]	Age of oldest surviving animal (days)[2]
Tsc1;Rptor;Emx1-Cre	$Tsc1^{wt/wt};Rptor^{wt/wt};Emx1\text{-}Cre^{+}$	M	n/a	n/a	>150
Tsc1;Rptor;Emx1-Cre	$Tsc1^{wt/wt};Rptor^{wt/wt};Emx1\text{-}Cre^{wt/+}$	F	n/a	n/a	>150
Tsc1;Rptor;Emx1-Cre	$Tsc1^{wt/wt};Rptor^{wt/fl};Emx1\text{-}Cre^{+}$	M	n/a	n/a	>150
Tsc1;Rptor;Emx1-Cre	$Tsc1^{wt/wt};Rptor^{wt/fl};Emx1\text{-}Cre^{+}$	F	n/a	n/a	>150
Tsc1;Rptor;Emx1-Cre	$Tsc1^{wt/wt};Rptor^{fl/fl};Emx1\text{-}Cre^{wt/+}$	M	n/a	n/a	>150
Tsc1;Rptor;Emx1-Cre	$Tsc1^{wt/wt};Rptor^{fl/fl};Emx1\text{-}Cre^{+}$	F	n/a	n/a	>150
Tsc1;Rptor;Emx1-Cre	$Tsc1^{wt/fl};Rptor^{wt/wt};Emx1\text{-}Cre^{+}$	M	n/a	n/a	>150
Tsc1;Rptor;Emx1-Cre	$Tsc1^{wt/fl};Rptor^{wt/wt};Emx1\text{-}Cre^{+}$	F	n/a	n/a	>150
Tsc1;Rptor;Emx1-Cre	$Tsc1^{wt/fl};Rptor^{wt/fl};Emx1\text{-}Cre^{+}$	M	n/a	n/a	>150
Tsc1;Rptor;Emx1-Cre	$Tsc1^{wt/fl};Rptor^{wt/fl};Emx1\text{-}Cre^{+}$	F	n/a	n/a	>150
Tsc1;Rptor;Emx1-Cre	$Tsc1^{wt/fl};Rptor^{fl/fl};Emx1\text{-}Cre^{+}$	M	n/a	n/a	>150
Tsc1;Rptor;Emx1-Cre	$Tsc1^{wt/fl};Rptor^{fl/fl};Emx1\text{-}Cre^{+}$	F	n/a	n/a	>150
Tsc1;Rptor;Emx1-Cre	$Tsc1^{fl/fl};Rptor^{wt/wt};Emx1\text{-}Cre^{+}$	M[3]	16	19	39
Tsc1;Rptor;Emx1-Cre	$Tsc1^{fl/fl};Rptor^{wt/wt};Emx1\text{-}Cre^{+}$	F[3]	16	18.5	20
Tsc1;Rptor;Emx1-Cre	$Tsc1^{fl/fl};Rptor^{wt/fl};Emx1\text{-}Cre^{+}$	M	18	24	>150
Tsc1;Rptor;Emx1-Cre	$Tsc1^{fl/fl};Rptor^{wt/fl};Emx1\text{-}Cre^{+}$	F	17	25	>150
Tsc1;Rptor;Emx1-Cre	$Tsc1^{fl/fl};Rptor^{fl/fl};Emx1\text{-}Cre^{+}$	M	n/a	n/a	>150
Tsc1;Rptor;Emx1-Cre	$Tsc1^{fl/fl};Rptor^{fl/fl};Emx1\text{-}Cre^{+}$	F	30	n/a[4]	>150

Tsc1;Rictor;Emx 1-Cre	*Tsc1$^{wt/wt}$;Rictor$^{wt/wt}$; Emx1-Cre^{+}*	M	n/a	n/a	-
Tsc1;Rictor;Emx 1-Cre	*Tsc1$^{wt/wt}$;Rictor$^{wt/wt}$; Emx1-Cre^{+}*	F	n/a	n/a	-
Tsc1;Rictor;Emx 1-Cre	*Tsc1$^{wt/wt}$;Rictor$^{wt/fl}$;Emx 1-Cre^{+}*	M	n/a	n/a	-
Tsc1;Rictor;Emx 1-Cre	*Tsc1$^{wt/wt}$;Rictor$^{wt/fl}$;Emx 1-Cre^{+}*	F	n/a	n/a	-
Tsc1;Rictor;Emx 1-Cre	*Tsc1$^{wt/wt}$;Rictor$^{fl/fl}$; Emx1-Cre^{+}*	M	n/a	n/a	-
Tsc1;Rictor;Emx 1-Cre	*Tsc1$^{wt/wt}$;Rictor$^{fl/fl}$;Emx 1-Cre^{+}*	F	n/a	n/a	-
Tsc1;Rictor;Emx 1-Cre	*Tsc1$^{wt/fl}$;Rictor$^{wt/wt}$; Emx1-Cre^{+}*	M	n/a	n/a	-
Tsc1;Rictor;Emx 1-Cre	*Tsc1$^{wt/fl}$;Rictor$^{wt/wt}$;Emx 1-Cre^{+}*	F	n/a	n/a	-
Tsc1;Rictor;Emx 1-Cre	*Tsc1$^{wt/fl}$;Rictor$^{wt/fl}$; Emx1-Cre^{+}*	M	n/a	n/a	-
Tsc1;Rictor;Emx 1-Cre	*Tsc1$^{wt/fl}$;Rictor$^{wt/fl}$;Emx 1-Cre^{+}*	F	n/a	n/a	-
Tsc1;Rictor;Emx 1-Cre	*Tsc1$^{wt/fl}$;Rictor$^{fl/fl}$; Emx1-Cre^{+}*	M	n/a	n/a	-
Tsc1;Rictor;Emx 1-Cre	*Tsc1$^{wt/fl}$;Rictor$^{fl/fl}$;Emx1 -Cre^{+}*	F	n/a	n/a	-
Tsc1;Rictor;Emx 1-Cre	*Tsc1$^{fl/fl}$;Rictor$^{wt/wt}$;Emx 1-Cre^{+}*	M	15	19	19
Tsc1;Rictor;Emx 1-Cre	*Tsc1$^{fl/fl}$;Rictor$^{wt/wt}$;Emx 1-Cre^{+}*	F	17	18	18
Tsc1;Rictor;Emx 1-Cre	*Tsc1$^{fl/fl}$;Rictor$^{wt/fl}$;Emx1 -Cre^{+}*	M	14	18	21
Tsc1;Rictor;Emx 1-Cre	*Tsc1$^{fl/fl}$;Rictor$^{wt/fl}$;Emx1 -Cre^{+}*	F	14	17	21
Tsc1;Rictor;Emx 1-Cre	*Tsc1$^{fl/fl}$;Rictor$^{fl/fl}$;Emx1-Cre^{+}*	M	18	19.5	22
Tsc1;Rictor;Emx 1-Cre	*Tsc1$^{fl/fl}$;Rictor$^{fl/fl}$;Emx1-Cre^{+}*	F	18	20	24

Footnotes:
[1] n/a = No animals died within the first 40 postnatal days
[2] - = Animals were not monitored past the first 40 postnatal days
[3] Three *Tsc1$^{fl/fl}$;Rptor$^{wt/wt}$;Emx1-Cre^{+}* mice were found dead before P10 and sex could not be determined
[4] One *Tsc1$^{fl/fl}$;Rptor$^{fl/fl}$;Emx1-Cre^{+}* female died at P30

Supplementary Table 2. Body weights of *Tsc1;Rptor;Emx1-Cre* and *Tsc1;Rictor;Emx1-Cre* mice. Related to Figure 4.

Mouse line	Genotype	Sex	Mean +/- SEM body weight at P15 (n)	Mean +/- SEM body weight at P150 (n)[1,2]
Tsc1;Rptor;Emx1-Cre	$Tsc1^{wt/wt};Rptor^{wt/wt};Emx1\text{-}Cre^{+}$	M	8.42 +/- 0.31 (14)	48.00 +/- 5.69 (3)
Tsc1;Rptor;Emx1-Cre	$Tsc1^{wt/wt};Rptor^{wt/wt};Emx1\text{-}Cre^{+}$	F	7.56 +/- 0.57 (9)	38.17 +/- 1.92 (3)
Tsc1;Rptor;Emx1-Cre	$Tsc1^{wt/wt};Rptor^{wt/fl};Emx1\text{-}Cre^{+}$	M	8.38 +/- 0.32 (14)	45.06 +/- 1.99 (9)
Tsc1;Rptor;Emx1-Cre	$Tsc1^{wt/wt};Rptor^{wt/fl};Emx1\text{-}Cre^{+}$	F	7.90 +/- 0.40 (13)	38.73 +/- 4.52 (6)
Tsc1;Rptor;Emx1-Cre	$Tsc1^{wt/wt};Rptor^{fl/fl};Emx1\text{-}Cre^{+}$	M	6.26 +/- 0.36 (7)	22.50 +/- 0.40 (2)
Tsc1;Rptor;Emx1-Cre	$Tsc1^{wt/wt};Rptor^{fl/fl};Emx1\text{-}Cre^{+}$	F	6.28 +/- 0.48 (10)	21.18 +/- 1.12 (5)
Tsc1;Rptor;Emx1-Cre	$Tsc1^{wt/fl};Rptor^{wt/wt};Emx1\text{-}Cre^{+}$	M	8.64 +/- 0.30 (23)	46.60 +/- 1.50 (6)
Tsc1;Rptor;Emx1-Cre	$Tsc1^{wt/fl};Rptor^{wt/wt};Emx1\text{-}Cre^{+}$	F	7.78 +/- 0.51 (11)	44.20 +/- 1.10 (2)
Tsc1;Rptor;Emx1-Cre	$Tsc1^{wt/fl};Rptor^{wt/fl};Emx1\text{-}Cre^{+}$	M	8.03 +/- 0.29 (38)	43.05 +/- 1.52 (16)
Tsc1;Rptor;Emx1-Cre	$Tsc1^{wt/fl};Rptor^{wt/fl};Emx1\text{-}Cre^{+}$	F	8.44 +/- 0.23 (39)	36.47 +/- 3.01 (11)
Tsc1;Rptor;Emx1-Cre	$Tsc1^{wt/fl};Rptor^{fl/fl};Emx1\text{-}Cre^{+}$	M	6.72 +/- 0.42 (17)	24.50 +/- 1.17 (3)
Tsc1;Rptor;Emx1-Cre	$Tsc1^{wt/fl};Rptor^{fl/fl};Emx1\text{-}Cre^{+}$	F	5.64 +/- 0.88 (9)	20.05 +/- 1.45 (2)
Tsc1;Rptor;Emx1-Cre	$Tsc1^{fl/fl};Rptor^{wt/wt};Emx1\text{-}Cre^{+}$	M	4.81 +/- 0.34 (11)	n/a

Tsc1;Rptor;Emx1-Cre	*Tsc1$^{fl/fl}$;Rptor$^{wt/wt}$;Emx1-Cre^{+}*	F	5.55 +/- 0.63 (8)	n/a
Tsc1;Rptor;Emx1-Cre	*Tsc1$^{fl/fl}$;Rptor$^{wt/fl}$;Emx1-Cre^{+}*	M	7.00 +/- 0.50 (16)	29.60 (1)
Tsc1;Rptor;Emx1-Cre	*Tsc1$^{fl/fl}$;Rptor$^{wt/fl}$;Emx1-Cre^{+}*	F	6.65 +/- 0.29 (23)	17.60 (1)
Tsc1;Rptor;Emx1-Cre	*Tsc1$^{fl/fl}$;Rptor$^{fl/fl}$;Emx1-Cre^{+}*	M	5.68 +/- 0.55 (8)	21.15 +/- 1.45 (2)
Tsc1;Rptor;Emx1-Cre	*Tsc1$^{fl/fl}$;Rptor$^{fl/fl}$;Emx1-Cre^{+}*	F	6.80 +/- 0.32 (9)	19.29 +/- 0.51 (7)
Tsc1;Rictor;Emx1-Cre	*Tsc1$^{wt/wt}$;Rictor$^{wt/wt}$;Emx1-Cre^{+}*	M	9.42 +/- 0.24 (12)	-
Tsc1;Rictor;Emx1-Cre	*Tsc1$^{wt/wt}$;Rictor$^{wt/wt}$;Emx1-Cre^{+}*	F	8.78 +/- 0.28 (12)	-
Tsc1;Rictor;Emx1-Cre	*Tsc1$^{wt/wt}$;Rictor$^{wt/fl}$;Emx1-Cre^{+}*	M	9.63 +/- 0.22 (6)	-
Tsc1;Rictor;Emx1-Cre	*Tsc1$^{wt/wt}$;Rictor$^{wt/fl}$;Emx1-Cre^{+}*	F	9.45 +/- 0.81 (6)	-
Tsc1;Rictor;Emx1-Cre	*Tsc1$^{wt/wt}$;Rictor$^{fl/fl}$;Emx1-Cre^{+}*	M	7.55 +/- 0.45 (6)	-
Tsc1;Rictor;Emx1-Cre	*Tsc1$^{wt/wt}$;Rictor$^{fl/fl}$;Emx1-Cre^{+}*	F	9.07 +/- 0.69 (3)	-
Tsc1;Rictor;Emx1-Cre	*Tsc1$^{wt/fl}$;Rictor$^{wt/wt}$;Emx1-Cre^{+}*	M	9.38 +/- 0.42 (19)	-
Tsc1;Rictor;Emx1-Cre	*Tsc1$^{wt/fl}$;Rictor$^{wt/wt}$;Emx1-Cre^{+}*	F	8.76 +/- 0.47 (14)	-
Tsc1;Rictor;Emx1-Cre	*Tsc1$^{wt/fl}$;Rictor$^{wt/fl}$;Emx1-Cre^{+}*	M	9.54 +/- 0.27 (27)	-
Tsc1;Rictor;Emx1-Cre	*Tsc1$^{wt/fl}$;Rictor$^{wt/fl}$;Emx1-Cre^{+}*	F	9.48 +/- 0.35 (30)	-
Tsc1;Rictor;Emx1-Cre	*Tsc1$^{wt/fl}$;Rictor$^{fl/fl}$;Emx1-Cre^{+}*	M	8.56 +/- 0.33 (24)	-
Tsc1;Rictor;Emx1-Cre	*Tsc1$^{wt/fl}$;Rictor$^{fl/fl}$;Emx1-Cre^{+}*	F	8.07 +/-0.32 (16)	-
Tsc1;Rictor;Emx1-Cre	*Tsc1$^{fl/fl}$;Rictor$^{wt/wt}$;Emx1-Cre^{+}*	M	5.31 +/- 0.54 (9)	n/a
Tsc1;Rictor;Emx1-Cre	*Tsc1$^{fl/fl}$;Rictor$^{wt/wt}$;Emx1-Cre^{+}*	F	5.60 +/- 0.39 (4)	n/a
Tsc1;Rictor;Emx1-Cre	*Tsc1$^{fl/fl}$;Rictor$^{wt/fl}$;Emx1-Cre^{+}*	M	5.82 +/- 0.59 (14)	n/a
Tsc1;Rictor;Emx1-Cre	*Tsc1$^{fl/fl}$;Rictor$^{wt/fl}$;Emx1-Cre^{+}*	F	4.81 +/- 0.38 (13)	n/a

Tsc1;Rictor;Emx1-Cre	*Tsc1$^{fl/fl}$;Rictor$^{fl/fl}$;Emx1-Cre^{+}*	M	5.91 +/- 0.34 (10)	n/a
Tsc1;Rictor;Emx1-Cre	*Tsc1$^{fl/fl}$;Rictor$^{fl/fl}$;Emx1-Cre^{+}*	F	4.76 +/- 0.34 (5)	n/a

Footnotes:
[1] n/a = No animals survived beyond postnatal day 40
[2] - = Animals were not monitored past the first 40 postnatal days

Supplementary Table 3. Summary of *in vivo* phenotypes in *Tsc1;Rptor;Emx1-Cre* mice by genotype and sex. Related to Figures 4 and 5.

Genotype	***Tsc1*$^{wt/wt}$*;Rptor*$^{wt/wt}$*; Emx1-Cre*$^{+}$		***Tsc1*$^{fl/fl}$*;Rptor*$^{wt/wt}$*; Emx1-Cre*$^{+}$		***Tsc1*$^{fl/fl}$*;Rptor*$^{wt/fl}$*; Emx1-Cre*$^{+}$	
Sex	**Females (n=4)**	**Males (n=4)**	**Females (n=4)**	**Males (n=4)**	**Females (n=4)**	**Males (n=4)**
	Mean +/- SEM		**Mean +/- SEM**		**Mean +/- SEM**	
Cortical thickness (µm)	963.50 +/- 37.62	990.10 +/- 54.72	1176.00 +/- 48.51	1262.00 +/- 24.62	1085.00 +/- 14.12	1105.00 +/- 46.99
CA1 thickness (µm)	56.85 +/- 3.16	56.03 +/- 4.83	83.58 +/- 7.54	95.01 +/- 5.33	80.26 +/- 13.22	69.82 +/- 7.62
DG suprapyramidal blade thickness (µm)	48.20 +/- 2.97	52.09 +/- 4.23	66.25 +/- 3.58	66.21 +/- 3.57	52.68 +/- 6.39	52.29 +/- 7.81
DG infrapyramydal blade thickness (µm)	38.52 +/- 2.19	44.01 +/- 4.47	55.92 +/- 3.88	66.53 +/- 1.22	51.90 +/- 2.33	43.33 +/- 4.45
GFAP intensity across cortical layers (a.u.)	213.30 +/- 3.07	190.80 +/- 2.72	288.60 +/- 6.09	292.10 +/- 5.37	300.70 +/- 5.81	236.30 +/- 5.77
GFAP intensity in CA1(a.u.)	278.90 +/- 53.94	263.10 +/- 23.43	363.40 +/- 32.79	457.00 +/- 51.27	339.40 +/- 14.30	312.20 +/- 28.31
MBP intensity (a.u.)	13340.00 +/- 670.00	13365.00 +/- 988.50	7561.00 +/- 418.40	7143.00 +/- 319.60	10059.00 +/- 933.40	9946.00 +/-790.20
# of ectopic neurons above CA1	4.25 +/- 0.25	3.75 +/- 0.85	33.00 +/- 6.49	45.50 +/- 4.83	23.00 +/- 9.00	26.00 +/- 1.47
Cortical neurons soma area (µm)	362.30 +/- 4.18	361.50 +/- 3.90	403.80 +/- 4.14	420.90 +/- 3.93	383.00 +/- 3.93	380.50 +/- 3.72
Cortical neurons p-S6 intensity (a.u.)	107.30 +/- 1.19	92.71 +/- 0.99	131.40 +/- 1.53	119.80 +/- 1.27	126.80+/- 1.57	97.96 +/- 1.37
CA1 neurons soma area (µm)	272.70 +/- 4.16	277.70 +/- 4.55	409.50 +/- 8.24	409.30 +/- 8.32	285.60 +/- 3.99	286.30 +/- 3.45
CA1 neurons p-S6 intensity (a.u.)	98.38 +/- 1.47	101.60 +/- 1.30	149.90 +/-2.27	124.20 +/- 2.32	118.50 +/- 1.86	85.92 +/- 1.53
DG neurons	209.00 +/- 3.27	217.60 +/- 3.34	233.30 +/- 3.56	259.80 +/- 4.57	232.50 +/- 3.24	216.80 +/- 3.39

soma area (μm)						
DG neurons p-S6 intensity (a.u.)	96.49 +/- 1.72	103.50 +/- 1.61	162.20 +/- 4.29	132.00 +/- 4.17	126.40 +/- 2.27	83.65 +/- 1.67

Supplementary Table 4. Mouse strains and genotyping primers

Mouse Line	Genotyping Primers	Source	Reference
Emx1-Cre	WT F: AAG GTG TGG TTC CAG AAT CG	JAX strain # 005628	[207]
	WT R: CTC TCC ACC AGA AGG CTG AG		
	Mut F: GCG GTC TGG CAG TAA AAA CTA TC		
	Mut R: GTG AAA CAG CAT TGC TGT CAC TT		
Tsc1$^{fl/fl}$	F: GTC ACG ACC GTA GGA GAA GC	JAX strain # 005680	[203]
	R: GAA TCA ACC CCA CAG AGC AT		
Rptor$^{fl/fl}$	F: AGCCTTTAGTACCCACTTGGC	JAX strain # 013188	[204]
	R: GGCATCTCACAAAGGGTACAG		
Rictor$^{fl/fl}$	F: ACTGATATGTTCATGGTTGTG	JAX strain # 020649	[205, 206]
	R: GACACTGGATTCAGTGGCTTG		
Ai9	WT F: AAG GGA GCT GCA GTG GAG TA	JAX strain # 007909	[244]
	WT R: CCG AAA ATC TGT GGG AAG TC		
	Mut F: CTG TTC CTG TAC GGC ATG G		
	Mut R: GGC ATT AAA GCA GCG TAT CC		

Supplementary Table 5. Viruses and titers.

Virus	Serotype	Promoter	Source	Titer of viral stock (vg/ml)	Dilution amount (*in vitro*)	Dilution amount (*in vivo*)
AAV1.hSyn.HI.eGFP-Cre.WPRE.SV40	1	hSyn	Penn Vector Core	$1.78x10^{13}$	1:20 0.5 µl/well	n/a
AAV1.hSyn.eGFP.WPRE.bGH	1	hSyn	Penn Vector Core	$3.86x10^{13}$	1:20 0.5 µl/well	n/a
AAV5.hSyn.eGFP	5	hSyn	UNC Vector Core	$4x10^{12}$	1:100 0.5	n/a
AAV1.CBA.mCherry-nCre.WPRE.bGH	1	CBA	Penn Vector Core	$1.04x10^{13}$	1:100 0.5 µl/well	n/a
AAV9.CAG.Flex.tdTomato.WPRE.bGH (AllenInstitute864)	9	CAG	Penn Vector Core	unknown	1:20 0.5 µl/well	n/a
AAV1.Syn.NES-jRGECO1a.WPRE.SV40	1	hSyn	Gift from Adesnik lab	$2.08x10^{13}$	1:20 0.5 µl/well	n/a
AAV9-U6-shRptor-EYFP	9	hU6	Caltech CLOVER Center	$1.93x10^{14}$	1:20 0.5 µl/well	1:4 500 nl/mouse
AAV9-U6-shContorl-EYFP	9	hU6	Caltech CLOVER Center	$2.17x10^{14}$	1:20 0.5 µl/well	1:4 500 nl/mouse

Supplementary Table 6. Antibodies and dilutions.

	Antibody	Host species	Company and catalog #	WB dilution	IHC dilution	ICC dilution
Primary	Tsc1	Rabbit	Cell Signaling 6935	1:800	-	-
	Raptor	Rabbit	Cell Signaling 2280	1:800	-	-
	Rictor	Rabbit	Cell Signaling 2114	1:600	-	-
	rpS6	Rabbit	Cell Signaling 2317	1:1000	-	-
	phospho-rpS6 Ser244/246	Rabbit	Cell Signaling 5364	1:2000	1:800	-
	Akt	Rabbit	Cell Signaling 4691	1:1500	-	-
	phospho-Akt Ser 473	Rabbit	Cell Signaling 4060	1:1000	-	-
	4E-BP1	rabbit	Cell Signaling 9644	1:1000	-	-
	phospho-4E-BP1 Thr37/46	Rabbit	Cell Signaling 2855	1:1000	-	-
	Histone 3	Mouse	Cell Signaling 3638	1:2000	-	-
	GFP	Chicken	AbCam ab13970	-	1:1000	1: 5000
	MBP	Rat	Abcam ab7349	-	1: 350	-
	GFAP	Rabbit	Fisher 180063	-	1: 400	-
	GFAP	Mouse	Cell Signaling 3670	-	1: 400	-
	NeuN	Mouse	Millipore MAB377	-	1: 800	-
	Antibody	**Species (reactivity)**	**Company and catalog #**	**WB dilution**	**IHC dilution**	**ICC dilution**
Secondary	Goat anti-Rabbit-HFP	Rabbit	Bio-Rad 170-5046	1:5000	-	-
	Goat anti-Mouse-HRP	Mouse	Bio-Rad 170-5047	1:5000	-	-
	Goat anti-Rat Alexa Fluor 488	Rat	Thermo Fisher A-11006	-	1:500	-

	Goat anti-Chicken Alexa Fluor 488	Chicken	Thermo Fisher A-11039	-	1:500	1:500
	Goat anti-Mouse Alexa Fluor 546	Mouse	Thermo Fisher A-11003	-	1:500	-
	Goat anti-Rabbit Alexa Fluor 633	Rabbit	Thermo Fisher A-21070	-	1:500	-

Chapter 3

The effects of mTORC1 inhibition on neuronal activity in Tsc1-KO hippocampal cultures

Vasiliki Karalis

Department of Molecular and Cell Biology
University of California, Berkeley

Introduction

Epilepsy is one of the most common neurologic conditions that significantly affects the quality of life of patients with Tuberous Sclerosis Complex (TSC) [90, 245, 246]. A recent study from the international Tuberous Sclerosis to increase Awareness (TOSCA) study showed that ~83% of TSC patients have epilepsy (1852/2216 patients)[90]. Seizure activity in TSC patients usually begins during infancy and is associated with increased rates of intellectual disability and other neuropsychiatric presentations such as autism [247, 248], that are collectively known as TSC-associated neuropsychiatric disorders (TAND)[76, 249].

TSC is a developmental multisystem genetic disorder. It is caused by mutations in either the *TSC1* or *TSC2* genes[68, 69], which form a complex that negatively regulates mTOR complex 1 (mTORC1) [73]. Studies of mTORC1 signaling revealed that it regulates several aspects of neuronal function and physiology in a cell type-dependent manner including intrinsic excitability, synaptic transmission, and long-term synaptic plasticity[147, 148, 153, 157, 163, 200, 250]. While mTORC1's involvement in neuronal function has been extensively investigated, the exact molecular mechanisms that underlie seizure activity in TSC patients with dysregulated mTOR signaling are still not completely understood.

Current pharmacological treatments include antiepileptic drugs (AEDs) hormonal therapy, surgery, ketogenic diet, vagus nerve stimulation and mTOR inhibitors[90]. However, about 2/3 of TSC patients develop refractory epilepsy[90]. Studies that focus on mTOR inhibition as a therapeutic strategy utilize rapalogs, analogs of a naturally occurring macrolide called rapamycin that was initially found to be a very strong mTORC1 inhibitor. One critical finding derived from these studies is that the onset of treatment in relation to the onset of seizure activity significantly affects the treatment outcome. Specifically, studies have reported that when therapeutic interventions occur before or near the onset of epileptiform activity, outcomes are improved [110, 111]. Currently, several clinical studies such as EPISTOP (https://clinicaltrials.gov/ct2/show/NCT02098759) and PREVENT (https://clinicaltrials.gov/ct2/show/NCT02849457) attempt to evaluate the impact of pre-symptomatic treatment and use the current pharmacologic approaches more as a prevention rather than a rescue strategy. Together, these studies highlight the idea that there are critical treatment windows for epilepsy in TSC patients.

The idea of critical periods for treatment of TSC related phenotypes has been previously explored and validated in several rodent models. For example, it has been shown that early onset rapamycin treatment in animals that lack *Tsc1* from cerebellar Purkinje cells can restore social behavior and stereotypic repetitive behavior deficits[157, 177]. However, later onset treatment could only reverse social behavior abnormalities. In addition, another study showed that there are critical treatment windows for rescuing dendritic arborization and spine deficits in Tsc1-KO cortical neurons in organotypic slices[175]. These studies raise two key questions: 1) Is rapamycin effective at treating some TSC-related phenotypes while it can only prevent others? And 2) Can we design alternative therapeutic strategies for better rescue, or do we need better prevention strategies?

In this study our goal was to generate an *in vitro* model for TSC-related epileptiform activity and determine whether mTORC1 downregulation via postnatal Raptor manipulation rescues neuronal hyperactivity *in vitro* as an alternative therapeutic approach to rapamycin. To do this, we generated primary hippocampal cultures from *Tsc1*$^{wt/wt}$*;Emx1Cre+* (WT) and *Tsc1*$^{fl/fl}$*;Emx1Cre+* (Tsc1-KO) mice and performed calcium imaging analysis.

We previously showed that postnatal Raptor downregulation via virally delivered shRNA was sufficient to normalize mTORC1 signaling and somatic hypertrophy in Tsc1-KO neurons in vitro[251]. In addition, we showed that it can rebalance mTORC1 signaling, reverse neuronal hypertrophy, improve myelination and extend survival of Tsc1-KO mice *in vivo*[251]. Here we found that when we transduced Tsc1-KO hippocampal neurons with AAV-shRNA targeting Raptor we did not improve the hyperactivity phenotype but rather enhanced it. We also unexpectedly found that while chronic rapamycin treatment ameliorates somatic hypertrophy and suppresses mTORC1 activity in Tsc1-KO cultures, it also enhances the hyperactivity phenotype. Our results suggest the possibility that neuronal hyperactivity may be mTORC1-dependent early on but at later stages this phenotype uncouples from mTORC1 activity. In addition, our data show that the somatic hypertrophy phenotype caused by loss of *Tsc1* is driven by a distinct mechanism to the one that causes hyperactivity and is dynamically regulated by mTORC1.

Results

Raptor downregulation does not improve Tsc1-KO related neuronal hyperexcitability

We have previously performed Ca^{2+} imaging analysis experiments and showed that primary hippocampal cultures from *Tsc1*$^{fl/fl}$;*Emx1Cre*$^{+}$ exhibit significant neuronal hyperactivity at 14 days *in vitro* (DIV14) (see Chapter 2 Fig. 6) [251]. We also showed that heterozygous loss of Raptor, an essential component of mTORC1 can ameliorate the hyperactivity phenotype caused by loss of *Tsc1* (see Chapter 2 Fig. 6). Here we investigated whether postnatal Raptor reduction could be a viable treatment avenue for TSC-related hyperactivity in neurons with embryonic loss of *Tsc1*. To do this, we transduced primary hippocampal cultures from *Tsc1*$^{fl/fl}$;*Emx1Cre*$^{+}$ (Tsc1-KO) and *Tsc1*$^{WT/WT}$;*Emx1Cre* (WT) mice with an AAV1 encoding shRNA targeting *Rptor* or control on DIV1 and AAV1 encoding the calcium indicator jRGECO1a[212] on DIV 2 and imaged calcium dynamics on DIV 15 (Fig 1a-l).

As expected, Tsc1-KO neurons transduced with AAV1-shCtrl (Tsc1-KO+shCtrl) exhibited significantly higher frequency and amplitude of individual calcium events in comparison to WT neurons transduced with AAV1-shCtrl (WT+shCtrl) (Fig. 1m,n). The duration of these events was not significantly changed (Fig 1o). Raptor downregulation in WT (WT+shRptor) neurons did not affect the frequency or duration of events; however, it did significantly reduce their amplitude in comparison to WT+shCtrl.

We previously verified that the shRptor construct used here rebalances mTORC1 activity and rescues somatic hypertrophy in *Tsc1*$^{fl/fl}$;*Emx1Cre*$^{+}$ neurons *in vitro* (see Chapter 2 Supplementary Fig. 9 i-j). Hence, we anticipated that Raptor downregulation would improve the hyperactivity phenotype. Surprisingly, while Raptor downregulation in Tsc1-KO neurons (Tsc1-KO +shRptor) slightly decreased the duration of Ca^{2+} events in comparison to Tsc1-KO+shCtrl neurons, it significantly increased the amplitude and showed a trend toward increasing the frequency of events (Fig. 1m-o). Together these data suggest that, at least *in vitro*, postnatal Raptor downregulation may exacerbate the hyperactivity of Tsc1-KO neurons.

Raptor downregulation does not improve Tsc1-KO related network hyperactivity

We next sought to examine whether Raptor downregulation improves TSC-related hyperactivity at the network level. We analyzed 'network events', which were defined by synchronous activity of more than 20% of neurons in the field of view (see methods for further details). As expected, in comparison to WT neurons (WT+shCtrl), deletion of *Tsc1* (Tsc1-KO+shCtrl) increased the frequency and amplitude of network events (Fig. 2a,b). While the duration of network events was not significantly altered, loss of Tsc1 significantly increased the proportion of time each culture had synchronous activity (Fig. 2c,d).

Similar to our observations with the single event analysis, postnatal Raptor downregulation was not sufficient to improve the network hyperactivity caused by loss of *Tsc1* and partially exacerbated it. Specifically, we observed that the frequency of network activity in Tsc1-KO+shRptor cultures was significantly increased in comparison to Tsc1-KO+shCntrl (Fig. 2a). In addition, the event amplitude and duration, the total duration of time the culture was synchronously active (duration of network activity) and the percentage of neurons participating in network events were comparable between the two

conditions (Fig. 2b-e). Together our data demonstrate that postnatal Raptor reduction in Tsc1-KO neurons does not improve the hyperactivity phenotype neither on the neuronal nor on the network level.

Rapamycin does not rescue Tsc1-KO related neuronal hyperexcitability

The results described above suggest that shRptor was not effective at ameliorating neuronal or network hyperactivity induced by loss of *Tsc1*. To investigate this further we compared our Raptor downregulation strategy with rapamycin treatment, which is the standard treatment approach for both *in vitro* and *in vivo* models of TSC. To do this, we treated Tsc1-KO cultures with 50nM rapamycin for four days starting at DIV10 and performed calcium imaging analysis at DIV14 (Fig. 3a-l). This is a treatment paradigm that we have previously shown suppresses mTORC1 signaling and rescues somatic hypertrophy of neurons with postnatal loss of *Tsc1 in vitro* (see Chapter 2, Fig. 1 and Fig. 3h) [251].

As expected, Tsc1-KO neurons treated with EtOH (Tsc1-KO+EtOH), the control vehicle, exhibited significantly higher frequency, amplitude and duration of spontaneous calcium events in comparison to WT + EtOH (Fig. 3m-o). Rapamycin treatment of WT (WT+Rapa) neurons significantly reduced the frequency of calcium events (Fig. 3m) but increased their amplitude and duration (Fig. 3n,o). Notably, this rapamycin treatment paradigm exhibited a similar phenotype to our Raptor manipulation approach in Tsc1-KO neurons. Specifically, we observed that the frequency and amplitude of events of Tsc1-KO neurons treated with rapamycin (Tsc1-KO+Rapa) were significantly increased in comparison to Tsc1-KO+EtOH cultures (Fig. 3m, n). The duration of these events was significantly decreased in comparison to Tsc1-KO+EtOH neurons while it remained significantly larger than WT+EtOH neurons (Fig. 3o).

Rapamycin does not rescue Tsc1-KO related network hyperactivity

We proceeded to examine the effect of rapamycin treatment on network hyperactivity in Tsc1 KO cultures. As with Raptor downregulation, we observed that the frequency of network events of Tsc1-KO+Rapa neuros was significantly increased in comparison to Tsc1-KO+EtOH neurons (Fig. 4a). The network event amplitude and duration, the duration of network activity, and the proportion of neurons participating in these events were comparable to Tsc1-KO+EtOH neurons and thus significantly larger than WT+EtOH neurons (Fig. 4b-e).

Rapamycin treatment suppresses mTOR signaling and improves somatic hypertrophy

Due to the unexpected calcium imaging results, we verified the effectiveness of rapamycin on other well established TSC-related phenotypes that we and others have previously shown can be rescued via rapamycin treatment.

First, we looked at changes induced by rapamycin on Tsc1-KO neurons at the biochemical level. Rapamycin is known to form a complex between itself, mTOR and FK506-binding protein 12 (FKBP12) and occlude access of some substrates to the catalytic site of the mTOR kinase[192]. While initially characterized as an mTORC1 inhibitor, long-term rapamycin treatment has been shown to also suppress mTORC2[118]. Recent studies have shown that mTORC2 suppression might also be beneficial for the seizure phenotypes in mTORopathies, specifically in the context of *Pten*

deletion [155]. Thus, we examined whether rapamycin treatment was effective at suppressing mTORC1 and mTORC2 activity in our system. To do this, we performed western blotting analysis and looked at the canonical readouts p-S6 S240/244 and p-4E-BP1-T37 for mTORC1[193] and pAkt-Ser473 for mTORC2[197] (Fig. 5a-g). Rapamycin treatment completely suppressed the phosphorylation of S6 in both WT and Tsc1-KO neurons (see Chapter 2 Fig. 1b,f), as expected. While we did not observe an increase in the phosphorylation of 4E-BP1 at Threonine 37 in Tsc1-KO+EtOH neurons in comparison to WT+EtOH (Fig. 5a, f) we did observe a significant increase in total 4EBP1 protein levels (Fig. 5a, e). Interestingly, this increase in the 4EBP1 was not affected by rapamycin treatment (Fig. 5a, e). As we have seen before (see Chapter 2 Fig. 1b,h), rapamycin treatment reduced the phosphorylation of Akt in WT and Tsc1-KO neurons. Together these data show that 4-day rapamycin treatment is sufficient to strongly suppress both mTORC1 and mTORC2 signaling.

Another common phenotypic manifestation in both *in vitro* and *in vivo* models of TSC is neuronal hypertrophy[160, 251, 252](see Chapter 2 Fig. 3h). We have previously shown that rapamycin rescues TSC related neuronal hypertrophy phenotype in primary hippocampal cultures with postnatal loss of *Tsc1* (see Chapter 2 Fig. 3h). To assess the effects of rapamycin in our model, where *Tsc1* loss occurs embryonically, we measured changes in neuronal soma size in WT and Tsc1-KO neurons with and without rapamycin. As expected, we found that loss of *Tsc1* caused a significant increase in soma size when compared to WT neurons (Fig. 5h-m). While rapamycin treatment did not affect WT neurons' soma size, it ameliorated the somatic hypertrophy of Tsc1-KO neurons (Fig. 5h-m). Together these data suggest that while this 4-day rapamycin treatment (DIV10-14) is sufficient to suppress mTOR signaling and improve somatic hypertrophy, it does not affect the neuronal hyperactivity phenotype of Tsc1-KO cultures.

Discussion

The goal of this study was test whether postnatal Raptor manipulation can rescue epileptiform activity *in vitro,* in neurons with embryonic loss of *Tsc1*. Our results were unexpected as we saw that while shRptor and rapamycin rescued mTOR signaling abnormalities and neuronal hypertrophy, neither of these treatments were sufficient to improve neuronal or network hyperactivity in cultured Tsc1-KO neurons. Furthermore, to our surprise, we saw that both approaches led to an apparent exacerbation of the existing phenotype.

Several studies have shown that rapamycin can treat hyperactivity phenotypes in mouse Tsc1-KO[153] and human TSC2-KO cultures[211, 253]. However, these studies either treated neurons with postnatal loss of *Tsc1*[153] or treated them near the onset of the epileptiform activity[211]. These results highlight an important factor, which is the onset of treatment with respect to the onset of hyperactivity phenotype. Specifically, treatment before or near the onset of this phenotype would prevent seizure activity while treatment after the phenotype has been established would aim at rescuing it.

In our Emx1-Cre^{+} *in vitro* model, loss of *Tsc1* occurs embryonically at ~E9.5-10. Thus, rapamycin treatment started on DIV10 begins approximately 21 days after *Tsc1* loss. While we have not examined the timing of Raptor protein downregulation with AAV-shRptor, based on the slow turnover of Raptor protein in the floxed mouse model (see Chapter 2 Supplementary Fig. 2a,c), we hypothesize that at least 7-8 days post shRNA application would be necessary for strong Raptor downregulation. Since AAV-shRNA was applied on DIV1, this manipulation likely occurred ~19-20 days post *Tsc1* loss. A study using tamoxifen-inducible Cre in mouse forebrain neurons showed that the mice developed epilepsy 8-12 days after *Tsc1* deletion providing a window between loss of *Tsc1* and the onset of seizures *in vivo*[254].

We have previously shown that in the same *in vitro* model, concomitant loss of *Tsc1* and one copy of *Rptor* prevents the hyperactivity phenotype observed in Tsc1-KO neurons to a certain extent[251] (see Chapter 2 Fig. 6). In the present study we were unable to rescue the hyperactivity phenotype neither via shRptor nor rapamycin treatment. These data suggest that while early on this seizure-like phenotype is mTORC1-dependent, later on the mechanism(s) that underlie neuronal hyperactivity are not controlled by mTORC1 in Tsc1-KO hippocampal cultures.

Spontaneous epileptiform activity has also been observed in multiple models of TSC with conditional loss of either *Tsc1* or *Tsc2* genes from different cell types including neuronal progenitor cells, excitatory or inhibitory postmitotic neurons and astrocytes[151, 152, 255, 256]. These findings suggest that there are potentially multiple independent mechanisms underlying seizure activity that can originate from different cell types and brain regions. While in our *in vitro* system we did not observe improvement in the neuronal hyperactivity phenotype upon rapamycin treatment, some studies have shown that *in vivo* rapamycin can rescue seizure activity including in the *Tsc1$^{fl/fl}$;Emx1-Cre^{+}* mouse model[151, 152, 255]. Several reasons could account for this discrepancy. In our *in vitro* system, we examine the cell-autonomous hyperactivity caused by loss of *Tsc1* from primarily excitatory hippocampal cultured neurons in an isolated highly interconnected network. In *in vivo* TSC mouse models*,* it is unknown where seizures originate, how they

interact with surrounding circuits, what type of cells drive and later sustain the epileptiform activity, and how rapamycin affects these parameters.

To examine whether our rescue strategies affect other TSC-related abnormalities we looked at some of the canonical manifestations observed in *in vitro* systems. We first examined signaling abnormalities. Loss of *Tsc1* has been consistently shown to increase mTORC1 activity and thus phosphorylation levels of the ribosomal protein S6 (p-S6) and the translation initiation factor 4E-BP1 (p-4E-BP1)[193, 198]. Interestingly, rapamycin completely suppressed p-S6 (see Fig. 5a,d) and Raptor downregulation near normalized p-S6 levels (see Chapter 2 Supplementary Fig. 9b,d), as expected. However, neither rapamycin (see Fig. 5a,e) nor shRprtor (data not shown) affected the increased total 4EBP1 protein levels. shRptor also did not affect the increased phosphorylation of 4E-BP1 observed in Tsc1-KO neurons (see Chapter 2 Supplementary Fig. 9a,g). This biased substrate inhibition by rapamycin has been previously reported[117]. Here we see that Raptor downregulation also exhibits the same substrate bias. Although it has been shown that changes in p-4EBPs are not involved in seizure activity[172], these data highlight that there might be other rapamycin/shRptor -insensitive targets that underlie seizure activity.

Neuronal hypertrophy due to loss of *Tsc1* has been reported both *in vitro* and *in vivo* in various neuronal subtypes including hippocampal, cortical, dopaminergic and striatal[160, 251, 252] neurons. *In vitro*, we consistently saw neuronal hypertrophy in Tsc1-KO cultured hippocampal neurons (Fig. 5h-m and Chapter 2 Supplementary Fig. 9i-j). Interestingly, 4-day rapamycin treatment significantly improved somatic hypertrophy (Fig. 5h-m) and shRptor completely normalized soma size to WT neuron levels (Chapter 2 Supplementary Fig. 9i-j). These data together suggest that somatic hypertrophy and neuronal hyperactivity are two distinct phenotypes driven by different mechanisms. Notably, somatic hypertrophy appears to be dynamically regulated by mTORC1 while seizure activity seems to be mTORC1-dependent early on (see prevention Chapter 2 Fig. 6) but later the mechanism(s) that drive neuronal hyperactivity uncouple from mTORC1 function (Fig. 1-4). Finally, the decrease in soma size of Tsc1-KO neurons might also explain the exacerbation we observe in the hyperactivity phenotype as a reduction in soma size would be expected to increase membrane resistance and render neurons even more excitable.

Overall, our *in vitro* model offers a unique opportunity to study in a “simplified” system the cell-autonomous mechanisms that drive neuronal hyperactivity upon loss of *Tsc1.* Using this system, future studies could 1) elucidate the time window during which these mechanism(s) are mTORC1 dependent, 2) determine when neuronal hyperactivity uncouples from mTORC1 function, and 3) identify the mechanism(s) that sustain hyperactivity after it has been established. With this information we will be able to develop better therapeutics and prevention strategies for TSC and potentially other mTORopathies.

Materials and Methods

Mice

All animal procedures were carried out in accordance with protocols approved by the University of California, Berkeley Institutional Animal Care and Use Committee (IACUC) AUP-2016-04-8684. Mice were on a mixed genetic background. Mice were housed with same-sex littermates in groups of 5–6 animals per cage and kept on a regular 12 h light/dark with ad libitum access to standard chow and water. For all experiments animals from at least 2-3 independent litters were used. Mouse genotypes were confirmed by PCR using genomic DNA obtained from tail samples. See Supplementary Table 1 for a list of the transgenic mouse lines used and genotyping primers.

Primary hippocampal cultures

Dissociated hippocampal cultures were prepared from postnatal day 0-1 (P0-1) mice using standard protocols. Briefly, hippocampi from single pups were dissected on ice. The tissue was dissociated using 34.4 µg/ml papain in dissociation media (HBSS Ca^{2+}, Mg^{2+} free, 1 mM sodium pyruvate, 0.1% D-glucose, 10 mM HEPES buffer) and incubated for 3 min at 37°C. Tissue digestion was stopped by incubation in trypsin inhibitor (1 mg/ml) in dissociation media at 37°C for 4 min. After trypsin inhibition, dissociation media was carefully removed and the tissue was gently manually triturated in 5 ml plating media (MEM, 10% FBS, 0.45% D-Glucose, 1 mM sodium pyruvate, 1 mM L-glutamine). Cell density was counted using a TC10 Automated cell counter (Bio-Rad) and ~2-2.25 × 10^5 neurons were plated onto 24-well plates pre-coated with Poly-D-Lysine (PDL) (Corning, Cat # 08774271). Plating media was removed after 3 h and 900 µl maintenance media (Neurobasal media (Fisher Scientific # 21103-049) with 2 mM glutamine, pen/strep, and B-27 supplement (Invitrogen # 17504-044)) were added per well. After 4 days *in vitro* (DIV 4), 1 µM Cytosine β-D-arabinofuranoside (Sigma-Aldrich # C6645) was added to prevent glial proliferation. Cultures were maintained in maintenance media for 14 - 18 days with partial media changes every 4 days.

Adeno-associated virus (AAV) transduction of primary cultures

Tsc1$^{fl/fl}$;Emx1Cre^{+} and *Tsc1$^{WT/WT}$;Emx1Cre^{+}* hippocampal cultures were transduced with AAV1-shRNA on DIV1 and AAV1-jRGeco on DIV2 AAVs. Amounts of AAVs were chosen after titration experiments for each virus to accomplish maximum while maintaining low toxicity levels. To determine the percentage of Cre-expressing neurons in primary hippocampal cultures from Emx1-Cre-positive pups we used AAV1-CAG-FLEX-GFP at a high titer (see Supplementary Fig 6a in Chapter 2). For calcium imaging experiments, we transduced neurons with AAV1-hSyn-jRGECO1a aiming for >95% transduction efficiency. For shRNA experiments, we transduced neurons with AAV9-hU6-shRNA-EYFP on DIV 1 and achieved 85-90% transduction. (See Supplementary Table 2 for the list of viruses, source, titer and number of viral genomes (vg) used.)

Protein extraction and western blot analysis

Hippocampal cultures were harvested on DIV 14. Neurobasal media was aspirated from one well at a time, wells were quickly rinsed with ice cold 1x PBS with Ca^{2+}/Mg^{2+}

and then 75 µl of lysis buffer were added (lysis buffer: 2 mM EDTA (Sigma: E5134), 2 mM EGTA (Sigma: E3889), 1% Triton-X (Sigma: T8787), and 0.5% SDS (Sigma: 71736) in 1× PBS with Halt phosphatase inhibitor cocktail (ThermoFisher: PI78420) and Complete mini EDTA-free protease inhibitor cocktail (Roche: 4693159001)). Wells were thoroughly scraped, and lysates were collected and sonicated for 5 sec. Total protein was determined by BCA assay (ThermoFisher: PI23227) and 10 µg of protein in 1X Laemmli sample buffer (Bio-Rad:161-0747) were loaded onto 4-15% Criterion TGX gels (Bio-Rad: 5671084). Proteins were transferred overnight at low voltage to PVDF membranes (Bio-Rad: 1620177), blocked in 5% milk in 1x TBS-Tween for one hour at RT, and incubated with primary antibodies diluted in 5% milk in 1x TBS-Tween overnight at 4°C. The following day, membranes were washed 3 x 10 min in 1x TBS-Tween and incubated with HRP-conjugated secondary antibodies (1:5000) for one hour at RT, washed 6 x 10 min in 1x TBS-Tween, incubated with chemiluminescence substrate (Perkin-Elmer: NEL105001EA) and developed on GE Amersham Hyperfilm ECL (VWR: 95017-661). Membranes were stripped by two 7 min incubations in stripping buffer (6 M guanidine hydrochloride (Sigma: G3272) with 1:150 □-mercaptoethanol) with shaking followed by four 2 min washes in 1x TBS with 0.05% NP-40 to re-blot on subsequent days. Bands were quantified by densitometry using ImageJ software (NIH). Phospho-proteins were normalized to their respective total proteins. Histone-3 was used as a loading control for every experiment. See Supplementary Table 3 for the list of antibodies, source and dilutions.

Rapamycin treatment *in vitro*

Primary hippocampal cultures were treated chronically for 4 days with rapamycin from DIV 10-14. A stock solution of 0.5 mM rapamycin (LC Laboratories: R-5000) was prepared in ethanol and stored at −20°C. Rapamycin stock was diluted in Neurobasal media 1:100 prior to use and then added to a final concentration of 50 nM. Rapamycin was first added on DIV 10 and in the final media change on DIV 12.

Fluorescence microscopy and image analysis

For soma size quantification, cultured neurons were imaged on an AxioObserver.A1 (Zeiss) inverted microscope using a 10x Zeiss A-Plan objective (Numerical Aperture: 0.25) with wide field fluorescence illumination (X-Cite series 120Q, Lumen Dynamics). Images were takes with a Hamamatsu Orca-er digital camera and Micro-Manager 1.4 software. For all quantitative comparison experiments, the same microscope and acquisition settings were used for each image and samples were processed in batches to include matched control and experimental samples. All images were processed using ImageJ software. Soma area was quantified by manually tracing neuronal cell bodies using ImageJ software.

Calcium imaging

Primary hippocampal cultures from P0-1 *Tsc1;Rptor;Emx1-Cre* mice of different genotypes were plated onto 24 well plates pre-coated with PDL (Corning, Cat # 08774271). On DIV 2, cultures were transduced with AAV1-jRGECO1a (Supplementary Table 5) and maintained for 12 days in Neurobasal media. On DIV 14, neurons were imaged on an AxioObserver.A1 (Zeiss) inverted microscope using a 10x Zeiss A-Plan

objective (Numerical Aperture: 0.25) with wide field fluorescence illumination (X-Cite series 120Q, Lumen Dynamics). Images were taken at 8.91 Hz with a Hamamatsu Orca-er digital camera and Micro-Manager 1.4 software. For all Ca^{2+} imaging experiments excitation light intensity, camera sensor gain, and exposure time used were identical. A single field of view (FOV) was imaged from at least 2-3 individual wells per culture (prepped from 1 pup) and approximately 40 neurons were randomly selected and analyzed. Before proceeding to the analysis, we verified that the neurons selected were active at least once during the recording period. At least 3 mice per genotype were examined from at least 3 different litters.

Calcium imaging analysis

Data analysis was performed using ImageJ 1.53c and custom programs written in Matlab 2020a.

Pre-processing

Circular ROIs corresponding to neuronal somata, were drawn manually in ImageJ on mean intensity projection images of the recorded FOV. Forty ROIs were drawn per FOV, beginning in the upper left quadrant of the image, and extending outward as necessary (to the right, bottom left, and bottom right quadrants, respectively), and were imported into Matlab for further analysis. Movies were motion corrected using the normcorre function[243], then normalized with respect to baseline, taken to be the minimum intensity projection of the FOV, to generate a ΔF/F movie. It was necessary to use the minimum projection as Tsc1-cKO neurons exhibited high Ca^{2+} activity and thus contained few baseline frames. Ca^{2+} traces were extracted as ΔF/F by computing the mean fluorescence within each ROI at each movie frame.

Single event analysis

Individual Ca^{2+} transients were detected by first filtering the ΔF/F traces with a four-frame moving mean, then using Matlab's findpeaks function to identify peaks in the ΔF/F trace. Event amplitude was defined as the difference between the event's peak ΔF/F and the minimum ΔF/F in the preceding inter-event-interval (see Supplementary Fig. 6c). Events with an amplitude < 0.5% were excluded from further analysis. Prior to measurement of event duration and area under the curve (AUC), Matlab's msbackadj function was used to shift the 1st percentile of the ΔF/F trace within 15 second time windows to zero. This reduced the reliance of event AUC on preceding bouts of Ca^{2+} activity, which would otherwise contribute significantly to AUC values in Tsc1-cKO neurons due to their high frequency activity. Event initiation and termination were identified by finding the 0.5% ΔF/F threshold (see Supplementary Fig. 6d) crossing preceding and following the event peak. Event termination was alternatively identified when the Ca^{2+} decay following the event peak ΔF/F was interrupted by a ΔF/F increase >1%, indicating the initiation of another event. Events without a clear initiation or termination were excluded from further analysis. AUC was defined as the area under the ΔF/F trace during the event (see Supplementary Fig. 6d) and measured using trapezoidal numerical integration implemented by the trapz function in Matlab.

Network event analysis

Network Ca^{2+} events were defined as time intervals over which more than 20% of neuronal ROIs in the imaged area were simultaneously active (activity for a single neuron was defined as $\Delta F/F \geq 0.5\%$) (See gray highlighted zones in Fig. 6e-g and Supplementary Fig. 8c,d). We did not use a standard deviation-based threshold, as it would have selectively reduced event detection in Tsc1-cKO cultures, due to their persistent Ca^{2+} activity. Events with a duration < 2.5 seconds were excluded from further analysis. Cell participation in events was defined as the percentage of neurons that were active at any time during the event. Response amplitude within a single neuron during a network event was defined as the difference between the maximum $\Delta F/F$ during the event and the minimum $\Delta F/F$ in the preceding inter-event-interval. Area under the curve (AUC) was defined as the area under the $\Delta F/F$ trace occurring during the event.

shRNA constructs

The AAV-Tet3-shRNA plasmid (Addgene plasmid # 85740) was used as a backbone to generate the AAV9-hU6-shRptor-EYFP construct. The restriction enzymes BamHI and XbaI were used to excise the Tet-3 shRNA sequence. The oligonucleotide sequence: 5'-GATCCGCCTCATCGTCAAGTCCTTCAAGAAGCTTGTTGAAGGACTTGACGATGAGG CTTTTTTT -3' that contains the *Rptor* shRNA sequence[215] flanked by restriction sites for BamHI and XbaI was subcloned into the plasmid backbone. AAV-hU6-shControl-EYFP (Addgene plasmid # 85741) that contains the 5'-GTTCAGATGTGCGGCGAGT-3' shRNA sequence was used as a control. For large-scale isolation and purification of the plasmids, DH5α NEB competent cells (New England Biolabs #C2987H) were transformed and Endofree Megaprep (Qiagen # 12381) was performed to generate plasmids for high titer viral packaging.

Statistical Analysis

Statistical analyses and graphing were performed using GraphPad Prism software (version 9). All datasets were first analyzed using the D'Agostino and Pearson normality test, and then parametric or non-parametric two-tailed statistical tests were employed accordingly to determine significance. Normally distributed datasets were analyzed using Welch's t-tests when comparing two groups or a one-way ANOVA with Holm-Sidak's multiple comparison tests when comparing three or more groups. Datasets that did not pass the normality test were analyzed using Kruskal–Wallis test with Dunn's multiple comparisons tests when comparing three or more groups. Cumulative distributions were analyzed using the Kruskal–Wallis test with Dunn's multiple comparisons tests (when comparing three or more groups. Significance was set as $*p < 0.05$, $**p < 0.01$, $***p < 0.001$, and $****p < 0.0001$. P values were corrected for multiple comparisons

Figures

Figure 1

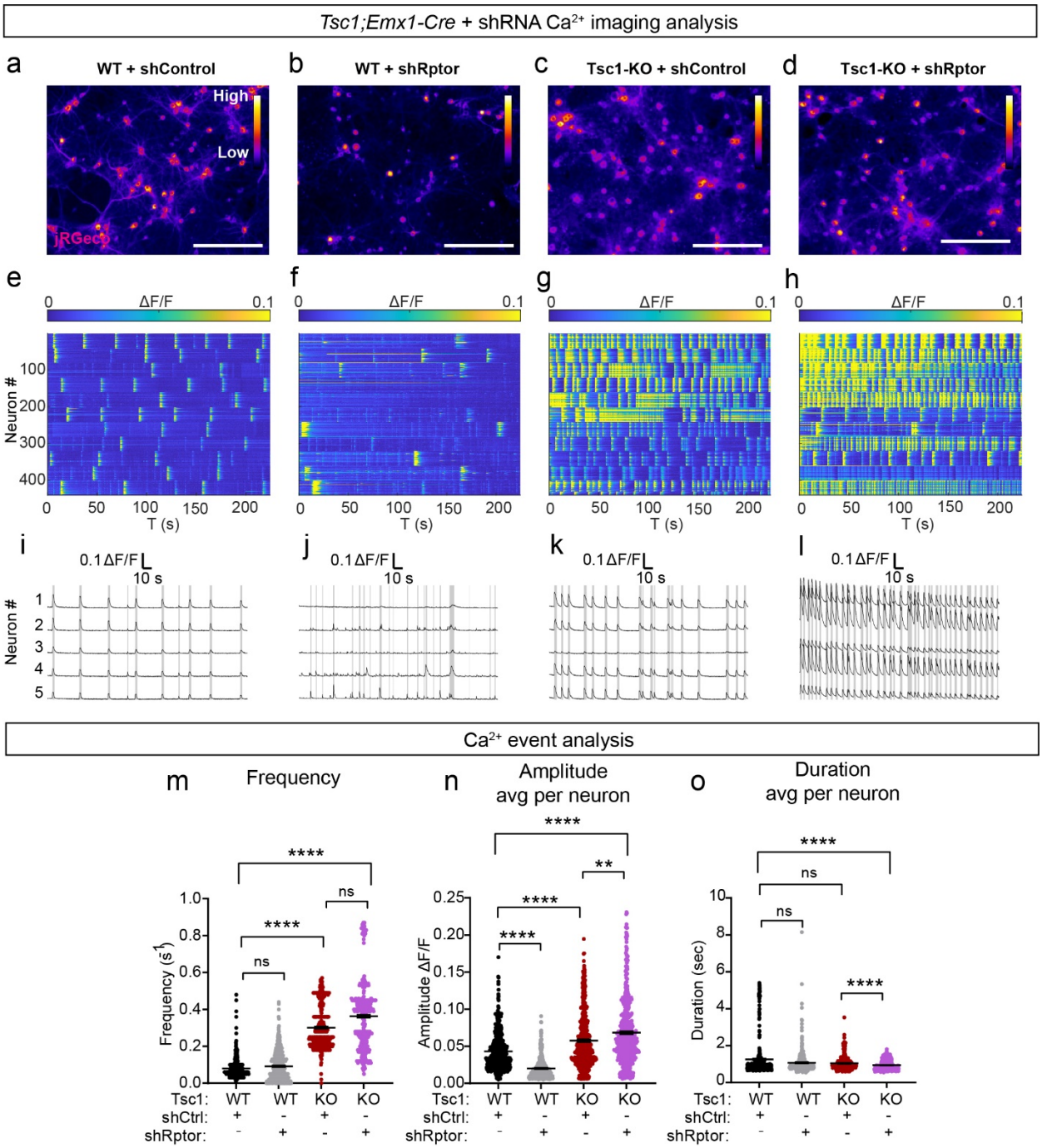

Figure 1. shRptor does not rescue neuronal hyperactivity of Tsc1-KO neurons.
a-d) Representative heatmaps of jRGeco fluorescent intensity of primary hippocampal cultures for *Tsc1$^{wt/wt}$;Emx1-Cre^{+}* + shControl (WT+shCtrl, a) *Tsc1$^{wt/wt}$;Emx1-Cre^{+}* + shRptor (WT+shRptor, b) *Tsc1$^{fl/fl}$;Emx1-Cre^{+}*+ shControl (KO+Ctrl, c) and *Tsc1$^{fl/fl}$;Emx1-Cre^{+}* + shRptor (KO+shRptor, d). Scale bars =250µm.
e-f)) Representative heatmaps of ΔF/F for *Tsc1$^{wt/wt}$;Emx1-Cre^{+}* + shControl (WT+shCtrl, e) *Tsc1$^{wt/wt}$;Emx1-Cre^{+}* + shRptor (WT+shRptor, f) *Tsc1$^{fl/fl}$;Emx1-Cre^{+}*+ shControl (KO+shCtrl, g) and *Tsc1$^{fl/fl}$;Emx1-Cre^{+}* + shRptor (KO+shRptor, h) cultures.
i-l) Ca^{2+} transients from 5 representative neurons *Tsc1$^{wt/wt}$;Emx1-Cre^{+}* + shControl (WT+shCtrl, i) *Tsc1$^{wt/wt}$;Emx1-Cre^{+}* + shRptor (WT+shRptor, j) *Tsc1$^{fl/fl}$;Emx1-Cre^{+}*+ shControl (KO+shCtrl, k) and *Tsc1$^{fl/fl}$;Emx1-Cre^{+}* + shRptor (KO+shRptor, l). cultures. Grey lines indicate network events with more than 20% of neurons in the field of view active at the same time.
m) Scatter dot plot (Mean+/-SEM) of the Ca2+ transient frequency per neuron for the indicated genotypes. n= 480 WT+shCtrl, n= 440 WT+shRptor, n=470 KO+shCtrl and n= 520 KO+shRptor neurons from 11-15 cultures wells, one pup per culture. Kruskal-Wallis test, p<0.0001; WT+shCtrl vs WT+shRptor, p>0.9999; WT+shCtrl vs KO+shCtrl, ****p<0.0001. WT+shCtrl vs KO+shRptor, ****p<0.0001; KO+shCtrl vs KO+shRptor, p=0.1851; Dunn's multiple comparisons tests
n) Scatter dot plot (Mean+/-SEM) of Ca^{2+} transients' amplitude per neuron for the indicated genotypes. . n= 480 WT+shCtrl, n= 440 WT+shRptor, n=470 KO+shCtrl and n= 520 KO+shRptor neurons from 11-15 cultures wells, one pup per culture. Kruskal-Wallis test, p<0.0001; WT+shCtrl vs WT+shRptor, ****p<0.0001; WT+shCtrl vs KO+shCtrl, ****p<0.0001. WT+shCtrl vs KO+shRptor, ****p<0.0001; KO+shCtrl vs KO+shRptor, **p<0.014; Dunn's multiple comparisons tests
o) Scatter dot plot (Mean+/-SEM) of Ca^{2+} transients' duration per neuron for the indicated genotypes. . n= 480 WT+shCtrl, n= 440 WT+shRptor, n=470 KO+shCtrl and n= 520 KO+shRptor neurons from 11-15 cultures wells, one pup per culture. Kruskal-Wallis test, p<0.0001; WT+shCtrl vs WT+shRptor, p=0.7667; WT+shCtrl vs KO+shCtrl, p>0.9999. WT+shCtrl vs KO+shRptor, ****p<0.0001; KO+shCtrl vs KO+shRptor, ****p<0.0001; Dunn's multiple comparisons tests

Figure 2

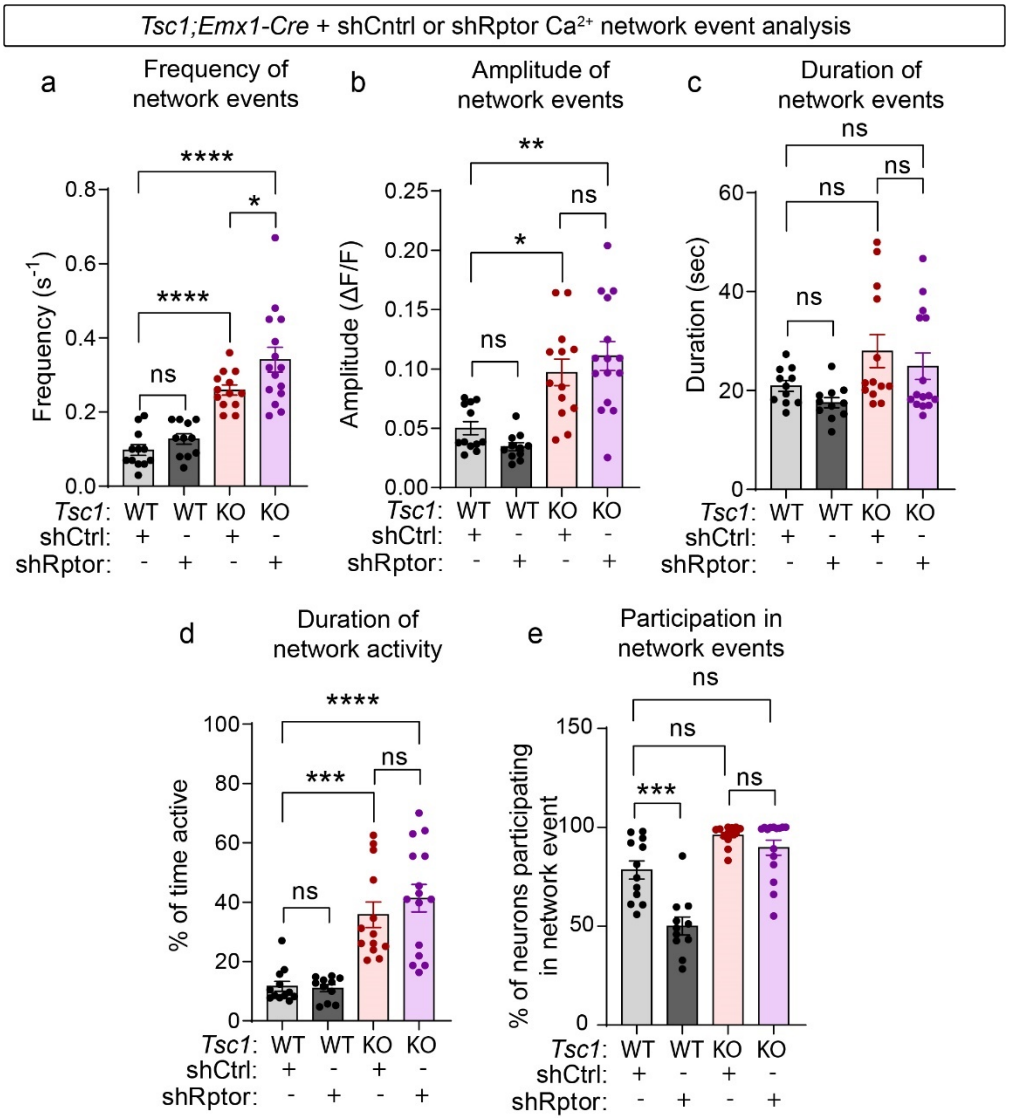

Figure 2. Tsc1-KO network hyperactivity is not improved by postnatal shRptor.

a) Mean +/- SEM frequency of network events per culture for the indicated genotypes. Each dot represents a single culture well. n= 12 WT+shCtrl, n= 11 WT+shRptor, n=13 KO+shCtrl and n= 15 KO+shRptor individual culture wells, from 4-5 independent culture preps, 1 pup per prep. One-way ANOVA, p<0.0001, F (3, 47) = 25.83; WT+shCtrl vs WT+shRptor, p=0.8579; WT+shCtrl vs KO+shCtrl, ****p<0.0001; WT+shCtrl vs KO+shRptor, ****p<0.0001; KO+shCtrl vs KO+shRptor, *p=0.0422. Sidak's multiple comparisons tests

b) Mean +/- SEM amplitude of network events per culture for the indicated genotypes. Each dot represents a single culture well. n= 12 WT+shCtrl, n= 11 WT+shRptor, n=13 KO+shCtrl and n= 15 KO+shRptor individual culture wells, from 4-5 independent culture preps, 1 pup per prep. Kruskal-Wallis, p<0.0001; WT+shCtrl vs WT+shRptor, p=0.7187; WT+shCtrl vs KO+shCtrl, *p=0.0270. WT+shCtrl vs KO+shRptor, **p=0.0074; KO+shCtrl vs KO+shRptor, p>0.9999. Dunn's multiple comparisons tests.

c) Mean +/- SEM duration of network events per culture for the indicated genotypes. Each dot represents a single culture well. n= 12 WT+shCtrl, n= 11 WT+shRptor, n=13 KO+shCtrl and n= 15 KO+shRptor individual culture wells, from 4-5 independent culture preps, 1 pup per prep. One-way ANOVA, p=0.0287, F (3, 46) = 3.294; WT+shCtrl vs WT+shRptor, p=0.8404; WT+shCtrl vs KO+shCtrl, p=0.1994; WT+shCtrl

vs KO+shRptor, p=0.6892; KO+shCtrl vs KO+shRptor, p=0.8318. Sidak's multiple comparisons tests.
d) Mean +/- SEM duration of network activity per culture, expressed as the percent of the recording time during which network events occurred for the indicated genotypes. Each dot represents a single culture well. n= 12 WT+shCtrl, n= 11 WT+shRptor, n=13 KO+shCtrl and n= 15 KO+shRptor individual culture wells, from 4-5 independent culture preps, 1 pup per prep. Kruskal-Wallis, p<0.0001; WT+shCtrl vs WT+shRptor, p>0.9999; WT+shCtrl vs KO+shCtrl, ***p=0.0004. WT+shCtrl vs KO+shRptor, ****p<0.0001; KO+shCtrl vs KO+shRptor, p>0.9999; Dunn's multiple comparisons tests.
e) Mean +/- SEM percentage of neurons in a field of view that participated in a network event per culture for the indicated genotypes. n= 12 WT+shCtrl, n= 11 WT+shRptor, n=13 KO+shCtrl and n= 15 KO+shRptor individual culture wells, from 4-5 independent culture preps, 1 pup per prep. Kruskal-Wallis, p=0.0002; WT+shCtrl vs WT+shRptor, ***p=0.001; WT+shCtrl vs KO+shCtrl, p>0.9999. WT+shCtrl vs KO+shRptor, p>0.9999; KO+shCtrl vs KO+shRptor, p>0.9999 Dunn's multiple comparisons tests.

Figure 3

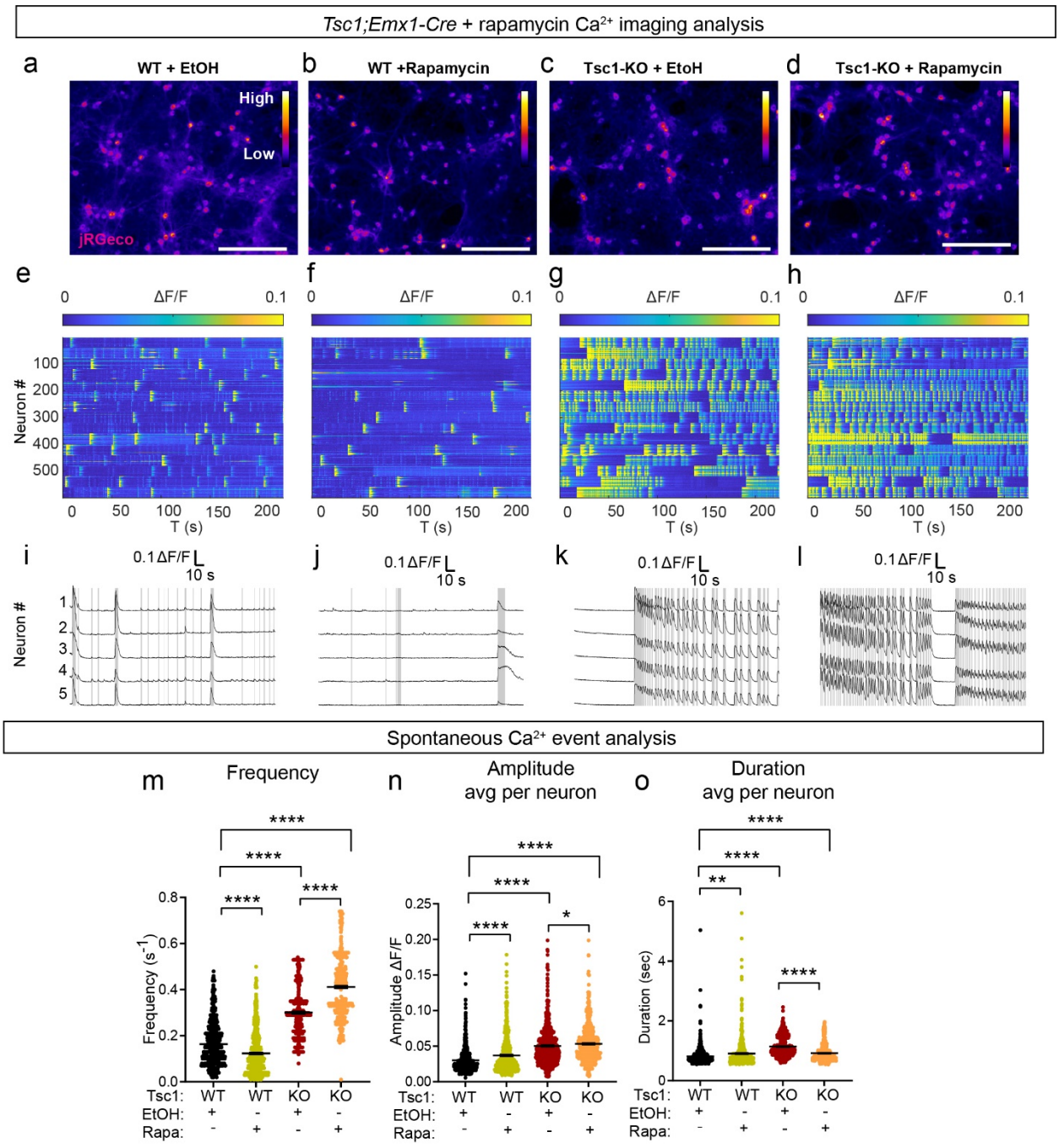
Tsc1;Emx1-Cre + rapamycin Ca2+ imaging analysis
a
WT + EtOH
b
WT +Rapamycin
c
Tsc1-KO + EtoH
d
Tsc1-KO + Rapamycin
High
Low
jRGeco
e
f
g
h
0 ΔF/F 0.1
Neuron #
T (s)
i
j
k
l
0.1 ΔF/F
10 s
Spontaneous Ca2+ event analysis
m
Frequency
n
Amplitude
avg per neuron
o
Duration
avg per neuron
Frequency (s-1)
Amplitude ΔF/F
Duration (sec)
Tsc1:
EtOH:
Rapa:
WT
KO

Figure 3. Rapamycin treatment exacerbates neuronal hyperactivity of Tsc1-KO neurons.
a-d) Representative heatmaps of jRGeco fluorescent intensity of primary hippocampal cultures for *Tsc1$^{wt/wt}$;Emx1-Cre^{+}* + EtOH (WT+ EtOH, a) *Tsc1$^{wt/wt}$;Emx1-Cre^{+}* + rapamycin from DIV10-14 (WT+Rapa, b) *Tsc1$^{fl/fl}$;Emx1-Cre^{+}*+ EtOH (KO+EtOH, c) and *Tsc1$^{fl/fl}$;Emx1-Cre^{+}* + rapamycin from DIV10-14 (KO+Rapa, d). Scale bars =250µm
e-f)) Representative heatmaps of ΔF/F for *Tsc1$^{wt/wt}$;Emx1-Cre^{+}* treated with EtOH from DIV10-14 (a), *Tsc1$^{wt/wt}$;Emx1-Cre^{+}* treated with 50nM rapamycin from DIV10-14 (b), *Tsc1$^{fl/fl}$;Emx1-Cre^{+}* treated with EtOH from DIV10-14 (c) and *Tsc1$^{fl/fl}$;Emx1-Cre^{+}* treated with 50nM rapamycin from DIV10-14 (d) cultures.
i-l) Ca^{2+} transients from 5 representative neurons for *Tsc1$^{wt/wt}$;Emx1-Cre^{+}* treated with EtOH from DIV10-14 (i), *Tsc1$^{wt/wt}$;Emx1-Cre^{+}* treated with 50nM rapamycin from DIV10-14 (j), *Tsc1$^{fl/fl}$;Emx1-Cre^{+}* treated with EtOH from DIV10-14 (k) and *Tsc1$^{fl/fl}$;Emx1-Cre^{+}* treated with 50nM rapamycin from DIV10-14 (l) cultures. Grey lines indicate network events with more than 20% of neurons in the field of view active at the same time.
m) Scatter dot plot (Mean+/-SEM) of Ca^{2+} transient frequency per neuron for the indicated genotypes. n=600 WT+EtOH, n=604 WT+Rapa, n=602 KO+EtOH and n=601 KO + Rapa individual neurons from 5-6 independent cultures, 1 pup per culture; Kruskal-Wallis test, p<0.0001; WT+EtOH vs WT+Rapa, ****p<0.0001; WT+EtOH vs KO+EtOH, ****p<0.0001; WT+EtOH vs KO+Rapa, ****p<0.0001; KO+EtOH vs KO+Rapa, ****p<0.0001; Dunn's multiple comparisons tests
n) Scatter dot plot (Mean+/-SEM) of Ca^{2+} transients' amplitude per neuron for the indicated genotypes. n=600 WT+EtOH, n=604 WT+Rapa, n=602 KO+EtOH and n=601 KO + Rapa individual neurons from 5-6 independent cultures, 1 pup per culture; Kruskal-Wallis test, p<0.0001; WT+EtOH vs WT+Rapa, ****p<0.0001; WT+EtOH vs KO+EtOH, ****p<0.0001; WT+EtOH vs KO+Rapa, ****p<0.0001; KO+EtOH vs KO+Rapa, *p<0.0462; Dunn's multiple comparisons tests
o) Scatter dot plot (Mean+/-SEM) of Ca^{2+} transients' duration per neuron for the indicated genotypes. n=600 WT+EtOH, n=604 WT+Rapa, n=602 KO+EtOH and n=601 KO + Rapa individual neurons from 5-6 independent cultures, 1 pup per culture; Kruskal-Wallis test, p<0.0001; WT+EtOH vs WT+Rapa, **p=0.0039; WT+EtOH vs KO+EtOH, ****p<0.0001; WT+EtOH vs KO+Rapa, ****p<0.0001; KO+EtOH vs KO+Rapa, ****p<0.0001; Dunn's multiple comparisons tests.

Figure 4

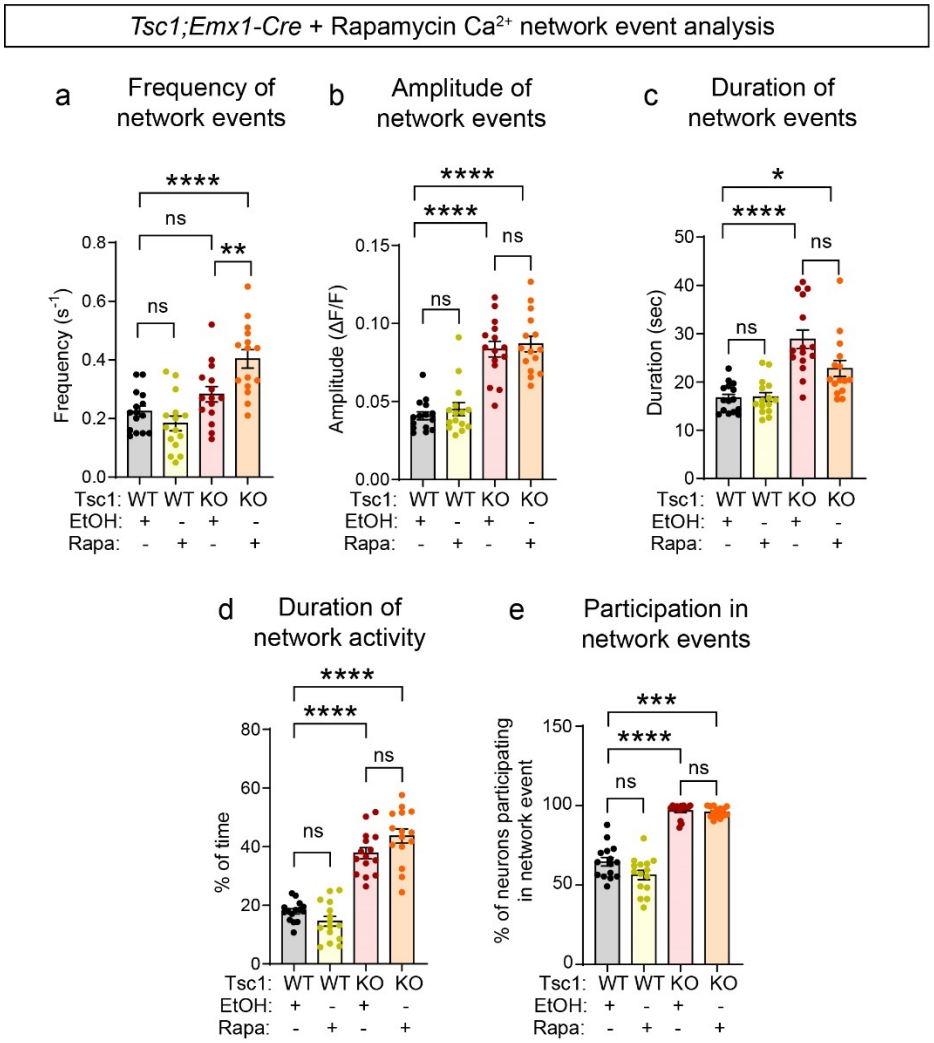

Figure 4. Tsc1-KO network hyperactivity is not restored by rapamycin treatment.
a) Mean +/- SEM frequency of network events per culture for the indicated genotypes. Each dot represents a single culture well. n= 15 individual culture wells for all genotypes, from 4-5 independent culture preps, 1 pup per prep. One-way ANOVA, p<0.0001, F (3, 56) = 14.05; WT+EtOH vs WT+Rapa, p=0.7054; WT+EtOH vs KO+EtOH, p=0.3735; WT+EtOH vs KO+Rapa, ****p<0.0001, KO+EtOH vs KO+Rapa, **p=0.006. Sidak's multiple comparisons tests
b) Mean +/- SEM amplitude of network events per culture for the indicated genotypes. Each dot represents a single culture well. n= 15 individual culture wells for all genotypes, from 4-5 independent culture preps, 1 pup per prep. Kruskal-Wallis, p<0.0001; WT+EtOH vs WT+Rapa, p>0.9999; WT+EtOH vs KO+EtOH, ****p<0.0001; WT+EtOH vs KO+Rapa, ****p<0.0001, KO+EtOH vs KO+Rapa, p>0.9999. Dunn's multiple comparisons tests.
c) Mean +/- SEM duration of network events per culture for the indicated genotypes. Each dot represents a single culture well. n= 15 individual culture wells for all genotypes, from 4-5 independent culture preps, 1 pup per prep. Kruskal-Wallis, p<0.0001; WT+EtOH vs WT+Rapa, p>0.9999; WT+EtOH vs KO+EtOH,

****p<0.0001; WT+EtOH vs KO+Rapa, *p=0.0112; KO+EtOH vs KO+Rapa, p=0.3458. Dunn's multiple comparisons tests.
d) Mean +/- SEM duration of network activity per culture, expressed as the percent of the recording time during which network events occurred for the indicated genotypes. Each dot represents a single culture well. n= 15 individual culture wells for all genotypes, from 4-5 independent culture preps, 1 pup per prep. One-way ANOVA, p=0.0443, F (3, 56) = 63.53; WT+EtOH vs WT+Rapa, p=0.5732; WT+EtOH vs KO+EtOH, ****p<0.0001; WT+EtOH vs KO+Rapa, ****p<0.0001, KO+EtOH vs KO+Rapa, p=0.0999. Sidak's multiple comparisons tests
e) Mean +/- SEM percentage of neurons in a field of view that participated in a network event per culture for the indicated genotypes. n Each dot represents a single culture well. n= 15 individual culture wells for all genotypes, from 4-5 independent culture preps, 1 pup per prep. Kruskal-Wallis, p=0.3916; WT+EtOH vs WT+Rapa, p>0.9999; WT+EtOH vs KO+EtOH, p=0.6292; WT+EtOH vs KO+Rapa, p>0.9999, KO+EtOH vs KO+Rapa, p=0.6292. Dunn's multiple comparisons tests.

Figure 5

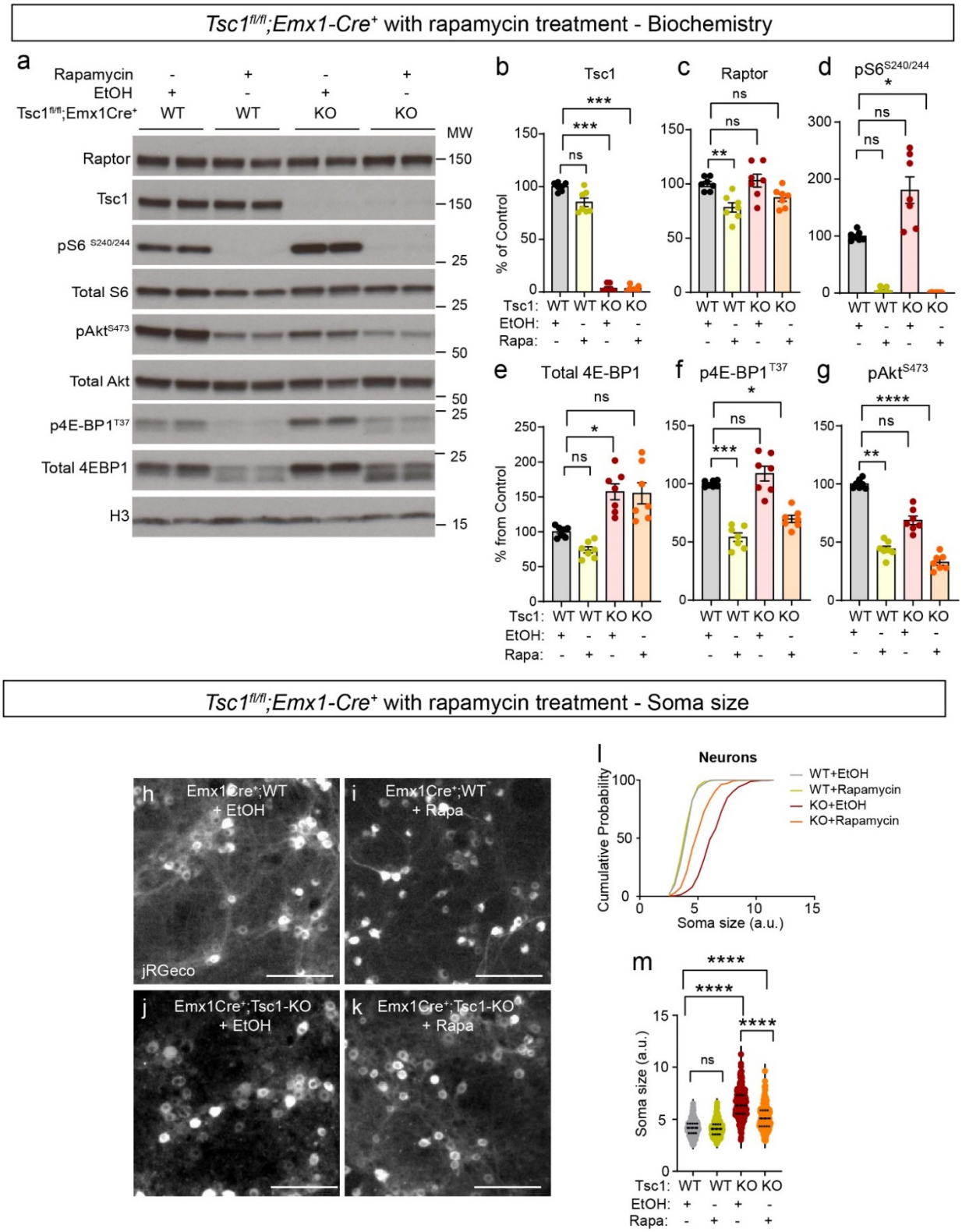
Tsc1fl/fl;Emx1-Cre+ with rapamycin treatment - Biochemistry
a
Rapamycin
EtOH
Tsc1fl/fl;Emx1Cre+
WT
KO
MW
Raptor
Tsc1
pS6 S240/244
Total S6
pAktS473
Total Akt
p4E-BP1T37
Total 4EBP1
H3
150
25
50
15
b
Tsc1
% of Control
c
Raptor
d
pS6S240/244
e
Total 4E-BP1
% from Control
f
p4E-BP1T37
g
pAktS473
ns
Tsc1fl/fl;Emx1-Cre+ with rapamycin treatment - Soma size
h
Emx1Cre+;WT
+ EtOH
jRGeco
i
Emx1Cre+;WT
+ Rapa
j
Emx1Cre+;Tsc1-KO
+ EtOH
k
Emx1Cre+;Tsc1-KO
+ Rapa
l
Neurons
Cumulative Probability
Soma size (a.u.)
WT+EtOH
WT+Rapamycin
KO+EtOH
KO+Rapamycin
m
Soma size (a.u.)

Figure 5. Rapamycin suppresses mTORC1 and mTORC2 signaling and improves somatic hypertrophy

a) Representative western blots of lysates collected from P0-1 *Tsc1$^{wt/wt}$;Emx1-Cre^{+}* (WT) and *Tsc1$^{fl/fl}$;Emx1-Cre^{+}* (Tsc1-KO) primary hippocampal cultures treated with EtOH or 50nM rapamycin from DIV10-DIV14. MW indicates molecular weight. Two-Three samples per genotype and treatment are shown; this experiment was replicated three times.

b-g) Bar graphs display western blot quantification (mean +/- SEM) for the indicated proteins, expressed as a percentage of control (WT + EtOH) levels. Phospho-proteins were normalized to their respective total proteins. Dots represent data from individual culture wells. n=7-9 culture wells per condition from 3 independent culture preps, 1 pup per prep.

b) Tsc1, Kruskal-Wallis, p<0.0001; WT+EtOH vs WT+Rapa, p=0.6154; WT+EtOH vs KO+EtOH, ***p=0.0005; WT+EtOH vs KO+Rapa, *** p=0.0003; Dunn's multiple comparisons tests.

c) Raptor, Kruskal-Wallis, p=0.0029; WT+EtOH vs WT+Rapa, **p=0.0075; WT+EtOH vs KO+EtOH, p>0.9999; WT+EtOH vs KO+Rapa, p=0.1041; Dunn's multiple comparisons tests

d) pS6 S240.244, Kruskal-Wallis, p<0.0001; WT+EtOH vs WT+Rapa, p= 0.0815; WT+EtOH vs KO+EtOH, p=0.4312; WT+EtOH vs KO+Rapa, *p= 0.0210; Dunn's multiple comparisons tests

e) Total 4EBP1, Kruskal-Wallis, p<0.0001; WT+EtOH vs WT+Rapa, p= 0.3803; WT+EtOH vs KO+EtOH, *p=0.0338; WT+EtOH vs KO+Rapa, p=0.0632; Dunn's multiple comparisons tests

f) p4EBP1 T37, Kruskal-Wallis, p<0.0001; WT+EtOH vs WT+Rapa, ***p=0.0006; WT+EtOH vs KO+EtOH, p>0.9999; WT+EtOH vs KO+Rapa, *p=0.0486; Dunn's multiple comparisons tests

g) pAkt S473, Kruskal-Wallis, p<0.0001; WT+EtOH vs WT+Rapa, **p=0.0022; WT+EtOH vs KO+EtOH, p=0.3342; WT+EtOH vs KO+Rapa, **** p<0.0001; Dunn's multiple comparisons tests

h-k)Representative images of Tsc1$^{wt/wt}$;Emx1-Cre^{+} + EtOH (WT+EtOH, h), Tsc1$^{wt/wt}$;Emx1-Cre^{+} + Rapa (WT+Rapa, i), Tsc1$^{fl/fl}$;Emx1-Cre^{+} + EtOH (KO+EtOH, j) and Tsc1$^{fl/fl}$;Emx1-Cre^{+} + Rapa (KO+Rapa, k) primary hippocampal cultures expressing jRGeco1a on DIV 14. Scale bars 100m.

l) Cumulative distributions of soma area for WT+EtOH, WT+Rapa, KO+EtOH and KO+Rapa cultured hippocampal neurons. n=241 WT+EtOH, n=240 WT+Rapa, n=240 KO+EtOH and n=240 KO+Rapa neurons from 6-7 independent cultures 1 pup per culture. Kruskal-Wallis test, p<0.0001; WT+EtOH vs WT+Rapa, p>0.9999; WT+EtOH vs KO+EtOH, ****p<0.0001; WT+EtOH vs KO+Rapa, ****p<0.0001; KO+EtOH vs KO+Rapa, ****p<0.0001Dunn's multiple comparison tests

m) Scatter dot plots of soma area for WT+EtOH, WT+Rapa, KO+EtOH and KO+Rapa cultured hippocampal neurons. n=241 WT+EtOH, n=240 WT+Rapa, n=240 KO+EtOH and n=240 KO+Rapa neurons from 6-7 independent cultures 1 pup per culture. Kruskal-Wallis test, p<0.0001; WT+EtOH vs WT+Rapa, p>0.9999; WT+EtOH vs KO+EtOH, ****p<0.0001; WT+EtOH vs KO+Rapa, ****p<0.0001; KO+EtOH vs KO+Rapa, ****p<0.0001Dunn's multiple comparison tests.

Supplementary Tables

Supplementary Table 1: Mouse Lines

Mouse Line	Genotyping Primers	Source	Reference
Emx1-Cre	WT F: AAG GTG TGG TTC CAG AAT CG	JAX strain # 005628	[207]
	WT R: CTC TCC ACC AGA AGG CTG AG		
	Mut F: GCG GTC TGG CAG TAA AAA CTA TC		
	Mut R: GTG AAA CAG CAT TGC TGT CAC TT		
Tsc1$^{fl/fl}$	F: GTC ACG ACC GTA GGA GAA GC	JAX strain # 005680	[203]
	R: GAA TCA ACC CCA CAG AGC AT		

Supplementary Table 2: Viruses and titers.

Virus	Serotype	Promoter	Source	Titer of viral stock (vg/ml)	Dilution amount (*in vitro*)
AAV1.Syn.NES-jRGECO1a.WPRE.SV40	1	hSyn	Gift from Adesnik lab	2.08×10^{13}	1:20 0.5 µl/well
AAV9-U6-shRptor-EYFP	9	hU6	Caltech CLOVER Center	1.93×10^{14}	1:20 0.5 µl/well
AAV9-U6-shContorl-EYFP	9	hU6	Caltech CLOVER Center	2.17×10^{14}	1:20 0.5 µl/well

Supplementary Table 3: Antibodies and dilutions.

	Antibody	Host species	Company and catalog #	WB dilution
Primary	Tsc1	Rabbit	Cell Signaling 6935	1:800
	Raptor	Rabbit	Cell Signaling 2280	1:800
	rpS6	Rabbit	Cell Signaling 2317	1:1000
	phospho-rpS6 Ser244/246	Rabbit	Cell Signaling 2215	1:2000
	Akt	Rabbit	Cell Signaling 4691	1:1500
	phospho-Akt Ser 473	Rabbit	Cell Signaling 4060	1:1000
	4E-BP1	rabbit	Cell Signaling 9644	1:1000
	rpS6	Rabbit	Cell Signaling 2317	1:1000
	phospho-4E-BP1 Thr37/46	Rabbit	Cell Signaling 2855	1:1000
	Histone 3	Mouse	Cell Signaling 3638	1:2000
	Antibody	**Species (reactivity)**	**Company and catalog #**	**WB dilution**
Secondary	Goat anti-Rabbit-HFP	Rabbit	Bio-Rad 170-5046	1:5000
	Goat anti-Mouse-HRP	Mouse	Bio-Rad 170-5047	1:5000

Chapter 4

Preliminary study of mTORC1 and mTORC2 interactions in neurons and concluding remarks

Vasiliki Karalis

Department of Molecular and Cell Biology
University of California, Berkeley

Introduction

The mechanistic target of rapamycin (mTOR) pathway is a signaling hub involved in a range of diverse processes that ultimately govern proper development and function of the central nervous system[12]. Deregulation in this pathway have been associated with a wide range of disorders including neurodevelopmental, neurodegenerative as a well as neuropsychiatric disorders [14, 89]. Due to mTOR's implication in disease pathology there have been extensive efforts to understand how this signaling pathway is regulated in normal and disease state, and how it can be therapeutically targeted[31].

Current therapeutic strategies for mTOR related disorders rely on rapamycin, the first known inhibitor of mTORC1, and its analogues (rapalogs). However, the use of rapalogs is only partially effective at treating the wide range of neurologic manifestations presented in mTOR related disorders. In addition, chronic administration of rapalogs has been shown to suppress both mTOR complexes and has been associated with severe side effects[119]. While this strong suppression might be beneficial for manifestations outside the central nervous system and in particular in the context of tumors, studies in animal models have shown that strong mTORC1 and mTORC2 suppression severely impairs brain development and function[28, 209, 251, 257]. To develop better therapeutics for the neurologic manifestations in mTOR-related disorders it is important to 1) understand which mTOR complex underlies each specific neurologic abnormality and 2) identify novel strategies to selectively target each complex in way that will eventually rebalance and not suppress the mTOR signaling.

Several studies have attempted to elucidate the function of the two mTOR complexes in neurons by targeting Raptor or Rictor proteins which are integral components of mTORC1 and mTORC2 respectively. One of the first studies to explore the function of each individual mTOR complex was conducted by Urbanska et al.[178]. In this study the authors selectively manipulated the two complexes via shRNA targeting Raptor or Rictor in rat hippocampal neurons and examined changes in dendritic arborization. Their results revealed that both complexes are essential for proper dendritic arbor morphology[178]. Another study conducted by McCabe et al. examined the role of the two complexes in synaptic function[28]. By genetically targeting and inactivating *Rptor* or *Rictor* in cultured mouse hippocampal neurons they showed that the two complexes differentially modulate postsynaptic and presynaptic functions. Specifically, they showed that loss of mTORC1, reduces evoked excitatory postsynaptic currents (eEPSCs) via postsynaptic changes and enhanced spontaneous vesicle fusion and replenishment. In contrast, they showed that mTORC2 inactivation led to reduced eEPSCs but via presynaptic changes. Additionally, a study by Zhu et al., showed that mTORC2 but not mTORC1 is important for hippocampal mGLUR dependent synaptic long-term depression[27]. Finally, a recent study in dopaminergic neurons showed that loss of *Rptor* causes somatodendritic hypotrophy, decreased excitability and impaired DA release. Interestingly, the effects of *Rictor* loss appeared to be cell-type specific and milder than those observed with *Rptor* loss [257]. These studies suggest that the two complexes control both overlapping and different mechanisms in a potentially tissue-specific manner.

While several studies have explored the effect of downregulation of each complex in neurons by Raptor and Rictor manipulations, not much work has been conducted to examine how specific to each complex these manipulations are. One of the first studies

to link the activity of the two complexes led by Urbanska et al[178]. In this study, they showed that in rat hippocampal neurons Rictor downregulation decreased phosphorylation of S6 protein suggestive of reduced mTORC1 activity. We have previously shown that downregulation of Raptor in primary hippocampal neurons affects mTORC1 but also mTORC2 activity in opposite directions (see Chapter 2 Supplementary Fig. 2h-j). Studies in non-neuronal systems have provided evidence for several possible points of crosstalk between the two complexes. For example, it has been shown that p70S6K1, a direct target of mTORC1, can phosphorylate both Rictor and mSin1, two mTORC2 components, and inhibit mTORC2-dependent Akt phosphorylation[229-231]. In oligodendrocytes and cancer cell lines it has been shown that loss of *Rptor* and thus mTORC1 suppression, leads to increased Akt phosphorylation at the mTORC2 site [216, 226]. These data suggest that targeting either Raptor or Rictor does not selectively manipulate one complex but both, in a cell type-dependent manner. Careful examination is warranted to elucidate the signaling relationships between the two complexes. This information will enable us to develop better strategies to manipulate the complexes in such a way that mTOR signaling is rebalanced in disease states and avoid mTOR suppression-associated side effects.

Here we used primary hippocampal cultures from $Rptor^{fl/fl}$, $Rictor^{fl/fl}$ and $Rptor^{fl/fl};Rictor^{fl/fl}$ animals to conditionally delete *Rptor* or *Rictor* or both simultaneously and study how mTORC1 and mTORC2 function is affected in each of these conditions. We found that downregulation of either Raptor or Rictor affects phosphorylation of downstream targets of both mTOR complexes. In addition, we found that decreased Raptor protein levels more strongly affect total mTOR protein levels compared to Rictor protein loss. Finally, we observed that neither Raptor not Rictor loss affected neuronal soma size in primary hippocampal cultures. Our preliminary results suggest that, at least in hippocampal cultures, these genetic strategies do not allow for selective manipulation of the two mTOR complexes and thus we need alternative methods to examine the function of these complexes independently.

Results

S6 phosphorylation is reduced in both Raptor-KO and Rictor-KO hippocampal neurons

To assess the mTORC1 signaling status in Raptor-KO, Rictor-KO and Raptor-KO;Rictor-KO hippocampal neurons, we quantified the phosphorylation levels of a canonical downstream phosphorylation target of mTORC1, the ribosomal S6 protein at serines 240/244 (Fig. 1a). We found that phosphorylation of S6 was reduced in Raptor-KO neurons (Fig. 1b,c) suggestive of reduced mTORC1 activity as expected. Interestingly, we saw that S6 phosphorylation was also reduced in Rictor-KO neurons (Fig. 1b,d). In the double Raptor-KO;Rictor-KO neurons we also observed a strong decrease in S6 phosphorylation that is potentially stronger than Raptor-KO alone. Our data show that loss of either *Rptor* or *Rictor* decrease mTORC1 activity, particularly at the p70S6K/S6 branch.

Akt phosphorylation is altered in both Raptor-KO and Rictor-KO hippocampal neurons

To examine the mTORC2 signaling status in Raptor-KO, Rictor-KO and Raptor-KO;Rictor-KO hippocampal neurons we quantified the phosphorylation levels of a canonical downstream phosphorylation target of mTORC2, the Akt protein at serine 473 (Fig. 2a). Interestingly we found that downregulation of Raptor protein significantly increased p-Akt levels (Fig. 2b,c) suggestive of increased mTORC2 activity. As expected, Rictor downregulation, which suppresses mTORC2 activity, significantly decreased Akt phosphorylation (Fig. 2b,d). When we looked at the Raptor-KO;Rictor-KO neurons we saw that p-Akt was reduced approximately as much as in Rictor-KO neurons alone. These data suggest that downregulation of Raptor and suppression of mTORC1 leads to a Rictor and potentially mTORC2-dependent increase of Akt phosphorylation.

Raptor downregulation significantly affects mTOR protein levels

To determine whether total levels of mTOR change upon loss of Raptor or Rictor proteins we measured changes in total mTOR protein in Raptor-KO, Rictor-KO and Raptor-KO;Rictor-KO hippocampal neurons. Interestingly we found that loss of Raptor reduced total mTOR by approximately 50% (Fig. 3a,b) while loss of Rictor affected total mTOR by less than ~25% (Fig. 3a,c). With concomitant loss of Raptor and Rictor, we observed a strong and additive downregulation of total mTOR levels (Fig. 3a,d). These data suggest that in primary hippocampal neurons, mTOR may participate mainly in mTORC1 formation and thus there is more mTORC1 than mTORC2 in our system(Fig. 3e). Finally, this almost complete suppression of total mTOR in the absence of Raptor and Rictor suggest that mTOR protein gets degraded if not bound to either one of these proteins.

Neither Raptor nor Rictor downregulation affect neuronal soma size

Since both mTOR complexes have been implicated in the control of cell soma size of various cell types including neurons[209, 237, 239, 257], we examined how downregulation of Raptor or Rictor affects hippocampal neuron soma size. Interestingly, we saw that neither deletion of *Rptor* (Fig. 4 a-c) nor *Rictor* (Fig. 4 d-f) significantly affected hippocampal neuron soma size *in vitro*.

Discussion

The goal of this study was to dissect the interactions between the two mTOR complexes in mouse primary hippocampal neurons. Out preliminary data show that downregulation of either Raptor or Rictor proteins, the obligatory components of mTORC1 and mTORC2 respectively, affects the activity of both complexes. Furthermore, we saw that more mTOR protein is associated with Raptor and hence within mTORC1 than Rictor and mTORC2. Finally, we found that neither Raptor nor Rictor suppression affects hippocampal soma size *in vitro*. Together these data strongly support the idea that the two complexes interact and that manipulation of Raptor or Rictor proteins is not the optimal strategy to dissociate mTOR complex activity in primary hippocampal cultures and potentially other systems.

Here we deleted *Rptor* or *Rictor* to test if and how their suppression affects both mTOR complexes. We observed that downregulation of Rictor decreased p-S6 levels and thus we hypothesize that under normal conditions mTORC2 is a positive regulator of mTORC1. Upon loss of *Rictor*, mTORC2 activity is downregulated and this positive feedback on mTORC1 is removed, hence mTORC1 signaling decreases. Interestingly, we noticed that p-S6 in Rictor-KO cultures was even further suppressed in comparison to Raptor-KO cultures. This unexpected observation can be explained by our previous findings (see Chapter 2 Supplementary Fig. 2a,c,e). Specifically, we found that after 14 days *in vitro* in Raptor-KO cultures there was still residual Raptor protein, which may be able to maintain significant levels of mTORC1 activity.

As we have previously shown, loss of Raptor leads to decreased mTORC1 activity and increased mTORC2 activity as indicated by levels of p-S6 and p-Akt respectively (see Chapter 2 Supplementary Fig. 2h-j). In this study we were able to recapitulate the same observation and hence we hypothesize that mTORC1 is a negative regulator of mTORC2. Specifically, we propose that upon loss of *Rptor* and mTORC1 downregulation, the negative feedback exerted from mTORC1 on mTORC2 is removed and thus mTORC2 activity is upregulated.

Finally, we wanted to explore whether mTOR kinase participates equally in the formation of the two complexes. Therefore, we examined the changes in the total mTOR protein levels upon Raptor and Rictor downregulation. We found that total mTOR levels were strongly downregulated in Raptor-KO cultures and mildly downregulated in Rictor-KO cultures. We hypothesize that in normal conditions, there is more mTORC1 than mTORC2 in our system (data summarized in Fig. 5). It will be interesting to examine whether in the absence of Raptor protein there is free mTOR that is available to bind on Rictor and promote mTORC2 formation. This could potentially partially underlie the increased mTORC2 activity levels in Raptor-KO cultures.

<u>Considerations and Future directions</u>

While these data clearly show that in primary hippocampal cultures the mTOR complexes regulate each other's function, our study is still very limited. Thus far, we have used only one downstream target as a readout to assess each mTOR complex's activity. It would be interesting to test whether other downstream targets of both complexes are affected the same way as the ones presented here. In an alternative scenario, the two complexes might affect each other's activity towards specific substrates. This substrate

bias has been observed in mTORC1 inhibition via rapamycin [117] which has been shown to affect some but not all mTORC1 substrates. Such substate bias could arise due to differential subcellular localization of the mTOR complexes within different cell types and across development. Localization could potentially affect access to certain substates and thus dictate which substrates will get primarily phosphorylated.

Several studies have showed that many mTOR functions are cell-type dependent. For instance, downregulation of either Raptor or Rictor decreases dopaminergic[257] and cortical[209] but not hippocampal neuronal soma size (Fig. 4a-f and Chapter 2 Fig. 7k,m). These data highlight that mTOR signaling might differ among different neuronal cell types and hence, the specific interactions we observe between the mTOR complexes in primary hippocampal neurons might be unique to that system. It would be interesting to examine whether we can recapitulate these observations in other types of neuronal cultures such as cortical or dopaminergic.

Studies have also shown that the developmental stage at which the mTOR pathway is perturbed dictates the range and severity of phenotypic manifestations in brain development and function. One of the most striking examples is embryonic vs postnatal loss of *Rptor*. We previously showed that embryonic loss of *Rptor* from forebrain excitatory neurons using the Emx1-Cre mouse line causes severely impaired forebrain development including cortical hypotrophy and absence of hippocampal structures(see Chapter 2 Supplementary Fig. 4f). In contrast, a study that used the CamKIIa-Cre mouse line to conditionally delete *Rptor* from neurons postnatally observed significantly less severe phenotypes and mice had fully formed hippocampal and cortical structures[239]. How the developmental time course affects the function of the two mTOR complexes has not been thoroughly explored, especially in postmitotic cells such as neurons. A study has previously shown that phosphorylation levels of S6 decrease over time in human differentiated neurons[166]. However, the exact mechanism(s) by which this activity change occurs are still unknown. Several parameters could potentially affect mTOR signaling across development. Such parameters include changes in 1) the total levels of the two complexes and/or the ratios among them, 2) the expression levels of mTORC1/2 upstream regulators either inhibitors or activators and 3) the subcellular localization patterns of the two complexes, and thus substrate access and availability. Such information will be critical to identify developmental time windows during which the mTOR complexes might regulate specific functions.

The neurologic abnormalities associated with mTOR deregulation are numerous and studies continue to associate mTOR signaling with essential brain functions. It will be important to understand how this signaling pathway is regulated in different cell types, across development, and in health and disease states. Such information will enable us to develop novel and more targeted therapeutics either to prevent or rescue neurologic abnormalities associated with the mTOR signaling pathway.

Materials and Methods

Mice

All animal procedures were carried out in accordance with protocols approved by the University of California, Berkeley Institutional Animal Care and Use Committee (IACUC) AUP-2016-04-8684. Mice of both sexes were used, and the ages are indicated in the methods for each experiment. Mice were on a mixed genetic background. Mice were housed with same-sex littermates in groups of 5–6 animals per cage and kept on a regular 12 h light/dark with ad libitum access to standard chow and water.

Mouse Line	Genotyping Primers	Source	Reference
Rptor$^{fl/fl}$	F: AGCCTTTAGTACCCACTTGGC R: GGCATCTCACAAAGGGTACAG	JAX strain # 013188	[204]
Rictor$^{fl/fl}$	F: ACTGATATGTTCATGGTTGTG R: GACACTGGATTCAGTGGCTTG	JAX strain # 020649	[205, 206]

Primary hippocampal cultures

Dissociated hippocampal cultures were prepared from postnatal day 0-1 (P0-1) mice using standard protocols. Briefly, hippocampi from 2-3 pups (floxed mouse lines, Figs. 1-3 and Supplementary Figs. 1-3) were dissected on ice. The tissue was dissociated using 34.4 µg/ml papain in dissociation media (HBSS Ca^{2+}, Mg^{2+} free, 1 mM sodium pyruvate, 0.1% D-glucose, 10 mM HEPES buffer) and incubated for 3 min at 37°C. Tissue digestion was stopped by incubation in trypsin inhibitor (1 mg/ml) in dissociation media at 37°C for 4 min. After trypsin inhibition, dissociation media was carefully removed and the tissue was gently manually triturated in 5 ml plating media (MEM, 10% FBS, 0.45% D-Glucose, 1 mM sodium pyruvate, 1 mM L-glutamine). Cell density was counted using a TC10 Automated cell counter (Bio-Rad) and ~2-2.25 × 10^5 neurons were plated for each experiment. For western blotting and Ca^{2+} imaging experiments, neurons were plated onto 24-well plates pre-coated with Poly-D-Lysine (PDL) (Corning, Cat # 08774271). For immunocytochemistry, neurons were plated onto 12 mm glass coverslips precoated overnight at room temperature (RT) with 0.5 mg/ml PDL in 0.1 M borate buffer (pH 8.5). On the plating day, the coverslips were rinsed 4 times with sterile water and then coated with 20 µg/ml laminin (GIBCO, 23017015) in 1x PBS for ~1.5h at 37°C. Subsequently, coverslips were rinsed 3 times with sterile water, and 400 µl of plating media were added prior to adding the dissociated neurons. For all cultures, plating media was removed after 3 h and 900 µl maintenance media (Neurobasal media (Fisher Scientific # 21103-049) with 2 mM glutamine, pen/strep, and B-27 supplement (Invitrogen # 17504-044)) were added per well. After 4 days *in vitro* (DIV 4), 1 µM Cytosine β-D-arabinofuranoside (Sigma-Aldrich # C6645) was added to prevent glial proliferation. Cultures were maintained in maintenance media for 14 days partial media changes every 4 days.

Adeno-associated virus (AAV) transduction of primary cultures

AAVs were added on DIV 2. Amounts of AAVs were chosen after titration experiments for each virus to accomplish either maximum or sparse transduction

efficiency while maintaining low toxicity levels. In primary cultures from *Rptor*$^{fl/fl}$, *Rictor*$^{fl/fl}$ and *Rptor*$^{fl/fl}$;*Rictor*$^{fl/fl}$ mice that were used for western blotting experiments, we aimed for >95% transduction efficiency using AAV1 human Synapsin 1 (*SYN1,* "hSyn") promoter-driven Cre-GFP or GFP to generate mutant and control cultures, respectively. For immunocytochemistry experiments, we aimed for sparse transduction to resolve individual neurons using AAV1-CBA-mCherry-Cre (nuclear localized), AAV9-CAG-FLEX-tdTomato, and AAV5-hSyn-GFP.

Virus	**Serotype**	**Promoter**	**Source**	**Titer of viral stock (vg/ml)**	**Dilution amount (*in vitro*)**
AAV1.hSyn.HI.eGFP-Cre.WPRE.SV40	1	hSyn	Penn Vector Core	$1.78x10^{13}$	1:20 0.5 µl/well
AAV1.hSyn.eGFP.WPRE.bGH	1	hSyn	Penn Vector Core	$3.86x10^{13}$	1:20 0.5 µl/well
AAV5.hSyn.eGFP	5	hSyn	UNC Vector Core	$4x10^{12}$	1:100 0.5
AAV1.CBA.mCherry-nCre.WPRE.bGH	1	CBA	Penn Vector Core	$1.04x10^{13}$	1:100 0.5 µl/well
AAV9.CAG.Flex.tdTomato.WPRE.bGH (AllenInstitute864)	9	CAG	Penn Vector Core	unknown	1:20 0.5 µl/well

Protein extraction and western blot analysis

Hippocampal cultures were harvested on DIV 14 -18. Neurobasal media was aspirated from one well at a time, wells were quickly rinsed with ice cold 1x PBS with Ca^{2+}/Mg^{2+} and then 75 µl of lysis buffer were added (lysis buffer: 2 mM EDTA (Sigma: E5134), 2 mM EGTA (Sigma: E3889), 1% Triton-X (Sigma: T8787), and 0.5% SDS (Sigma: 71736) in 1× PBS with Halt phosphatase inhibitor cocktail (ThermoFisher: PI78420) and Complete mini EDTA-free protease inhibitor cocktail (Roche: 4693159001)). Wells were thoroughly scraped, and lysates were collected and sonicated for 5 sec. Total protein was determined by BCA assay (ThermoFisher: PI23227) and 10 µg of protein in 1X Laemmli sample buffer (Bio-Rad:161-0747) were loaded onto 4-15% Criterion TGX gels (Bio-Rad: 5671084). Proteins were transferred overnight at low voltage to PVDF membranes (Bio-Rad: 1620177), blocked in 5% milk in 1x TBS-Tween for one hour at RT, and incubated with primary antibodies diluted in 5% milk in 1x TBS-Tween overnight at 4°C. The following day, membranes were washed 3 x 10 min in 1x TBS-Tween and incubated with HRP-conjugated secondary antibodies (1:5000) for one hour at RT, washed 6 x 10 min in 1x TBS-Tween, incubated with chemiluminescence substrate (Perkin-Elmer: NEL105001EA) and developed on GE Amersham Hyperfilm ECL (VWR: 95017-661). Membranes were stripped by

two 7 min incubations in stripping buffer (6 M guanidine hydrochloride (Sigma: G3272) with 1:150 beta-mercaptoethanol) with shaking followed by four 2 min washes in 1x TBS with 0.05% NP-40 to re-blot on subsequent days. Bands were quantified by densitometry using ImageJ software (NIH). Phospho-proteins were normalized to their respective total proteins. Histone-3 was used as a loading control for every experiment.

	Antibody	**Host species**	**Company and catalog #**	**WB dilution**
Primary	Raptor	Rabbit	Cell Signaling 2280	1:800
	Rictor	Rabbit	Cell Signaling 2114	1:600
	rpS6	Rabbit	Cell Signaling 2317	1:1000
	phospho-rpS6 Ser244/246	Rabbit	Cell Signaling 5364	1:2000
	Akt	Rabbit	Cell Signaling 4691	1:1500
	phospho-Akt Ser 473	Rabbit	Cell Signaling 4060	1:1000
	Histone 3	Mouse	Cell Signaling 3638	1:2000
	Antibody	**Species (reactivity)**	**Company and catalog #**	**WB dilution**
Secondary	Goat anti-Rabbit-HFP	Rabbit	Bio-Rad 170-5046	1:5000
	Goat anti-Mouse-HRP	Mouse	Bio-Rad 170-5047	1:5000

Figures

Figure 1

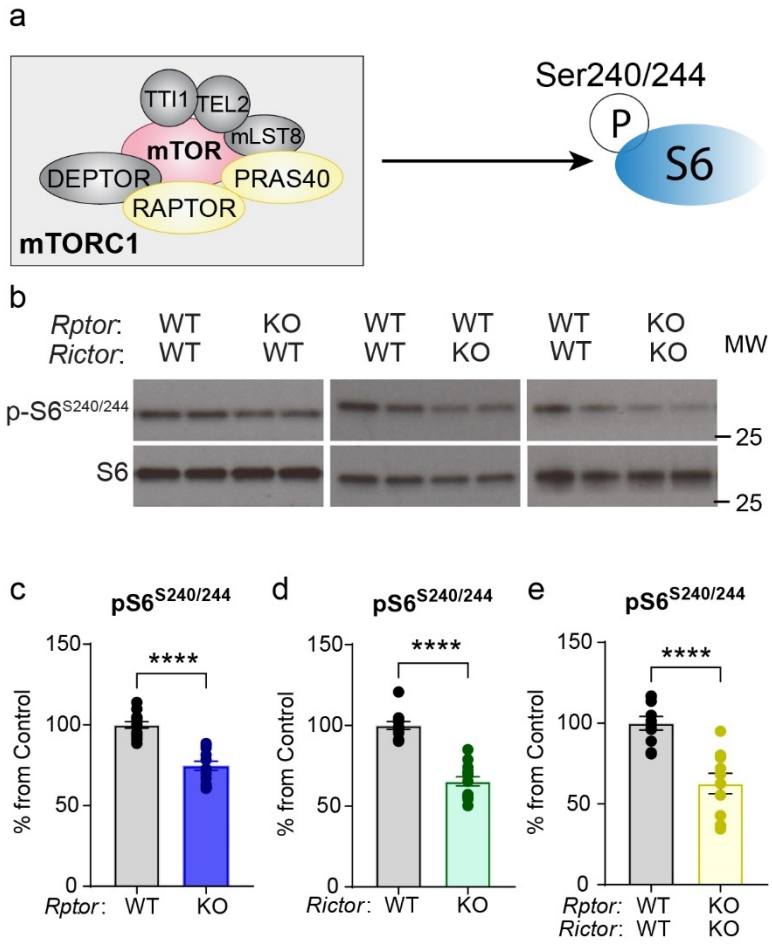

Figure 1: Loss of *Rptor* or *Rictor* reduces phosphorylation of S6 protein
a) Schematic representation of mTORC1 showing in addition to other components its obligatory component Raptor. mTORC1 phosphorylates S6 at Ser240/244.
b) Representative western blots from *Rptor*$^{fl/fl}$, *Rictor*$^{fl/fl}$ *and Rptor*$^{fl/fl}$*;Rictor*$^{fl/fl}$ hippocampal cultures treated with AAV-GFP (WT;WT) or AAV-Cre-GFP (KO or KO;KO) and harvested on DIV 14. MW indicates molecular weight. Two independent samples per genotype are shown; this experiment was replicated three times.
c-e) Bar graphs display western blot quantification (mean +/- SEM) for p-S6-Ser240/244 normalized to Total S6 and expressed as a percentage of Control (WT) levels in c) *Rptor*$^{fl/fl}$. Mann-Whitney test, ****p<0.0001; *d) Rictor*$^{fl/fl}$, Mann-Whitney test, ****p<0.0001; *and e) Rptor*$^{fl/fl}$*;Rictor*$^{fl/fl}$ Mann-Whitney test, ****p<0.0001. n=9-12 culture wells from 3-4 independent cultures per genotype; 2 mice per culture.

Figure 2

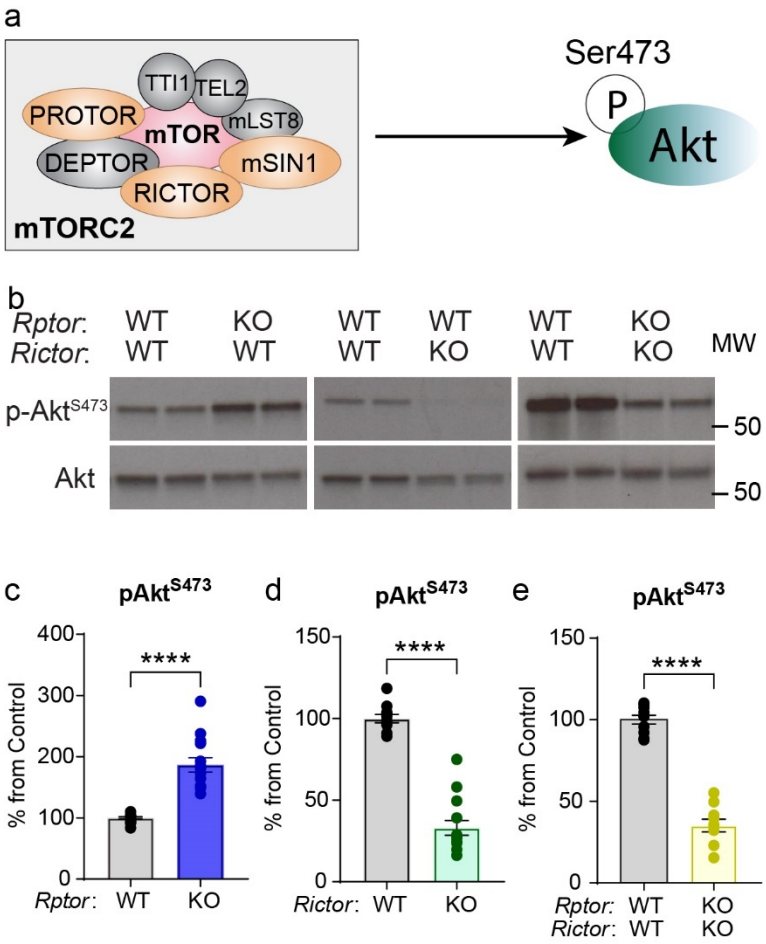

Figure 2: Deletion of *Rptor* or *Rictor* oppositely affects phosphorylation of Akt.
a) Schematic representation of mTORC2 showing in addition to other components it's obligatory component Rictor. mTORC2 phosphorylates Akt at Ser473.
b) Representative western blots from *Rptor*$^{fl/fl}$, *Rictor*$^{fl/fl}$ *and Rptor*$^{fl/fl}$*;Rictor*$^{fl/fl}$ hippocampal cultures treated with AAV-GFP (WT;WT) or AAV-Cre-GFP (KO or KO;KO) and harvested on DIV 14. MW indicates molecular weight. Two independent samples per genotype are shown; this experiment was replicated three times.
c-e) Bar graphs display western blot quantification (mean +/- SEM) for p-Akt-Ser473 normalized to Total Akt and expressed as a percentage of Control (WT) levels in c) *Rptor*$^{fl/fl}$. Mann-Whitney test, ****p<0.0001; *d) Rictor*$^{fl/fl}$, Mann-Whitney test, ****p<0.0001; *and e) Rptor*$^{fl/fl}$*;Rictor*$^{fl/fl}$ Mann-Whitney test, ****p<0.0001. n=9-12 culture wells from 3-4 independent cultures per genotype; 2 mice per culture.

Figure 3

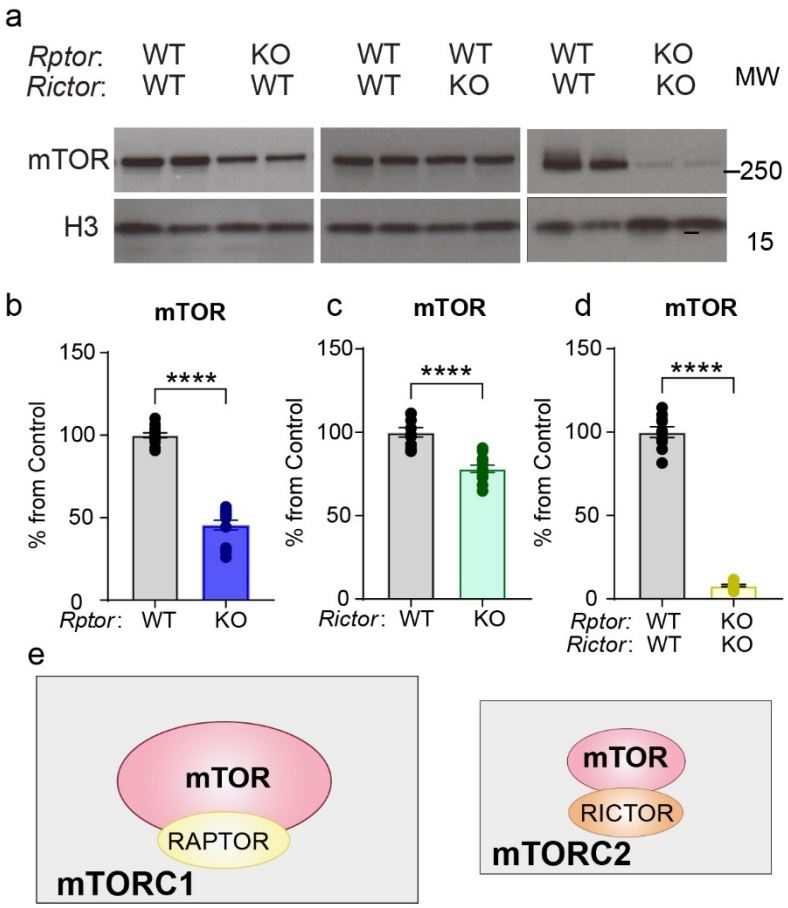

Figure 3: Total mTOR levels are strongly reduced by deletion of *Rptor*

a) Representative western blots from *Rptor*$^{fl/fl}$, *Rictor*$^{fl/fl}$ *and Rptor*$^{fl/fl}$*;Rictor*$^{fl/fl}$ hippocampal cultures treated with AAV-GFP (WT;WT) or AAV-Cre-GFP (KO or KO;KO) and harvested on DIV 14. MW indicates molecular weight. Two independent samples per genotype are shown; this experiment was replicated three times.

b-d) Bar graphs display western blot quantification (mean +/- SEM) for Total mTOR expressed as a percentage of Control (WT) levels in b) *Rptor*$^{fl/fl}$. Mann-Whitney test, ****p<0.0001; *c) Rictor*$^{fl/fl}$, Mann-Whitney test, ****p<0.0001; *and d) Rptor*$^{fl/fl}$*;Rictor*$^{fl/fl}$ Mann-Whitney test, ****p<0.0001. n=9-12 culture wells from 3-4 independent cultures per genotype; 2 mice per culture.

e) Schematic representation of the hypothesized ratio between mTORC1 and mTORC2

Figure 4

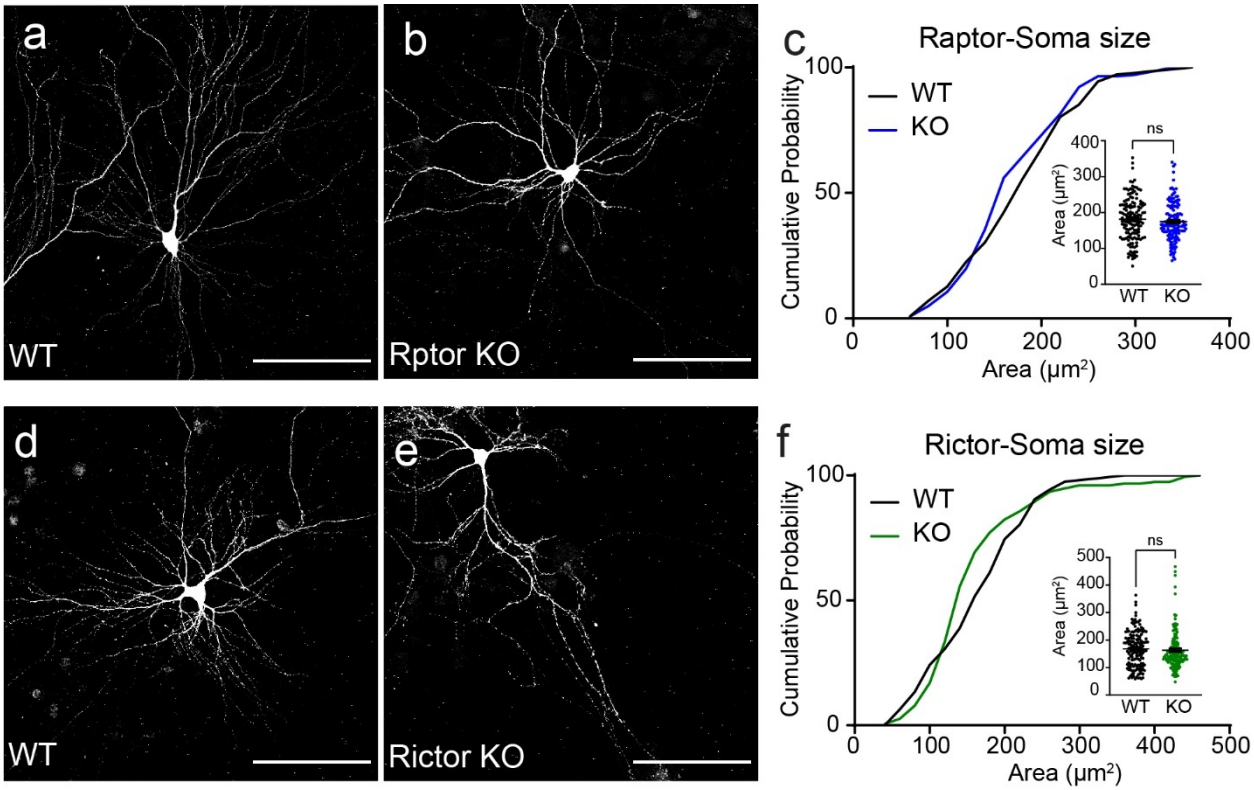

Figure 4: Soma size is not significantly altered in *Rptor* or *Rictor* KO primary hippocampal neurons.
a-b) Example fluorescence images of a) *Rptor*$^{fl/fl}$ neurons expressing GFP (WT, control) and b) *Rptor*$^{fl/fl}$ neurons expressing Cre dependent tdTomato (Rptor-KO). Scale bars = 100μm
c) Cumulative distributions of soma area for cultured *Rptor*$^{fl/fl}$ neurons treated with AAV-GFP (control) or AAV-Cre-mCherry and AAV-FLEx-TdTomato (Rptor-KO). n=142 GFP+ and 141 Cre+ neurons. Inset scatter dot plot of the same data. Black lines indicated mean +/- SEM. Mann-Whitney, p=0.2330.
d-e) Example fluorescence images of e) *Rictor*$^{fl/fl}$ neurons expressing GFP (WT, control) and f) *Rictor*$^{fl/fl}$ neurons expressing Cre dependent tdTomato (Rptor-KO). Scale bars=100μm
f) Cumulative distributions of soma area for cultured *Rictor*$^{fl/fl}$ neurons treated with AAV-GFP (control) or AAV-Cre-mCherry and AAV-FLEx-TdTomato (Rictor-KO). n=157 GFP+ and 153 Cre+ neurons. Inset scatter dot plot of the same data. Black lines indicated mean +/- SEM. Mann-Whitney, p=0.1033.

Figure 5

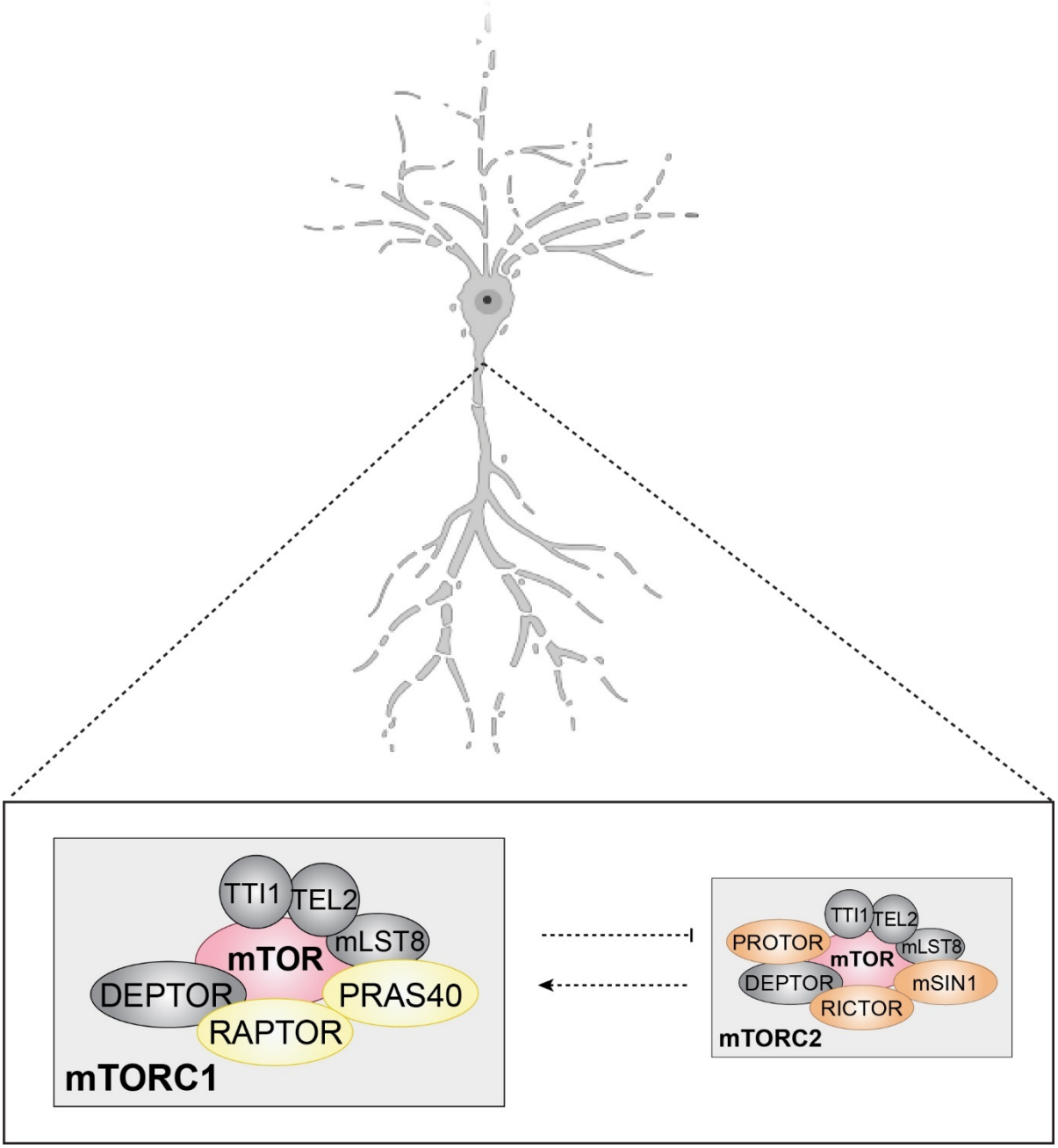

Figure 5: Proposed model of mTOR complexes' relationships in primary hippocampal neurons. In primary hippocampal cultured neurons mTOR kinase participates mainly in the mTORC1 formation. Under normal conditions mTORC1 negatively regulates mTORC2 while mTORC2 behaves as a positive regulator of mTORC1. Created with BioRender.com

References

1. Vezina, C., A. Kudelski, and S.N. Sehgal, *Rapamycin (AY-22,989), a new antifungal antibiotic. I. Taxonomy of the producing streptomycete and isolation of the active principle.* J Antibiot (Tokyo), 1975. **28**(10): p. 721-6.
2. Heitman, J., N.R. Movva, and M.N. Hall, *Targets for cell cycle arrest by the immunosuppressant rapamycin in yeast.* Science, 1991. **253**(5022): p. 905-9.
3. Koltin, Y., et al., *Rapamycin sensitivity in Saccharomyces cerevisiae is mediated by a peptidyl-prolyl cis-trans isomerase related to human FK506-binding protein.* Mol Cell Biol, 1991. **11**(3): p. 1718-23.
4. Sabatini, D.M., et al., *RAFT1: a mammalian protein that binds to FKBP12 in a rapamycin-dependent fashion and is homologous to yeast TORs.* Cell, 1994. **78**(1): p. 35-43.
5. Sabers, C.J., et al., *Isolation of a protein target of the FKBP12-rapamycin complex in mammalian cells.* J Biol Chem, 1995. **270**(2): p. 815-22.
6. Fingar, D.C., et al., *mTOR controls cell cycle progression through its cell growth effectors S6K1 and 4E-BP1/eukaryotic translation initiation factor 4E.* Mol Cell Biol, 2004. **24**(1): p. 200-16.
7. Sarbassov, D.D., S.M. Ali, and D.M. Sabatini, *Growing roles for the mTOR pathway.* Curr Opin Cell Biol, 2005. **17**(6): p. 596-603.
8. Fifkova, E., et al., *Effect of anisomycin on stimulation-induced changes in dendritic spines of the dentate granule cells.* J Neurocytol, 1982. **11**(2): p. 183-210.
9. Frey, U., et al., *Anisomycin, an inhibitor of protein synthesis, blocks late phases of LTP phenomena in the hippocampal CA1 region in vitro.* Brain Res, 1988. **452**(1-2): p. 57-65.
10. Gingras, A.C., B. Raught, and N. Sonenberg, *Regulation of translation initiation by FRAP/mTOR.* Genes Dev, 2001. **15**(7): p. 807-26.
11. Tang, S.J., et al., *A rapamycin-sensitive signaling pathway contributes to long-term synaptic plasticity in the hippocampus.* Proc Natl Acad Sci U S A, 2002. **99**(1): p. 467-72.
12. Switon, K., et al., *Molecular neurobiology of mTOR.* Neuroscience, 2017. **341**: p. 112-153.
13. Jaworski, J. and M. Sheng, *The growing role of mTOR in neuronal development and plasticity.* Mol Neurobiol, 2006. **34**(3): p. 205-19.
14. Lipton, J.O. and M. Sahin, *The neurology of mTOR.* Neuron, 2014. **84**(2): p. 275-91.
15. Costa-Mattioli, M. and L.M. Monteggia, *mTOR complexes in neurodevelopmental and neuropsychiatric disorders.* Nat Neurosci, 2013. **16**(11): p. 1537-43.
16. Wong, M., *Mammalian target of rapamycin (mTOR) pathways in neurological diseases.* Biomed J, 2013. **36**(2): p. 40-50.
17. Hara, K., et al., *Raptor, a binding partner of target of rapamycin (TOR), mediates TOR action.* Cell, 2002. **110**(2): p. 177-89.
18. Kim, D.H., et al., *mTOR interacts with raptor to form a nutrient-sensitive complex that signals to the cell growth machinery.* Cell, 2002. **110**(2): p. 163-75.

19. Sarbassov, D.D., et al., *Rictor, a novel binding partner of mTOR, defines a rapamycin-insensitive and raptor-independent pathway that regulates the cytoskeleton.* Curr Biol, 2004. **14**(14): p. 1296-302.
20. Kim, D.H., et al., *GbetaL, a positive regulator of the rapamycin-sensitive pathway required for the nutrient-sensitive interaction between raptor and mTOR.* Mol Cell, 2003. **11**(4): p. 895-904.
21. Peterson, T.R., et al., *DEPTOR is an mTOR inhibitor frequently overexpressed in multiple myeloma cells and required for their survival.* Cell, 2009. **137**(5): p. 873-86.
22. Kaizuka, T., et al., *Tti1 and Tel2 are critical factors in mammalian target of rapamycin complex assembly.* J Biol Chem, 2010. **285**(26): p. 20109-16.
23. Sancak, Y., et al., *PRAS40 is an insulin-regulated inhibitor of the mTORC1 protein kinase.* Mol Cell, 2007. **25**(6): p. 903-15.
24. Frias, M.A., et al., *mSin1 is necessary for Akt/PKB phosphorylation, and its isoforms define three distinct mTORC2s.* Curr Biol, 2006. **16**(18): p. 1865-70.
25. Pearce, L.R., et al., *Identification of Protor as a novel Rictor-binding component of mTOR complex-2.* Biochem J, 2007. **405**(3): p. 513-22.
26. Liu, G.Y. and D.M. Sabatini, *mTOR at the nexus of nutrition, growth, ageing and disease.* Nat Rev Mol Cell Biol, 2020. **21**(4): p. 183-203.
27. Zhu, P.J., et al., *mTORC2, but not mTORC1, is required for hippocampal mGluR-LTD and associated behaviors.* Nat Neurosci, 2018. **21**(6): p. 799-802.
28. McCabe, M.P., et al., *Genetic inactivation of mTORC1 or mTORC2 in neurons reveals distinct functions in glutamatergic synaptic transmission.* Elife, 2020. **9**.
29. Crino, P.B., *Focal brain malformations: seizures, signaling, sequencing.* Epilepsia, 2009. **50 Suppl 9**: p. 3-8.
30. Crino, P.B., *mTOR: A pathogenic signaling pathway in developmental brain malformations.* Trends Mol Med, 2011. **17**(12): p. 734-42.
31. Crino, P.B., *The mTOR signalling cascade: paving new roads to cure neurological disease.* Nat Rev Neurol, 2016. **12**(7): p. 379-92.
32. Pilarski, R., *PTEN Hamartoma Tumor Syndrome: A Clinical Overview.* Cancers (Basel), 2019. **11**(6).
33. Song, M.S., L. Salmena, and P.P. Pandolfi, *The functions and regulation of the PTEN tumour suppressor.* Nat Rev Mol Cell Biol, 2012. **13**(5): p. 283-96.
34. Elia, M., et al., *An atypical patient with Cowden syndrome and PTEN gene mutation presenting with cortical malformation and focal epilepsy.* Brain Dev, 2012. **34**(10): p. 873-6.
35. Adachi, T., et al., *Cowden Syndrome with a Novel PTEN Mutation Presenting with Partial Epilepsy Related to Focal Cortical Dysplasia.* Intern Med, 2018. **57**(1): p. 97-99.
36. Cheung, K.M., et al., *Atypical focal cortical dysplasia in a patient with Cowden syndrome.* Hong Kong Med J, 2014. **20**(2): p. 165-7.
37. Varga, E.A., et al., *The prevalence of PTEN mutations in a clinical pediatric cohort with autism spectrum disorders, developmental delay, and macrocephaly.* Genet Med, 2009. **11**(2): p. 111-7.

38. Satterstrom, F.K., et al., *Large-Scale Exome Sequencing Study Implicates Both Developmental and Functional Changes in the Neurobiology of Autism.* Cell, 2020. **180**(3): p. 568-584 e23.
39. Pang, T., R. Atefy, and V. Sheen, *Malformations of cortical development.* Neurologist, 2008. **14**(3): p. 181-91.
40. Blumcke, I., et al., *The clinicopathologic spectrum of focal cortical dysplasias: a consensus classification proposed by an ad hoc Task Force of the ILAE Diagnostic Methods Commission.* Epilepsia, 2011. **52**(1): p. 158-74.
41. Pavone, P., et al., *A clinical review on megalencephaly: A large brain as a possible sign of cerebral impairment.* Medicine (Baltimore), 2017. **96**(26): p. e6814.
42. Mirzaa, G.M. and A. Poduri, *Megalencephaly and hemimegalencephaly: breakthroughs in molecular etiology.* Am J Med Genet C Semin Med Genet, 2014. **166C**(2): p. 156-72.
43. Leventer, R.J., R. Guerrini, and W.B. Dobyns, *Malformations of cortical development and epilepsy.* Dialogues Clin Neurosci, 2008. **10**(1): p. 47-62.
44. Desbiens, R., et al., *Life-threatening focal status epilepticus due to occult cortical dysplasia.* Arch Neurol, 1993. **50**(7): p. 695-700.
45. Barkovich, A.J., W.B. Dobyns, and R. Guerrini, *Malformations of cortical development and epilepsy.* Cold Spring Harb Perspect Med, 2015. **5**(5): p. a022392.
46. Baybis, M., et al., *mTOR cascade activation distinguishes tubers from focal cortical dysplasia.* Ann Neurol, 2004. **56**(4): p. 478-87.
47. Miyata, H., A.C. Chiang, and H.V. Vinters, *Insulin signaling pathways in cortical dysplasia and TSC-tubers: tissue microarray analysis.* Ann Neurol, 2004. **56**(4): p. 510-9.
48. Ljungberg, M.C., et al., *Activation of mammalian target of rapamycin in cytomegalic neurons of human cortical dysplasia.* Ann Neurol, 2006. **60**(4): p. 420-9.
49. Aronica, E., et al., *Co-expression of cyclin D1 and phosphorylated ribosomal S6 proteins in hemimegalencephaly.* Acta Neuropathol, 2007. **114**(3): p. 287-93.
50. Jansen, L.A., et al., *PI3K/AKT pathway mutations cause a spectrum of brain malformations from megalencephaly to focal cortical dysplasia.* Brain, 2015. **138**(Pt 6): p. 1613-28.
51. Zhao, S., et al., *A brain somatic RHEB doublet mutation causes focal cortical dysplasia type II.* Exp Mol Med, 2019. **51**(7): p. 84.
52. Lim, J.S., et al., *Brain somatic mutations in MTOR cause focal cortical dysplasia type II leading to intractable epilepsy.* Nat Med, 2015. **21**(4): p. 395-400.
53. Lim, J.S., et al., *Somatic Mutations in TSC1 and TSC2 Cause Focal Cortical Dysplasia.* Am J Hum Genet, 2017. **100**(3): p. 454-472.
54. Baldassari, S., et al., *Dissecting the genetic basis of focal cortical dysplasia: a large cohort study.* Acta Neuropathol, 2019. **138**(6): p. 885-900.
55. Bar-Peled, L., et al., *A Tumor suppressor complex with GAP activity for the Rag GTPases that signal amino acid sufficiency to mTORC1.* Science, 2013. **340**(6136): p. 1100-6.

56. Baulac, S., *mTOR signaling pathway genes in focal epilepsies.* Prog Brain Res, 2016. **226**: p. 61-79.
57. Ribierre, T., et al., *Second-hit mosaic mutation in mTORC1 repressor DEPDC5 causes focal cortical dysplasia-associated epilepsy.* J Clin Invest, 2018. **128**(6): p. 2452-2458.
58. Iffland, P.H., 2nd, et al., *GATORopathies: The role of amino acid regulatory gene mutations in epilepsy and cortical malformations.* Epilepsia, 2019. **60**(11): p. 2163-2173.
59. Hawley, S.A., et al., *Complexes between the LKB1 tumor suppressor, STRAD alpha/beta and MO25 alpha/beta are upstream kinases in the AMP-activated protein kinase cascade.* J Biol, 2003. **2**(4): p. 28.
60. Lau, N., et al., *Loss of neurofibromin is associated with activation of RAS/MAPK and PI3-K/AKT signaling in a neurofibromatosis 1 astrocytoma.* J Neuropathol Exp Neurol, 2000. **59**(9): p. 759-67.
61. Puffenberger, E.G., et al., *Polyhydramnios, megalencephaly and symptomatic epilepsy caused by a homozygous 7-kilobase deletion in LYK5.* Brain, 2007. **130**(Pt 7): p. 1929-41.
62. Nix, J.S., J. Blakeley, and F.J. Rodriguez, *An update on the central nervous system manifestations of neurofibromatosis type 1.* Acta Neuropathol, 2020. **139**(4): p. 625-641.
63. Hoeffer, C.A., et al., *Altered mTOR signaling and enhanced CYFIP2 expression levels in subjects with fragile X syndrome.* Genes Brain Behav, 2012. **11**(3): p. 332-41.
64. Troca-Marin, J.A., et al., *The Akt-mTOR pathway in Down's syndrome: the potential use of rapamycin/rapalogs for treating cognitive deficits.* CNS Neurol Disord Drug Targets, 2014. **13**(1): p. 34-40.
65. Tang, G., et al., *Loss of mTOR-dependent macroautophagy causes autistic-like synaptic pruning deficits.* Neuron, 2014. **83**(5): p. 1131-43.
66. Olney, N.T., et al., *Linking tuberous sclerosis complex, excessive mTOR signaling, and age-related neurodegeneration: a new association between TSC1 mutation and frontotemporal dementia.* Acta Neuropathol, 2017. **134**(5): p. 813-816.
67. Bateup, H.S., et al., *Temporal dynamics of a homeostatic pathway controlling neural network activity.* Front Mol Neurosci, 2013. **6**: p. 28.
68. van Slegtenhorst, M., et al., *Identification of the tuberous sclerosis gene TSC1 on chromosome 9q34.* Science, 1997. **277**(5327): p. 805-8.
69. European Chromosome 16 Tuberous Sclerosis, C., *Identification and characterization of the tuberous sclerosis gene on chromosome 16.* Cell, 1993. **75**(7): p. 1305-15.
70. Nakashima, A., et al., *Identification of TBC7 having TBC domain as a novel binding protein to TSC1-TSC2 complex.* Biochem Biophys Res Commun, 2007. **361**(1): p. 218-23.
71. Dibble, C.C., et al., *TBC1D7 is a third subunit of the TSC1-TSC2 complex upstream of mTORC1.* Mol Cell, 2012. **47**(4): p. 535-46.
72. Garami, A., et al., *Insulin activation of Rheb, a mediator of mTOR/S6K/4E-BP signaling, is inhibited by TSC1 and 2.* Mol Cell, 2003. **11**(6): p. 1457-66.

73. Tee, A.R., et al., *Tuberous sclerosis complex gene products, Tuberin and Hamartin, control mTOR signaling by acting as a GTPase-activating protein complex toward Rheb.* Curr Biol, 2003. **13**(15): p. 1259-68.
74. Mizuguchi, M. and S. Takashima, *Neuropathology of tuberous sclerosis.* Brain Dev, 2001. **23**(7): p. 508-15.
75. Ertan, G., et al., *Cerebellar abnormality in children and young adults with tuberous sclerosis complex: MR and diffusion weighted imaging findings.* J Neuroradiol, 2010. **37**(4): p. 231-8.
76. Curatolo, P., R. Moavero, and P.J. de Vries, *Neurological and neuropsychiatric aspects of tuberous sclerosis complex.* Lancet Neurol, 2015. **14**(7): p. 733-45.
77. Ma, T.S., et al., *Electrocorticographic evidence of perituberal cortex epileptogenicity in tuberous sclerosis complex.* J Neurosurg Pediatr, 2012. **10**(5): p. 376-82.
78. Sosunov, A.A., et al., *Epileptogenic but MRI-normal perituberal tissue in Tuberous Sclerosis Complex contains tuber-specific abnormalities.* Acta Neuropathol Commun, 2015. **3**: p. 17.
79. Grayson, L.E., et al., *Pilot Study of Neurodevelopmental Impact of Early Epilepsy Surgery in Tuberous Sclerosis Complex.* Pediatr Neurol, 2020. **109**: p. 39-46.
80. Northrup, H., D.A. Krueger, and G. International Tuberous Sclerosis Complex Consensus, *Tuberous sclerosis complex diagnostic criteria update: recommendations of the 2012 Iinternational Tuberous Sclerosis Complex Consensus Conference.* Pediatr Neurol, 2013. **49**(4): p. 243-54.
81. Magri, L. and R. Galli, *mTOR signaling in neural stem cells: from basic biology to disease.* Cell Mol Life Sci, 2013. **70**(16): p. 2887-98.
82. Henske, E.P., et al., *Allelic loss is frequent in tuberous sclerosis kidney lesions but rare in brain lesions.* Am J Hum Genet, 1996. **59**(2): p. 400-6.
83. Sepp, T., J.R. Yates, and A.J. Green, *Loss of heterozygosity in tuberous sclerosis hamartomas.* J Med Genet, 1996. **33**(11): p. 962-4.
84. Au, K.S., et al., *Complete inactivation of the TSC2 gene leads to formation of hamartomas.* Am J Hum Genet, 1999. **65**(6): p. 1790-5.
85. Crino, P.B., et al., *Biallelic TSC gene inactivation in tuberous sclerosis complex.* Neurology, 2010. **74**(21): p. 1716-23.
86. Qin, W., et al., *Analysis of TSC cortical tubers by deep sequencing of TSC1, TSC2 and KRAS demonstrates that small second-hit mutations in these genes are rare events.* Brain Pathol, 2010. **20**(6): p. 1096-105.
87. Martin, K.R., et al., *The genomic landscape of tuberous sclerosis complex.* Nat Commun, 2017. **8**: p. 15816.
88. Chan, J.A., et al., *Pathogenesis of tuberous sclerosis subependymal giant cell astrocytomas: biallelic inactivation of TSC1 or TSC2 leads to mTOR activation.* J Neuropathol Exp Neurol, 2004. **63**(12): p. 1236-42.
89. de Vries, P.J., et al., *A clinical update on tuberous sclerosis complex-associated neuropsychiatric disorders (TAND).* Am J Med Genet C Semin Med Genet, 2018. **178**(3): p. 309-320.
90. Nabbout, R., et al., *Epilepsy in tuberous sclerosis complex: Findings from the TOSCA Study.* Epilepsia Open, 2019. **4**(1): p. 73-84.

91. Crino, P.B., K.L. Nathanson, and E.P. Henske, *The tuberous sclerosis complex.* N Engl J Med, 2006. **355**(13): p. 1345-56.
92. Curatolo, P., M. Verdecchia, and R. Bombardieri, *Tuberous sclerosis complex: a review of neurological aspects.* Eur J Paediatr Neurol, 2002. **6**(1): p. 15-23.
93. Numis, A.L., et al., *Identification of risk factors for autism spectrum disorders in tuberous sclerosis complex.* Neurology, 2011. **76**(11): p. 981-7.
94. Chu-Shore, C.J., et al., *The natural history of epilepsy in tuberous sclerosis complex.* Epilepsia, 2010. **51**(7): p. 1236-41.
95. Simao, G., et al., *Diffusion tensor imaging of commissural and projection white matter in tuberous sclerosis complex and correlation with tuber load.* AJNR Am J Neuroradiol, 2010. **31**(7): p. 1273-7.
96. Arulrajah, S., et al., *Magnetic resonance imaging and diffusion-weighted imaging of normal-appearing white matter in children and young adults with tuberous sclerosis complex.* Neuroradiology, 2009. **51**(11): p. 781-6.
97. Capo-Chichi, J.M., et al., *Disruption of TBC1D7, a subunit of the TSC1-TSC2 protein complex, in intellectual disability and megalencephaly.* J Med Genet, 2013. **50**(11): p. 740-4.
98. Alfaiz, A.A., et al., *TBC1D7 mutations are associated with intellectual disability, macrocrania, patellar dislocation, and celiac disease.* Hum Mutat, 2014. **35**(4): p. 447-51.
99. Komiya, T., et al., *A Pilot Study of Sirolimus in Subjects with Cowden Syndrome or Other Syndromes Characterized by Germline Mutations in PTEN.* Oncologist, 2019. **24**(12): p. 1510-e1265.
100. Weiss, B., et al., *Sirolimus for progressive neurofibromatosis type 1-associated plexiform neurofibromas: a neurofibromatosis Clinical Trials Consortium phase II study.* Neuro Oncol, 2015. **17**(4): p. 596-603.
101. Parker, W.E., et al., *Rapamycin prevents seizures after depletion of STRADA in a rare neurodevelopmental disorder.* Sci Transl Med, 2013. **5**(182): p. 182ra53.
102. Choi, J., et al., *Structure of the FKBP12-rapamycin complex interacting with the binding domain of human FRAP.* Science, 1996. **273**(5272): p. 239-42.
103. Franz, D.N., et al., *Rapamycin causes regression of astrocytomas in tuberous sclerosis complex.* Ann Neurol, 2006. **59**(3): p. 490-8.
104. Franz, D.N., et al., *Efficacy and safety of everolimus for subependymal giant cell astrocytomas associated with tuberous sclerosis complex (EXIST-1): a multicentre, randomised, placebo-controlled phase 3 trial.* Lancet, 2013. **381**(9861): p. 125-32.
105. Krueger, D.A., et al., *Everolimus long-term safety and efficacy in subependymal giant cell astrocytoma.* Neurology, 2013. **80**(6): p. 574-80.
106. Cardamone, M., et al., *Mammalian target of rapamycin inhibitors for intractable epilepsy and subependymal giant cell astrocytomas in tuberous sclerosis complex.* J Pediatr, 2014. **164**(5): p. 1195-200.
107. French, J.A., et al., *Adjunctive everolimus therapy for treatment-resistant focal-onset seizures associated with tuberous sclerosis (EXIST-3): a phase 3, randomised, double-blind, placebo-controlled study.* Lancet, 2016. **388**(10056): p. 2153-2163.

108. Samueli, S., et al., *Efficacy and safety of Everolimus in children with TSC - associated epilepsy - Pilot data from an open single-center prospective study.* Orphanet J Rare Dis, 2016. **11**(1): p. 145.
109. Overwater, I.E., et al., *Sirolimus for epilepsy in children with tuberous sclerosis complex: A randomized controlled trial.* Neurology, 2016. **87**(10): p. 1011-8.
110. Jozwiak, S., et al., *Antiepileptic treatment before the onset of seizures reduces epilepsy severity and risk of mental retardation in infants with tuberous sclerosis complex.* Eur J Paediatr Neurol, 2011. **15**(5): p. 424-31.
111. Cusmai, R., et al., *Long-term neurological outcome in children with early-onset epilepsy associated with tuberous sclerosis.* Epilepsy Behav, 2011. **22**(4): p. 735-9.
112. Curatolo, P., M. Verdecchia, and R. Bombardieri, *Vigabatrin for tuberous sclerosis complex.* Brain Dev, 2001. **23**(7): p. 649-53.
113. Krueger, D.A., et al., *Everolimus for treatment of tuberous sclerosis complex-associated neuropsychiatric disorders.* Ann Clin Transl Neurol, 2017. **4**(12): p. 877-887.
114. Overwater, I.E., et al., *A randomized controlled trial with everolimus for IQ and autism in tuberous sclerosis complex.* Neurology, 2019. **93**(2): p. e200-e209.
115. Mizuguchi, M., et al., *Everolimus for epilepsy and autism spectrum disorder in tuberous sclerosis complex: EXIST-3 substudy in Japan.* Brain Dev, 2019. **41**(1): p. 1-10.
116. Thoreen, C.C. and D.M. Sabatini, *Rapamycin inhibits mTORC1, but not completely.* Autophagy, 2009. **5**(5): p. 725-6.
117. Choo, A.Y., et al., *Rapamycin differentially inhibits S6Ks and 4E-BP1 to mediate cell-type-specific repression of mRNA translation.* Proc Natl Acad Sci U S A, 2008. **105**(45): p. 17414-9.
118. Sarbassov, D.D., et al., *Prolonged rapamycin treatment inhibits mTORC2 assembly and Akt/PKB.* Mol Cell, 2006. **22**(2): p. 159-68.
119. Kaplan, B., Y. Qazi, and J.R. Wellen, *Strategies for the management of adverse events associated with mTOR inhibitors.* Transplant Rev (Orlando), 2014. **28**(3): p. 126-33.
120. Lamming, D.W., et al., *Rapamycin-induced insulin resistance is mediated by mTORC2 loss and uncoupled from longevity.* Science, 2012. **335**(6076): p. 1638-43.
121. Kleinert, M., et al., *Acute mTOR inhibition induces insulin resistance and alters substrate utilization in vivo.* Mol Metab, 2014. **3**(6): p. 630-41.
122. Arriola Apelo, S.I., et al., *Alternative rapamycin treatment regimens mitigate the impact of rapamycin on glucose homeostasis and the immune system.* Aging Cell, 2016. **15**(1): p. 28-38.
123. Rensing, N., L. Han, and M. Wong, *Intermittent dosing of rapamycin maintains antiepileptogenic effects in a mouse model of tuberous sclerosis complex.* Epilepsia, 2015. **56**(7): p. 1088-97.
124. Schreiber, K.H., et al., *A novel rapamycin analog is highly selective for mTORC1 in vivo.* Nat Commun, 2019. **10**(1): p. 3194.
125. Schenone, S., et al., *ATP-competitive inhibitors of mTOR: an update.* Curr Med Chem, 2011. **18**(20): p. 2995-3014.

126. Mahoney, S.J., et al., *A small molecule inhibitor of Rheb selectively targets mTORC1 signaling.* Nat Commun, 2018. **9**(1): p. 548.
127. Chung, C.Y., et al., *Covalent targeting of the vacuolar H(+)-ATPase activates autophagy via mTORC1 inhibition.* Nat Chem Biol, 2019. **15**(8): p. 776-785.
128. Shokat K, Z.Z., Fan Q, Luo X, Lou K, Weiss W, *Brain-Restricted mTOR Inhibition with Binary Pharmacology.* bioRxiv 10.21203/rs.3.rs-92256/v1, 2020.
129. Ito, N. and G.M. Rubin, *gigas, a Drosophila homolog of tuberous sclerosis gene product-2, regulates the cell cycle.* Cell, 1999. **96**(4): p. 529-39.
130. Tapon, N., et al., *The Drosophila tuberous sclerosis complex gene homologs restrict cell growth and cell proliferation.* Cell, 2001. **105**(3): p. 345-55.
131. Eker R., M.J., *A dominant gene for renal adenomas in the rat.* Nature, 1961. **189**: p. 858–859.
132. Yeung, R.S., et al., *Predisposition to renal carcinoma in the Eker rat is determined by germ-line mutation of the tuberous sclerosis 2 (TSC2) gene.* Proc Natl Acad Sci U S A, 1994. **91**(24): p. 11413-6.
133. Hino, O., et al., *The predisposing gene of the Eker rat inherited cancer syndrome is tightly linked to the tuberous sclerosis (TSC2) gene.* Biochem Biophys Res Commun, 1994. **203**(2): p. 1302-8.
134. Orlova, K.A., et al., *STRADalpha deficiency results in aberrant mTORC1 signaling during corticogenesis in humans and mice.* J Clin Invest, 2010. **120**(5): p. 1591-602.
135. Dang, L.T., et al., *Multimodal Analysis of STRADA Function in Brain Development.* Front Cell Neurosci, 2020. **14**: p. 122.
136. Gutmann, D.H. and M. Giovannini, *Mouse models of neurofibromatosis 1 and 2.* Neoplasia, 2002. **4**(4): p. 279-90.
137. Yuskaitis, C.J., et al., *A mouse model of DEPDC5-related epilepsy: Neuronal loss of Depdc5 causes dysplastic and ectopic neurons, increased mTOR signaling, and seizure susceptibility.* Neurobiol Dis, 2018. **111**: p. 91-101.
138. Kobayashi, T., et al., *A germ-line Tsc1 mutation causes tumor development and embryonic lethality that are similar, but not identical to, those caused by Tsc2 mutation in mice.* Proc Natl Acad Sci U S A, 2001. **98**(15): p. 8762-7.
139. Kobayashi, T., et al., *Renal carcinogenesis, hepatic hemangiomatosis, and embryonic lethality caused by a germ-line Tsc2 mutation in mice.* Cancer Res, 1999. **59**(6): p. 1206-11.
140. Onda, H., et al., *Tsc2(+/-) mice develop tumors in multiple sites that express gelsolin and are influenced by genetic background.* J Clin Invest, 1999. **104**(6): p. 687-95.
141. Di Cristofano, A., et al., *Pten is essential for embryonic development and tumour suppression.* Nat Genet, 1998. **19**(4): p. 348-55.
142. Sato, A., et al., *Rapamycin reverses impaired social interaction in mouse models of tuberous sclerosis complex.* Nat Commun, 2012. **3**: p. 1292.
143. Goorden, S.M., et al., *Cognitive deficits in Tsc1+/- mice in the absence of cerebral lesions and seizures.* Ann Neurol, 2007. **62**(6): p. 648-55.
144. Kirschstein, T., *Synaptic plasticity and learning in animal models of tuberous sclerosis complex.* Neural Plast, 2012. **2012**: p. 279834.

145. Clipperton-Allen, A.E. and D.T. Page, *Pten haploinsufficient mice show broad brain overgrowth but selective impairments in autism-relevant behavioral tests.* Hum Mol Genet, 2014. **23**(13): p. 3490-505.
146. Li, L., et al., *PTEN in neural precursor cells: regulation of migration, apoptosis, and proliferation.* Mol Cell Neurosci, 2002. **20**(1): p. 21-9.
147. Ehninger, D., et al., *Reversal of learning deficits in a Tsc2+/- mouse model of tuberous sclerosis.* Nat Med, 2008. **14**(8): p. 843-8.
148. Tavazoie, S.F., et al., *Regulation of neuronal morphology and function by the tumor suppressors Tsc1 and Tsc2.* Nat Neurosci, 2005. **8**(12): p. 1727-34.
149. Auerbach, B.D., E.K. Osterweil, and M.F. Bear, *Mutations causing syndromic autism define an axis of synaptic pathophysiology.* Nature, 2011. **480**(7375): p. 63-8.
150. Jeong A and W. M, *Tuberous Sclerosis and Other mTORopathies*, in *Models of Seizures and Epilepsy (Second edition)*. 2017, Elsevier Inc. p. 797-810.
151. Meikle, L., et al., *A mouse model of tuberous sclerosis: neuronal loss of Tsc1 causes dysplastic and ectopic neurons, reduced myelination, seizure activity, and limited survival.* J Neurosci, 2007. **27**(21): p. 5546-58.
152. Carson, R.P., et al., *Neuronal and glia abnormalities in Tsc1-deficient forebrain and partial rescue by rapamycin.* Neurobiol Dis, 2012. **45**(1): p. 369-80.
153. Bateup, H.S., et al., *Excitatory/inhibitory synaptic imbalance leads to hippocampal hyperexcitability in mouse models of tuberous sclerosis.* Neuron, 2013. **78**(3): p. 510-22.
154. McMahon, J., et al., *Impaired autophagy in neurons after disinhibition of mammalian target of rapamycin and its contribution to epileptogenesis.* J Neurosci, 2012. **32**(45): p. 15704-14.
155. Chen, C.J., et al., *Therapeutic inhibition of mTORC2 rescues the behavioral and neurophysiological abnormalities associated with Pten-deficiency.* Nat Med, 2019. **25**(11): p. 1684-1690.
156. Zou, J., et al., *Postnatal reduction of tuberous sclerosis complex 1 expression in astrocytes and neurons causes seizures in an age-dependent manner.* Epilepsia, 2017. **58**(12): p. 2053-2063.
157. Tsai, P.T., et al., *Autistic-like behaviour and cerebellar dysfunction in Purkinje cell Tsc1 mutant mice.* Nature, 2012. **488**(7413): p. 647-51.
158. Reith, R.M., et al., *Loss of Tsc2 in Purkinje cells is associated with autistic-like behavior in a mouse model of tuberous sclerosis complex.* Neurobiol Dis, 2013. **51**: p. 93-103.
159. Cupolillo, D., et al., *Autistic-Like Traits and Cerebellar Dysfunction in Purkinje Cell PTEN Knock-Out Mice.* Neuropsychopharmacology, 2016. **41**(6): p. 1457-66.
160. Kosillo, P., et al., *Tsc1-mTORC1 signaling controls striatal dopamine release and cognitive flexibility.* Nat Commun, 2019. **10**(1): p. 5426.
161. McMahon, J.J., et al., *Seizure-dependent mTOR activation in 5-HT neurons promotes autism-like behaviors in mice.* Neurobiol Dis, 2015. **73**: p. 296-306.
162. Benthall KN, C.K., Agopyan-Miu AHCW,Chen EY, Bateup HS, *Loss of Tsc1 from striatal direct pathway neurons impairs endocannabinoid-LTD and enhances motor routine learning.* bioRxiv 10.1101/2019.12.15.877126, 2019.

163. Normand, E.A., et al., *Temporal and mosaic Tsc1 deletion in the developing thalamus disrupts thalamocortical circuitry, neural function, and behavior.* Neuron, 2013. **78**(5): p. 895-909.
164. Feliciano, D.M., et al., *Single-cell Tsc1 knockout during corticogenesis generates tuber-like lesions and reduces seizure threshold in mice.* J Clin Invest, 2011. **121**(4): p. 1596-607.
165. Nguyen, L.H., T. Mahadeo, and A. Bordey, *mTOR Hyperactivity Levels Influence the Severity of Epilepsy and Associated Neuropathology in an Experimental Model of Tuberous Sclerosis Complex and Focal Cortical Dysplasia.* J Neurosci, 2019. **39**(14): p. 2762-2773.
166. Blair, J.D., D. Hockemeyer, and H.S. Bateup, *Genetically engineered human cortical spheroid models of tuberous sclerosis.* Nat Med, 2018. **24**(10): p. 1568-1578.
167. Blair, J.D. and H.S. Bateup, *New frontiers in modeling tuberous sclerosis with human stem cell-derived neurons and brain organoids.* Dev Dyn, 2020. **249**(1): p. 46-55.
168. Costa, V., et al., *mTORC1 Inhibition Corrects Neurodevelopmental and Synaptic Alterations in a Human Stem Cell Model of Tuberous Sclerosis.* Cell Rep, 2016. **15**(1): p. 86-95.
169. Li, Y., et al., *Induction of Expansion and Folding in Human Cerebral Organoids.* Cell Stem Cell, 2017. **20**(3): p. 385-396 e3.
170. Afshar Saber, W. and M. Sahin, *Recent advances in human stem cell-based modeling of Tuberous Sclerosis Complex.* Mol Autism, 2020. **11**(1): p. 16.
171. Meikle, L., et al., *Response of a neuronal model of tuberous sclerosis to mammalian target of rapamycin (mTOR) inhibitors: effects on mTORC1 and Akt signaling lead to improved survival and function.* J Neurosci, 2008. **28**(21): p. 5422-32.
172. Lin, T.V., et al., *Normalizing translation through 4E-BP prevents mTOR-driven cortical mislamination and ameliorates aberrant neuron integration.* Proc Natl Acad Sci U S A, 2016. **113**(40): p. 11330-11335.
173. Getz, S.A., et al., *Rapamycin prevents, but does not reverse, aberrant migration in Pten knockout neurons.* Neurobiol Dis, 2016. **93**: p. 12-20.
174. Tsai, P.T., et al., *Sensitive Periods for Cerebellar-Mediated Autistic-like Behaviors.* Cell Rep, 2018. **25**(2): p. 357-367 e4.
175. Cox, R.L., et al., *Multiple Critical Periods for Rapamycin Treatment to Correct Structural Defects in Tsc-1-Suppressed Brain.* Front Mol Neurosci, 2018. **11**: p. 409.
176. Zeng, L.H., N.R. Rensing, and M. Wong, *The mammalian target of rapamycin signaling pathway mediates epileptogenesis in a model of temporal lobe epilepsy.* J Neurosci, 2009. **29**(21): p. 6964-72.
177. Tsai, P.T., et al., *Prenatal rapamycin results in early and late behavioral abnormalities in wildtype C57BL/6 mice.* Behav Genet, 2013. **43**(1): p. 51-9.
178. Urbanska, M., et al., *Mammalian target of rapamycin complex 1 (mTORC1) and 2 (mTORC2) control the dendritic arbor morphology of hippocampal neurons.* J Biol Chem, 2012. **287**(36): p. 30240-56.

179. Angliker, N., et al., *mTORC1 and mTORC2 have largely distinct functions in Purkinje cells.* Eur J Neurosci, 2015. **42**(8): p. 2595-612.
180. Huang, W.C., Y. Chen, and D.T. Page, *Hyperconnectivity of prefrontal cortex to amygdala projections in a mouse model of macrocephaly/autism syndrome.* Nat Commun, 2016. **7**: p. 13421.
181. Weston, M.C., H. Chen, and J.W. Swann, *Loss of mTOR repressors Tsc1 or Pten has divergent effects on excitatory and inhibitory synaptic transmission in single hippocampal neuron cultures.* Front Mol Neurosci, 2014. **7**: p. 1.
182. Sharma, A., et al., *Dysregulation of mTOR signaling in fragile X syndrome.* J Neurosci, 2010. **30**(2): p. 694-702.
183. Yan, J., et al., *Activation of autophagy rescues synaptic and cognitive deficits in fragile X mice.* Proc Natl Acad Sci U S A, 2018. **115**(41): p. E9707-E9716.
184. Sare, R.M., et al., *Negative Effects of Chronic Rapamycin Treatment on Behavior in a Mouse Model of Fragile X Syndrome.* Front Mol Neurosci, 2017. **10**: p. 452.
185. Wang, D., P.W.L. Tai, and G. Gao, *Adeno-associated virus vector as a platform for gene therapy delivery.* Nat Rev Drug Discov, 2019. **18**(5): p. 358-378.
186. Fellmann, C., et al., *Cornerstones of CRISPR-Cas in drug discovery and therapy.* Nat Rev Drug Discov, 2017. **16**(2): p. 89-100.
187. Adli, M., *The CRISPR tool kit for genome editing and beyond.* Nat Commun, 2018. **9**(1): p. 1911.
188. Ingusci, S., et al., *Gene Therapy Tools for Brain Diseases.* Front Pharmacol, 2019. **10**: p. 724.
189. Deverman, B.E., et al., *Gene therapy for neurological disorders: progress and prospects.* Nat Rev Drug Discov, 2018. **17**(9): p. 641-659.
190. Karalis, V. and H.S. Bateup, *Current Approaches and Future Directions for the Treatment of mTORopathies.* Dev Neurosci, 2021: p. 1-16.
191. Yang, H., et al., *Structural insights into TSC complex assembly and GAP activity on Rheb.* Nat Commun, 2021. **12**(1): p. 339.
192. Yang, H., et al., *mTOR kinase structure, mechanism and regulation.* Nature, 2013. **497**(7448): p. 217-23.
193. Burnett, P.E., et al., *RAFT1 phosphorylation of the translational regulators p70 S6 kinase and 4E-BP1.* Proc Natl Acad Sci U S A, 1998. **95**(4): p. 1432-7.
194. Hara, K., et al., *Regulation of eIF-4E BP1 phosphorylation by mTOR.* J Biol Chem, 1997. **272**(42): p. 26457-63.
195. Fingar, D.C., et al., *Mammalian cell size is controlled by mTOR and its downstream targets S6K1 and 4EBP1/eIF4E.* Genes Dev, 2002. **16**(12): p. 1472-87.
196. Scaiola, A., et al., *The 3.2-A resolution structure of human mTORC2.* Sci Adv, 2020. **6**(45).
197. Sarbassov, D.D., et al., *Phosphorylation and regulation of Akt/PKB by the rictor-mTOR complex.* Science, 2005. **307**(5712): p. 1098-101.
198. Saxton, R.A. and D.M. Sabatini, *mTOR Signaling in Growth, Metabolism, and Disease.* Cell, 2017. **168**(6): p. 960-976.
199. Xie, J. and C.G. Proud, *Signaling crosstalk between the mTOR complexes.* Translation (Austin), 2014. **2**(1): p. e28174.

200. Bateup, H.S., et al., *Loss of Tsc1 in vivo impairs hippocampal mGluR-LTD and increases excitatory synaptic function.* J Neurosci, 2011. **31**(24): p. 8862-9.
201. Chevere-Torres, I., et al., *Metabotropic glutamate receptor-dependent long-term depression is impaired due to elevated ERK signaling in the DeltaRG mouse model of tuberous sclerosis complex.* Neurobiol Dis, 2012. **45**(3): p. 1101-10.
202. Potter, W.B., et al., *Reduced juvenile long-term depression in tuberous sclerosis complex is mitigated in adults by compensatory recruitment of mGluR5 and Erk signaling.* PLoS Biol, 2013. **11**(8): p. e1001627.
203. Kwiatkowski, D.J., et al., *A mouse model of TSC1 reveals sex-dependent lethality from liver hemangiomas, and up-regulation of p70S6 kinase activity in Tsc1 null cells.* Hum Mol Genet, 2002. **11**(5): p. 525-34.
204. Sengupta, S., et al., *mTORC1 controls fasting-induced ketogenesis and its modulation by ageing.* Nature, 2010. **468**(7327): p. 1100-4.
205. Tang, F., et al., *A critical role for Rictor in T lymphopoiesis.* J Immunol, 2012. **189**(4): p. 1850-7.
206. Magee, J.A., et al., *Temporal changes in PTEN and mTORC2 regulation of hematopoietic stem cell self-renewal and leukemia suppression.* Cell Stem Cell, 2012. **11**(3): p. 415-28.
207. Gorski, J.A., et al., *Cortical excitatory neurons and glia, but not GABAergic neurons, are produced in the Emx1-expressing lineage.* J Neurosci, 2002. **22**(15): p. 6309-14.
208. Magri, L., et al., *Sustained activation of mTOR pathway in embryonic neural stem cells leads to development of tuberous sclerosis complex-associated lesions.* Cell Stem Cell, 2011. **9**(5): p. 447-62.
209. Carson, R.P., et al., *Deletion of Rictor in neural progenitor cells reveals contributions of mTORC2 signaling to tuberous sclerosis complex.* Hum Mol Genet, 2013. **22**(1): p. 140-52.
210. Kulkarni, R.U., et al., *Voltage-sensitive rhodol with enhanced two-photon brightness.* Proc Natl Acad Sci U S A, 2017. **114**(11): p. 2813-2818.
211. Winden, K.D., et al., *Biallelic Mutations in TSC2 Lead to Abnormalities Associated with Cortical Tubers in Human iPSC-Derived Neurons.* J Neurosci, 2019. **39**(47): p. 9294-9305.
212. Dana, H., et al., *Sensitive red protein calcium indicators for imaging neural activity.* Elife, 2016. **5**.
213. Nadadhur, A.G., et al., *Neuron-Glia Interactions Increase Neuronal Phenotypes in Tuberous Sclerosis Complex Patient iPSC-Derived Models.* Stem Cell Reports, 2019. **12**(1): p. 42-56.
214. Alsaqati, M., V.M. Heine, and A.J. Harwood, *Pharmacological intervention to restore connectivity deficits of neuronal networks derived from ASD patient iPSC with a TSC2 mutation.* Mol Autism, 2020. **11**(1): p. 80.
215. Thoreen, C.C., et al., *An ATP-competitive mammalian target of rapamycin inhibitor reveals rapamycin-resistant functions of mTORC1.* J Biol Chem, 2009. **284**(12): p. 8023-32.
216. Lebrun-Julien, F., et al., *Balanced mTORC1 activity in oligodendrocytes is required for accurate CNS myelination.* J Neurosci, 2014. **34**(25): p. 8432-48.

217. Shi, Q., et al., *mTORC1 Activation by Loss of Tsc1 in Myelinating Glia Causes Downregulation of Quaking and Neurofascin 155 Leading to Paranodal Domain Disorganization.* Front Cell Neurosci, 2018. **12**: p. 201.
218. Ercan, E., et al., *Neuronal CTGF/CCN2 negatively regulates myelination in a mouse model of tuberous sclerosis complex.* J Exp Med, 2017. **214**(3): p. 681-697.
219. Bercury, K.K., et al., *Conditional ablation of raptor or rictor has differential impact on oligodendrocyte differentiation and CNS myelination.* J Neurosci, 2014. **34**(13): p. 4466-80.
220. Carracedo, A. and P.P. Pandolfi, *The PTEN-PI3K pathway: of feedbacks and cross-talks.* Oncogene, 2008. **27**(41): p. 5527-41.
221. Yang, G., et al., *A Positive Feedback Loop between Akt and mTORC2 via SIN1 Phosphorylation.* Cell Rep, 2015. **12**(6): p. 937-43.
222. Bhattacharya, K., S. Maiti, and C. Mandal, *PTEN negatively regulates mTORC2 formation and signaling in grade IV glioma via Rictor hyperphosphorylation at Thr1135 and direct the mode of action of an mTORC1/2 inhibitor.* Oncogenesis, 2016. **5**(5): p. e227.
223. Inoki, K., et al., *Rheb GTPase is a direct target of TSC2 GAP activity and regulates mTOR signaling.* Genes Dev, 2003. **17**(15): p. 1829-34.
224. Huang, J., et al., *The TSC1-TSC2 complex is required for proper activation of mTOR complex 2.* Mol Cell Biol, 2008. **28**(12): p. 4104-15.
225. Huang, J. and B.D. Manning, *A complex interplay between Akt, TSC2 and the two mTOR complexes.* Biochem Soc Trans, 2009. **37**(Pt 1): p. 217-22.
226. Breuleux, M., et al., *Increased AKT S473 phosphorylation after mTORC1 inhibition is rictor dependent and does not predict tumor cell response to PI3K/mTOR inhibition.* Mol Cancer Ther, 2009. **8**(4): p. 742-53.
227. Yu, Y., et al., *Phosphoproteomic analysis identifies Grb10 as an mTORC1 substrate that negatively regulates insulin signaling.* Science, 2011. **332**(6035): p. 1322-6.
228. Yoneyama, Y., et al., *Serine Phosphorylation by mTORC1 Promotes IRS-1 Degradation through SCFbeta-TRCP E3 Ubiquitin Ligase.* iScience, 2018. **5**: p. 1-18.
229. Dibble, C.C., J.M. Asara, and B.D. Manning, *Characterization of Rictor phosphorylation sites reveals direct regulation of mTOR complex 2 by S6K1.* Mol Cell Biol, 2009. **29**(21): p. 5657-70.
230. Julien, L.A., et al., *mTORC1-activated S6K1 phosphorylates Rictor on threonine 1135 and regulates mTORC2 signaling.* Mol Cell Biol, 2010. **30**(4): p. 908-21.
231. Liu, P., et al., *Sin1 phosphorylation impairs mTORC2 complex integrity and inhibits downstream Akt signalling to suppress tumorigenesis.* Nat Cell Biol, 2013. **15**(11): p. 1340-50.
232. Jones, A.C., et al., *Comprehensive mutation analysis of TSC1 and TSC2-and phenotypic correlations in 150 families with tuberous sclerosis.* Am J Hum Genet, 1999. **64**(5): p. 1305-15.
233. Dabora, S.L., et al., *Mutational analysis in a cohort of 224 tuberous sclerosis patients indicates increased severity of TSC2, compared with TSC1, disease in multiple organs.* Am J Hum Genet, 2001. **68**(1): p. 64-80.

234. Tyburczy, M.E., et al., *Mosaic and Intronic Mutations in TSC1/TSC2 Explain the Majority of TSC Patients with No Mutation Identified by Conventional Testing.* PLoS Genet, 2015. **11**(11): p. e1005637.
235. Benthall, K.N.C., K.R.; Agopyan-Miu, A.H.C.W.; Chen, E.Y.; Bateup, H.S., *Loss of Tsc1 from striatal direct pathway neurons impairs endocannabinoid-LTD and enhances motor routine learning.* bioRxiv, 2020.
236. Hentges, K.E., et al., *FRAP/mTOR is required for proliferation and patterning during embryonic development in the mouse.* Proc Natl Acad Sci U S A, 2001. **98**(24): p. 13796-801.
237. Cloetta, D., et al., *Inactivation of mTORC1 in the developing brain causes microcephaly and affects gliogenesis.* J Neurosci, 2013. **33**(18): p. 7799-810.
238. Ka, M., et al., *mTOR regulates brain morphogenesis by mediating GSK3 signaling.* Development, 2014. **141**(21): p. 4076-86.
239. Zhang, Y., et al., *Neuronal mTORC1 Is Required for Maintaining the Nonreactive State of Astrocytes.* J Biol Chem, 2017. **292**(1): p. 100-111.
240. Diez, H., J.J. Garrido, and F. Wandosell, *Specific roles of Akt iso forms in apoptosis and axon growth regulation in neurons.* PLoS One, 2012. **7**(4): p. e32715.
241. Vanderplow, A.M., et al., *Akt-mTOR hypoactivity in bipolar disorder gives rise to cognitive impairments associated with altered neuronal structure and function.* Neuron, 2021. **109**(9): p. 1479-1496 e6.
242. Machado-Vieira, R., et al., *Decreased AKT1/mTOR pathway mRNA expression in short-term bipolar disorder.* Eur Neuropsychopharmacol, 2015. **25**(4): p. 468-73.
243. Pnevmatikakis, E.A. and A. Giovannucci, *NoRMCorre: An online algorithm for piecewise rigid motion correction of calcium imaging data.* J Neurosci Methods, 2017. **291**: p. 83-94.
244. Madisen, L., et al., *A robust and high-throughput Cre reporting and characterization system for the whole mouse brain.* Nat Neurosci, 2010. **13**(1): p. 133-40.
245. Vergeer, M., et al., *Epilepsy, impaired functioning, and quality of life in patients with tuberous sclerosis complex.* Epilepsia Open, 2019. **4**(4): p. 581-592.
246. Devlin, L.A., et al., *Tuberous sclerosis complex: clinical features, diagnosis, and prevalence within Northern Ireland.* Dev Med Child Neurol, 2006. **48**(6): p. 495-9.
247. Winterkorn, E.B., M.B. Pulsifer, and E.A. Thiele, *Cognitive prognosis of patients with tuberous sclerosis complex.* Neurology, 2007. **68**(1): p. 62-4.
248. Askalan, R., et al., *Prospective preliminary analysis of the development of autism and epilepsy in children with infantile spasms.* J Child Neurol, 2003. **18**(3): p. 165-70.
249. de Vries, P.J., et al., *Tuberous sclerosis associated neuropsychiatric disorders (TAND) and the TAND Checklist.* Pediatr Neurol, 2015. **52**(1): p. 25-35.
250. Yang, S.B., et al., *Rapamycin ameliorates age-dependent obesity associated with increased mTOR signaling in hypothalamic POMC neurons.* Neuron, 2012. **75**(3): p. 425-36.

251. Karalis, V., F. Caval-Holme, and H.S. Bateup, *Raptor downregulation rescues neuronal phenotypes in mouse models of Tuberous Sclerosis Complex.* bioRxiv, 2021.
252. Benthall, K.N., S.L. Ong, and H.S. Bateup, *Corticostriatal Transmission Is Selectively Enhanced in Striatonigral Neurons with Postnatal Loss of Tsc1.* Cell Rep, 2018. **23**(11): p. 3197-3208.
253. Hisatsune, C., et al., *Tuberous Sclerosis Complex (TSC) Inactivation Increases Neuronal Network Activity by Enhancing Ca(2+) Influx via L-Type Ca(2+) Channels.* J Neurosci, 2021. **41**(39): p. 8134-8149.
254. Koene, L.M.C., et al., *Effects of antiepileptic drugs in a new TSC/mTOR-dependent epilepsy mouse model.* Ann Clin Transl Neurol, 2019. **6**(7): p. 1273-1291.
255. Malik, R., et al., *Tsc1 represses parvalbumin expression and fast-spiking properties in somatostatin lineage cortical interneurons.* Nat Commun, 2019. **10**(1): p. 4994.
256. Zeng, L.H., et al., *Rapamycin prevents epilepsy in a mouse model of tuberous sclerosis complex.* Ann Neurol, 2008. **63**(4): p. 444-53.
257. Kosillo, P., et al., *Dopamine neuron morphology and output are differentially controlled by mTORC1 and mTORC2.* bioRxiv, 2021.